

Earth Chemistry Introduction

Earth Chemists are primarily interested in the evolution of the Earth through measuring chemical and isotopic systems in relevant materials. Our studies range from the earliest solar system through the earliest Earth environments and on to processes that are actively taking place today. Most of our analytical work involves detailed analysis on the microscale, or concentrating trace elements from larger samples for high precision analysis. Isotopic systems can reveal both the nature of the processes involved (stable isotopes) as well as the timing of events (radiogenic isotopes), while chemical abundances can reflect protolith contributions and processes affecting various systems. As revealed in this year's research contributions, analytical work can be applied to topics in tectonics, ore genesis, metamorphic petrology, paleoclimate, and regolith dating. Several of these contributions have made their way to the pages of *Science* and *Nature*, an outstanding effort.

SHRIMP

A focus of research for many RSES researchers is the SHRIMP arsenal. The last year has seen several important breakthroughs in our attempts to produce analytical protocols that allow high precision, robust and reproducible stable isotope ratios on the SHRIMP II multiple collector. These developments are extremely important as we commit to the final designs of the SHRIMP SI (supported by ARC LIEF in Y2005). In addition, high precision Pb isotope measurements by multiple collection are becoming more routine further supporting the success of the multiple collector rebuild. SHRIMP I continues to produce quality data, but this year saw substantial changes to the sample stage and handling system to allow automated, unattended operation as is now routine for SHRIMP II and SHRIMP RG.

Personnel

This year we welcome QEII Fellow Dr Jochen Brocks who has introduced organic geochemistry to Earth Chemistry. Jochen's research interests focus on the signatures of earliest life (biomarkers) and the evolution of the Earth from a chemically hostile realm to a flourishing ecosystem.

Earth Chemistry also welcomes QEII Fellow Dr Daniela Rubatto to the area. Daniela has been at the Australian National University for several appointments and continues her work in to trace element behaviour particularly in high-grade metamorphic rocks.

Dr Yuri Amelin of the Canadian Geological Survey, Ottawa, has accepted a position funded the Planetary Science Institute and is expected to arrive in mid-2006. Yuri's specialty is high precision geochronology, latterly focused on the earliest chronology of the solar system.

ARC

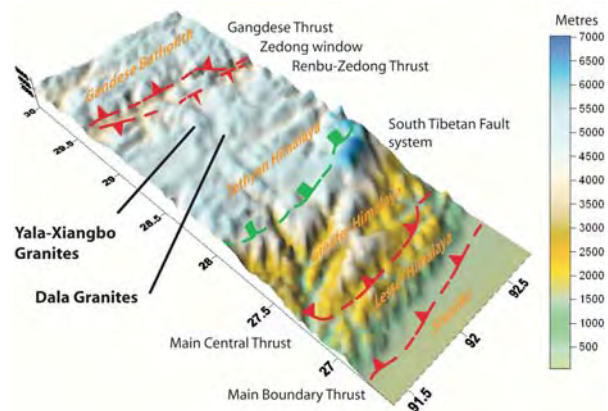
This year saw three ARC Discovery awards to EC personnel. Professor Mark Harrison will continue his work on the Hadean through studies of detrital zircons. Drs Trevor Ireland and Yuri Amelin will focus on the chronology of the earliest solar system. Dr Ian Williams in collaboration with Professor Rainer Grun (Earth Environment) will examine oxygen isotope distributions in teeth as an environmental indicator. Dr Jochen Brocks was successful in his ARC LIEF bids for a high resolution double-sector mass-spectrometer (GC-MS/MS) instrument for biomarker analyses to be housed at RSES and a HPLC-MS/MS to be located at Curtin University, while Dr Trevor Ireland supported a successful bid for a High Resolution Simultaneous DSC/DTA-TGA-FTIR System with UWS.

New constraints on evolutionary models for the Himalayan orogen from Eocene-Miocene granitoid bodies in the eastern North Himalaya

Amos B. Aikman¹

¹ *Research School of Earth Sciences, Australian National University, Canberra, ACT 0200, Australia*

The record of granitoid magmatism preserved in the eastern North Himalaya and the southern Tibetan plateau places important constraints on the structural architecture and locus of tectonic activity in the Himalayan orogen since at least the mid-Eocene.



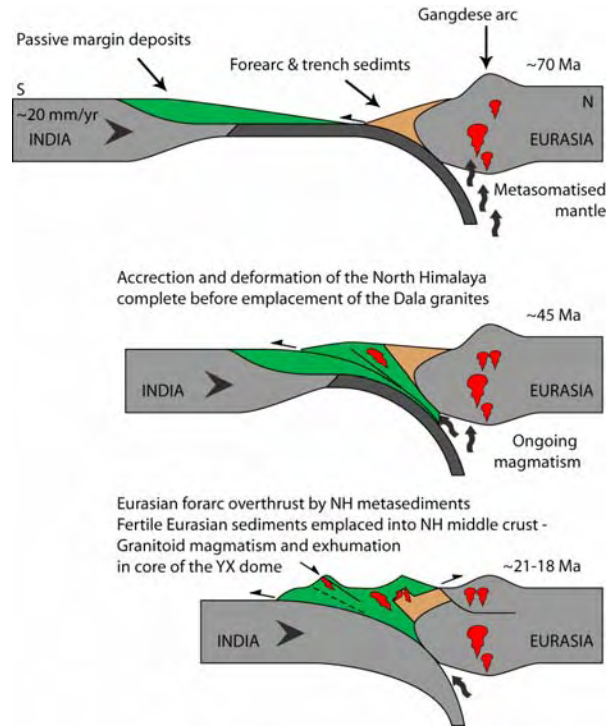
The North Himalaya (NH) comprise a sequence of predominantly low-grade metasediments that originated as passive margin deposits north of the Indian Shield prior to closure of the Tethys Ocean. The sequence is bounded to the south by the South Tibetan Detachment (STD), a segmented normal-sense movement zone cropping out along the peaks of the high Himalaya, and to the north by the Indus Tsangpo Suture (ITS), which marks the surface boundary between rocks of Indian and Eurasian continental affinity.

Undeformed Eocene (45 Ma) granitoid plutons (the Dala granites, DG) emplaced into deformed sub-greenschist facies metasediments of the North Himalaya constrain the timing of deformation in the structurally highest units of the Himalayan fold and thrust belt (HFTB). Combined isotopic and thermometric studies of the DG indicate they formed by mixing between a juvenile magma and a crustal derived component. In terms of major and trace elements, the DG are virtually indistinguishable from granites of the Gangdese Batholith (an Andean type complex which formed above a north dipping subduction zone on the southern margin of Eurasia, GB). Isotopically however, they are distinct from any of the major Himalayan lithotectonic units outcropping today. Combined, these observations suggest that the base of the North Himalaya was exposed to the Gangdese metasomatised mantle wedge in the mid-Eocene, and that high-grade units such as the Greater Himalayan Crystallines (GHC) did not underlie the present-day structurally highest units of the HFTB at that time.

Miocene (~20 Ma) granites (the Yala-Xiangbo granites, YG) emplaced into the high grade core of the Yala-Xiangbo dome (YD) record low zircon and monazite saturation temperatures ($660 \pm 50^\circ\text{C}$), indicative of hydrous melting conditions.

High-grade pelites in the core of the YD are both isotopically and geochemically similar to rocks of the GB and southern Lhasa Block (LB). These observations are attributed to formation of the YG by dehydration melting of the Xigaze Forearc (XF) sediments during burial associated with activity on the South-Tibetan Detachment (STD) – Renbu Zedong Thrust (RZT) fault system.

Petrogenesis of the DG, combined with documented evidence for ongoing magmatism in the GB as recently as ~12 Ma (possibly <10 Ma) argue strongly against underthrusting of Indian lithosphere beneath southern Tibet, either as a means of thickening the crust, or providing insulation to promote development of a weak mid-crustal layer. These data are in agreement with recent tomographic studies. Combined with abundant evidence that the middle crust of the southern LB is not partially molten, we suggest that the presence of Eurasian material in the exhumed remnants of the North Himalayan middle crust (high-grade core of the YD) can be explained by localised thrust dynamics, without the need to invoke complex processes such as channel flow.



Identifying ancient lunar impactor populations using high precision siderophile element determinations: A new look at early Moon-Earth Connections

Vickie C. Bennett¹, Marc D. Norman¹

¹Research School of Earth Sciences, Australian National University, Canberra, ACT 0200, Australia

The most prominent features on the Moon's surface, visible even by eye from the Earth, are the impact craters. Many of these craters, including the largest basins were formed between 3.8 and 3.9 Ga, and may represent an episode of intense meteorite bombardment referred to as the "lunar cataclysm". A record of the materials that hit the Moon, and almost certainly the Earth, during this catastrophic period is preserved in lunar impact breccias; samples of which were collected during the Apollo missions.



During 2005, as part of our on-going program aimed at linking siderophile and lithophile element chemistry of lunar breccias with their chronology to explore the impact history of the Moon, we determined precise Re, Ir, Ru, Pt and Pd concentrations, and lithophile trace element abundances for a suite of Apollo 16 impact melt breccias. The Apollo 16 samples, allocated to us by NASA for this study, were collected from the edge of Nectaris, the oldest nearside lunar basin. Our approach is based on recent work demonstrating that different types of potential impactors have subtly different compositions of the highly siderophile elements. Thus through high precision siderophile element concentration measurements of suites of Lunar impact breccias we can potentially determine both the type and diversity of impactors at a given site.

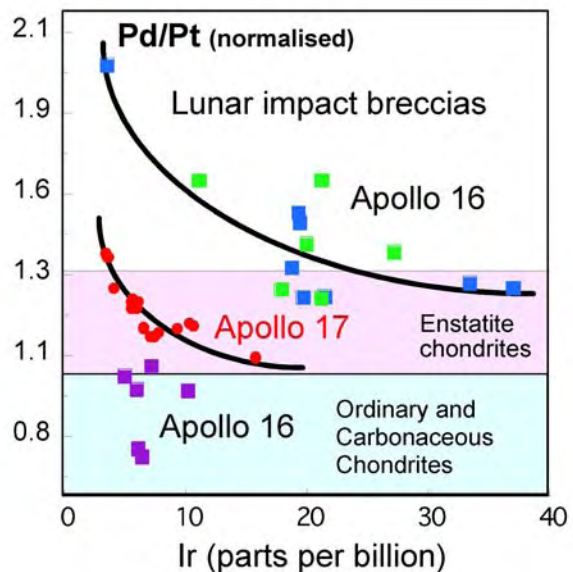


Figure 1. Top, lunar impact crater. Bottom, iridium, palladium and platinum data for Apollo 16 and 17 lunar impact breccias showing affinities to different types of potential impactors.

potentially determine both the type and diversity of impactors at a given site.

The analytical work is accomplished in a purpose built, metal-free, clean lab using novel sample digestion and chemical extraction protocols with the PGE lab at RSES being one of only a few places in the world capable of these measurements.

The comparison of our data from Apollo 16 samples with a primitive meteorite reference composition (CI-chondrite- Orgueil) demonstrates two fundamentally different types of signatures. One group has "W-shaped" CI-normalized patterns with enrichments of Ir, Ru and Pd, relative to Ir and Pt, whereas a second group has flat CI-normalized patterns, with Re/Ir and Pd/Pt characteristics more like ordinary or carbonaceous chondrites. These data demonstrate that at least two different events involving two different types of meteorite impactors can be identified from the PGE-Re patterns of these Apollo 16 breccias. The identification of distinctive enstatite chondrite-like signatures at both the Apollo 16 and 17 sites suggests that these were common types of impactors in the 3.9 Ga bombardment of the Moon. Thus, enstatite chondrites may have had a role in establishing the highly siderophile element characteristics of the Earth's mantle.

In addition to revealing early lunar history, determining the number, timing and compositional diversity of materials that struck the Moon provides a mechanism for testing models of solar system dynamics. For example, the various types of potential impactors originated in spatially distinct regions of the solar nebula e.g. inner versus outer solar system, such that establishing their presence or absence in the cratering record on the Moon provides information on the parent body trajectories.

Somewhat ironically, establishing the early impact history for the Moon may provide a clearer image of early Earth processes, particularly on the much speculated role of impacts in hindering or fostering early life and tectonic cycles. The Earth and Moon likely experienced related early impact histories, but owing to continuous terrestrial tectonic activity with only limited preservation of >3.7 Ga rocks, this record has been largely obliterated. The Moon, tectonically static by comparison, retains a much more extensive image of this mutual early history.

Australia's ancient oceans: toxic and purple

Jochen J. Brocks

¹ *Research School of Earth Sciences, Australian National University, Canberra, ACT 0200, Australia*

1.64 billion years ago, the ancient seas in Australia's north were toxic seas of sulfide. The marine waters harbored phototrophic green and purple sulfur bacteria (Chlorobiaceae and Chromatiaceae, respectively), but were hostile to eukaryotic algae. It was an ecosystem unlike anything we know of in the Earth's history, according to new investigations of the Earth Chemistry Group in the Research School of Earth Sciences at ANU.



The oldest known liquid petroleum in the world seeping out of dolomitic mudstone of the 1.64 Ga Barney Creek Formation, McArthur Group, Northern Territory. The oil contains molecular fossils (biomarkers) of green and purple sulfur bacteria.

Today, Earth's oceans are teeming with life, and even deep marine trenches contain enough oxygen to support complex organisms.

However, oceans in Earth's distant past were fundamentally different. In the first half of Earth history, ~4.5 to 1.8 billion years ago, the world's oceans were almost entirely devoid of oxygen. Surprisingly, for the following one billion years, the state of the oceans remains rather mysterious. Scientists debate whether at this time the deep oceans became more oxygenated, in parallel with the Earth's atmosphere, or whether they remained oxygen-starved and additionally accumulated toxic hydrogen sulfide.

In a recent paper published in *Nature*, Dr Jochen Brocks from the Research School of Earth Sciences, found the molecular remains of lipids in the world's best preserved rocks of the time, the Barney Creek Formation in the McArthur Basin, northern Australia. The 1.64 billion year old dolomitic mudstones that formed at the bottom of a deep marine trench near the present Gulf of Carpentaria contain an oil preserving the molecular fossils (biomarkers) of green and purple colored carotenoid pigments that were used by bacteria to conduct photosynthesis. Purple and green sulfur bacteria require reduced sulfur species and light to live. They provide the first evidence independent of isotopic findings that the waters remained oxygen-starved and sulfidic from the bottom of the water column to probably less than 20 meters below the water surface. Fossil

lipids of more complex eukaryotic organisms, the ancestors of algae, plants, animals and fungi, were conspicuously scarce in the samples, possibly because these organisms were asphyxiated by toxic hydrogen sulfide or lacked essential trace elements precipitated under sulfidic conditions.

Sulfidic oceans throughout Earth's middle age may thus explain why the world was ruled by bacteria for such a long time. When the oxygen-free and toxic waters finally retreated about 800 million years ago, complex and multicellular eukaryotes finally conquered the world's open oceans. Their development culminated in the Cambrian Explosion 542 million years ago, the sudden appearance of most groups of animals in the fossil record as we know them today.

Brocks J. J., Love G. D., Summons R. E., Knoll A. H., Logan G. A., and Bowden S. A. (2005) Biomarker evidence for green and purple sulphur bacteria in a stratified Paleoproterozoic sea. *Nature* **437**, 866-870.

The Origin of Shoshonites: New insights from the Tertiary High-Potassium Intrusions of Eastern Tibet

Ian H. Campbell¹, Hua-Ying Liang^{1,2}, Charlotte M. Allen¹, Yu-Qiang Zhang², Ying-Wen Xie², Cong-Qiang Liu³, Heng-Xiang Yu⁴

¹*Research School of Earth Sciences, Australian National University, Canberra, ACT 0200, Australia*

²*Laboratory of Marginal Sea Geology, Guangzhou Institute of Geochemistry & South China Sea Institute of Oceanology, Chinese Academy of Sciences, Guangzhou 510640, China*

³*Institute of Geochemistry, Chinese Academy of Sciences, Guizhou 55002, China*

⁴*Guilin Institute of Technology, Guilin 541004*

The shoshonitic intrusions of eastern Tibet, which range in age from 33 to 41 Ma and in composition from ultramafic ($\text{SiO}_2 = 42\%$) to felsic ($\text{SiO}_2 = 76\%$), were produced during the collision of India with Eurasia. The mafic and ultramafic members of the suite are characterized by phenocrysts of phlogopite, olivine and clinopyroxene, low SiO_2 , high MgO and Mg/Fe ratios, and olivine forsterite contents of Fo_{87} to Fo_{93} , indicative of equilibrium with mantle olivine and orthopyroxene. Direct melting of the mantle, on the other hand, cannot have produced the felsic members. They have a phenocryst assemblage of plagioclase, amphibole and quartz, high SiO_2 , and low MgO and Mg/Fe ratios well below the values expected for a melt in equilibrium with mantle olivine and orthopyroxene. Furthermore, lack of variation of Cr with SiO_2 and MgO in the mafic and ultramafic rocks precludes the possibility that they were derived by fractional crystallization from the more mafic members (Fig. 1). Yet all members of the suite share similar incompatible element and radiogenic isotope ratios, which suggests a common origin and source (Figs. 2, 3 & 4). We suggest that melting for all members of the shoshonite suite was initiated in continental crust that was thrust into the upper mantle at various points along the trans-pressional Red River-Ailao Shan-Batang-Litang fault system. The melt produced was quartz-saturated and reacted with the overlying mantle to produce garnet and pyroxene during its ascent. The felsic shoshonites reacted little with the adjacent mantle and preserved the essential features of their original chemistry, including their high SiO_2 , low Ni, Cr and MgO contents, and low Mg/Fe ratio, whereas the mafic and ultramafic magmas reacted extensively. Although they preserved the incompatible element and radiogenic isotope ratios of their crustal source, their MgO, Ni, Cr, SiO_2 contents and Mg/Fe ratio were buffered by olivine and orthopyroxene. As a consequence, their MgO, Ni, Cr, SiO_2 concentrations and Mg/Fe ratios were extensively modified to values dictated by equilibrium with mantle olivine and orthopyroxene. Fig. 5 shows trace element modelling of the eastern Tibet shoshonites. The better known shoshonitic rocks of central and western Tibet have been attributed to small degrees of partial melting of remnant lithospheric mantle that had been enriched previous to melt generation between 1 and 20 Ma. Our data indicate that the tectonics of shoshonite

generation could be very different than that previously interpreted at least for the case of the Red River-Ailao Shan-Batang-Litang fault system.

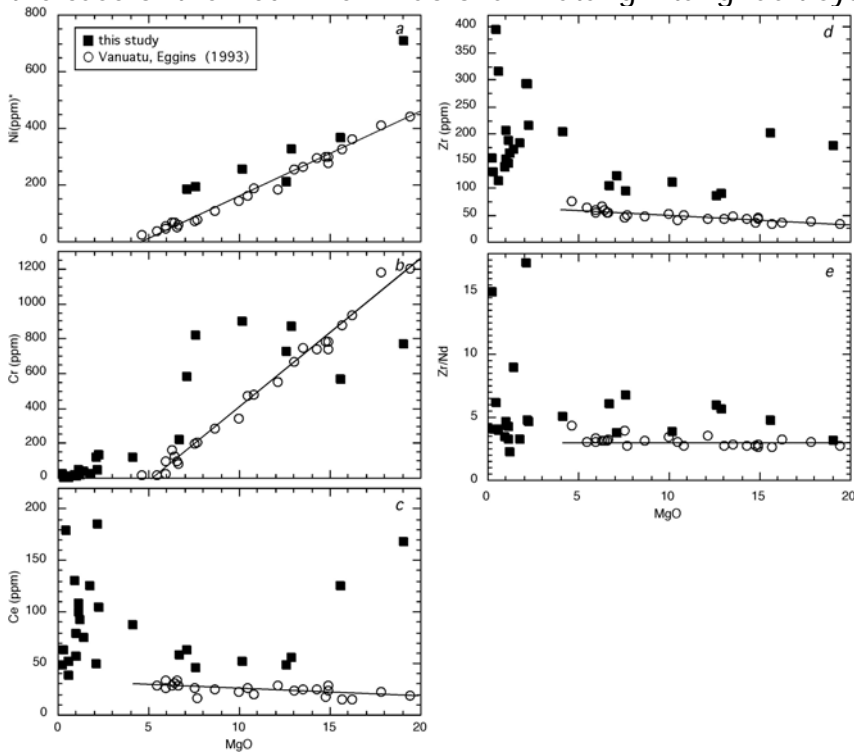


Figure 1: Variations in trace elements (ICP-MS) against MgO (XRF) for samples from eastern Tibet and Vanuatu (Eggins, 1993). Data from the Vanuatu oceanic arc are plotted with open symbols and are shown for comparative purposes. *Data for Ni from XRF.

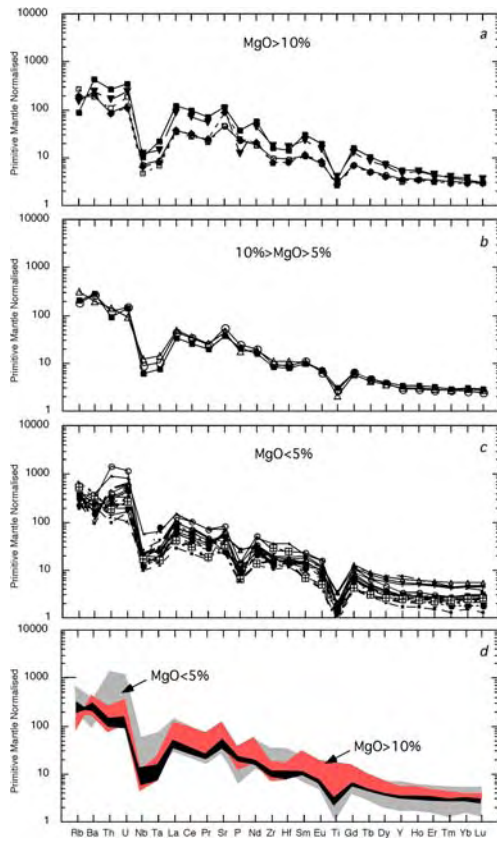


Figure 2: Primitive mantle-normalized trace element patterns for representative igneous rocks from the western Yunnan and eastern Tibet. The normalizing values used are those of Sun and McDonough (1989). The similarity among the compositional groups is demonstrated by the overlapping fields in (d).

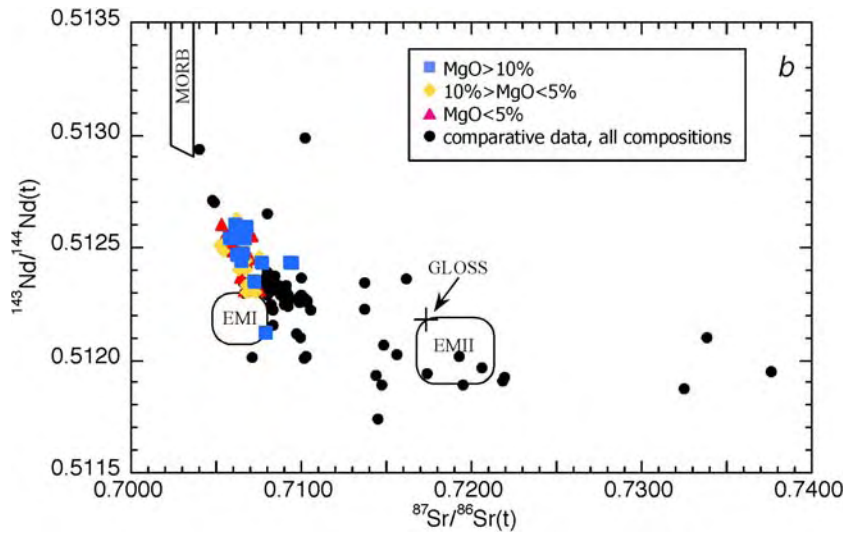


Figure 3: Plot for igneous rocks from west Yunnan and east Tibet. The fields for MORB, EMI, EMII and GLOSS (global average subducted sediment, Plank and

Langmuir, 1998) are shown for comparative purposes. Data sources: Xu et al. (2001); Wang et al. (2001) Zhu et al. (1992) and Zhang et al. (1997). Comparative data are for younger shoshonites from central and western Tibet taken from Arnaud et al. (1992), Turner et al. (1996), Miller et al. (1999), and Williams et al. (2004).

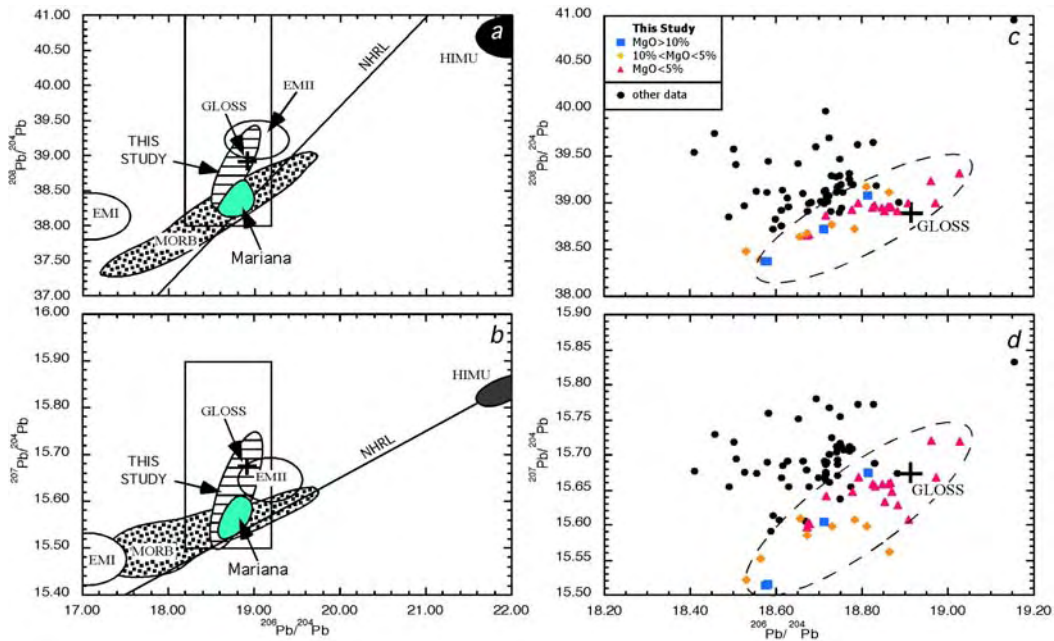


Figure 4: Lead isotope plots for igneous rocks from west Yunnan and east Tibet. The fields for MORB, EMI, EMII, HIMU, GLOSS, Mariana ocean arc basalts and the northern hemisphere reference line (NHRL) are shown for comparative purposes. Horizontally ruled ellipse in (a) and (b) corresponds to dashed on in (c) and (d). Mariana data compiled by Jon Woodhead. Other data source as for Fig. 3.

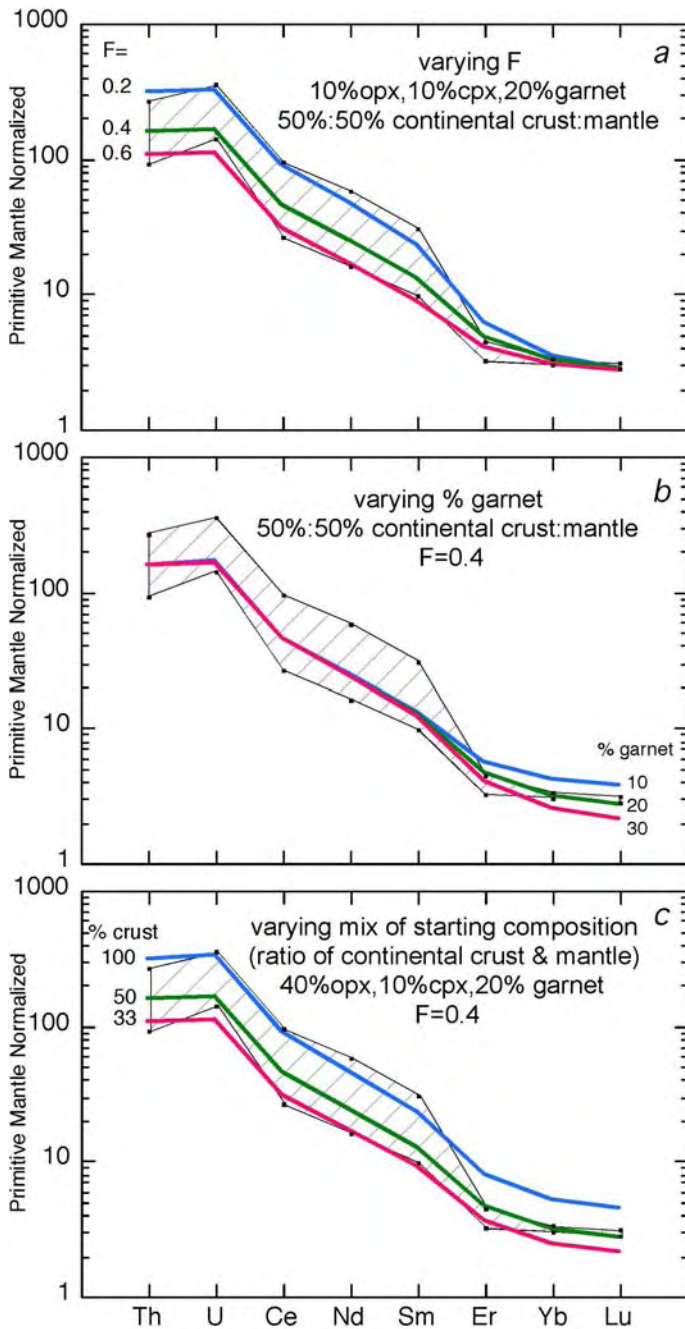


Figure 5: Incompatible trace element models of batch melting of average continental crust and continental crust-mantle mixtures. (a) The influence of varying the melt fraction F at constant mineralogy (10% orthopyroxene, 10% clinopyroxene and 20% garnet) and at a constant continental crust-mantle mass ratio. (b) The affect of varying the amount of garnet in the residue at constant F and crust-mantle ratio. (c) The effect of varying the continental crust to mantle ratio (as a proxy for the extent of melt-mantle reaction) at constant F and residual mineralogy. Partition coefficients from Salters et al. (2002) and average continental crust composition from McLennan (2001)

- Arnaud N.O., Vidal, Ph., Tapponnier, P., Matte, Ph., and Deng, W.M. (1992) The High K₂O volcanism of northwestern Tibet: geochemistry and tectonic implications. *Earth and Planetary Science Letters*, **111**, 351-367.
- Eggins, S.M. (1993) Origin and differentiation of picritic arc magmas, Ambae (Aoba), Vanuatu. *Contributions to Mineralogy and Petrology* **114**, 79-100.
- McLennan, S.M. (2001) Relationships between the trace element composition of sedimentary rocks and upper continental crust. *Geochemistry Geophysics Geosystems* **2**, 2000GC000109.
- Miller, C., Schuster, R., Klötzli, U, Frank, W., and Purtscheller, F. (1999) Post-collisional potassic and ultrapotassic magmatism in SW Tibet: geochemical and Sr-Nd-Pb-O isotopic constraints for mantle source characteristics and petrogenesis. *Journal of Petrology* **40**, 1399-1424.
- Salters, V.J.M., Longhi, J.E., and Bizimis, N (2002) Near mantle solidus trace element partitioning at pressures up to 3.4 GPa. *Geochemistry Geophysics Geosystems* **3**, 2001GC000148.
- Sun, S-s and McDonough, W.F. (1993) Chemical and isotopic systematics of oceanic basalts; implications for mantle composition and processes. In: Saunders A.D., Norry, M.J. (eds) *Magmatism in the ocean basins. Geological Society of London Special Publication* **42**, 315-345.
- Turner, S. Arnaud, N, Liu, J., Rogers, N, Hawkesworth, C, Harris, N., Kelley, S., van Calsteren, P, and Deng, W. (1996) Post-collision, shoshonitic volcanism on the Tibetan plateau; implications for convective thinning of the lithosphere and the source of ocean island basalts. *Journal of Petrology* **37**, 45-71.
- Wang, J.H., Yin, A., Harrison, T.M., Grove, M., Zhang, Y.Q., Xie, G.H. (2001) A tectonic model for Cenozoic igneous activities in the eastern Indo-Asian collision Zone. *Earth and Planetary Science Letters* **188**, 123-133.
- Williams, H.M., Turner, S.P., Pearce, J.A., Kelley, S.P., and Harris, N.B.W. (2004) Nature of the source regions for post-collisional, potassic magmatism in southern and northern Tibet from geochemical variations and inverse trace element modelling. *Journal of Petrology* **45**, 555-607.
- Xu, Y.G., Menzies, M.A, Thirlsall, M.F., and Xie, G.H., 2001, Exotic lithosphere mantle beneath the western Yangtze craton: Petrogenetic links to Tibet using highly magnesian ultrapotassic rocks. *Geology* **29**, 863-866
- Zhang, Y.Q., Xie, Y.W., 1997, Age and Nd, Sr isotopic characteristics of alkali intrusions along the Ailao Shan-Jin Sha River, China, *Science in China (Series D)*, v.27, p. 289-293.
- Zhu, B-Q, Zhang, Y-Q, Xie Y-W, 1992, Nd, Sr and Pb isotopic characteristics of Cenozoic ultrapotassic volcanic rocks from eastern Erhai, Yunnan and their implications for subcontinent-mantle evolution in southwestern China, *Cosmochemica Geochemica Acta*, (3): 201-212

The thermal and structural evolution of the Kumaun Lesser Himalaya, north west India.

Julien C  lerier¹

¹ *Research School of Earth Sciences, Australian National University, Canberra, ACT 0200, Australia*

The Himalaya have been described as the 'world's best natural laboratory in which to study processes associated with large-scale continent-continent collision' and as such play a key role in our understanding of both modern and ancient collisional orogens. It is, therefore, somewhat surprising that quantitative descriptions of the conditions of metamorphism, patterns of deformation and exhumation in the Himalaya are currently largely restricted to a narrow strip of amphibolite grade rocks known as the Greater Himalayan Crystallines (GHC). The GHC, though coinciding with the regions of highest relief and what we instinctively think of as the Himalayan mountains, actually only account for <20% of the exposure. Owing to perceived and real problems related to understanding the petrogenesis of rocks of low metamorphic grade, quantitative constraints concerning the evolution of the other 80% of the rock volume are lacking. In the last year of research I have been able to integrate metamorphic and thermochronological data with structural geology to begin documenting and deciphering the complex internal deformation of the Lesser Himalaya of Kumaun, India (Figure 1).



Figure 1. Digital Elevation Model of the western Himalaya, Tibetan plateau and Tarim basin, showing the position of the Kumaun Himalaya within the orogenic system.

The Lesser Himalayan Series (LHS) is composed of Proterozoic to Palaeozoic metasedimentary rocks of Indian continental affinity which have been accreted to the mountain range since the early Miocene and define one of four principal tectonometamorphic units of the Himalayan mountains (Heim & Gansser, 1939). The sequence is bounded to the north by the Main Central Thrust (MCT), a major crustal thickening structure believed to have been episodically active at ~20 Ma and ~4Ma (Harrison et al., 1997), placing the GHC over the LHS, whilst to the south, the Main Boundary Thrust places the LHS over the Tertiary foreland basin. Several erosional remnants of the crystalline thrust sheet which covered LHS are preserved as klippen within the Lesser Himalaya.

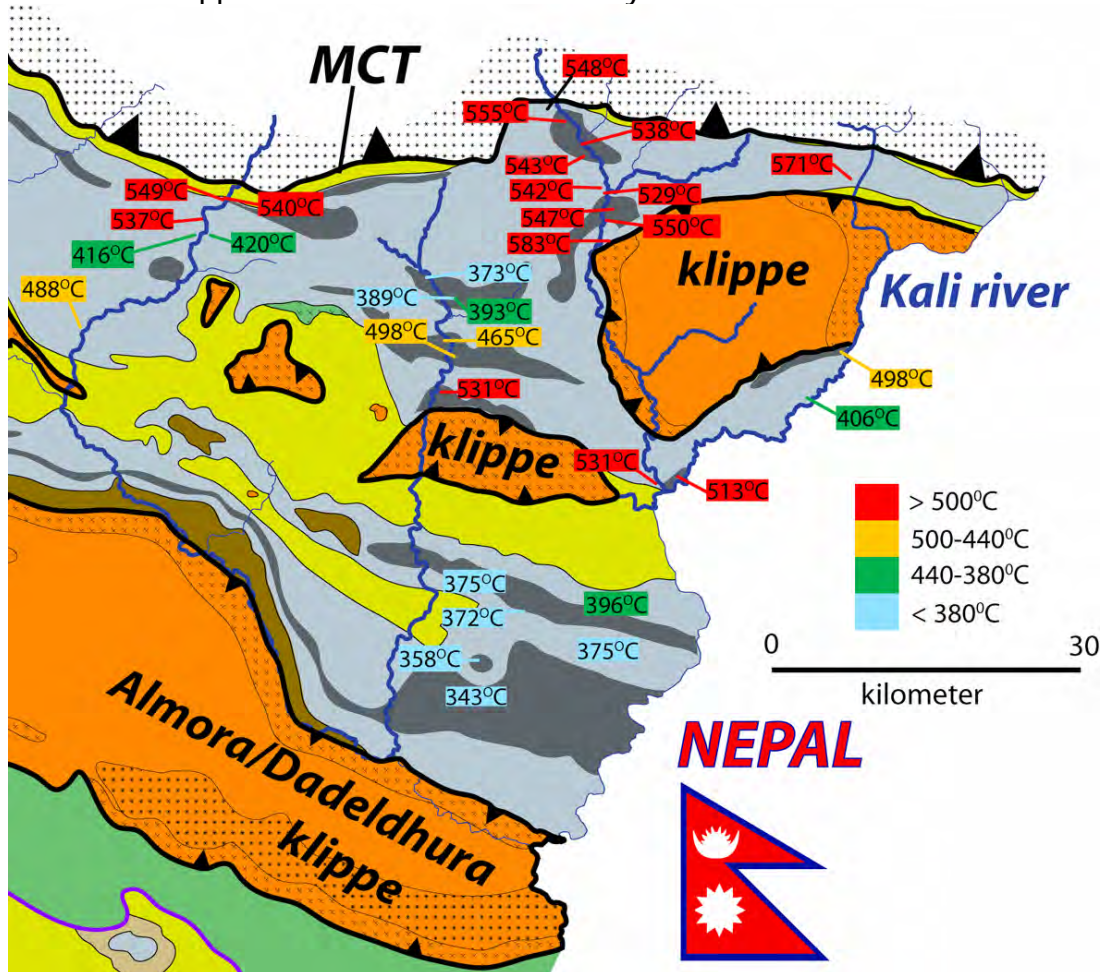


Figure 2. Portion of a geological map of the eastern Kumaun Lesser Himalaya. Peak metamorphic temperatures, as measured by Raman Spectroscopy of Organic Material are shown in coloured boxes scaled to temperature.

Raman Spectroscopy of Organic Material (Beyssac et al., 2002) has been used to constrain the conditions of metamorphism within the metasedimentary pile. Samples of graphitic schist and slate collected along 5 parallel transects reveal that adjacent to the MCT, peak metamorphic temperatures are in the vicinity of 550°C. Down structural section from the MCT (south), thermal gradients are

relatively steep, in the range of 30°C - 50°C/km. Beyond <25km south of the MCT, towards the contact with the foreland basin, metamorphic temperatures fall below the range of the technique (<330°C). My work has also shown that the overriding crystalline thrust sheets of the GHC strongly influence the thermal structure of the underlying Lesser Himalayan metasedimentary pile. This relationship is demonstrated in Figure 2 where LHS samples from beneath several klippen show increasing peak metamorphic temperatures with increasing proximity to the contact with the overlying crystalline rocks.

$^{40}\text{Ar}/^{39}\text{Ar}$ geochronology of white micas, separated from Lesser Himalayan quartzites, is contributing to a growing geochronological framework for the LHS. Results reveal a range of ages from Pliocene to Early Miocene. These cooling ages, the first of their kind from the Lesser Himalaya, define a trend of younger ages upsection, i.e. towards the MCT, with the youngest age of 4.3 Ma coming from an MCT footwall quartzite directly adjacent to the thrust contact. Samples within <15km south of the MCT are characterized by cooling ages less than 10 Ma, whilst ages range between 10 and 26 Ma beyond <15km south (downsection) of the MCT. Many of the ages obtained fit chronological frameworks proposing episodic, out of sequence, movement along the MCT (Harrison et al., 1997), yet there are also several ages which fall outside the Miocene and Pliocene MCT motion paradigm. These ages, and the continuum which they define, are particularly interesting as they suggest that exhumation of the Lesser Himalayan metasedimentary pile has been continuous since the Miocene and independent of motion on the MCT.

Integrating these thermal data sets with microstructural analysis of quartz dislocation creep regimes has enabled the quantification of transitions in deformation styles (brittle to ductile) within Kumaun Lesser Himalaya. The observed deformation and thermal structure can be represented in cross-sections composed of four thrust sheets comprising a duplex which evolves from brittle deformation, close to the MBT, towards ductile with increasing proximity to the MCT. These cross-sections are a significant departure from currently published reconstructions which represent deformation in the Lesser Himalaya as a solely brittle process.

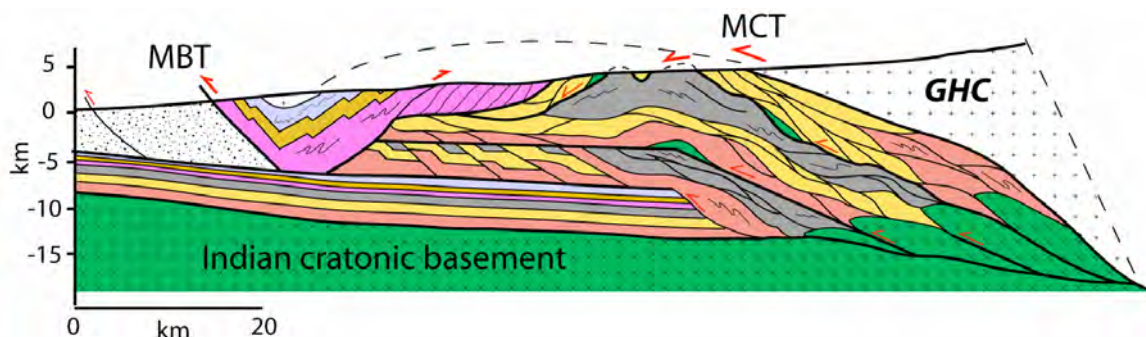


Figure 3. Cross section through the western Kumaun Lesser Himalaya.

References

Beyssac, O., Goffe, B., Chopin, C., and Rouzaud, J.N. Raman spectra of carbonaceous material in metasediments: a new geothermometer, *Journal of Metamorphic Geology*, 20 (2002) 859–871.

Harrison, T. M., Ryerson, F. J., Le Fort, P., Yin, A., Lovera, O. M., E.J. Catlos, 1997, A Late Miocene-Pliocene origin for the Central Himalayan inverted metamorphism. *Earth and Planetary Science Letters* 146, E1-E8.

Heim, A. and Gansser, A., 1939, Central Himalaya geological observations of Swiss expedition, 1936, 246 p.

Second-order instrumental effects in zircon Pb/U age determinations using SHRIMP

William Compston¹

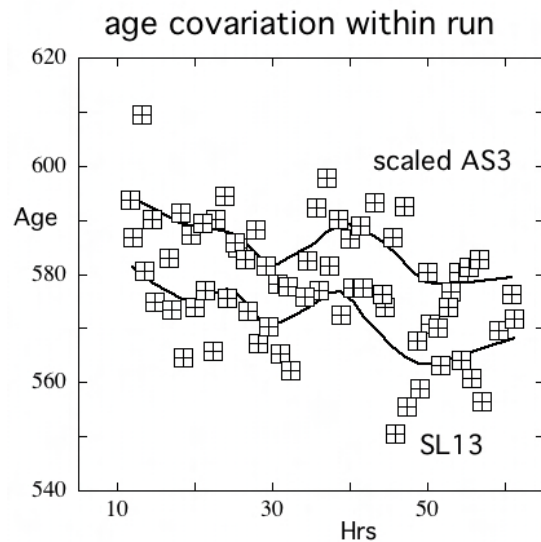
¹ Research School of Earth Sciences, Australian National University, Canberra, ACT 0200, Australia

Although the SHRIMP ion microprobe has been used for the dating of zircon for the past twenty-five years, new small instrumental effects continue to be discovered as we endeavor to make the age determinations more precise. Precision is especially important for definition of the geological time scale, for which the elemental ratio $^{206}\text{Pb}/^{238}\text{U}$ must be measured. This is done by dividing $^{206}\text{Pb}^+ / ^{238}\text{U}^+$ ion ratios from the sample zircons by those from a known standard zircon, which gives the sample ages relative to that of the standard.

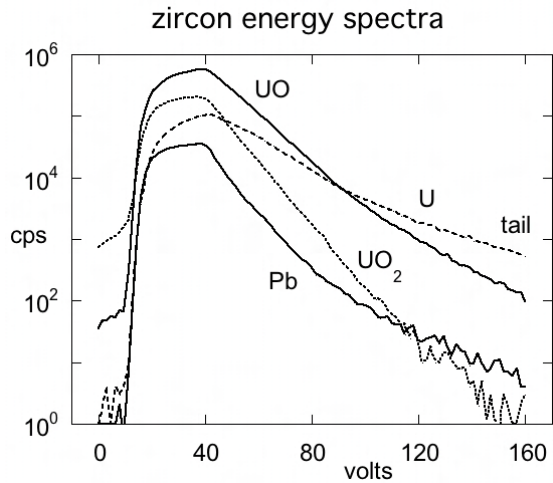
Previously, the sample ages so derived during an analytical session were placed in a table for statistical and geochemical testing. Only rarely were they plotted against their times of analysis because no such correlation was expected, which proved to be a mistake. Instead, several analytical sessions showed irregular but definite variations when the time plot was applied, which can account for most of the residual variance in age per session. In addition, the time variation can be quantified by fitting a localized weighted least squares curve (the 'lowess' curve), and importantly, the

lowess curves are *strongly correlated* between the sample and standard ages (Compston & Clement, 2006). Such correlations had been obscured in the past by scatter in age due to counting statistics. Earlier data can now be corrected and previous SHRIMP points for the geological time-scale sharpened.

Two new observations clarify the origin of the above instrumental effect. The first is the explanation of why $^{206}\text{Pb}^+ / ^{238}\text{U}^+$ ion ratios correlate with $^{238}\text{UO}^+ / ^{238}\text{U}^+$ ion ratios. The latter has been known since the earliest studies of the sputtering of zircon and remains an essential part of routine data-reduction for $^{206}\text{Pb}/^{238}\text{U}$ ages. However the physical reasons for the occurrence of $^{206}\text{Pb}^+ / ^{238}\text{U}^+$ changes and their particular correlation slope with $^{238}\text{UO}^+ / ^{238}\text{U}^+$ remained a mystery until recently. The first clue came from the digitized energy spectra for sputtered secondary ions from zircon. The measured ion current for each ion species is that part of its energy spectrum that fits within the energy slit set at 10.0 mm



(ca. 100eV). Truncation of the beam by the energy slit can be simulated by progressively deleting successive ion counts from the low- or high-energy edge. The beam intensities are reduced and the ion ratios are changed because of the different shapes of the spectra for different ion species. Truncation at the low-energy edge, *i.e.* loss of low-energy ions, gives correlated changes in $^{206}\text{Pb}^+ / ^{238}\text{U}^+$ and $^{238}\text{UO}^+ / ^{238}\text{U}^+$ that have a slope of 2.0, exactly as found during measurement operation, while truncation of high-energy ions gives a much flatter slope. Thus, the observed slope is explicable by selective loss of low energy ions and the problem is to find where and why this is happening.



The second clue is isotopic fractionation traced to the source-slit during measurement of the light isotopes by I.S. Williams, P. Holden and J.J. Foster, combined with the long-known fact that the UO^+ and Pb^+ beam beams require slightly different steering for maximum transmission through the source-slit. Williams *et al.* showed that the Earth's magnetic field causes sufficient mass dispersion along the ion path between the analyzed spot and the source-slit to partially separate the oxygen isotopes. Consequently, when the UO^+ secondary beam is centered through the source slit, the Earth's field will steer the Pb^+ ions, which are 23% lighter, slightly off-centre. The lowest energy Pb^+ ions will be the more deflected and hence the more truncated at the source-slit edge.

Compston, W. and Clement, SWJ (*in press*) The geological ion probe: the first twenty-five years of dating zircon. *SIMS XV Elsevier Press*

Contrasting depositional age inferences for the Au-bearing Mount Charles Formation, Tanami Region Australia

Andrew Cross

¹ *Research School of Earth Sciences, Australian National University, Canberra, ACT 0200, Australia*

The Tanami Region is currently Australia's pre-eminent Palaeoproterozoic Au-province. Located approximately 600 km northwest of Alice Springs and overlapping both the Northern Territory and Western Australia, the region in recent years has seen a continued effort by the Northern Territory Geological Survey, Geoscience Australia and the Research School of Earth Sciences to further understand its geological history. A part of this work has been to establish the timing of sedimentation for the various sedimentary units. Only two sedimentary units in the Tanami region contain significant Au, the Tanami Group and the Mount Charles Formation. No dateable interlayered felsic volcanics have yet been identified in the Mount Charles Formation, which has meant that the timing of sedimentation for this unit has been interpreted from structural observations. This age contrasts markedly with the ages of detrital zircons from this unit. The sedimentary sequence in the Tanami from base to top comprises of the Dead Bullock Formation (siltstone and sandstone with lesser iron formation), the Killi Killi Formation (turbidite) of the Tanami Group, the Ware Group (coarse sandstone with interlayered volcanic rocks), the Mount Charles Formation (turbiditic siliciclastics and basalt), the Pargee Sandstone (sandstone and conglomerate), and Gardiner Sandstone (marine to fluvial sandstone and conglomerate) of the Birrindudu Group. Based on structural grounds, the Mount Charles Formation is thought to post date the Tanami and Ware Groups and to have been deposited at ~1800 Ma (Crispe and Vandenburg, in press). SHRIMP U–Pb detrital zircon ages from three samples of the Mount Charles Formation contrast markedly with samples from the Killi Killi Formation, Ware group, Pargee Sandstone and Gardiner Sandstone. These units contain zircon populations that are dominated by ~1.87 Ga detritus. By comparison, Mount Charles Formation sediments are dominated by Archaean aged zircon, which is also the major detrital component in the basal Ferdies Member of the Dead Bullock Formation. The youngest zircon component in all Mount Charles samples are euhedral grains and grain fragments that have a crystallisation age of ~1.91 Ga. These zircon may have been derived from contemporaneous igneous activity and therefore may approximate the timing of sediment deposition. If this is the case, the Au-bearing Mount Charles Formation may be ~100 million years older than current estimates. In an attempt to determine the depositional age of the Mount Charles Formation, future SHRIMP work will be undertaken on recently collected tuffaceous rocks and also sandstones where diagenetic xenotime will be targeted for U–Pb SHRIMP analysis.

Crispe, AJ and Vandenburg L. (in press) Geology of the Tanami Region, Northern Territory. *Northern Territory Geological Survey Bulletin*.

Solubility of Oxygen in Sulphide melts as a function of fO_2 , at 1 bar and 1200°C

Fonseca, R., Campbell I.H. and O'Neill, H.Stc.

¹ *Research School of Earth Sciences, Australian National University, Canberra, ACT 0200, Australia*

It is known that oxygen dissolves into sulphide melts as oxygen fugacity approaches QFM. The extent of that dissolution and the nature of the Oxygen species in the sulphide melt are not well known. The aim of this work was to: (1) Measure oxygen concentrations in sulphide melts at different fO_2 ; (2) Investigate the nature of oxygen bearing phase in the quench; (3) Discuss possible oxygen species in the sulphide melt.

Experiments were conducted in a vertical muffle furnace, equipped with gas mixture, at 1200°C for 96 hours. Five experiments were run between 10^{-15} atm and 10^{-11} fO_2 . Pure silica crucibles containing 1 gram of troilite powder were used. At the end of each experimental run, the sulphide was quenched in cold water. Quenching times were calculated to be about one second. Typical quenching textures consisted of sulphide crystals and another phase containing Fe, S and O, which occupies the interstitial spaces (Figure 1).

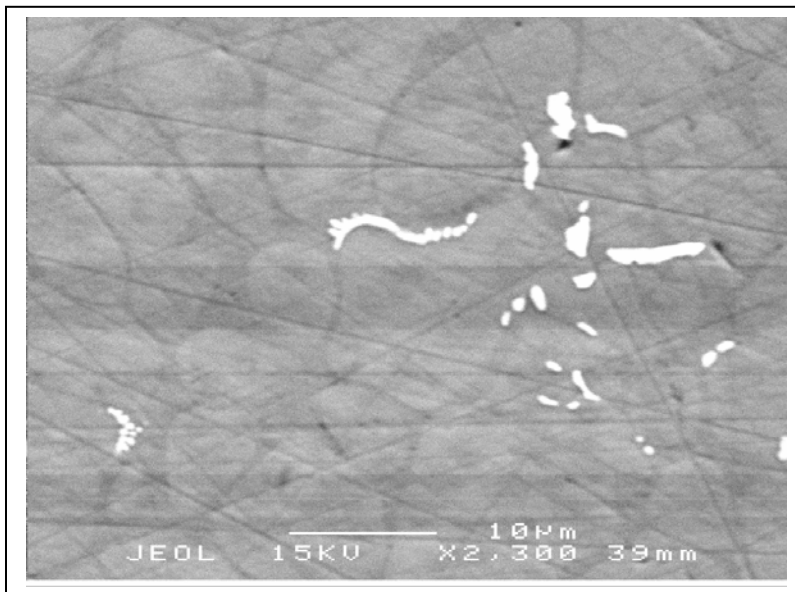


Figure 1: Typical quenching textures present in high fO_2 runs. The light gray phase consists of stoichiometric FeS and the dark grey phase is a glass containing Fe, S and O. In white are PtFe crystals.

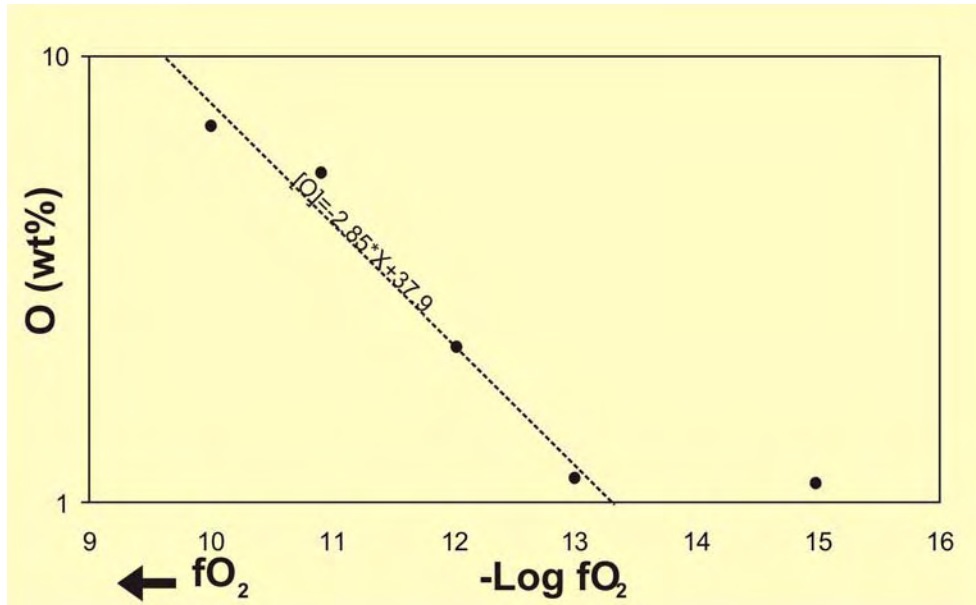


Figure 2: Oxygen concentrations in sulphide melt as a function of fO_2

Oxygen concentrations were analyzed independently by 3 methods: Electron Microprobe, SEM and image analysis. Oxygen in the sulphide melt was shown to increase with increasing fO_2 (Figure 2). Oxygen concentrations in the sulphide melt is as high as 7 wt% at 10^{-10} atm fO_2 . However, obtaining accurate measurements of O is hard given the analytical problems inherent in analyzing oxygen.

One of the major problems which needed explaining was the presence of the interstitial phase. No such Fe, S, O compounds are documented to occur in Nature so it is unlikely to be a crystalline mineral. The interstitial phase is present at fO_2 ranging from 10^{-12} to 10^{-10} atm. Identification of the oxygen bearing phase was done by both X-ray diffraction (XRD) and Transmission electron microscopy (TEM).

The XRD yielded 3 phases: Troilite, Cristobalite and, at a much lesser extent, wustite which do not explain the observed oxygen contents of the sulphide melt. The interstitial phase does not have Si so Cristobalite cannot be used to explain the presence of oxygen in the melt. Moreover the wustite peak is too small to explain the amounts of oxygen present. The failure of the XRD pattern to show peaks for the unknown phase suggest that the Fe-S-O phase may be an amorphous glass.

Confirmation of the existence of a glass phase was done by the use of the TEM. As with the XRD, the TEM identified the presence of Troilite, Cristobalite and Wustite, however it also identified the presence of a glass phase. This glass phase has an EDS spectrum with O, S and Fe. The x-ray diffraction patterns for this phase (Figure 3) demonstrate that it is an amorphous phase, however it also

shows minor reflections which indicate that there is some incipient nucleation of a crystalline phase occurring within the glass, which given the close association. The crystalline phase appears to be the result of a transition between glass and crystalline wustite.

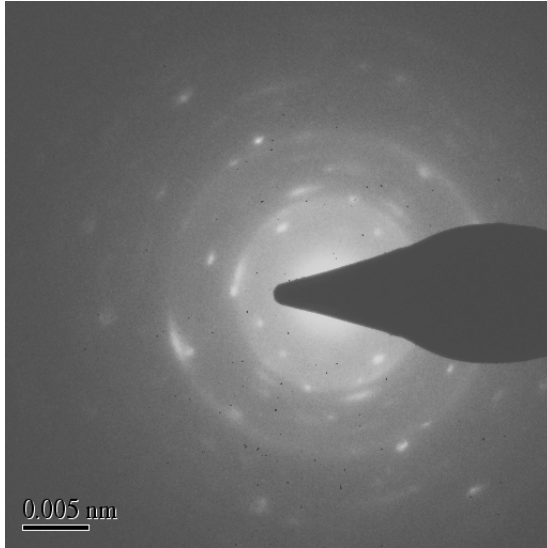


Figure 3: TEM diffraction pattern of the glass phase present in the sulphide quench. The presence of minor reflections indicates that there was some incipient nucleation of a crystalline phase within the glass phase.

The results present here may provide a mechanism that allows the existence of crystals of spinel within sulphide ore deposits such as the Merensky Reef of the Bushveld complex (South Africa) and the massive sulphide deposit of Kambalda (Western Australia), without having to resort to hydrothermal alteration.

Dating of Australian arid landforms using cosmogenic Ne/Be exposure dating

Toshiyuki Fujioka, John Chappell, Masahiko Honda, Igor Yatsesevich, Keith Fifield¹ and Derek Fabel²

¹ Research School of Physical Sciences and Engineering, ANU

² Department of Geographical and Earth Sciences, University of Glasgow, Scotland, UK

In principle, the history of aridity in Australia can be determined by dating the landforms and deposits that form under arid conditions. Over 75% of Australian continent is semi-arid to arid, and stony deserts are a major feature of these regions. Stony deserts are characterized by a surface monolayer of pebble- to cobble-sized rocks (gibbers), which, once formed, tend to remain in place with little subsequent modification. Some gibbers were formed *in situ* by breakdown of their underlying parent rock; others were fluvially transported to their present positions. We propose that the age of the stony deserts can be estimated by determining the time when gibbers were formed.

In this study, we measured cosmogenic nuclides, ²¹Ne and ¹⁰Be, in silcrete gibber samples collected from stony deserts in central Australia, to determine their exposure ages (Fujioka et al., 2005). The use of cosmogenic ²¹Ne, which is a stable cosmogenic nuclide, allows us to examine the history of gibber formation beyond the exposure dating range of ¹⁰Be, which is limited by radioactive decay to a few million years. We note that we have developed a reliable method for determining cosmogenic ²¹Ne in the presence of ²¹Ne from other sources.

Apparent exposure ages calculated from the concentrations of cosmogenic ²¹Ne and ¹⁰Be in the gibber samples from stony deserts west of Lake Eyre in northern South Australia ranged from two to five million years, but the apparent ²¹Ne ages are significantly greater than the apparent ¹⁰Be ages. The discordance indicates that the parent silcrete, from which the gibbers were derived, was buried at a shallow depth for a considerable period before being stripped and broken into gibbers. Calculations indicate that the silcrete was stripped and gibbers began to form around 4 m.y. ago, and that gibber-mantled tablelands were widely developed and dissected around 2-3 m.y. ago. These ages correspond to the time of late Cenozoic global cooling inferred from benthic oxygen isotope records in marine sediment cores (Figure).

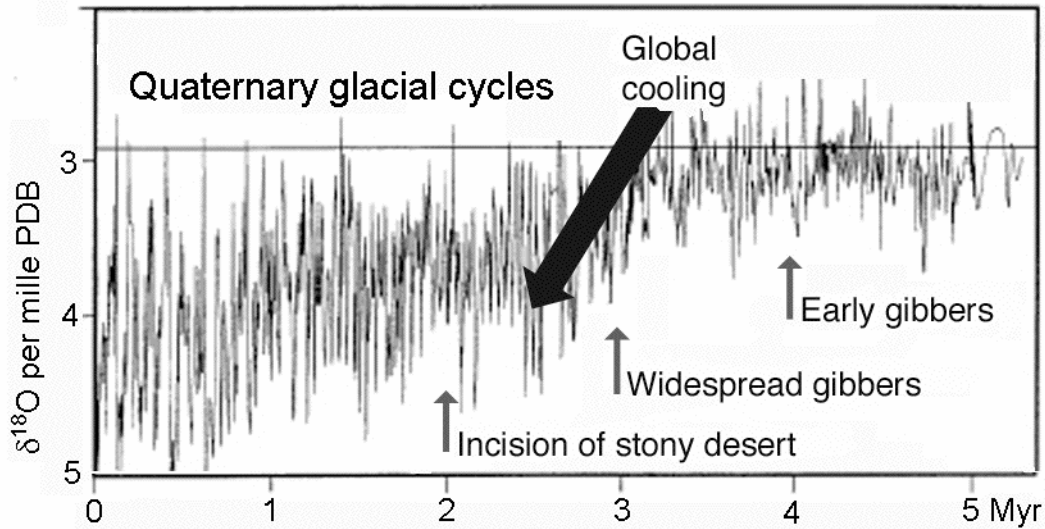


Figure. Relationship between the timing of the formation of gibber plains in Australia and benthic oxygen isotope record in marine sediment cores (east Atlantic Ocean Drilling Program Site 659; Tiedemann et al., 1994). Gibber ages (arrows) indicate that Australia's stony deserts formed during late Cenozoic global cooling as seen in marine sediments, that led to Quaternary glacial cycles. PDB: Peedee belemnite.

References:

- Fujioka T., Chappell J., Honda M., Yatsevich I, Fifield K., and Fabel D. (2005) Global cooling initiated stony deserts in central Australia 2-4 Ma, dated by cosmogenic ^{21}Ne - ^{10}Be . *Geology* **33**, 993-996.
- Tiedemann R., Sarnthein M., and Shackleton N. J. (1994) Astronomic timescale for the Pliocene Atlantic $\delta^{18}\text{O}$ and dust flux records of Ocean Drilling Program Site 659. *Paleoceanography* **9**, 619-638.

Young high-grade metamorphism: Linking U, Th-Pb ages to metamorphic conditions

Courtney J. Gregory¹

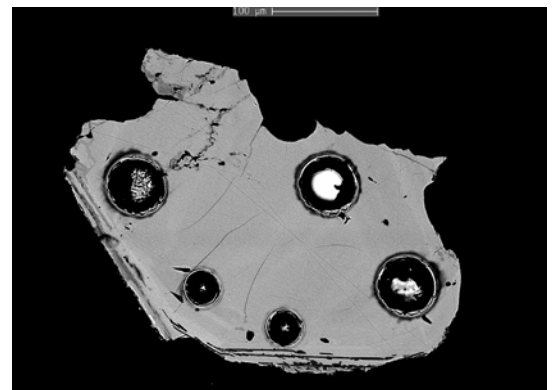
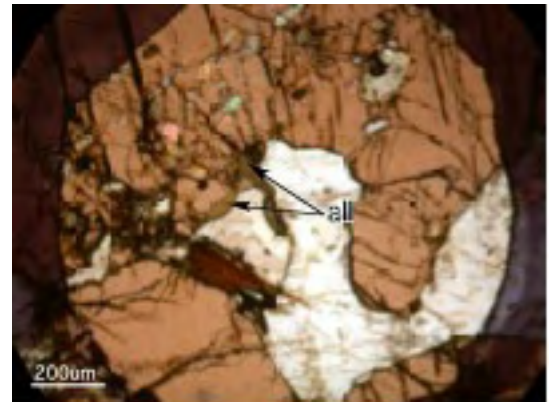
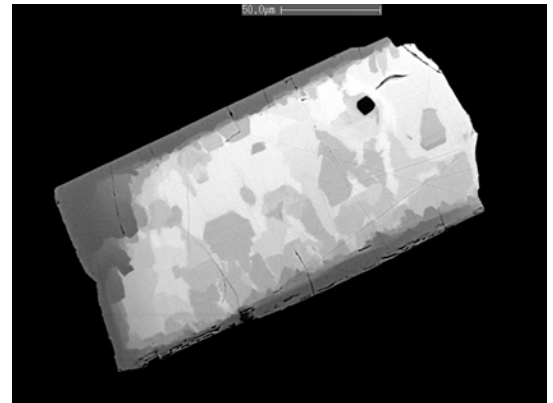
¹ Research School of Earth Sciences, Australian National University, Canberra, ACT 0200, Australia

Over the last decade evidence of short geological time spans for high-grade metamorphism has become apparent. The timing and especially the rates at which such processes occur provide first order constraints on the dynamics of the Earth's crust. Such information can be obtained by linking isotopic ages to metamorphic conditions. Recent studies of accessory minerals such as allanite have shown that they play a key role in the storage and mobility of geochemically important trace elements and thus can be effective recorders of metamorphic episodes.

Allanite is a LREE, Th (U)-rich trace mineral that occurs in a wide range of rock types. Of particular interest is its common presence in mafic and high-pressure rocks, which potentially provide important geochemical constraints for tectonic processes, but which have proved more difficult to date by well-established minerals such as zircon.

In situ U, Th-Pb isotopic analysis of magmatic and metamorphic allanite has been carried out at RSES. Established SHRIMP dating methods have been used in conjunction with the development of advanced dating techniques on the ArF excimer Laser Ablation quadrupole ICP-MS instrument. To date, isotopic results have shown that allanite can reliably date magmatic events with an accuracy of 1-5% (2σ).

Migmatitic and high-pressure metamorphic allanite from the Central European Alps were analysed as part of a case study on the temporal evolution of the polymetamorphic terrane. Preliminary results have proved successful, with meaningful and comparable Th-Pb ages obtained



Top: Back-scatter electron (BSE) image of a chemically zoned magmatic allanite. Middle: Textural relationship between garnet and metamorphic allanite, PPL. Bottom: BSE image of Laser Ablation ICPMS pits in a standard allanite sample used for isotopic dating.

Crystallization temperatures of Hadean zircons

T.M. Harrison and E.B. Watson¹

¹*Dept. of Earth and Environmental Sciences, Rensselaer Polytechnic Institute, Troy, NY 12180, USA*

We applied a new thermometer based on the concentration of Ti in zircon to Hadean detrital zircons from Jack Hills, Western Australia and obtained significant constraints on the nature of magmatism during the first 500 Ma of Earth history. Jack Hills zircons ranging from 4.0 to 4.35 Ga yield a peak in crystallization temperature at 680°C, suggesting that a limited range of mechanisms produced zircon-bearing rocks during that period. Together with results from other studies (e.g., $d^{18}\text{O}$, Lu-Hf, inclusion mineralogy), these data suggest that the following conditions may have obtained throughout the Hadean: 1) wet, minimum melting, 2) 700-800°C collisional-type melting, 3) formation of clay minerals under ambient conditions, 4) peraluminous melting of pelitic protoliths, 5) isotopic fractionations requiring a major Hadean continental crust forming event, 6) a continent-mantle recycling time constant varying from 200-50 m.y., 7) global heat flow 3 times higher than present, and 8) Mg-rich mantle lithospheres. We view constraints 1, 3 and 4 to imply the existence of liquid water at or near the Earth's surface, constraints 1, 2, 5 and 6 imply the existence of continental crust throughout the Hadean, and we speculate that constraints 1 and 4 reflect Hadean thrust burial. These three inferences are most easily explained by the existence of some form of collisional boundary interaction among surface plates, whether rigid or not. The plausibility of plate tectonic-like behaviour operating during the Hadean has recently been bolstered by ^{142}Nd studies that suggest the Earth's mantle may have experienced MORB-like depletion within a few 10's of millions of years of planetary accretion.

Evidence of continental crust by 4.5 Ga

T.M. Harrison, J. Blichert-Toft¹, W. Müller, F. Albarede¹, S.J. Mojzsis², and P. Holden

¹*CNRS UMR 5570, Ecole Normale Supérieure, 69364 Lyon Cedex 7, France*
²*Dept. of Geological Sciences, University of Colorado, Boulder, CO 80309, USA*

The paradigm for continent formation long favoured by isotope geochemists is that growth began at ~4 Ga and was ~80% of its present mass by 2.5 Ga. This view reflects the absence of a >4 Ga rock record and the systematic post-4 Ga evolution of depleted mantle $^{143}\text{Nd}/^{144}\text{Nd}$ and $^{176}\text{Hf}/^{177}\text{Hf}$. The observations of some early Nd and Hf isotopic heterogeneities leave open the possibility of earlier global fractionations and a minority view has persisted that continental crust was widespread in the early Hadean (the "Armstrong" model). In this regard, the relative lack of evidence of earlier depletions (from a magma ocean or continent formation) reflects remixing of these heterogeneities. Detrital zircons from Jack Hills, Australia, with 4.0-4.4 Ga U-Pb ages transcend this ambiguity as they represent pieces of crust that have been sequestered for up to ~4.4 Ga. Zircons have very low Lu/Hf and thus record near initial $^{176}\text{Hf}/^{177}\text{Hf}$ at the time given by the U-Pb age. Amelin et al. (1999) used Jack Hills zircons as old as 4.14 Ga to investigate early crustal evolution and inferred the existence of re-melted Hadean crust. We have carried out $^{176}\text{Hf}/^{177}\text{Hf}$ analyses by both solution and laser ablation MC-ICPMS on 104 Jack Hills zircons ranging in age from 3.96 to 4.35 Ga. These results indicate very large positive and negative $\epsilon_{\text{Hf}(T)}$ deviations from CHUR ($\lambda_{176} = 0.01867/\text{Ga}$; $^{176}\text{Hf}/^{177}\text{Hf} = 0.282772$; $^{176}\text{Lu}/^{177}\text{Hf} = 0.0332$). Negative values of $\epsilon_{\text{Hf}(T)}$ equivalent to $(^{176}\text{Hf}/^{177}\text{Hf})_{4.5 \text{ Ga}}$ observed between 4.35 and 4.2 Ga are consistent with development of a Lu/Hf = 0 reservoir by 4.5 Ga. Positive $\epsilon_{\text{Hf}(T)}$ deviations in the same age interval imply a depleted reservoir with Lu/Hf up to 0.1. We interpret these results as indicating either that significant continental crust had formed by ~4.5 Ga, consistent with recent inferences from $\Delta^{142}\text{Nd}$ systematics.

Crustal noble gases in Jwaneng diamonds with links to seismic tomography

Masahiko Honda, David Phillips¹, Jeff Harris² and Igor Yatsevich

¹ *School of Earth Sciences, The University of Melbourne, Melbourne, Victoria 3010*

² *Division of Earth Sciences, University of Glasgow, Glasgow, G12 8QQ, UK*

Recent seismic tomography studies of the Kaapvaal-Zimbabwe craton of southern Africa reveal distinct seismic velocity profiles at 150 km depth within the diamond stability field, that appear to correlate with differences in diamond paragenesis. Diamond mines with predominantly eclogitic diamond inclusions (e.g. Jwaneng, Orapa, Premier) overlie lithospheric mantle with relatively slow P-wave velocities, whereas localities with predominantly peridotitic diamond inclusions (e.g. Kimberley, Finsch) are associated with faster P-wave velocities at 150 km depth in the mantle. This distinction in P-wave velocities between the two groups can be interpreted in terms of different chemical compositions in the lithospheric mantle. Thus, the region with slower P-wave velocities could correlate with an oceanic lithospheric component and/or metasomatising fluids introduced by ancient subduction-related processes. In contrast, the region with faster P-wave velocities may reflect mid-Archean mantle depletion events initiated by craton keel formation.

As the mantle beneath the Jwaneng mine is characterized by slower P-wave velocities at 150 km depth, our finding of crustal noble gases in Jwaneng diamonds (gem-quality diamond aggregates and framesites) appears to be consistent with the tomographic observations. It is noteworthy that early helium work on diamonds from the Orapa mine also showed radiogenic He-enriched $^3\text{He}/^4\text{He}$ ratios, as low as 0.16 R/Ra (where Ra represents the atmospheric value of 1.4×10^{-6}), which could indicate the involvement of crustal helium; consistent with our findings from the Jwaneng diamonds.

Thus, it is postulated that diamonds from eclogitic mines could clarify whether or not material subducted into the deep mantle retained crustal and atmospheric noble gases, and could quantify the influence of subducted material through time. In contrast, diamonds from the peridotitic mines could contain pristine ancient mantle noble gas compositions at the time of their formation. Verification of our hypothesis will be significant in providing a basis for the reconciliation of geophysical and geochemical observations in terms of mantle structure and mantle geodynamics.

EXTREME ISOTOPIC ANOMALIES IN METEORITIC HIBONITES

Trevor R. Ireland and Chris. B. Thomson (Student Intern)

Research School of Earth Sciences, Australian National University, Canberra, ACT 0200, Australia

Large variations in calcium and titanium compositions are well known in the mineral hibonites, which is found in carbonaceous meteorites such as Murchison [e.g. 1]. Percent level variations are commonly found in the heaviest isotopes of these elements. In some cases extremely large positive anomalies are found with the most extreme being a 27% excess in ^{50}Ti . The magnitude of this anomaly rivals that in presolar SiC grains albeit with a different isotopic signature. The anomalies in the heaviest isotopes are consistent with nucleosynthesis in a quasi-equilibrium process, such as in the precursor of a Type I or IIa supernova, whereas the SiC grains have V-shaped Ti isotopic patterns more consistent with slow addition of neutrons (s-process) that commonly occurs in Red Giant stars (or Asymptotic Giant Branch (AGB) stars). While the preservation of large variations in circumstellar condensates is not surprising, the magnitude of the Ti isotopic variations in meteoritic hibonites far exceeds that in any other solar nebula products.

These inclusions therefore offer an intriguing view of the incorporation of Fe-group isotopic anomalies into the solar system. Thus far are very few anomalous grains with extreme excesses of ^{50}Ti (>10%). Two grains from Murray both have 10% ^{50}Ti excesses [2], and there appear to be two crystals with near 27% excesses of ^{50}Ti [1,3]. Some of the crystals may be fragments of larger inclusions and thus there may be only two extreme compositions. We have reinitiated a search for hibonite crystals with large Ti and Ca isotopic anomalies. This requires analysis of many grains because of their low abundance even within the hibonite population. We have developed a protocol on the SHRIMP RG for rapid characterization (approx 10 minutes) to a level of around $\pm 5\text{‰}$ in Ca and Ti isotopes. Using this approach we now have three hibonite inclusions with ^{50}Ti abundances 20% or more above terrestrial. Characterization of these grains for other systems will be carried out but thus far there is little to indicate exceptional behaviour in REE, O isotopes, or Mg isotope systematics. Oxygen isotopes probably underwent exchange with an ambient nebular gas. REE abundance patterns suggest a nebular source and little input from presolar sources. Mg isotopes are near terrestrial consistent with the low $^{26}\text{Al}/^{27}\text{Al}$ environment for these grains. This probably reflects the presence of nonradiogenic ^{27}Al in the precursors [4].

Individual crystals appear to represent discrete entities with their own characteristics. The precursors were probably originally refractory dust; the hibonite crystals reflecting homogenization and crystallization in the early solar nebula. The outstanding issue with these grains is where they fit within the chronology of the solar system.

- Ireland T. R. (1990) Presolar isotopic and chemical signatures in hibonite-bearing refractory inclusions from the Murchison carbonaceous chondrite. *Geochim. Cosmochim. Acta* **54**, 3219-3237.
- Fahey, A.; Goswami, J. N.; McKeegan, K. D.; Zinner, E. (1985) Evidence for extreme Ti-50 enrichments in primitive meteorites *Astrophysics Journal (Lett.)*, **296**, L17-L20.
- Ireland T. R. and Meibom A. (2002) Fe-group element isotopic compositions from meteoritic hibonites. *Meteoritics and Planetary Science* **37**, A69.
- Ireland T. R. and Fegley B. Jr (2000) The solar system's earliest chemistry: Systematics of refractory inclusions. *International Geological Review* **42**, 865-894.

The Geochemistry of Early Archaean basic and ultrabasic rocks from southern West Greenland: tectonic setting and mantle sources

Frances Jenner¹, Vickie Bennett¹, Allen Nutman¹

¹Research School of Earth Sciences, Australian National University, Canberra, ACT 0200, Australia

Little is known about the earliest Archaean (>3800 Ma) tectonic environments because very few rocks of this age have survived to the present day. Debate centres on whether plate tectonics existed, and if so, how similar were ancient and modern tectonic regimes. To provide information on the dominant tectonic mechanisms in the Early Archaean we have collected samples of the world's oldest mafic rocks as part of an integrated field, geochronological and geochemical study. All these rocks occur as fragments of their original sequences scattered as enclaves and tectonic lenses within more voluminous orthogneisses. Sample suites include volcanic and layered gabbro-ultramafic sequences (*Figure 1*) from several islands located south of Ameralik Fjord, southern West Greenland. Ages of ≥ 3850 Ma have been ascribed to these units (e.g. Krogh et al. 2002; Nutman et al. 2002) making them the world's oldest supracrustal rocks. None of the supracrustal rocks contain protolith zircons, therefore minimum age constraints were obtained by U/Pb SHRIMP dating of zircons from younger intrusive gneisses.

Complete trace element compositions were determined on fused glass discs using the LA-ICPMS. Major and trace element chemistry indicate that our samples of the supracrustal rocks, despite having been to granulite conditions, suffered only minimal secondary alteration of key diagnostic elements (i.e. the rare earth and high field strength elements).

Geochemical modelling has identified members of these suites that underwent minimal fractional crystallisation such that they can be used to reconstruct the composition and melting conditions of their mantle source regions. The supracrustal rocks display LREE depleted to slightly enriched patterns, indicating that mantle sources were already depleted by 3850 Ma. The low La/Sm ratios also indicate that the parental magma was not contaminated by felsic continental crust. Consequently, there is no evidence for felsic crust older than the supracrustal rocks within this area; it is likely that the earliest crust in this region was predominantly mafic. Detailed modelling of the geochemistry of the various supracrustal suites indicates that by 3850 Ma there were diverse source materials for the mafic melts, pointing to tectonic complexity similar to that seen in modern day settings.

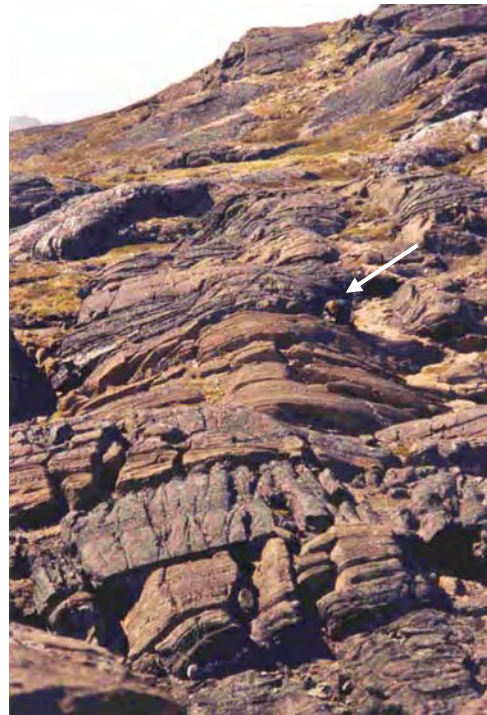


Figure 1: The world's oldest known layered ultramafic complex, southern West Greenland. Arrow points to person for scale.

Krogh, T. E., Kamo, S. L. and Kwok, Y.Y. (2002), An isotope dilution, etch abrasion solution to the Akilia Island U-Pb age controversy. Abstracts of the 12th annual V. M. Goldschmidt conference. Anonymous, Pergamon. Oxford, International.

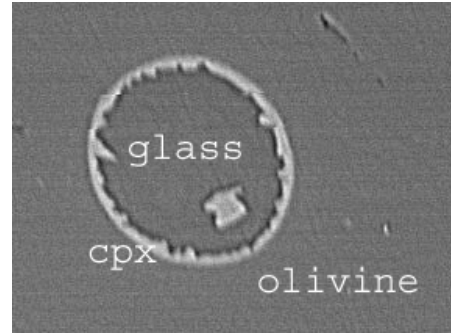
Nutman, A.P., McGregor, V.R., Shiraishi, K., Friend, C.R.L., Bennett, V.C. and Kinny, P.D. (2002), ≥ 3850 Ma BIF and mafic inclusions in the early Archaean Itsaq gneiss complex around Akilia, southern West Greenland? The difficulties of precise dating of zircon-free protoliths in migmatites. *Precambrian Research* **117**(3-4): 185-224.

Progress in analysis of Rb-Cs-Ba in silicate melt inclusions from old greenstone belts

Antti P. A. Kallio¹

¹ *Research School of Earth Sciences, Australian National University, Canberra, ACT 0200, Australia*

During 2005, important progress was made in the analysis of Cs-Rb-Ba from melt inclusions. In the current preferred scheme, Ba/Cs is analyzed with SHRIMP and Ba/Rb and other incompatible trace elements with LA-ICPMS from the same olivine-hosted melt inclusions. Successful analyses have been done on targets with down to 5 ppb Cs, with a ~20 μm spot diameter. Modern reference samples and samples from several greenstone belts in the 3.5-2 Ga age range have been analyzed. Correct results from multiple reference samples validate the suitability of the techniques, but unexpected complexities in the results from old samples make it difficult to draw quick conclusions on mantle evolution. Discoveries like that of mostly glassy 3.5 Ga melt inclusions (Figure), make it possible to quantitatively work on problems of how much old inclusions are altered or contaminated – and will help in uncovering the Rb-Cs-Ba chemistry of the early mantle.



Extrasolar Planets

Charles H. Lineweaver

Planetary Science Institute, Research School of Astronomy and Astrophysics, Research School of Earth Sciences, Australian National University, Canberra, ACT, Australia

Sun-like stars have stellar, brown dwarf and planetary companions. Relatively few brown dwarfs (compared to the number of planets and stellar companions) have been found in close orbits around sun-like stars. Why this should be so is unknown. With PhD student Grether, Lineweaver compiled, analysed and interpreted the world's data on exoplanet, brown dwarf and stellar companions. Our analysis i) confirmed that the brown dwarf desert was not a selection effect and ii) located the position of the driest part of the brown dwarf desert (the mass at which the fewest number of companions exist) at $M = 31^{+25}_{-18} M_{\text{Jupiter}}$. We found that approximately 16% of Sun-like stars have close companions more massive than Jupiter: 11% +/- 3% are stellar, <1% are brown dwarf and 5% +/- 2% are giant planets. Our results are published in the paper,

``How Dry is the Brown Dwarf Desert?: Quantifying the Relative Number of Planets, Brown Dwarfs and Stellar Companions around Nearby Sun-like Stars"
D. Grether and C.H.Lineweaver *Astrophysical Journal*, accepted December, 2005.

In observational work, we searched for water masers around stars hosting exoplanets. We were unable to duplicate previous reported detections. Our results are published in the paper:

"A search for water masers toward extrasolar planets"
V. Minier, & C.H.Lineweaver, *Astronomy and Astrophysics*, accepted December 2005

Astrobiology

In theoretical work in collaboration with Paul Davies, we showed that if life emerges readily under Earth-like conditions, the possibility arises of multiple terrestrial genesis events. We quantified the probability of this scenario using estimates of the Archean bombardment rate and the fact that life established itself fairly rapidly on Earth. We found a significant likelihood that at least one more sample of life may have emerged on Earth, and could have coexisted with known life. We found that it is difficult to rule out the possibility of extant alien life. Our results are published in the paper:

"Finding a Second Sample of Life on Earth"

Davies, P.C.W. and Lineweaver, C.H., *Astrobiology*, Vol 5, No. 2, April 2005, pp 154-163

In theoretical work I challenged the assumption that we have not yet found extraterrestrial life. I argued that by redefining life in a more general way, we can legitimately conclude that we have already detected extraterrestrial life. I argued that thermodynamic justifications for a broader definition of life are compelling and more universal than the traditional definitions of life based on DNA, "self-reproduction" and the chemical complexity of the terrestrial life most familiar to us. These ideas are published in the paper,

"`We Have Not Detected Extraterrestrial Life, Or Have We?"

Lineweaver, C.H. in "`Life As We Know It" ed. J. Seckbach, Vol. 10 of a series on Cellular Origin, Life in Extreme Habitats and Astrobiology, Springer, Dordrecht in press, ISBN 1-4020-4394-5

I reinterpreted biogeographical and plate tectonic observations as the best evidence we currently have to evaluate the question: Is human-like intelligence a convergent feature of evolution? I found that this evidence indicates that human-like intelligence is not a convergent feature of evolution. This result is published in a review essay,

"`Intelligent Life in the Universe: From Common Origins to the Future of Humanity"

C. H. Lineweaver. Review of "`Intelligent Life in the Universe: from common origins to the future of humanity" by Peter Ulmschneider, *Astrobiology*, Vol 5, No. 5, 2005 pp 674-677

Cosmology

We identified the most common misconceptions about the Big Bang held by astronomers and the public. We analyzed and made these misconceptions explicit for a popular audience in the paper,

"Misconceptions about the Big Bang"

Lineweaver, C.H. and Davis, T.M., *Scientific American*, 292, Part No 3, March, 2005, pp 36-45.

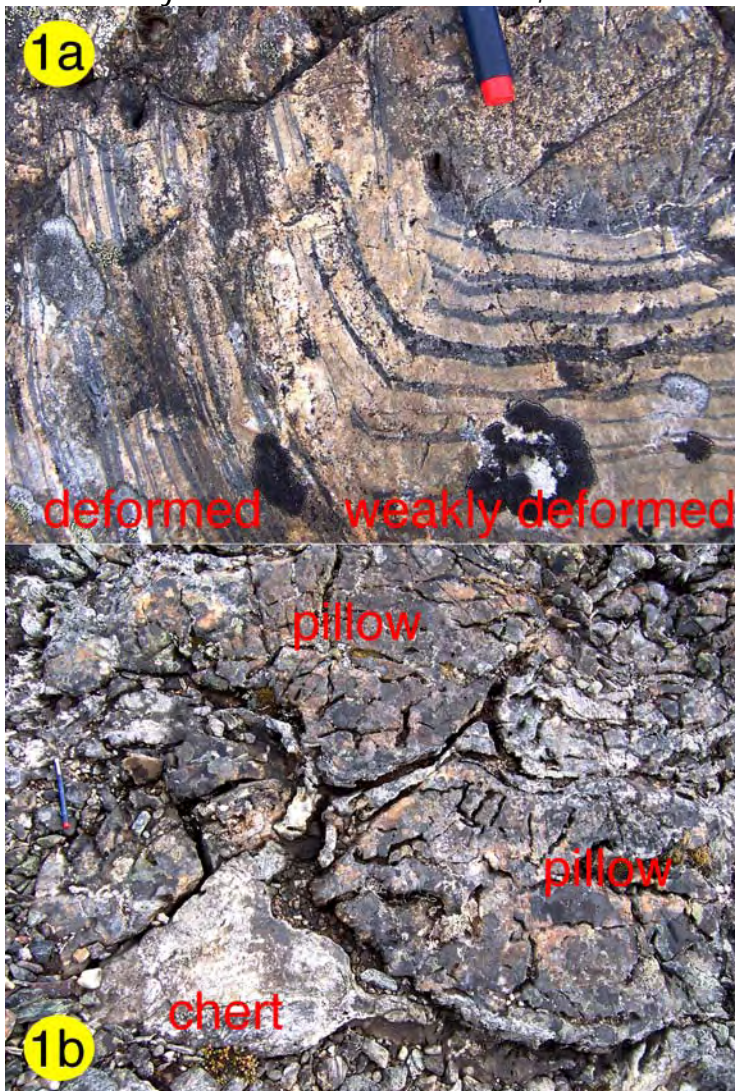
New discoveries of volcanic and sedimentary structures in the 3800-3700 million year old Isua supracrustal belt, Greenland: Tools for understanding the ancient Earth

Clark R. L. Friend¹ and Allen P. Nutman²

¹ 45, Stanway Road, Headington, Oxford, U.K.

² Research School of Earth Sciences, Australian National University, Canberra, ACT 0200 Australia

The Isua supracrustal belt (ISB) in W. Greenland is a 35 km long body of amphibolite facies rocks that contains the world's best record of ancient 3800-3700 Ma volcanism and sedimentation. Strong deformation destroyed most of its sedimentary and volcanic structures, and metasomatism causes difficulties in



interpreting the rocks. Nonetheless, for 30 years the ISB has been a magnet for early Earth studies, ranging from its mafic rocks providing insight into ancient tectonic environments and mantle chemistry – to searching for earliest evidence of life. However, it is rarely communicated that the best study areas with low deformation and relics of volcanic and sedimentary structures are extremely rare – we estimate they are preserved in less than a millionth of the belt! We have been finding more of these relics (funded by ARC DP-4707011) to obtain important new resources for early Earth studies via geochemical techniques.

The ISB contains quartz + magnetite banded iron formations (BIF) that were precipitated out of the oceans 3800-3700 million years ago. Banding in the BIF is mostly entirely tectonic i.e., transposed, attenuated sedimentary layering combined with new quartz and magnetite fabrics (left side of Fig. 1a). Such rocks cannot be taken to pieces sedimentary layer by layer to obtain detailed environmental information on the

early oceans, or be used to seek chemical signatures of individual meteorite impacts. In 2005 we found a small low strain zone (albeit still deformed) of $\sim 2\text{m}^2$ in BIF (right hand side of Fig. 1a). Individual quartz-rich and magnetite-rich layers are sedimentary and have internal fine structure. This rare sample will be taken to pieces layer by layer in geochemical studies with our RSES colleagues Vickie Bennett and Marc Norman.

Relict pillow structures not only show the sub-aqueous basaltic protoliths of Isua amphibolites, but also allow the most controlled geochemical studies of early terrestrial basalt petrogenesis and their depositional environment than by working on strongly deformed, banded amphibolites. Our 2005 discovery ($\sim 15\text{m}^2$) of more pillows (Fig. 1b) is the least deformed in Isua yet, and have well-preserved triangular domains of siliceous inter-pillow material and also they preserve their facing direction (Fig. 1b). The facing direction demonstrates that they are *capped* by an adjacent BIF unit. The structural top of this BIF is an early Archaean mylonite, above which is another package of amphibolites. Thus this locality provides a new important constraint on the early tectonics of the belt, a new opportunity to study basalt petrogenesis and a unique chance to study a 3800-3700 Ma inter-pillow environment – a potential early life habitat.

These are two examples of several new discoveries of original structures we made in Isua this year. Thus even in such well-trodden ground that has been the focus of 30 years study, continued field work still brings forth new discoveries for multidisciplinary research on the early Earth.

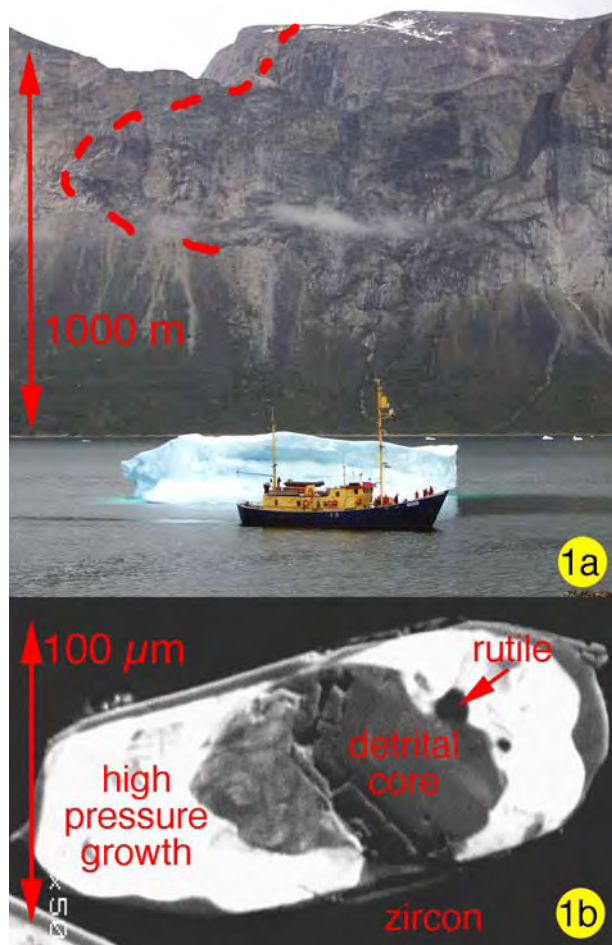
Archaean alpine-style collisions in Greenland (Nuuk district): Sequential high pressure metamorphic events followed by nappe development

Allen P. Nutman¹ and Clark R. L. Friend²

¹ *Research School of Earth Sciences, Australian National University, Canberra, ACT 0200 Australia*

² *45, Stanway Road, Headington, Oxford, U.K.*

The Nuuk district of West Greenland is a deeply eroded and glacially-incised section of Archaean basement crust (with recumbent isoclinal folds - Fig. 1a). Very small (100µm) zircons provide unique information to reconstruct tectonic evolution in monotonous Archaean basement gneiss terranes. Our field mapping, zircon SHRIMP dating, trace element geochemistry and inclusion studies were funded by ARC DP4707012. In structurally-deep levels in the southern part of the district, decompression (~10-5 Kbar) metamorphism occurred at ~2700 Ma. High pressure melt patch zircons contain garnet, clinopyroxene or rutile inclusions (Fig. 1b), whereas lower pressure melt patches that are the same age within errors of 2 million years contain sillimanite inclusions. The deep structural levels of the central part of the Nuuk district consists of rocks of different ages to deep structural levels to the south, but has relicts of 2650 Ma high pressure assemblages. The terranes with 2700 Ma and 2650 Ma high pressure assemblages were tectonically juxtaposed along a major mylonite zone prior to development of a northerly directed nappe-stack that was imprinted on several already-assembled terranes. Sequential high pressure events in different terranes increases the similarity between the Archaean tectonic evolution of the Nuuk district and collisional Phanerozoic orogens such as the European Alps.



Trace elements as key to the interpretation of zircon and monazite ages in high-grade rocks

Daniela Rubatto and Jörg Hermann

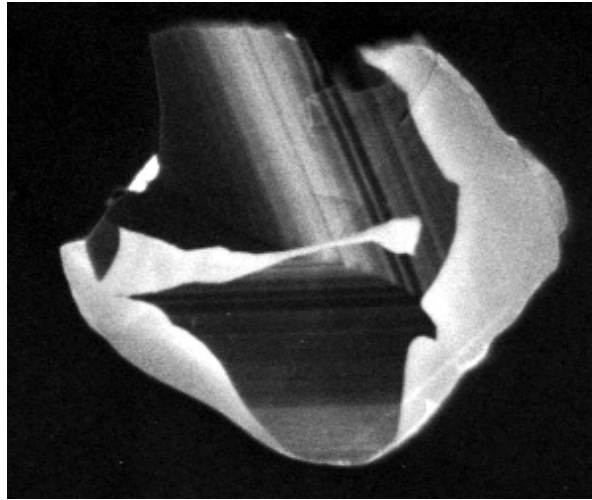
¹ *Research School of Earth Sciences, Australian National University, Canberra, ACT 0200, Australia*

The formation of metamorphic zircon and/or monazite in high-grade rocks is virtually ubiquitous and occurs in a variety of rock types from metapelitic granulites to metaperidotites. These minerals can provide not only absolute ages through U-Pb dating, but also important information on the petrological evolution of the rock and the timing of specific events. The combined study of textural relationships, inclusion suites and trace element composition of accessory and major minerals is used to link geochronology with petrology and achieve a rigorous interpretation of age data.

The formation, age and trace element composition of zircon and monazite were investigated across the prograde, low pressure, granulite sequence at Mount Stafford (central Australia). Three pairs of inter-layered, relatively melt-rich and melt-poor rocks (metapelite and metapsammites, respectively) were sampled in migmatites together with a sample of the nearby granite. U-Pb SHRIMP geochronology on metamorphic zircon rims and on monazite indicate that granulite facies metamorphism occurred between ~1795 and 1805 Ma. The granite intrusion was coeval with metamorphism at 1802 ± 3 Ma and is unlikely to be the heat source for the prograde metamorphism. Metamorphic growth of zircon started at temperatures of ~750°C well above the pelite solidus and is more abundant in the melt-rich rocks. In contrast, monazite growth had already begun under prograde sub-solidus conditions. At granulite facies conditions two distinct metamorphic domains were observed in monazite. Textural observations, petrology and the trace element composition of monazite and garnet provide evidence that the first metamorphic monazite domain grew prior to garnet during prograde conditions and the second in equilibrium with garnet and zircon close to the metamorphic peak. Ages from sub-solidus, prograde and peak metamorphic monazite and zircon are within error not distinguishable, indicating that heating took place in less than 20 Ma.

The Duria garnet peridotite (Adula nappe, Central Alps) contains two generations of metamorphic zircon formed in sub-solidus conditions, which have inclusions of amphibole and clinopyroxene. The first domain is oscillatory zoned, with high U, REE and moderately high Ti contents (32 ppm) and Th/U (0.1-0.3). It was determined that this zircon formed during decompression, likely at the transition from Zr-rich peak metamorphic rutile to Zr-poor retrograde ilmenite. Additionally, textures and trace element contents of clinopyroxene, orthopyroxene and amphibole that formed contemporaneously with the zircon suggest that peridotite recrystallization was assisted by the influx of crustal derived fluids,

which probably also favoured zircon formation. The second zircon domain is the product of recrystallization of zircon 1 and is characterised by low CL emission, low REE and Ti contents (5.4 ppm). The Ti content of zircon in the peridotites is buffered by the assemblage ilmenite, olivine and orthopyroxene. Application of the Ti in zircon thermometer indicates that significant cooling occurred between the formation of zircon domain 1 at $\sim 850^{\circ}\text{C}$ and its recrystallization (zircon domain 2) at $\sim 700^{\circ}\text{C}$. SHRIMP dating of the two domains yield ages of 34.15 ± 0.24 Ma and 32.94 ± 0.27 Ma, respectively, indicating fast exhumation of the peridotite within the spinel stability field. We suggest that the Duria garnet peridotite originate from the mantle wedge above the tertiary subduction of the European continental margin and that it was assembled to the country rock gneisses between 34 and 33 Ma.



Cathodoluminescence image of zircon from the Duria peridotite showing the two cross cutting metamorphic domains.

Contrasting marginal basin development in Fennoscandia and northern Australia 2.30 to 1.85 billion years ago

R.W. Roye Rutland¹ and Ian S. Williams¹

¹ *Research School of Earth Sciences, Australian National University, Canberra, ACT 0200 Australia.*

Remnants of the Earth's crust between 2.30 and 1.85 billion years old are relatively rare, but they provide a critical link in the record of crustal evolution through time. Two of the best preserved areas, relatively unaffected by younger geological events, are found in northern Australia and northern Sweden and Finland.

These two Palaeoproterozoic provinces developed by broadly similar sequences of geological events (e.g. Rutland, 1997). The oldest sedimentary sequences in both areas have been related to rifting of the Archaean crust, evidenced in Finland by several phases of mafic magmatism between 2.10 and 1.95 billion

years ago. Early volcanic rocks and tonalitic intrusions dating from between 1.93 and 1.91 b.y. ago occur in both the Savo Belt of the Svecofennian province in Finland and in the Halls Creek orogenic domain in the North Australian province. The main episode of plutonism, volcanism and associated mineralisation in the Svecofennian province of Fennoscandia occurred between 1.89 and 1.86 b.y. ago, and the corresponding events in northern Australia took place between 1.88 and 1.85 b.y. ago.

Both provinces contain significant gold deposits, but whilst the most important mineral deposits in Fennoscandia occur in the pre-1.85 b.y. old province, deposits of this age are not prominent in Australia. The Svecofennian province shows little evidence of an Archaean basement, and there is abundant mantle derived magmatism, with which the principal ore deposits are associated. In contrast, coherent Archaean basement to the North Australian province is exposed in several areas.



Against this background, quite different models of crustal evolution have been applied in the two regions; rapid arc accretion in Fennoscandia and ensialic marginal basin development in Australia. Our recent work in collaboration with colleagues in Sweden and Finland has combined data from regional aeromagnetic mapping with new field studies and ion microprobe studies of critical samples to test the models in those countries (Rutland et al., 2001a and b; 2004; Skiöld and Rutland, in press). We have focused on zircon populations in metasedimentary rocks. The detrital grains provide a tracer of the source materials of the sediments and overgrowths on the grains can provide a record of post-depositional metamorphism.

We have found that the widespread Svecofennian metamorphic complexes in both Sweden and Finland are significantly older than previously assumed and originally probably formed an extensive oceanic marginal basin that was deformed and metamorphosed about 1.92 b.y. ago. Thus, the first stage of Svecofennian crustal growth was by marginal basin accretion. Igneous rocks previously attributed to rapid arc accretion, and their associated ore deposits, actually postdate the basin development, and a re-evaluation of their tectonic setting is required. This marginal basin accretion hypothesis has a younger analogue in the Lachlan province of Eastern Australia.

Work in progress in Ostrobothnia will provide a further test of the hypothesis and allow correlation of tectonic evolution between northern Sweden and Finland across the Gulf of Bothnia.

Rutland R. W. R. (1997) Palaeoproterozoic of Northern Australia and Fennoscandia: an Introduction. *In* Palaeoproterozoic Tectonics and Metallogenesis: Comparative analysis of parts of the Australian and Fennoscandian Shields. *Australian Geological Survey Organisation Record*, 1997/44, 1-5.

Rutland R. W. R., Kero L., Nilsson G. & Stølen L. K. (2001a) Nature of a major tectonic discontinuity in the Svecofennian province of northern Sweden. *Precambrian Research* 112, 211-237.

Rutland, R. W. R., Skiöld, T. and Page, R. W. (2001b) Age of deformation episodes in the Palaeoproterozoic domain of northern Sweden, and evidence of a pre-1.9 Ga crustal layer. *Precambrian Research* 112, 239-259.

Rutland R. W. Roye, Williams, Ian S. and Korsman Kalevi (2004) Pre-1.91 Ga deformation and metamorphism in the Palaeoproterozoic Vammala Migmatite Belt, southern Finland, and implications for Svecofennian tectonics. *Bulletin of the geological Society of Finland* 76, 93-140.

ELA-Q-ICP-MS for the analyses of $^{207}\text{Pb}/^{206}\text{Pb}$ and $^{208}\text{Pb}/^{206}\text{Pb}$ in carbonates

Amanda. Stoltze, Ian Campbell, Charlotte Allen

¹ *Research School of Earth Sciences, Australian National University, Canberra, ACT 0200, Australia*

Isotope dilution may give the highest quality isotopic data but it is often unsuited for the analyses of old samples where post formation mobility of the parent and/or daughter isotope can lead to the calculation of incorrect initial ratios. Analyzing mineral separates that have a very low parent to daughter ratio can minimize the problem but most mineral separates have small mineral or fluid inclusions. Moreover it is often difficult to obtain pure separates of fine-grained material. *In situ* ELA-Q-ICP-MS offers a viable alternative method. It is substantially less precise than isotope dilution but allows greater control on sample selection and avoids problems associated with inclusions and fine grain size. The other advantage *in situ* ELA-Q-ICP-MS has over standard isotope dilution methods is shorter analytical time.

We have applied the ELA-ICP-Q-MS to analyses of Pb in carbonates from monzonite-syenite-carbonatite associated with the Wallaby gold deposit in Western Australia. The aim was to test whether the Pb in the gold mineralization was derived from the same source as the intrusions. The biggest problem with the application of this method to Pb isotopes is that the interference of ^{204}Hg on ^{204}Pb excludes the measurement of ^{204}Pb , therefore, limiting the measured ratios to $^{207}\text{Pb}/^{206}\text{Pb}$ and $^{208}\text{Pb}/^{206}\text{Pb}$. The comparison of ELA-Q-ICP-MS to isotope dilution values from the same lithologies was used to characterize the success of the application for the analyses of carbonate minerals (calcite, strontianite and dolomite).

During each analyses the background counts were measured for 20 seconds and the unknown for 40 seconds during which time each isotope was measured approximately 100 times. Each ratio was averaged and multiplied by a factor determined by comparing the average measured ratio of NIST612 (bracketing standard) to the published value of Woodhead and Hergt (2001). The standard BCR-2g was analyzed a total of fourteen times and gave averages of $^{207}\text{Pb}/^{206}\text{Pb} = 0.831 \pm 4$ and $^{208}\text{Pb}/^{206}\text{Pb} = 2.051 \pm 9$ which were compared to the published values of Woodhead and Hergt (2000) and Jochum et al (2005). The ratios obtained were within error of the published values, giving confidence in the data. Uranium and Th were also analyzed so that inclusions rich in these elements could be excluded from the average calculation, and correction for radiogenic decay since formation could be applied.

The average Pb isotopic ratios of ore, dikes, Wallaby conglomerate calcite, Lancefield conglomerate calcite, and Chatterbox limestone are displayed in figure 1. All three Pb isotopic groups at Wallaby cluster in a tight range and data collected from locations 10's Km distance from Wallaby are distinctly different (Lancefield and Chatterbox).

The results of Laser analyses are compared to ratios determined by isotope dilution using the methods of Kuritani and Nakamura (2002) in the figure. The comparison of the two methods shows that laser produced isotopes are consistent with those produced by isotope dilution but with less scatter. The values produced by the less precise method but with better sample control have lower scatter suggesting that variable radiogenic decay of U and Th is producing the scatter, therefore the sample composition is producing most of the variability found by isotope dilution. The data is also consistent with a common source of Pb in the dike suit and gold mineralization.

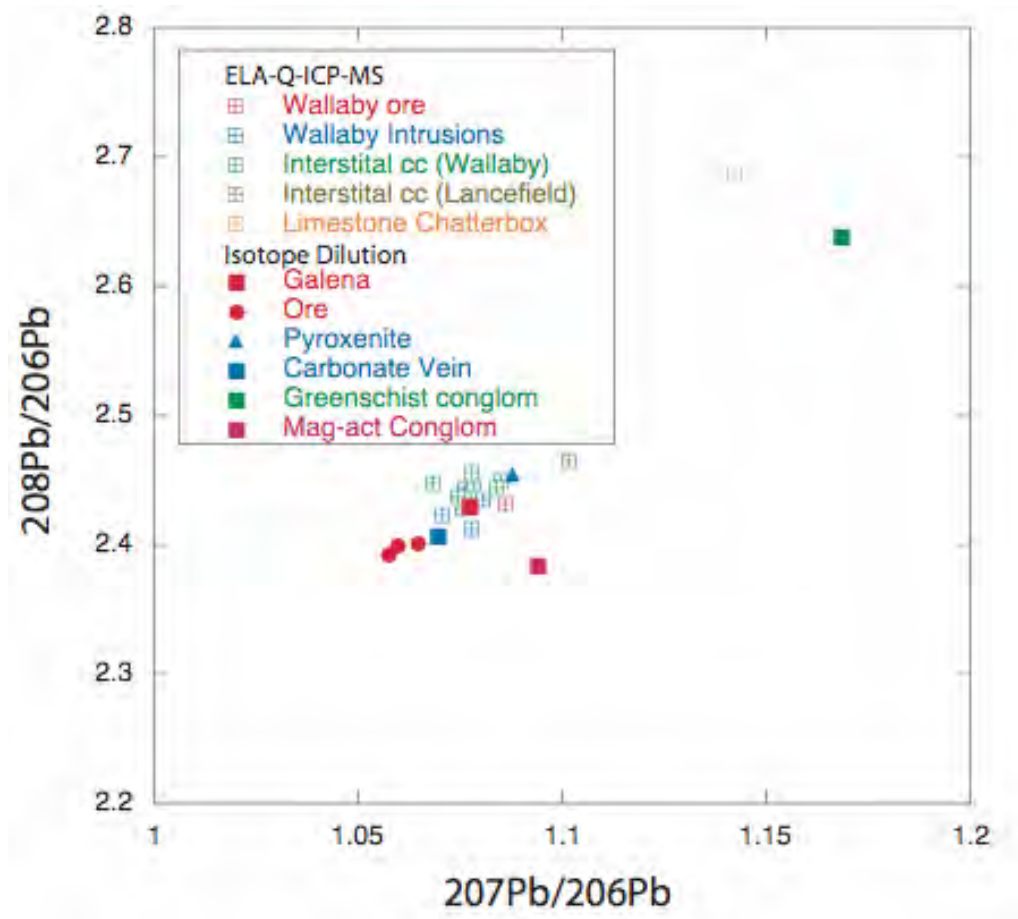


Figure 1. A graph of the LA-ICP-Q-MS ratios compared to those determined by the method of Kuritani and Nakamura (2002) shown in solid symbols.

- Jochum K. P., Stoll B., Herwig K., Amini M., Abouchami W. and Hofmann A. W. (2005) Lead isotope ratio measurements in geological glasses by laser ablation-sector field-ICP mass spectrometry (LA-SF-ICP-MS). *International Journal of Mass Spectrometry* **242(2-3)**, 281-289.
- Kuritani T. and Nakamura E. (2002) Precise isotope analyses of nanogram-level Pb for natural rock samples without use of double spikes. *Chemical Geology* **186**, 31-40.
- Woodhead J. D. and Hergt J. M. (2000) Pb-isotope analyses of USGS reference materials. *Geostandards Newsletter: The Journal of Geostandards and Geoanalysis* **24(1)**, 33-38.
- Woodhead J. D. and Hergt J. M. (2001) Strontium, neodymium and lead isotope analyses of NIST glass certified reference materials: SRM 610, 612, 614. *Geostandards Newsletter: The Journal of Geostandards and Geoanalysis* **25(2-3)**, 261-266.

THERMAL REVERSALS: EVIDENCE FOR MAGMA MIXING LEADING TO THE EVOLUTION OF PORPHYRY COPPER DEPOSITS?

Dianne L. Valente

Research School of Earth Sciences, Australian National University, Canberra, ACT 0200, Australia

The El Abra Porphyry Copper Deposit is a major deposit located in the El Loa Province, Region II, Chile, and is spatially associated with a suite of intermediate to felsic composition, calc-alkaline intrusions, called the Pajonal-El Abra complex. The deposit is located 1650km north of Santiago and lies within the Late Eocene-Oligocene aged, north-south trending Domeyko Cordillera which hosts other major porphyry copper mines including Chuquicamata, and Escondida (AMBRUS, 1977; GRAICHEN et al., 1995; MAKSAEV and ZENTILLI, 1999; GERWE, 2005).

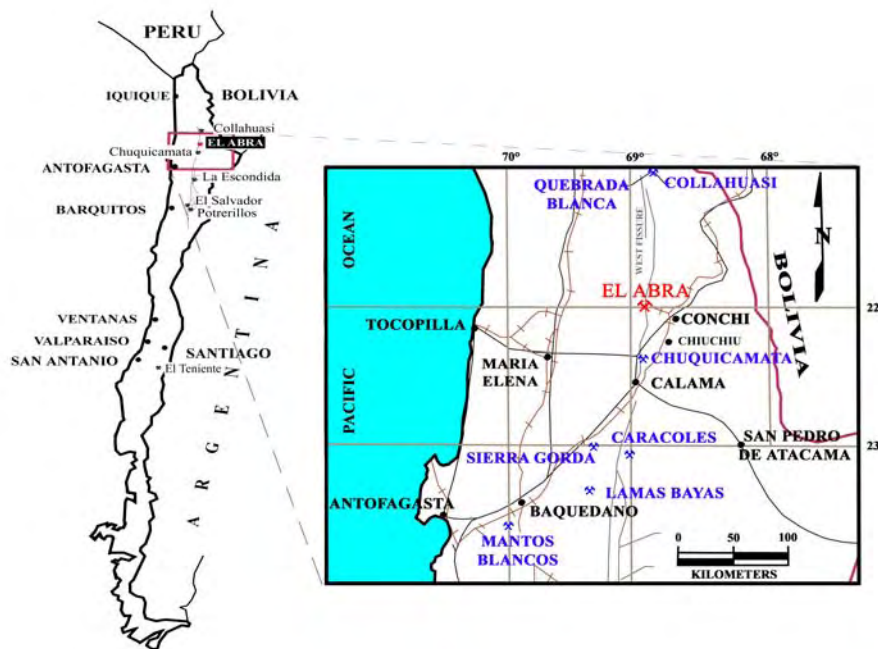


Figure 1: Regional location plan of the El Abra mine site and PhD project area. Figure modified from GERWE (2005) and GRAICHEN et al. (1995).

The Pajonal-El Abra suite of rocks have a shared petrochemical history which culminated in the formation of the copper porphyry deposit associated with the El Abra porphyry. These rocks, which are defined in age and by whole rock

chemistry as three distinct suites, were emplaced between 35-43Ma. They formed through a combination of processes including assimilation, magma mixing and fractional crystallisation, with the latter process only being significant within suites, whilst the processes of assimilation and magma mixing are more important between suites. A feature of these rocks, especially for Clara suite, is that they are sulphur saturated.

The preliminary thermal history, dating and whole rock chemical data indicates the three suites of rocks at El Abra define three magmatic cycles, initiated by a magma mixing event, followed by combined processes such as crystal fractionation and assimilation. The rate of cooling is exponential over the life of the Pajonal-El Abra batholith, with initial, hot, thermal mixing events followed by rapid cooling (Figure 2).

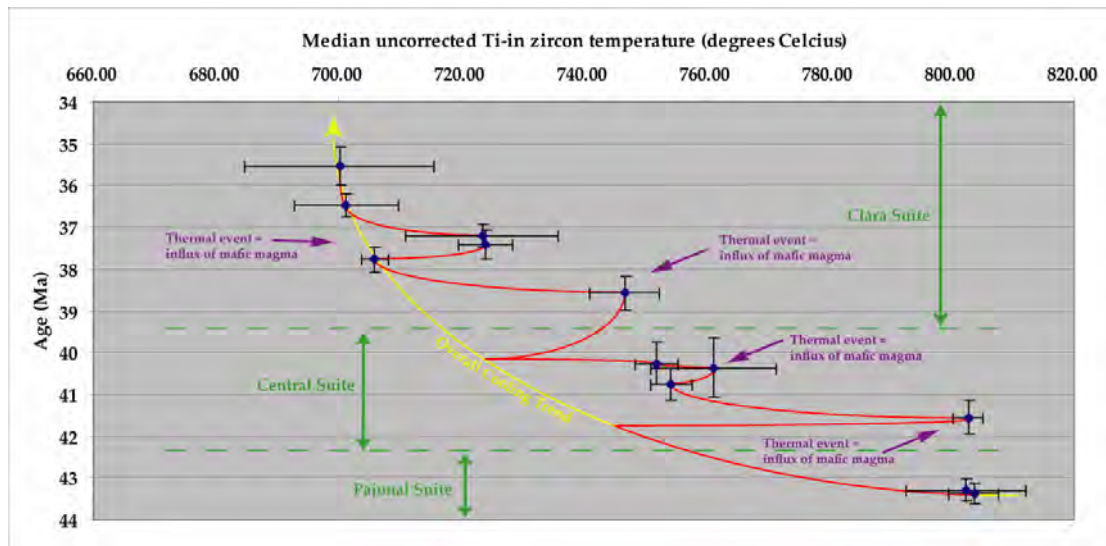


Figure 2: Uncorrected Ti-in-zircon temperature versus age (Ma)

- Ambrus J. (1977) Geology of the El Abra Porphyry Copper Deposit, Chile. *Economic Geology* 72(6), 1062-1085.
- Gerwe J. (2005) The El Abra Porphyry Copper Deposit: An overview. SCM El Abra (Unpublished company presentation).
- Graichen R. E., Dean D. A., Barrett L. F., Burton W. D., and Christenson D. K. (1995) Geologic Overview of the El Abra Porphyry Copper Deposit, Chile, pp. 1-11. Cyprus Amax Minerals Company: Unpublished company report.
- Maksaev V. and Zentilli M. (1999) Fission track thermochronology of the Domeyko Cordillera, northern Chile; implications for Andean tectonics and porphyry copper metallogensis. In *Latin American mineral deposits.*, Vol. 8; 1-2 (ed. L. Sangster Alan and M. Zentilli), pp. 65-89. Canadian Institute of Mining, Metallurgy and Petroleum.

Wrigglers and wombats: improved precision and accuracy in light isotope analysis using the SHRIMP II ion microprobe

Ian Williams¹, Peter Holden¹, Julie Trotter¹, Peter Lanc¹, Rainer Grün¹, John Foster¹, Trevor Ireland¹, Norm Schram¹, Ben Jenkins¹, Rebecca Fraser¹ and Dmitry Matukov²

¹ Research School of Earth Sciences, The Australian National University

² VSEGEI All Russian Geological Research Institute, St Petersburg

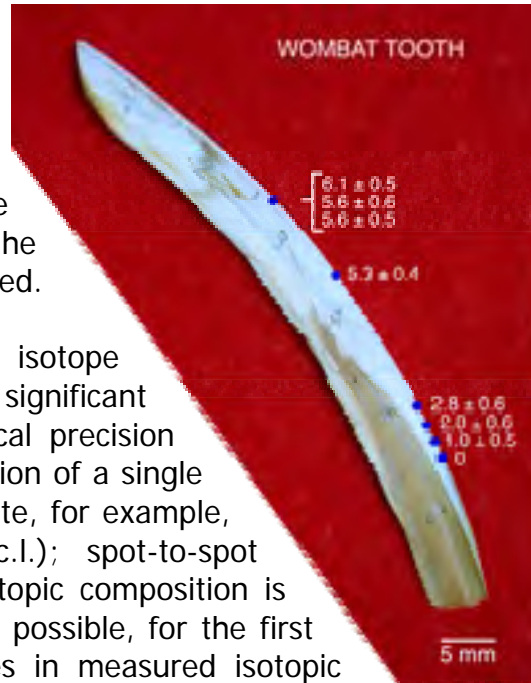
Coinciding with the development of a multiple collector for the SHRIMP II ion microprobe, there has been a resurgence of interest at RSES in the *in situ* isotopic analysis of light elements, particularly S and O. Initially the main emphasis was on improving the performance of the collector itself; refining the mechanical design, optimising the ion counting system and enhancing the computer control. This work was largely completed in 2005, with the multiple collector development reaching the stage where the main limiting factor in the analysis of light isotopes became the performance of the SHRIMP II secondary ion optics.



Early experiments with light isotope analysis of major elements showed that it was relatively easy to achieve sub permille precision in a rapid analysis of a single spot. However, systematic shifts in the apparent isotopic composition during a longer analysis, and even larger random shifts when moving to a new spot, made it extremely difficult to reproduce analyses on a uniform target to better than one permille. The cause of the isotopic variability was traced to a partial separation of the isotopes occurring before the secondary ion beam entered the secondary mass analyzer. The separation did not, as first suspected, reflect dispersion due to mass-dependent differences in ion energies, but apparently the influence of a magnetic field.

Experiments on the ANU SHRIMP II showed that the separation was very small, just a few microns, so it was possible that the cause was the magnetic field of the Earth. This was checked by repeating the experiment on the multiple-collector SHRIMP II at VSEGEI in St. Petersburg. The separation was indeed

found to occur in the reverse sense, consistent with a field reversal. The solution was to fit the SHRIMP II source with Helmholtz coils and, although the Earth's field is probably not the sole reason for the mass separation, the variable fractionation effect at the entrance to the mass analyser can now be virtually eliminated.



This and other advances in the light isotope analysis protocol have led to significant improvements in both single spot analytical precision and spot-to-spot reproducibility. The precision of a single 10-minute spot analysis of $^{18}\text{O}/^{16}\text{O}$ in apatite, for example, is typically better than 0.5‰ (95% c.l.); spot-to-spot reproducibility on a crystal of uniform isotopic composition is similar. This level of precision has made it possible, for the first time, to explore small systematic changes in measured isotopic compositions as a function of other parameters, in particular those dependent upon changes in the immediate environment of the spot from which secondary ions are being extracted.

With this improved precision, the study of oxygen isotopic compositions in early Paleozoic conodonts (Williams et al., 2004) has been revisited, including an expanded sampling of stratigraphic units from the Late Ordovician and Early Silurian. The progressive change in isotopic composition up section has now been measured more accurately. However, despite testing several samples from close to the Ordovician-Silurian boundary, we could not detect any excursions in oxygen isotopic composition that might reflect the proposed terminal Ordovician glaciation and consequent rapid drop in global sea water temperatures. Whether this is due to an hiatus in the stratigraphic sequence we sampled has yet to be resolved.

In preparation for a research program on human teeth to be commenced in 2006, techniques are being refined for the analysis of oxygen isotopes in mammalian tooth enamel. Single spot (25 μm diameter) analyses of the enamel from a wombat tooth have achieved precisions of $\sim 0.5\text{‰}$ (95% c.l.) relative to bracketing analyses of a standard and identified a similar shift in isotopic composition to that measured by conventional methods. No change in composition across the enamel layer was detected.

Williams, I.S., Holden, P. and Trotter, J.A. (2004) Towards the analysis of oxygen isotopes in insulators using the SHRIMP II. *Abstracts of the SHRIMP Workshop Hiroshima 2004*, 63.

Mounting evidence for a continuation of the Dabie-Sulu ultra-high pressure metamorphic belt into Korea

Ian S. Williams¹, Daniela Rubatto¹, Chang Whan Oh² and Sung Won Kim³

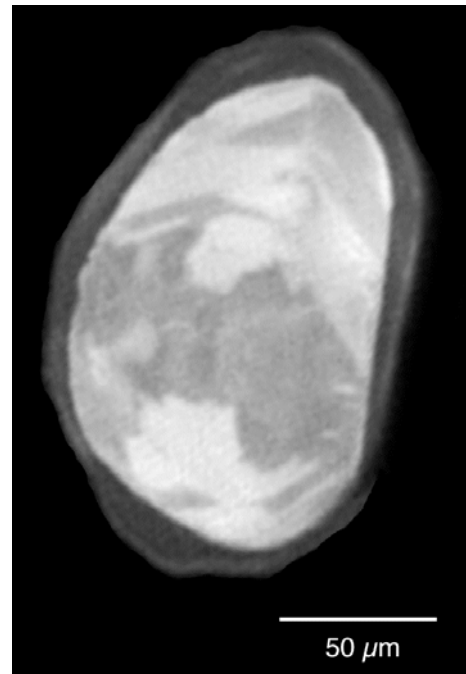
¹ *Research School of Earth Sciences, The Australian National University*

² *Department of Earth and Environmental Sciences, Chonbuk National University, Chonju, South Korea*

³ *Basic Science Research Institute, Chonbuk National University, Chonju, South Korea*

The Dabie-Sulu metamorphic belt in central and eastern China contains some of the highest pressure crustal metamorphic rocks presently known to be exposed at the Earth's surface. Peak pressures up to 7 GPa have been inferred, equivalent to depths of burial of over 200 km (Ye et al., 2000). These enormous pressures were generated by the subduction of crust as a result of several continent-continent collisions between the North and South China Blocks, the last and largest of which occurred in the Triassic. The eastern end of the metamorphic belt is terminated abruptly at the Yellow Sea coast, so there has been much speculation over whether the collision zone might extend into the Korean peninsula, and possibly even as far east as Japan. The idea has remained speculative until recently, when high pressure metamorphic rocks yielding Permo-Triassic isotopic ages have first been found in South Korea (Oh et al., 2005).

A visit to RSES this year by two leading researchers from Chonbuk National University, Prof. Oh Chang Whan and Dr Kim Sung Won, initiated a collaboration between the two institutes to study key aspects of the geological history of South Korea using SHRIMP U-Pb dating. Amongst the samples chosen for the initial work was one from the Hongseong area in the southeastern Gyeonggi Massif, the area from which retrogressed eclogite with Permo-Triassic garnet Sm-Nd ages had previously been reported (Oh et al., 2005). The results obtained strongly supported the earlier interpretation that some of the garnet granulites and amphibolites in the Hongseong area are retrogressed eclogites, and that the age of the high pressure metamorphism is Triassic.



The new evidence came from zircon recovered from a garnet granulite collected from a large lenticular body of metabasite at Bibong. Many of the zircon grains

are similar to the one illustrated, consisting of a low-U, sector zoned core surrounded by a distinct younger overgrowth. SHRIMP *in situ* U-Pb dating of these two zircon types showed that the cores are late Neoproterozoic in age, whilst the overgrowths are Middle Triassic. The interpretation was that the garnet granulite derives from a Neoproterozoic igneous rock, probably of intermediate to mafic composition, that was metamorphosed to high grade in the Middle Triassic.

It could be inferred from the type and chemical composition of the major minerals in the granulite that its igneous protolith had been metamorphosed under eclogite facies conditions (1.6–2.0 GPa), followed by partial re-equilibration at granulite facies (1.1–1.6 GPa), followed in turn by an amphibolite facies (0.8–0.9 GPa) overprint. To determine which stage of the metamorphism produced the zircon overgrowths, several cores and overgrowths were analysed for trace elements by laser ablation ICP-MS. The cores are enriched in heavy rare earth elements (REE) relative to middle and light REE and have a pronounced negative Eu anomaly, consistent with zircon precipitated from a magma. In contrast, the overgrowths have relatively low total trace element contents, virtually no heavy REE enrichment and only weak Eu anomalies, consistent with growth in the presence of garnet but not feldspar, namely growth under eclogite facies conditions. Even though the granulite no longer has an eclogite facies mineralogy, the zircon overgrowths preserve their eclogite facies chemical fingerprint, and the U-Pb ages of those overgrowths record the age of that event. There is now little doubt that the continent-continent collision zone in mainland China extends eastward, running north east across the Korean peninsula approximately parallel to the international border.

Oh, C.W., Kim, S.W., Choi, S.G., Zhai, M., Guo, J. and Krishnan, S. (2005) First finding of eclogite facies metamorphic event in South Korea and its correlation with the Dabie-Sulu collision belt in China. *The Journal of Geology* 113, 226-232.

Ye, K., Cong, B. and Ye, D. (2000) The possible subduction of continental material to depths greater than 200 km. *Nature* 407, 734-736.

Earth Environment Introduction

Research in the Earth Environment Group is focused on environmental change and long-term interactions between humans and our environment. Research is directed toward understanding globally significant processes within the themes of climate and sea-level change, landscape evolution, human evolution and extinctions and the impact of ongoing global change on the marine environment. Our research is based around the application of a unique group of World-class research facilities that enable analysis of a wide range of trace element and isotopic systems, with an emphasis on the timing and rate of change of major environmental and Earth surface processes. Emphasis is on developing detailed chronologic records that span a few tens to several hundred thousand years of the Earth's history, and using these as a basis for understanding past and present environmental change and predicting future trends. Earth Environment specialises in the reconstruction of high-resolution environmental records from growth banding preserved in fossil and modern corals, speleothems (cave deposits), layered sedimentary deposits and anthropologic sites of special significance.

ARC

During 2005 there were a number of highlights. Academic staff continued their high level of success with ARC proposals from both Professor Grün and Dr Gagan being funded. Professor Grün's proposal is being undertaken jointly with Professor Roberts from the University of Wollongong and involves dating of a number of key archeological sites using both OSL and ESR methods. Dr Gagan will continue his important research in the Indonesian region with two projects being funded. The first project is for five years and involves the use of coral records to better constrain the recurrence interval of major earthquakes in the Sumatra region. The second project is for three years and is being undertaken jointly with Dr Zhao from the University of Queensland and Dr Drysdale from the University of Newcastle and addresses the important question of the environmental impacts of early human history in southern Australasia. This will be tackled using geochemical microanalysis of precisely dated speleothems to document climate and environmental change in southern Indonesia.

Coral Reef Centre of Excellence

Earth Environment is also a key member of the newly established Coral Reef centre of Excellence where Professor McCulloch is an Associate Director. This is an ARC funded initiative and provides new opportunities to undertake and expand our research in coral reefs with a world-leading group of researchers. The centre is based at James Cook University

under the Directorship of Professor Hughes from Marine Biology together with the Marine Sciences Centre at University of Queensland led by Professor Hugh-Guldberg (Associate Director). In addition to providing additional funding for Post Doctoral positions across wide interdisciplinary fields there are also many opportunities for PhD students to undertake research utilising the combined resources and talents of the Centre.

New instrumentation

New LIEF funded state-of-the-art equipment is now being installed in the Earth Environment Group to enable us to continue our cutting-edge research. This includes an ~\$2 million gas source AMS which will revolutionise our capacity to undertake ^{14}C dating terrestrial materials and an ultra-short wavelength (157 nm) laser ICPMS combination to enable direct in-situ analyses of a wider variety of Geological materials with greatly enhanced sensitivity.

Research highlights

The following section describes some of the research highlights of our group. Major break-throughs have been made in understanding how Australia's desert environment has responded to climate change during the past million years. On shorter timescales the effects of ENSO variability in the Philippine region has now been clarified during the Holocene period, and using new refined thermal ionisation methods, boron isotope variations in corals have been used to determine variability of seawater pH due to uptake of anthropogenic CO_2 during the industrial and preindustrial periods.

Long-term perspectives on monsoon dynamics, environmental shifts, and early human impacts in southern Australasia

Late Holocene reconstruction of strong El Niño events

Rose D. Berdin¹, Michael K. Gagan¹, Fernando P. Siringan²,
Atsushi Suzuki³ and Hodaka Kawahata⁴

¹*Research School of Earth Sciences, The Australian National University, Canberra, 0200 ACT, Australia*

²*National Institute of Geological Sciences, University of the Philippines, Diliman, 1100 Quezon City, Philippines*

³*Geological Survey of Japan, National Institute of Advanced Industrial Science and Technology (AIST), Tsukuba, Ibaraki 305-8567, Japan*

⁴*Graduate School of Science, Tohoku University, 980-8578 Sendai, Japan*

Annually-resolved $\delta^{18}\text{O}$ records were derived from a modern and a 2.3 ky coral acquired in Maydolong, eastern Samar, Philippines to reconstruct past El Niño events. The two records are comparable in length: the modern coral spans the past 82 years (1922 to 2003) whereas the 2.3 ky coral includes 91 years. Replicate measurements of samples milled at annual increments were made until the standard error of the mean fell below 0.05‰. $\delta^{18}\text{O}$ anomalies were then calculated by subtracting the 7-year running mean from the average of each year.

Strong El Niño events in the past 82 years exhibited positive $\delta^{18}\text{O}$ anomalies. The most recent events, which occurred in 1972/3, 1982/3, 1991-3 and 1997/8, registered values from 0.09 to 0.18‰ (Fig. 1). To identify strong El Niño events in the 2.3 ky coral record, we used the threshold value of 0.10‰ as weak to moderate El Niños have an average $\delta^{18}\text{O}$ anomaly of 0.05‰. Eight events occurring at fairly regular intervals (approximately every 10 years) were identified in the late Holocene record (Fig. 1). Relative to modern-day events starting from the 1970s, the frequency as well as the amplitude of strong El Niños is similar to that of the late Holocene. The tendency for more frequent and stronger El Niño events in the late Holocene has been shown in a climate model (Clement et al., 2000) and in coral records from Papua New Guinea (Tudhope et al., 2001; McGregor and Gagan, 2004). However, persistent events (lasting more than 1 year) are more common in the late Holocene record relative to the modern. This corroborates findings of multi-year El Niño events based on coral reconstructions (Tudhope et al., 2001; McGregor and Gagan, 2004) but not captured in models.

Clement, A.C., Seager, R., and Cane, M.A., 2000. Suppression of El Niño during the mid-Holocene by changes in the Earth's orbit. *Paleoceanography*, 15: 731-737.

McGregor, H.V., and Gagan, M.K., 2004. Western Pacific coral $\delta^{18}\text{O}$ records of anomalous Holocene variability in the El Niño-Southern Oscillation. *Geophysical Research Letters*, 31: doi:10.1029/2004GL019972.

Tudhope, A.W., Chilcott, C.P., McCulloch, M.T., Cook, E.R., Chappell, J., Ellam, R.M., Lea, D.W., Lough, J.M., and Shimmield, G.B., 2001. Variability in the El Niño-Southern Oscillation through a glacial-interglacial cycle. *Science*, 291: 1511-1517.

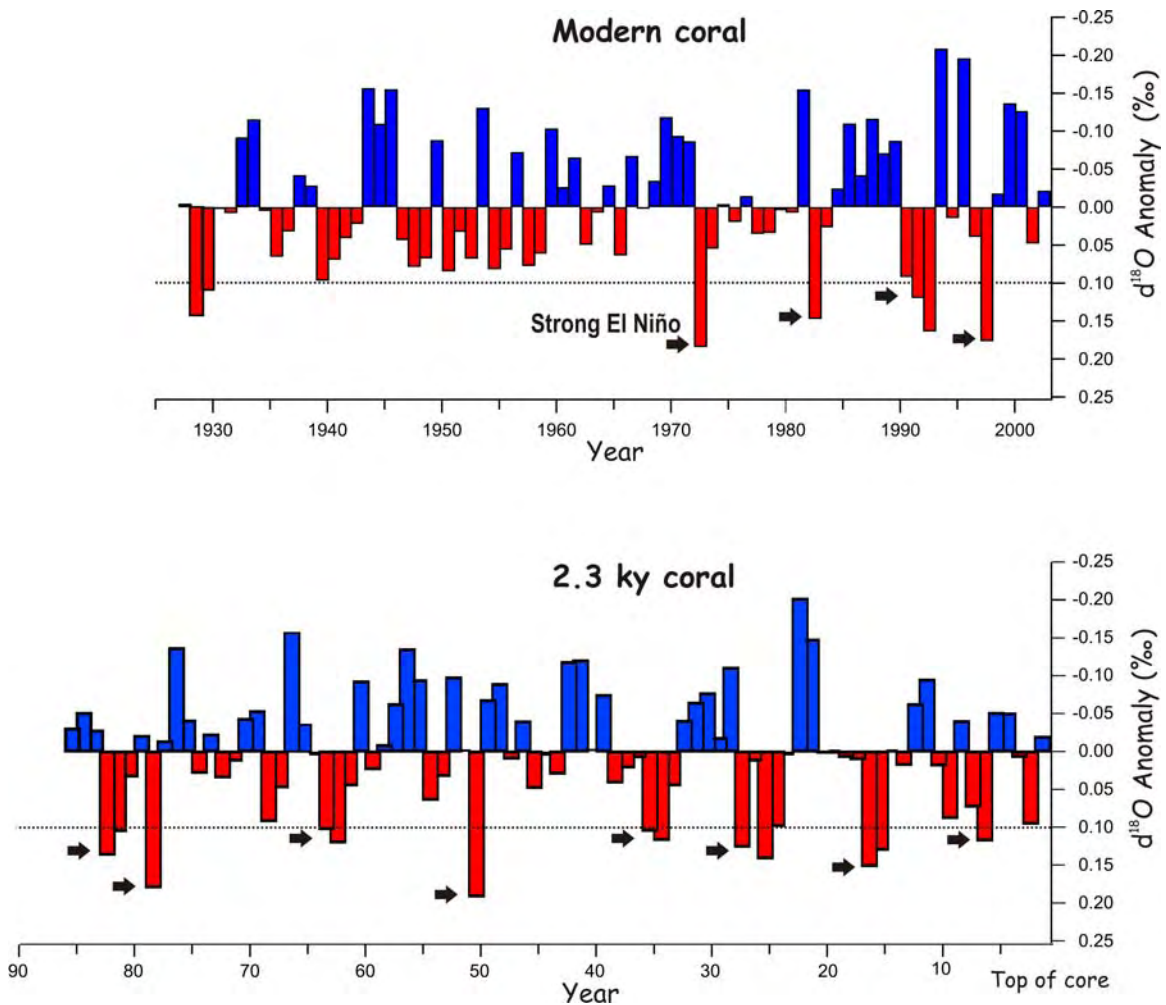


Figure 1. $\delta^{18}\text{O}$ anomalies in the modern (top) and 2.3 ky (bottom) coral records from Maydolong, eastern Samar, Philippines. Black arrows indicate strong El Niño events. The threshold for strong events is marked by the dashed line

Geochemical ecology of a high latitude coral: establishing high resolution records to evaluate potential as a paleoclimate archive

Samantha N Burgess¹

¹Research School of Earth Sciences, The Australian National University, Canberra, 0200 ACT, Australia

Corals growing in high latitude waters are sensitive to changes in climate, especially seasonal fluctuations in sea surface temperature. The annual nature of density bands of *Plesiastrea versipora* were verified using U/Th ages derived from multi-collector ICP-MS analyses and the resulting extension rates varied from an average of 1.2 mm yr⁻¹ to 9 mm yr⁻¹ for different colonies located within the same reef. High resolution (~fortnightly) laser-ablation ICP-MS analyses of established paleo-temperature proxies including B/Ca, Mg/Ca, Sr/Ca and U/Ca and milled $\delta^{18}\text{O}$ and $\delta^{13}\text{C}$ analyses were obtained from several cores of *P. versipora* from Gulf St Vincent (34.5°S) and Spencer Gulf (35°S), South Australia. Elemental compositions were compared to *in situ* sea surface temperature (SST) and satellite (IGOSS) records. There was a significant correlation between $\delta^{18}\text{O}$ and Ba/Ca ($r^2 = 0.82$) and a significant inverse correlation was observed between $\delta^{18}\text{O}$ and $\delta^{13}\text{C}$.

Sea surface temperature linear regressions provided the following calibration equations:

$$\delta^{18}\text{O} = 0.9 - 0.16 \text{ SST } (^{\circ}\text{C}), r^2 = 0.77.$$

$$\text{Ba/Ca } (\mu\text{mol/mol}) = 8.35 - 0.13 \text{ SST } (^{\circ}\text{C}), r^2 = 0.65.$$

$$\text{Sr/Ca } (\text{mmol/mol}) = 10.55 - 0.06 \text{ SST } (^{\circ}\text{C}), r^2 = 0.62.$$

$$\text{B/Ca } (\text{mmol/mol}) = 0.96 - 0.13 \text{ SST } (^{\circ}\text{C}), r^2 = 0.55.$$

$$\text{U/Ca } (\mu\text{mol/mol}) = 2.3 - 0.16 \text{ SST } (^{\circ}\text{C}), r^2 = 0.6.$$

Barium may not have been recognised as a temperature covarying proxy in previous studies due to the smaller temperature range for lower latitude environments (~5°C versus 12°C for this study) and other factors masking the Ba signal such as terrestrially-derived or upwelled sources. However, it could not be determined whether the covariance was directly related to temperature or another factor which varies with winter periods such as phytoplankton blooms or increased oceanic mixing.

Other trace elements analysed gave an indication of both the nutrient availability (P and Mn) and terrestrially derived pollutants (V, Y, Mo, Sn and Pb) correlating strongly with luminescent bands. Several of the stronger luminescent bands coincide temporally with known oil spills at a nearby port refinery and research is ongoing to determine if this is the point source of pollution. These data taken together suggest that *P. versipora* can provide valuable paleoclimate information in high-latitude environments, recording large seasonal variation in both temperature and productivity regimes with high fidelity and may also be employed to reconstruct anthropogenic activity.

Regional and continental-scale erosion in the Yangtse River catchment, China, from cosmogenic nuclides

John Chappell¹ Keith Fifield², Hongbo Zheng³

¹Research School of earth Sciences, The Australian National University, Australia

²Research School of Physical Sciences and Engineering, The Australian National University, Australia

³School of Marine and Earth Science, Tongji University, Shanghai

Regional erosion arising from land clearing undeniably has increased in wide tracts of agricultural land but human impacts on erosion are less clear for high mountain areas, where natural erosion rates are high. With a long history of intensive human occupation, the Yangtse River basin in China is an ideal test case. The river rises in the northeast Tibetan Plateau and descends through ranges of very high mountains, passing eastwards across China, collecting water and sediment from a series of tributaries, before passing through the Yangtse Delta into the East China Sea. To determine regional erosion prior to the impact of agriculture, we used measurements of cosmogenic nuclides in eroding rock surfaces and sedimentary quartz grains. These nuclides are produced by cosmic rays impacting common nuclei in surface rocks; their abundance decreases with increasing erosion, and this signature is preserved in sediment from the eroding surfaces. Results from high mountain catchments of the western Yangtse River basin are similar to rates derived from sediment gauges along the river system and range to over 700 m Ma⁻¹, while cosmogenic determinations from headwater tributaries on the northeast Tibetan plateau gave much lower long-term rates, around 20–30 m Ma⁻¹. For lowland and lesser mountains in the eastern reaches of the Yangtse River catchments, rates from cosmogenic nuclides were around 30 m Ma⁻¹, which is about half the present-day regional average derived from sediment gauges. In summary, human land use has sensibly increased catchment-scale erosion in eastern China, but regionally the effect in high mountains of the western Yangtse River appears to be minor.

The history of aridity in Australia

John Chappell¹, Ed Rhodes¹, Brad Pillans¹, Toshiyuki Fujioka¹, Masahiko Honda¹,
John Magee¹ and Kath Fitzsimmons²

¹*Research School of earth Sciences, The Australian National University, Australia*

²*Department of Earth and Marine Sciences, The Australian National University, Australia*

Australia became progressively drier while it drifted northwards in the Cenozoic but the picture is complex and wet periods punctuated the drying trend. Regolith, groundwater and salts actively interact with the landscape and with each other, during these climatic changes. The project is a study of Upper Cenozoic climate changes in the Australian interior and their effects on the regolith. Targets include aeolian landscapes (longitudinal dunefields, source-bordering dunes and lunettes), stony desert and dissected silcrete and ferricrete landforms, surfaces with thick regolith and deep weathering with mine-pit access, and palaeochannel systems.

The broad timing of major phases of silcrete and ferricrete formation followed by landscape dissection and falling groundwater have been established by palaeomagnetic dating of ferruginous regolith dating of relict fluvial deposits. A key study concerns the age structure of major dunefields and stony deserts, which are the most widespread regolith materials in the arid zone. The ages of other arid-climate deposits including aeolian silt mantles are also being determined.

Stony deserts are durable indicators of aridity but hitherto have not been directly dated. We have successfully determined the age of the stony deserts, using ²¹Ne and ¹⁰Be produced in surface rocks by cosmic rays, and have shown that Australian stony deserts formed 2–4 Ma ago, at the time when global cooling initiated the Quaternary ice ages and intensified aridity induced major landscape changes in central Australia. To achieve this, we developed new methods for determining cosmogenic ²¹Ne in the presence of neon components from other sources. Using our cosmogenic toolkit (²¹Ne, ¹⁰Be and ²⁶Al), we have also found that the Simpson Desert dunefield has existed for at least the last 1.5 Ma, whereas optical dating (OSL) of drill-core samples shows that individual dunes were active during global cold episodes of the Late Pleistocene ice ages, when many dunes were extensively reworked. In short, the cosmogenic data have allowed us to determine the antiquity of Australia's most characteristic arid landforms, while OSL dating allows us to assess the degree to which arid landscape processes have been episodic.

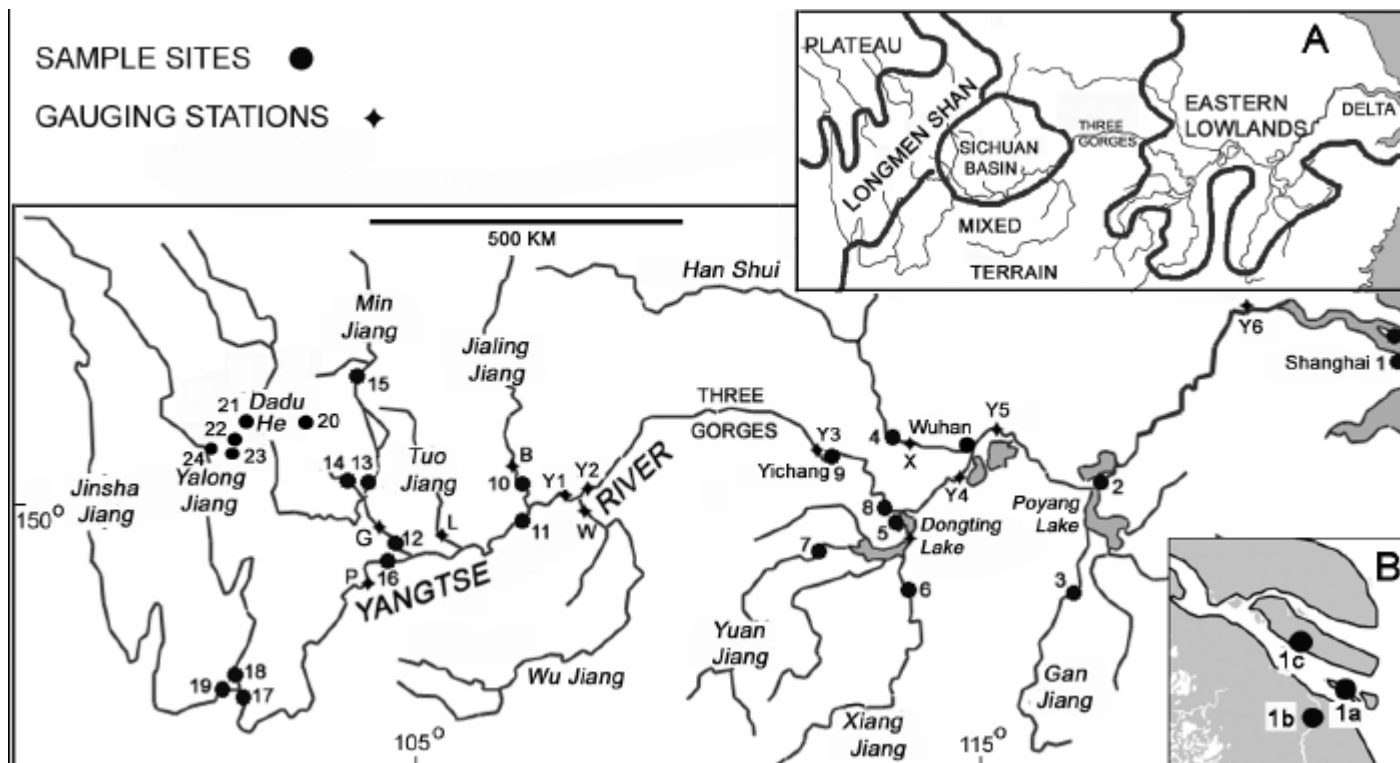


Figure 1 Regional erosion in China – major river sampling sites in China

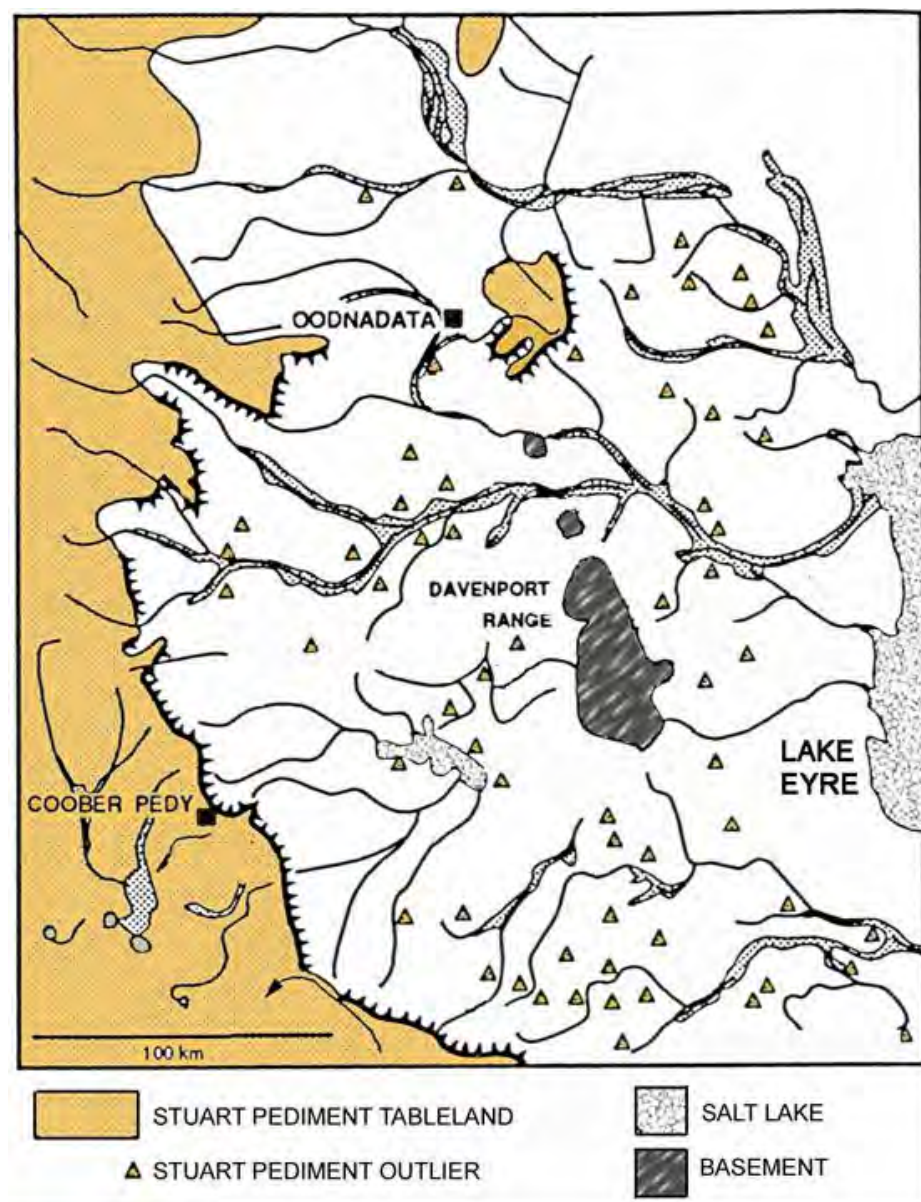


Figure 2 History of aridity: sampling site for cosmogenic determination of stony desert ages

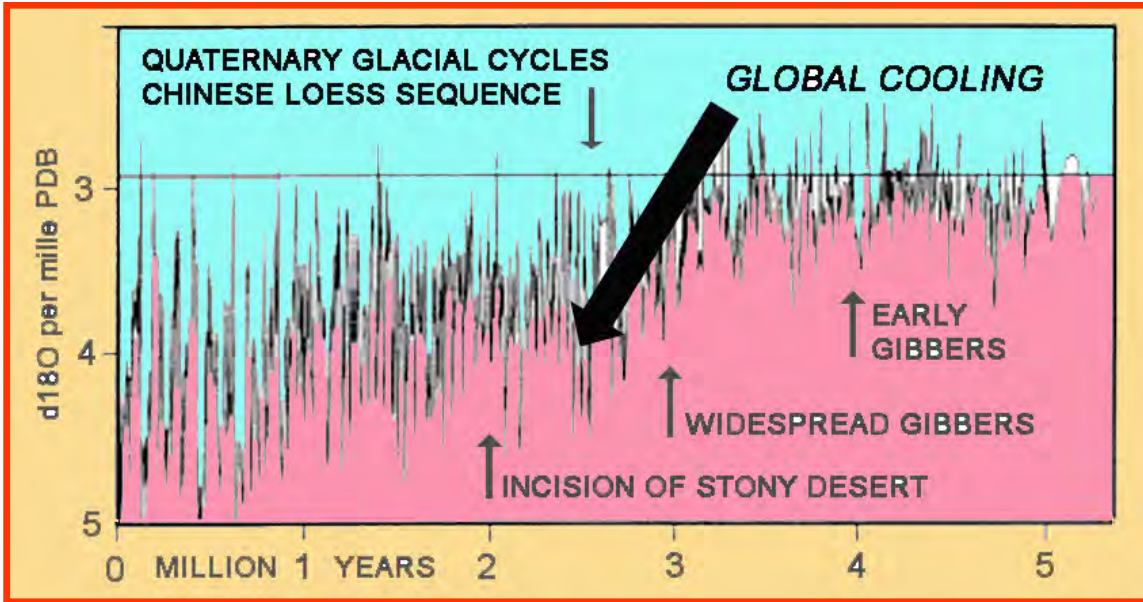


Figure 3. Timing of the formation of stony "gibber" pavements in central Australia

Micro-sampling of skeletal mass accumulation in the tissue layer of *Porites*: implications for paleo-environmental reconstruction

Gavin B. Dunbar¹ & Michael K. Gagan¹

¹ Research School of Earth Sciences, The Australian National University, Canberra ACT 0200, Australia

Stable isotope and trace element geochemical records obtained from *Porites* corals are an important source of quantitative paleoclimate information. The depth over which aragonite is deposited within the growing tissue layer of these corals determines the amount of biological smoothing imparted to environmental signals that are preserved in their skeletons. If these distortions are not accounted for when transforming raw data into estimates of sea surface temperature (SST) and salinity, substantial inaccuracies in paleoclimatic reconstruction may result. In order to estimate the magnitude of this problem we have measured the mass of aragonite in consecutive 200 μm thick samples through the upper 10-12 mm of five corals from four locations and have found that growth can be characterised by two patterns: “sharp” growth when all aragonite is deposited in the upper 2mm of the coral skeleton; and, “smooth” growth when aragonite is deposited throughout the tissue layer, typically 6 to 10 mm in thickness (Fig.1). Ningaloo is the only coral that shows a smooth growth pattern in our dataset.

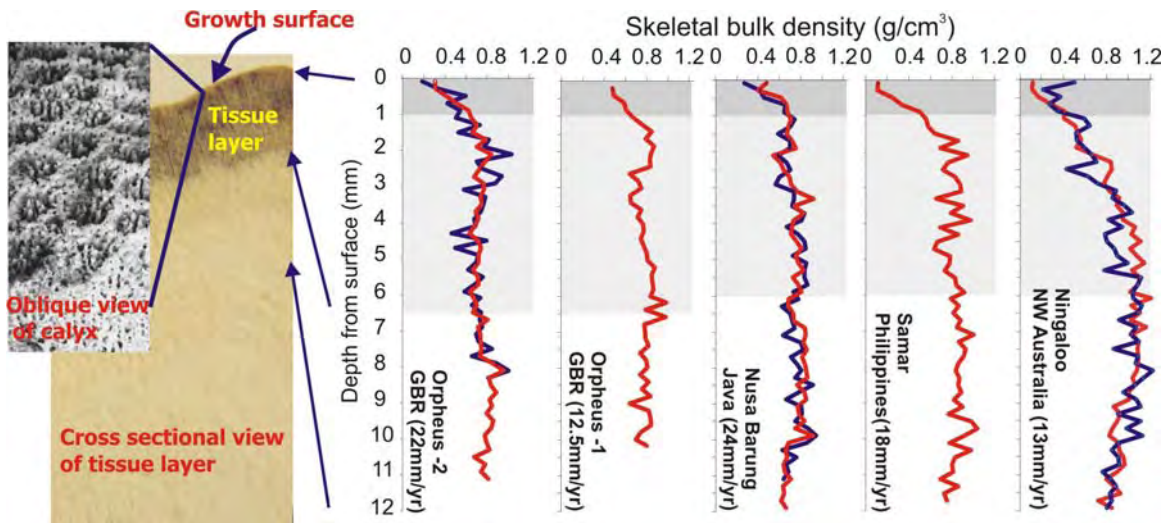


Figure 1. Plots showing variations in bulk density with depth for five corals. Where possible each milling transect was replicated (blue curves). Note that with the exception of Ningaloo, systematic increases in density are confined to the upper 2 mm of each coral.

By adopting two smoothing functions (for sharp and smooth growth measurements) to a sine wave (which approximates the kind of variability evident in many environmental signals) it is possible to model the degree of

attenuation of environmental cycles of different periods for different rates of coral growth (Fig. 2).

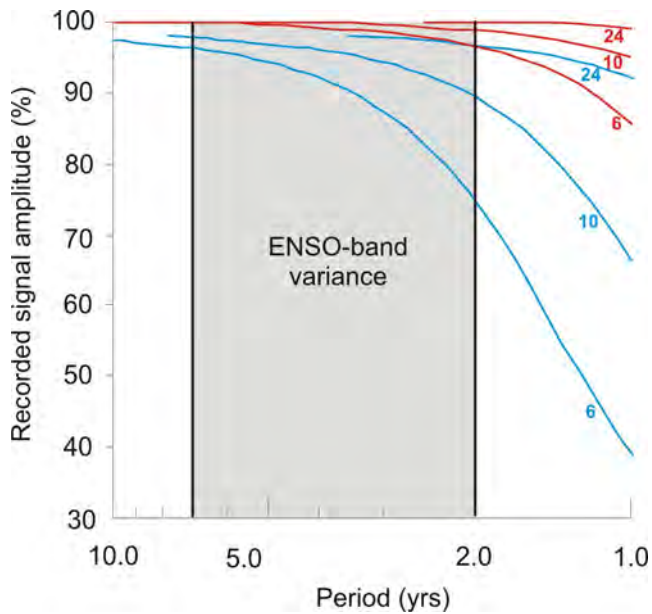


Fig. 2. The attenuation of sine waves with periods between 1 and 10 years for modelled coral growth at 6, 10 and 24 mm/yr (labelled on graph) as a result of bio-smoothing. Results are shown for “sharp” (red) and “smooth” (blue) calcification patterns as defined in the text.

This model suggests attenuation of annual and longer cycles is limited to <10% for most *Porites* corals over a wide range of growth rates, consistent with published environmental records that assume limited smoothing (e.g. Alibert & McCulloch, 1997; Gagan et al., 1994; 1998; Wellington et al., 1996). However, where aragonite deposition takes place throughout the tissue layer (“smooth” – type calcification) significant smoothing of environmental signals will occur. The difficulty for researchers is that this type of growth does not appear to be environment or species specific and cannot be determined directly in fossil corals where the outer coral skeleton is typically not preserved.

References

- Alibert, C. & McCulloch, M. T., 1997. Strontium/calcium ratios in modern *Porites* corals from the Great Barrier Reef as a proxy for sea surface temperature: Calibration of the thermometer and monitoring of ENSO. *Paleoceanography*, 12, 345-363.
- Gagan, M. K., Chivas, A. R., & Isdale, P. J., 1994. High-resolution isotopic records from corals using ocean temperature and mass-spawning chronometers: *Earth and Planetary Science Letters*, 121, 549–558.
- Gagan, M.K., Aylife, L.K., Hopley, D., Cali, J.A., Mortimer, G.E., Chappell, J., McCulloch, M.T. & Head, M.J., 1998. Temperature and surface-ocean water balance of the mid-Holocene tropical western Pacific. *Science*, 279, 1014-1018.
- Wellington, G. M., Dunbar, R. B. & Merlen, G., 1996. Calibration of stable isotope signatures in Galapagos corals. *Paleoceanography*, 11, 467-480.

Dating of Australian arid landforms using cosmogenic Ne/Be exposure dating

Toshiyuki Fujioka¹, John Chappell¹, Masahiko Honda¹, Igor Yatssevich¹, Keith Fifield² and Derek Fabel³

¹*Research School of Earth Sciences, The Australian National University, Australia*

²*Research School of Physical Sciences and Engineering, The Australian National University, Australia*

3

In principle, the history of aridity in Australia can be determined by dating the landforms and deposits that form under arid conditions. Over 75% of Australian continent is semi-arid to arid, and stony deserts are a major feature of these regions. Stony deserts are characterized by a surface monolayer of pebble- to cobble-sized rocks (gibbers) which, once formed, tend to remain in place with little subsequent modification. Some gibbers were formed *in situ* by breakdown of their underlying parent rock; others were fluvially transported to their present positions. We propose that the age of the stony deserts can be estimated by determining the time when gibbers were formed.

In this study, we measured cosmogenic nuclides, ²¹Ne and ¹⁰Be, in silcrete gibber samples collected from stony deserts in central Australia, to determine their exposure ages (Fujioka et al., 2005). The use of cosmogenic ²¹Ne, which is a stable cosmogenic nuclide, allows us to examine the history of gibber formation beyond the exposure dating range of ¹⁰Be, which limited by radioactive decay to a few million years. We note that we have developed a reliable method for determining cosmogenic ²¹Ne in the presence of ²¹Ne from other sources.

Apparent exposure ages calculated from the concentrations of cosmogenic ²¹Ne and ¹⁰Be in the gibber samples from stony deserts west of Lake Eyre in northern South Australia ranged from two to five million years, but the apparent ²¹Ne ages are significantly greater than the apparent ¹⁰Be ages. The discordance indicates that the parent silcrete, from which the gibbers were derived, was buried at a shallow depth for a considerable period before being stripped and broken into gibbers. Calculations indicate that the silcrete was stripped and gibbers began to form around 4 m.y. ago, and that gibber-mantled tablelands were widely developed and dissected around 2-3 m.y. ago. These ages correspond to the time of late Cenozoic global cooling inferred from benthic oxygen isotope records in marine sediment cores (Figure).

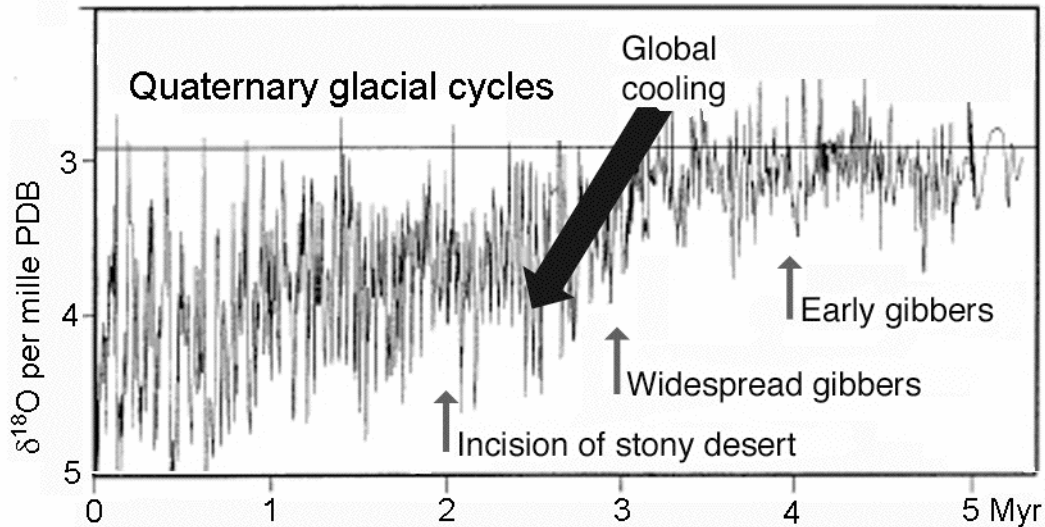


Figure. Relationship between the timing of the formation of gibber plains in Australia and benthic oxygen isotope record in marine sediment cores (east Atlantic Ocean Drilling Program Site 659; Tiedemann et al., 1994). Gibber ages (arrows) indicate that Australia's stony deserts formed during late Cenozoic global cooling as seen in marine sediments, that led to Quaternary glacial cycles. PDB: Peedee belemnite.

References

- Fujioka T., Chappell J., Honda M., Yatsevich I, Fifield K., and Fabel D. (2005) Global cooling initiated stony deserts in central Australia 2-4 Ma, dated by cosmogenic ^{21}Ne - ^{10}Be . *Geology* **33**, 993-996.
- Tiedemann R., Sarnthein M., and Shackleton N. J. (1994) Astronomic timescale for the Pliocene Atlantic $\delta^{18}\text{O}$ and dust flux records of Ocean Drilling Program Site 659. *Paleoceanography* **9**, 619-638.

Long-term perspectives on monsoon dynamics, environmental shifts, and early human impacts in southern Australasia

Michael K. Gagan¹

¹ *Research School of Earth Sciences, The Australian National University, Canberra, ACT, 0200, Australia*

The Earth Environment Stable Isotope Laboratory contributed to advances along several fronts in 2005 to improve our understanding of the late Quaternary history of the Australasian monsoon, palaeo-environmental shifts, and early human impacts in southern Australasia. Two papers describing new coral geochemical records were published in *Earth and Planetary Science Letters* (Sun et al., 2005) and *Science* (Pelejero et al., 2005). Sun et al. (2005) developed a 54-year long, high-resolution skeletal $\delta^{18}\text{O}$ record for a massive *Porites* sp. coral from Hainan Island, South China Sea, to investigate East Asian monsoon variability during summer and winter ~4,400 calendar years ago. The East Asian monsoon is a prominent feature of the tropical general circulation that impacts the lives of ~25% of the world's population, yet its year-to-year variability is still difficult to predict. The coral record shows that ENSO-related sea-surface temperature anomalies were well established in the South China Sea by ~4,400 years ago, despite ENSO variability being significantly weaker in the Pacific region at that time. Our findings indicate that the monsoon is sensitive to forces, other than ENSO, that could act as alternative drivers of interannual monsoon variability. If this is the case, greater interannual climate variability could accompany the strengthening of the Asian monsoon predicted to occur during the 21st century as transient greenhouse warming preferentially warms Eurasia, even if ENSO perturbations remain relatively stable.

Pelejero et al. (2005) reported on a new coral record for a *Porites* sp. from Flinders Reef in the Coral Sea, which provides a continuous time-series of seawater $\delta^{13}\text{C}$ and pH commencing in 1708 AD, well before the start of the industrial revolution. The most striking feature of the coral $\delta^{13}\text{C}$ curve is the trend towards lower values commencing in 1800 AD. The secular decrease in coral $\delta^{13}\text{C}$ can be ascribed to the Suess effect, which is due to uptake by the oceans of atmospheric CO_2 that has been progressively depleted in ^{13}C by the combustion of fossil fuels. The likely consequence of this absorption of anthropogenic CO_2 is that the surface-ocean will become progressively acidic. The impact of progressive ocean acidification on marine ecosystems is unclear, but will likely depend on species adaptability and the rate of change in seawater pH relative to its natural variability. To address this issue, coral $\delta^{11}\text{B}$ was used as a "palaeo-pH meter" to show that Flinders Reef seawater pH has varied over ~50 year cycles in tandem with the Interdecadal Pacific

Oscillation. The results suggest that natural cycles in reef-water pH will modulate the impact of future ocean acidification on coral reef ecosystems.

In 2005, the Earth Environment Group's progress and potential in the area of high-resolution coral-based palaeoclimatology was rewarded through new research funding for the next five years (2006-2010) from the Australian Research Council Discovery grants scheme. This stream of research, The Indian Ocean Dipole, Australasian drought, and the great-earthquake cycle: Long-term perspectives for improved prediction, will be driven by team-members from RSES, Indonesian Institute of Sciences, Australian Institute of Marine Science, CSIRO, University of Wisconsin, and Caltech. The team will combine cutting-edge geochemical microanalysis of recently discovered corals with world-leading palaeoclimate modelling to quantify the Indian Ocean Dipole system, and mechanistic links with Australasian drought, over the past 130,000 years. Our other primary goal is to develop an innovative submarine earthquake hindcasting technique that will improve understanding of the recurrence intervals of great-earthquakes and tsunamis in Australasia.

In addition to our contributions to the new ANU Marine Science Initiative, the Earth Environment Stable Isotope Laboratory also contributed to the production of novel terrestrial palaeoclimate records. The highlight of these was the paper published by Miller et al. (2005) in *Science* describing a unique 140,000-year time-series of dietary $\delta^{13}\text{C}$ in fossil eggshells of the Australian emu and extinct *Genyornis newtoni*. This comprehensive data set represents the culmination of 15 years of field collecting by John Magee (DEMS, ANU) and Gifford Miller (U. Colorado) and more than 1,400 $\delta^{13}\text{C}$ analyses on a subset of over 100,000 eggshell fragments. The 140,000-year record of dietary $\delta^{13}\text{C}$ documents a permanent reduction in food sources available to the Australian emu beginning about the time of human colonisation of Australia (55-45 ka). The unprecedented shift in dietary $\delta^{13}\text{C}$ is best explained by human firing of landscapes and rapid conversion of a drought-adapted mosaic of trees, shrubs, and nutritious grasslands to the modern fire-adapted desert scrub. Given this profound ecosystem shift, animals that could adapt survived, while those that could not became extinct.

Johnson et al. (2005) analysed the Holocene portion of the emu eggshell $\delta^{13}\text{C}$ record from Lake Eyre, South Australia, and found that the proportion of C_4 plants in emu diets has been reduced by ~20% over the last 200 years at Lake Eyre. Probable causes of the recent reduction in C_4 plants at Lake Eyre include overgrazing by both introduced and native animals, increasing drought, and a change in fire regime beginning in the late 1890s. The eggshell $\delta^{13}\text{C}$ record provides the first evidence for major environmental change at Lake Eyre soon after Europeans settled the arid zone.

Treble et al. (2005) made significant progress in understanding the nature of seasonal-scale $\delta^{18}\text{O}$ and $\delta^{13}\text{C}$ variations in speleothems via high-resolution analysis of an 81-year old stalagmite from Moondyne Cave, southwest Australia. For this study, seasonal variations in calcite $\delta^{18}\text{O}$ were measured in situ by ion microprobe at UCLA, whilst interannual variations of $\delta^{18}\text{O}$ and $\delta^{13}\text{C}$ were measured by gas-source mass spectrometry at RSES. The key point is that the seasonal range in speleothem $\delta^{18}\text{O}$ at Moondyne Cave is larger than any interannual-decadal variation in $\delta^{18}\text{O}$ observed in the record. This finding raises the possibility that even small changes in the relative masses of speleothem calcite deposited in winter and summer could produce significant shifts in mean $\delta^{18}\text{O}$ and $\delta^{13}\text{C}$ determined by "bulk sampling" of speleothems. Therefore, long-term trends in speleothem records may have a complex relation to climate, particularly those for shallow cave sites where seasonal variations in geochemical tracers are large, including most of the sub-tropical monsoon belts and mid- to high-latitudes with distinctly seasonal rainfall.

In 2005, the Earth Environment Group was awarded a 3-year Australian Research Council Discovery grant (2006-2008) to pursue the production of novel speleothem records in Indonesia. This new stream of research, Monsoon extremes, environmental shifts, and catastrophic volcanic eruptions: Quantifying impacts on the early human history of southern Australasia, will be pursued by team-members from RSES, Indonesian Institute of Sciences, University of Queensland, University of Newcastle, and NASA. The team will use novel geochemical microanalysis of precisely dated speleothems from southern Indonesia and state-of-the-art palaeoclimate modelling to document, for the first time, millennial to seasonal extremes in monsoonal rainfall, environmental shifts, and catastrophic volcanic eruptions over the past 150,000 years. These new records will provide the basis for evaluating the relative influence of natural and human-induced environmental change on early human dispersal in Australasia, including the surprisingly recent extinction of *Homo floresiensis* ("the Hobbit").

In summary, palaeo-records provide valuable insights into how climate variability and change has and could affect our marine and terrestrial environments. Readers who are interested in what Quaternary palaeo-science can reveal about climate change and its potential impacts in Australia should refer to the comprehensive report compiled by Harle et al. (2005) for the Australian Greenhouse Office.

References

- Gagan, M.K., Hantoro, W.S., Natawidjaja, D.H., Lough, J.M., Meyers, G.A., Liu, Z. and K. Sieh. The Indian Ocean Dipole, Australasian drought, and the great-earthquake cycle: Long-term perspectives for improved prediction. ARC Discovery Grant DP0663227 (2006-

- 2010).
- Gagan, M.K., Zhao, J.-x., Drysdale, R.N., Hantoro, W.S. and G.S. Schmidt. Monsoon extremes, environmental shifts, and catastrophic volcanic eruptions: Quantifying impacts on the early human history of southern Australasia. ARC Discovery Grant DP0663274 (2006-2008).
- Harle, K., Etheridge, D., Whetton, P., Jones, R., Hennessy, K., Goodwin, I., Brooke, B., van Ommen, T., Barbetti, M., Barrows, T., Chappell, J., De Deckker, P., Fink, D., Gagan, M., Haberle, S., Heijnis, H., Henderson-Sellers, A., Hesse, P., Hope, G., Kershaw, P. and N. Nicholls (2005). Building a future on knowledge from the past: what palaeo-science can reveal about climate change and its potential impacts in Australia. Report for the Australian Greenhouse Office, 46 p.
- Johnson, B.J., Miller, G.H., Magee, J.W., Gagan, M.K., Fogel, M.L. and P.D. Quay (2005). Carbon isotope evidence for abrupt grassland loss coincident with European settlement of Lake Eyre, South Australia. *The Holocene*, 15(6): 888-896.
- Miller, G.H., Fogel, M.L., Magee, J.W., Gagan, M.K., Clarke, S.J. and B.J. Johnson (2005). Ecosystem collapse in Pleistocene Australia and a human role in megafaunal extinction. *Science*, 309: 287-290.
- Paper highlighted in *Science Perspectives*: Johnson, C.N. (2005). The remaking of Australia's ecology. *Science*, 309: 255-256.
- Pelejero, C., Calvo, E., McCulloch, M.T., Marshall, J.M., Gagan, M.K., Lough, J.M. and B.N. Opdyke (2005). Preindustrial to modern interdecadal variability in coral reef pH. *Science*, 309: 2204-2207.
- Sun, D., Gagan, M.K., Cheng, H., Scott-Gagan, H., Dykoski, C.A., Edwards, R.L. and R. Su (2005). Seasonal and interannual variability of the mid-Holocene East Asian monsoon in coral $\delta^{18}\text{O}$ records from the South China Sea. *Earth and Planetary Science Letters*, 237: 69-84.
- Treble, P.C, Chappell, J., Gagan, M.K., McKeegan, K.D. and T.M. Harrison (2005). In situ measurement of seasonal $\delta^{18}\text{O}$ variations and analysis of isotopic trends in a precisely dated speleothem from southwest Australia. *Earth and Planetary Science Letters*, 233: 17-32.

In situ U-series microanalysis of fossil human remains

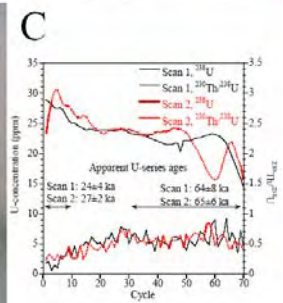
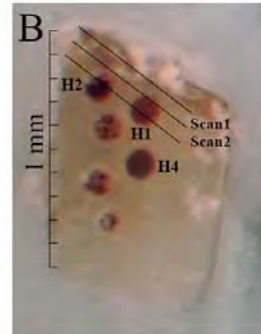
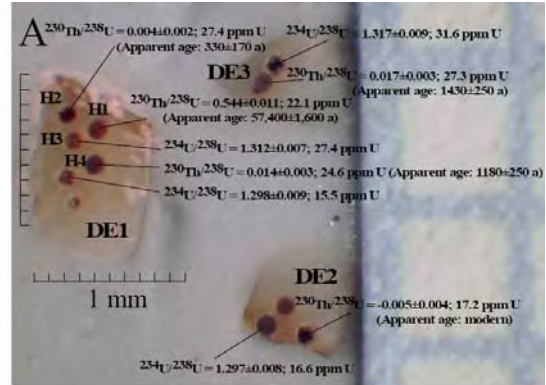
Rainer Grün^{1,2}, Stephen Eggins¹ and Julia Maroto³

¹Research School of Earth Sciences, The Australian National University, Canberra, ACT 0200, Australia

²Research School of Pacific and Asian Studies, The Australian National University, Canberra, ACT 0200, Australia

³Area de Prehistoria, Universitat de Girona, Spain

When dating human remains, it is necessary to keep any destruction to an absolute minimum. During an ESR dating study on the Neanderthal Banyoles mandible, it was necessary to analyse the U-series isotopes on dentine adjacent to the enamel piece that had previously been analysed by ESR. We were able to obtain three small dentine fragments (DE1 to DE3), the largest had a maximum dimension of 1 mm (Figure 1). These were analysed for U-series isotopes by drilling holes with the laser (see Figure 6A) and subsequent analysis with the Neptune multicollector ICP MS. Because of the configuration of the Neptune with a single central ion counter, this can either be used for the measurement of ^{234}U or ^{230}Th . Thus the material ablated from the holes give either $^{234}\text{U}/^{238}\text{U}$ or $^{230}\text{Th}/^{238}\text{U}$ ratios. The



The $^{234}\text{U}/^{238}\text{U}$ ratio is very homogeneous, four measurements yielding a mean of 1.306 ± 0.009 (1- σ s.d.). In contrast, the $^{230}\text{Th}/^{238}\text{U}$ ratios and the U concentrations varied greatly: the $^{230}\text{Th}/^{238}\text{U}$ ratio between virtual background and 0.544 ± 0.011 , and the U-concentration between about 15.5 and 32 ppm. The large variation of the $^{230}\text{Th}/^{238}\text{U}$ values is astonishing, particularly considering that the high U-concentrations and the extremes measured on the material ablated from holes H1 and H2 in dentine fragment DE1 are less than 0.2 mm apart. Because of the surprising small scale variation in the $^{230}\text{Th}/^{238}\text{U}$ values, two laser ablation scans were run across the top of DE1 in the same track (the second scan ablating material from deeper into the sample). The approximate positions of the scans are indicated in Figure 1B. Note that the three-dimensional symmetry of the sample is somewhat different than can be estimated from the surface shown in Figure 1B. The first scan did not penetrate either of holes H1 and H2, while the second scan ran completely through H1 (causing the apparent drop in U-concentration in Scan 2; see Figure

1C) and just the top of H2. It can be clearly seen that the U-concentrations increase from H1 to H2, while the $^{230}\text{Th}/^{238}\text{U}$ values decrease, confirming the observations made from the holes. The average U-concentration of the dentine is 24 ± 5.5 ppm. Because of the small-scale variations in the $^{230}\text{Th}/^{238}\text{U}$ ratio, it is difficult to estimate an average $^{230}\text{Th}/^{238}\text{U}$ value for the dentine. All results below 0.5 mm below the surface (i.e. hole H4 and below) and the other two dentine fragments, whose exact spatial relationship to DE1 cannot be reconstructed, correspond to U-series ages of younger than about 1400 years (apparent U-series age on DE3).

The dentine clearly underwent at least two U-accumulation stages, one several tens of thousands of years ago, possibly during the initial burial phase, and a second one, perhaps starting about 1400 years ago and continuing to very recent times. This later U-accumulation phase was most likely initiated by the activation of percolating waters from historic quarrying and drainage activities. In 812, Abbot Bonitus founded the monastery of Sant Esteve on what was then waste land. To control the level of the lake, the monks laid a network of irrigation ditches which turned an uninhabitable place into an agricultural and industrial area which would soon become prosperous. In the 13th and 14th centuries, the area underwent great expansions with the establishment of varied industries.

With conventional analytical techniques we may have been able to obtain one single U-series result on the combined dentine. The micro analytical capabilities of the laser ablation system do not only allow repeated, detailed analyses of the material, they also give hitherto unobtainable insights into the mechanism of U-migration in dental material.

Proliferation and Demise of Deep-Sea Corals in the Mediterranean During the Younger Dryas

Malcolm T. McCulloch¹, Marco Taviani², Paolo Montagna³, Graham Mortimer¹
and Alessandro Remia²

¹ *Research School of Earth Sciences, Australian National University, Canberra, Australia.*

² *ISMAR-CNR, via Gobetti 101, I-40129 Bologna, Italy. 19/01/2006 19/01/2006*

³ *ICRAM, Italian Institute for Marine Research, Rome, Italy*

Deep-sea, cold-water corals have been recognised in the Mediterranean for some time, but it is only in the last several years that oceanographic surveys have begun to reveal their full extent and distribution. Living specimens are relatively rare, with the main reef framebuilders, the colonial *Madrepora oculata* and the solitary coral *Desmophyllum dianthus* being the most widespread, while the colonial *Lophelia pertusa* is known in only several locations. Although deep, cold-water corals are now in recession, pre-modern or sub-fossil examples were much more abundant, occurring throughout the Mediterranean basin (Figure 1) either as in situ assemblages, patch reefs, or as coral-bearing sedimentary mounds, at depths ranging from 250 to 3000 m. Many of these latter sites are now covered in a veneer of muddy sediment which together with their excellent state of preservation indicates that they were exposed on the sea-floor for only a limited time before burial. Thus in contrast to fossil occurrences in the N. Atlantic where specimens are commonly patinated by thin films of Fe-Mn, in the Mediterranean the post-LGM occurrences found on the continental shelves, still often maintain their original luster, making it difficult to discriminate between sub-fossil and modern sample.

In the Mediterranean all the major taxa (*Lophelia pertusa* *Madrepora oculata*, *Desmophyllum dianthus*,) are represented in sub-fossil and pre-modern patch reefs and coral mounds at intermediate water-depths. Specimens from the western and central Mediterranean give a surprisingly narrow range of U-Th ages, with the majority falling between 13,500 to 11,000 yrs BP, indicating that deep-sea corals flourished during the cooler more glacial-like conditions of the Younger Dryas (YD) period. Radiocarbon ages from these corals show that since the Last Glacial Maximum (LGM), the intermediate depth waters of the Mediterranean generally had similar $\Delta^{14}\text{C}$ compositions to surface waters (Figure 2), except for a narrow period in the early YD ($12,500 \pm 100$ yrs) when corals approached atmospheric-like compositions. This followed the peak in ^{14}C production in the early YD and implies a very brief, ~200 yr period, of extremely rapid ventilation. Prolific deep-sea coral growth ended abruptly at ~11,000 yrs BP, ~500 yrs after the cessation of the YD with many of the deposits being draped in a thin veneer of mud. Consequently, their demise was probably due to a combination of factors, the rapid 6-8°C rise in sea surface temperatures that occurred at the end of the YD, together with the unusually high sedimentation in

the Mediterranean caused by a massive increase in river discharge from glacial meltwater pulses associated with the termination of the YD.

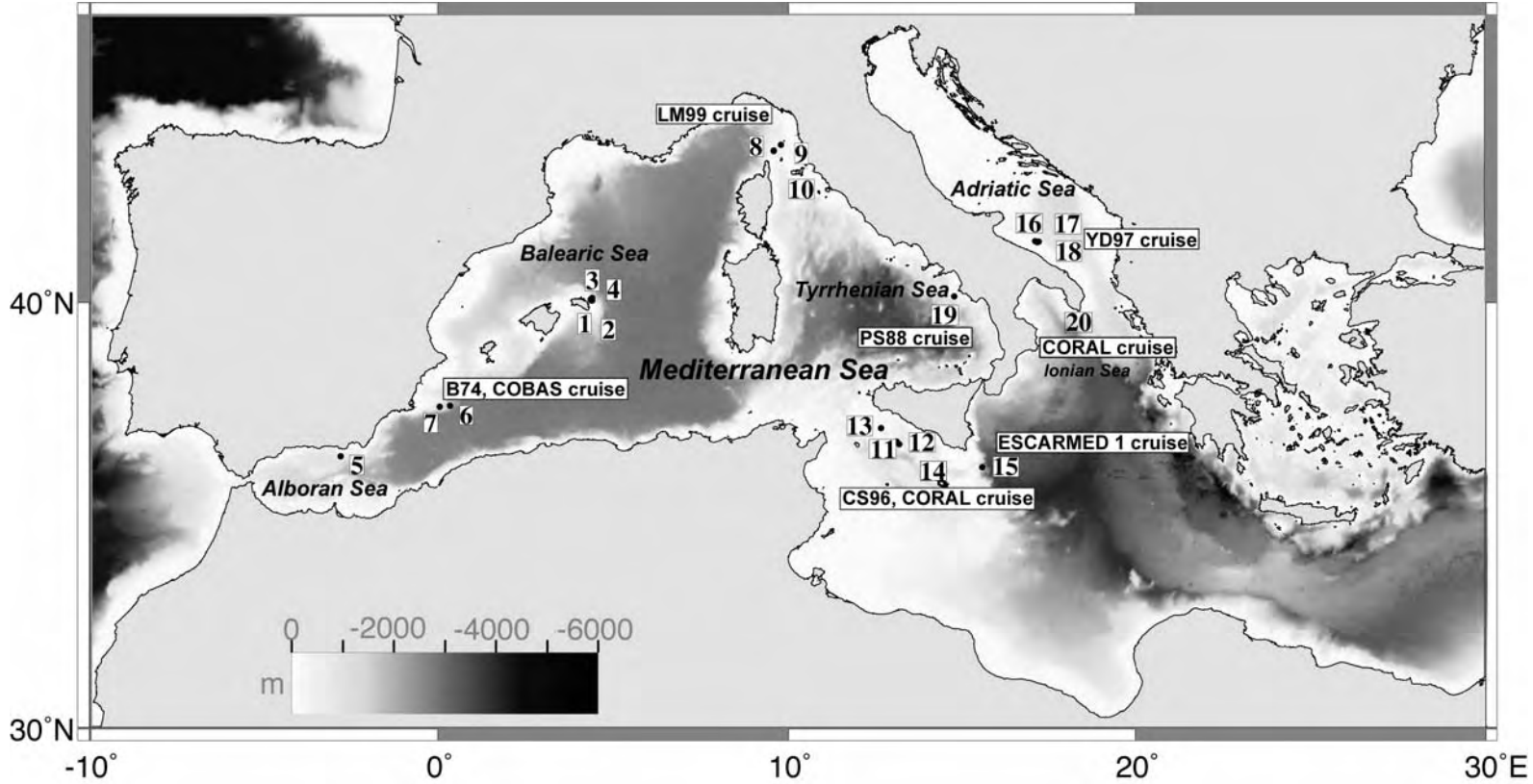


Figure 1. Map showing localities of deep-sea coral sites from the Mediterranean basin. The sample cruises are shown in closed rectangles and the number key to individual samples is given in Table 1 (supp material)

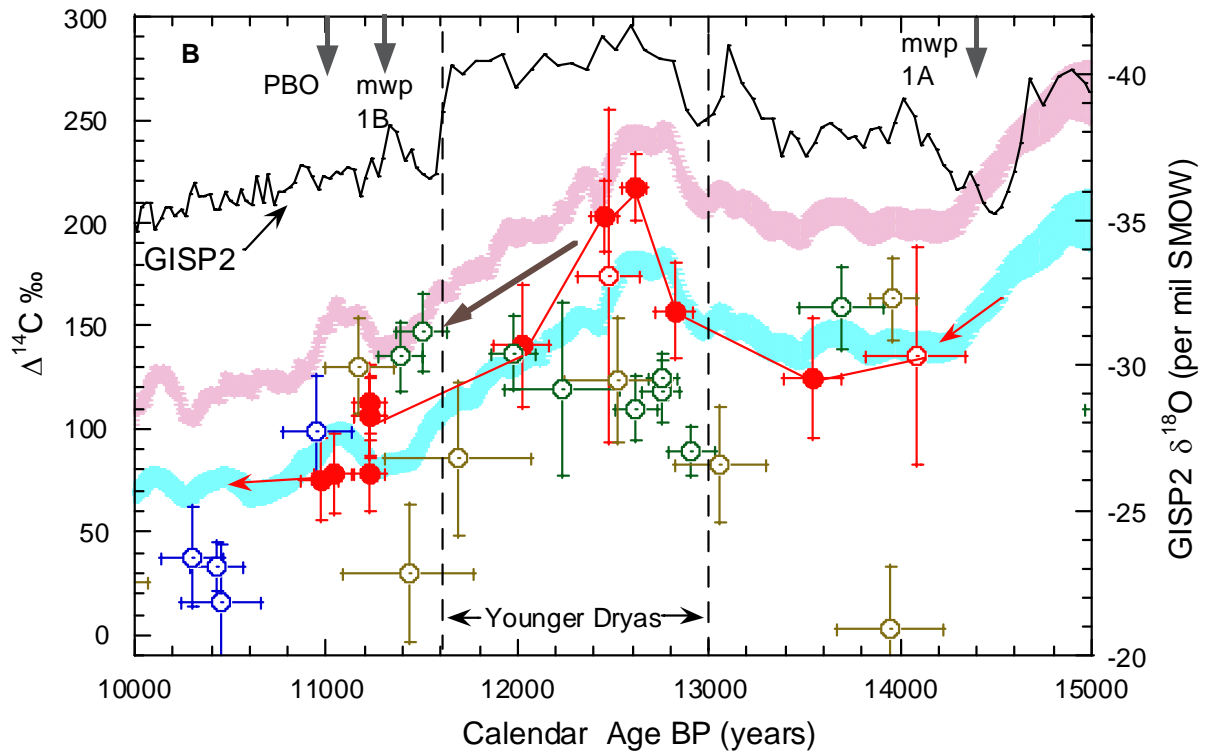
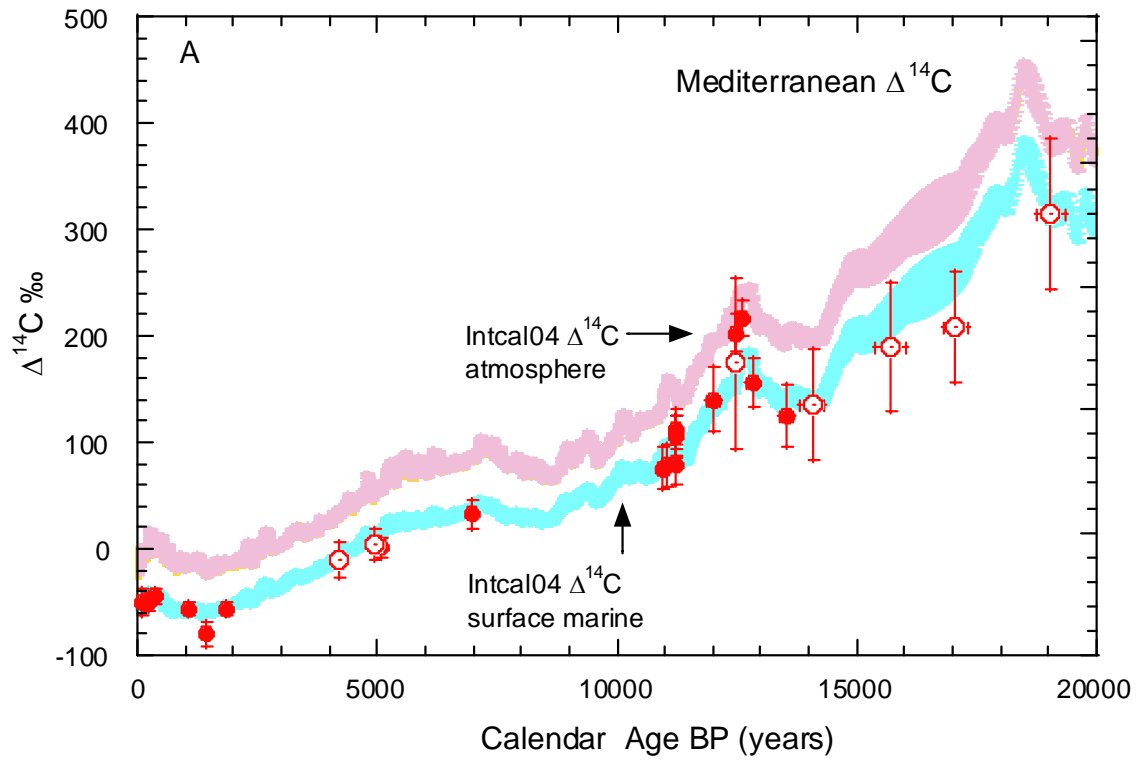


Figure 2A. Plot of $\Delta^{14}\text{C}$ values for the Mediterranean for the last 20,000 yrs. Values determined in this study using combined U-Th and ^{14}C ages are shown in solid symbols. With the exception of two samples from the early YD period which have near atmospheric $\Delta^{14}\text{C}$ values, all deep-sea coral samples have $\Delta^{14}\text{C}$ values within error of the Intcal04 surface marine curve¹³. $\Delta^{14}\text{C}$ values determined from ^{14}C ages of planktonic foraminifera and contemporaneous tephra pairs from Siani et al. are shown in open symbols and also lie error of the surface marine curve.

2B. Expanded plot showing $\Delta^{14}\text{C}$ values of the Mediterranean compared to deep sea coral data from N. Atlantic from other workers (green, blue, olive). The increased near atmospheric-like values found in this study (solid red symbols) during the YD occur shortly after the rapid rise in $\Delta^{14}\text{C}$ values, are coincident with a decrease in $\Delta^{14}\text{C}$ values from GISP2. This indicates that the initiation of the YD involved a close link between cooling (lower $\Delta^{14}\text{C}$ values) and increased $\Delta^{14}\text{C}$ from shutdown of deep water formation in the N. Atlantic. In contrast the termination of the YD is marked by rapid warming (higher $\Delta^{14}\text{C}$ values) without perturbation of the steadily decreasing $\Delta^{14}\text{C}$ values suggesting that factors other than deep-water formation in the N. Atlantic were responsible for the steadily decreasing $\Delta^{14}\text{C}$ values from $\sim 12,500$ yrs to 11,200 yrs. At $\sim 11,400$ yrs, several deep-sea corals from the N. Atlantic have atmospheric $\Delta^{14}\text{C}$ compositions. These appear to be anomalous as they require isolation of surface water masses for over 1000 yrs. A sequence of $\Delta^{14}\text{C}$ values (supp. Fig1) determined from a single septal element covering ~ 100 yrs time period for specimen LM99-124D (*D. dianthus* of age 11,230 yrs) from the Mediterranean exhibits a range of $\Delta^{14}\text{C}$ values of from 79 ± 19 ‰ (surface marine) to 113 ± 18 (‰). These values overlap with the surface marine curve and approach atmospheric values, consistent with a period of rapidly fluctuating $\Delta^{14}\text{C}$ values as previously found for an earlier period in the N. Atlantic. Solid arrow shows trajectory for decreasing $\Delta^{14}\text{C}$ due to ^{14}C decay.

High resolution coral record of Indo-Pacific Warm Pool climate during the penultimate deglaciation, Sumba, Indonesia

Dingchuang Qu¹, Michael K. Gagan¹, Gavin B. Dunbar¹, Wahyoe S. Hantoro², Bambang W. Suwargadi², Graham E. Mortimer¹, Malcolm T. McCulloch¹,

¹Research School of Earth Sciences, The Australian National University, Canberra, ACT 0200, Australia

²Research and Development Center for Geotechnology, Indonesian Institute of Sciences, Bandung 40135, Indonesia

Ocean-atmosphere interactions in the tropical Indo-Pacific Warm Pool are fundamental drivers of the global meridional Hadley and zonal Walker circulations. Recent research indicates that changes in sea surface temperatures and atmospheric convection in this region play important roles in modulating global climate on interannual, decadal, millennial, and even glacial-interglacial time-scales. Knowing the natural bounds of past ocean-atmosphere variability in the Warm Pool region will enhance our ability to predict the climate in the future. Massive, long-lived corals are one of the only paleoclimate archives capable of providing high resolution records (weekly to monthly) for periods when climate boundary conditions were different from those of the present day. Here we report a 28-year-long high resolution $\delta^{18}\text{O}$ record for a sea-level highstand during the penultimate deglaciation (140 to 130 ka) reconstructed from a massive *Porites* coral from the Mondu raised reefs, located southwest of Cape Laundi on the island of Sumba, eastern Indonesia.

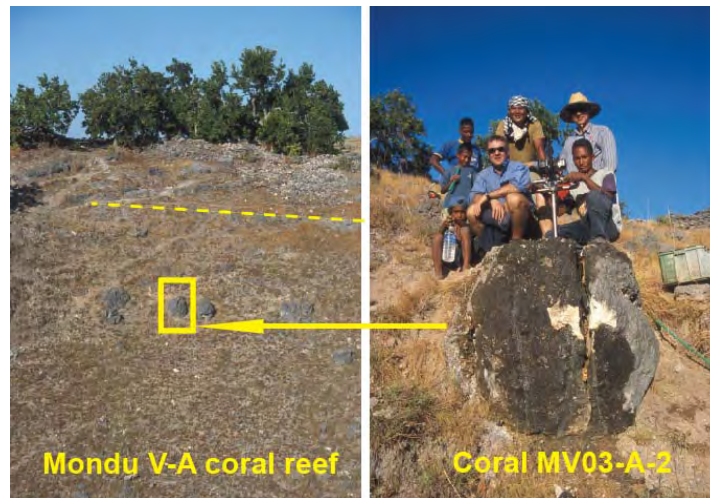


Fig.1 A 1.2 metre long fossil *Porites* coral core MV03-A-2c has been drilled from the Mondu V-A raised reef, 1.5 km inland from the sea. The coral is now 39 m above modern sea level. This coral has an average annual skeletal extension rate of 16 mm/yr, which is typical for modern and Holocene Sumba *Porites* corals

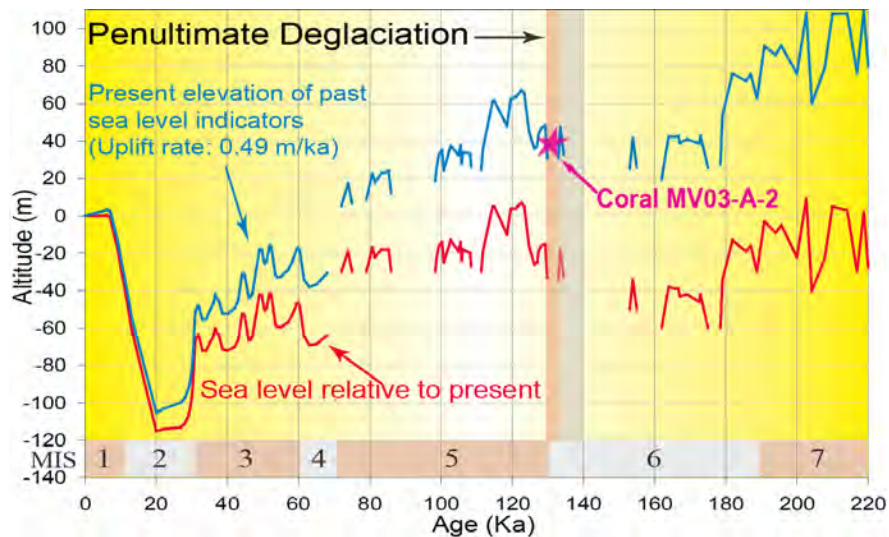


Fig.2 The present elevation of past sea level indicators in study area is shown by the blue curve based on a constant uplift rate of 0.49 m/ka (Pirazzoli *et al.* 1991). Sea level change (red curve) is based on data from John Chappell (Pers. Comm.) and Thompson and Goldstein (2005). The closed-system U/Th age for coral MV03-A-2 is 136 ± 1.5 ka. However, because the $\delta^{234}\text{U}_i$ is slightly high (158.8‰), we believe that the open-system age of 131 ka is more correct (Thompson *et al.* 2003). Both ages are in the penultimate deglaciation and are consistent with topographic surveys and stratigraphic analysis.

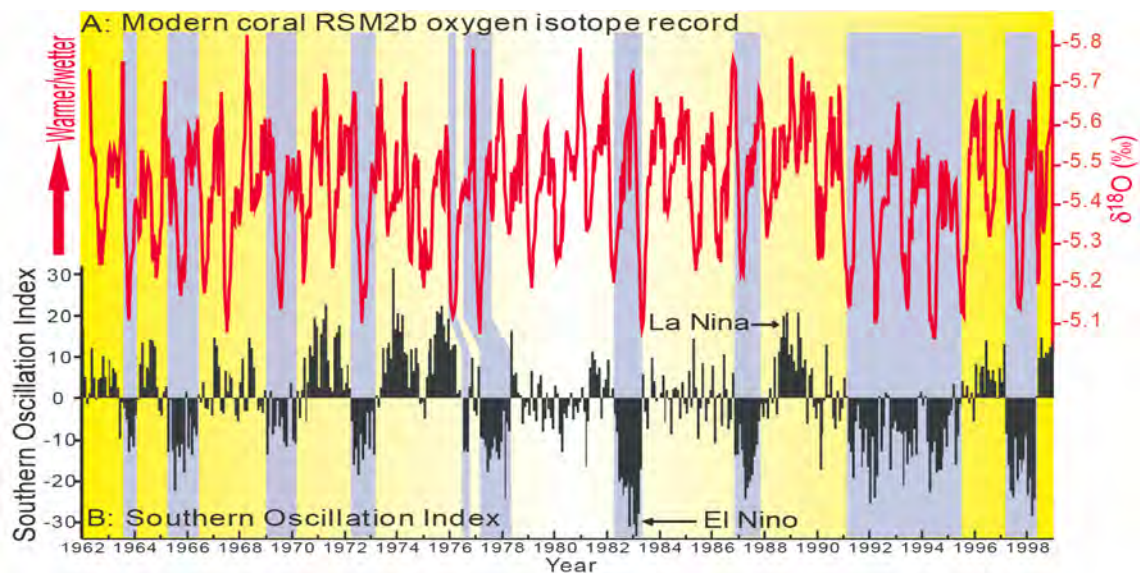


Fig.3 A modern coral was drilled from a nearby fringing reef to establish the basis of the coral climate reconstruction. The coral $\delta^{18}\text{O}$ mostly reflects SST, with superimposition of a salinity (rainfall) signal. The Mondu coral $\delta^{18}\text{O}$ records ENSO events very well, especially the winter values. During El Nino events, the winter is relatively dry and cool, reflected by higher $\delta^{18}\text{O}$ values; in contrast, during La Nina events, the warmer/wetter winter climate is reflected by lower $\delta^{18}\text{O}$ values.

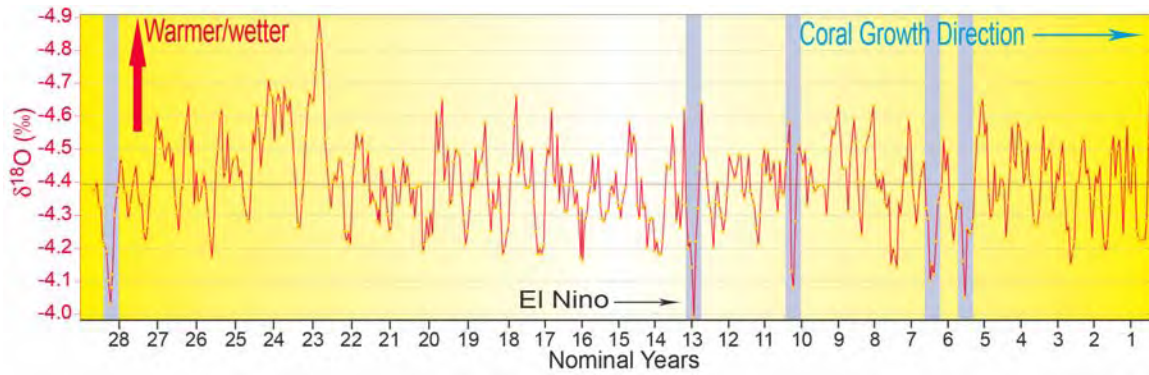


Fig.4 Coral record of the penultimate deglaciation: This coral MV03-A-2c $\delta^{18}O$ record covers a 28-year period of the penultimate deglaciation climate signal, showing good preservation of annual cycles, and, in many years, a double peak indicating the seasonal development of the wet/warm summer monsoon. The double peak reflects the cross-equatorial movement of the Inter-Tropical Convergence Zone, presumably during years when monsoon rainfall is strong. 5 El Nino events are recognized in this record according to the drier and cooler winters.

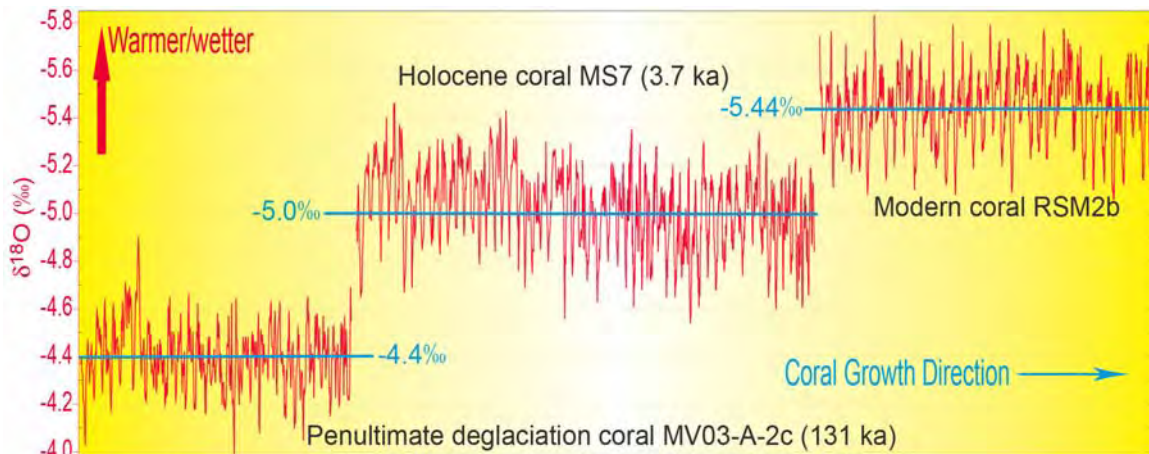


Fig.5 Comparison of penultimate deglaciation and Holocene coral records:

a. The average $\delta^{18}O$ for the penultimate deglaciation coral is -4.4‰ , which is 0.6‰ higher than the average value of the mid-late Holocene coral and 1.0‰ higher than the modern coral on the Mondu reefs. Taking into account the ice volume effect, and assuming constant surface salinity, the shift in $\delta^{18}O$ indicates that the SST during this period of the penultimate deglaciation at 131 ka was $2\text{ }^{\circ}\text{C}$ cooler than it is today.

b. The average annual range in $\delta^{18}O$ between summer and winter of this penultimate deglaciation coral record is smaller than that in the Holocene and modern corals. This change might result from reduction of seasonal difference in insolation or monsoon during that time.

c. The fossil coral record also shows that the frequency of cooler/drier years, indicative of El Nino events, was lower than today.

References

- Pirazzoli, P. A., U. Radtke, et al. (1991). "Quaternary raised coral-reef terraces on Sumba Island, Indonesia." *Science* 252: 1834-1836.
- Thompson, W. G. and S. L. Goldstein (2005). "Open-System Coral Ages Reveal Persistent Suborbital Sea-Level Cycles." *Science* 308(5720): 401-404.
- Thompson, W. G., M. W. Spiegelman, et al. (2003). "An open-system model for U-series age determinations of fossil corals." *Earth and Planetary Science Letters* 210(1-2): 365-381.

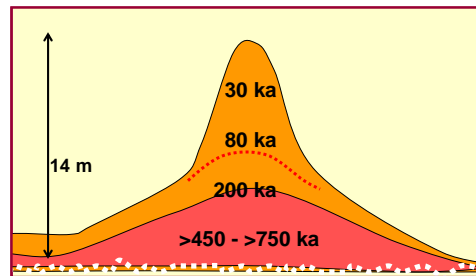
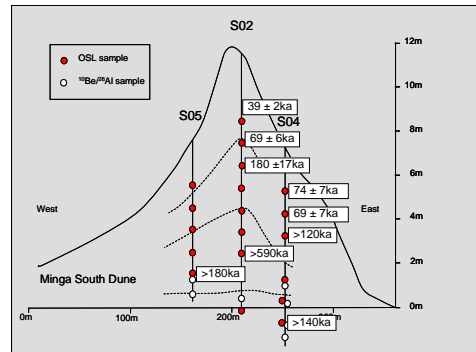
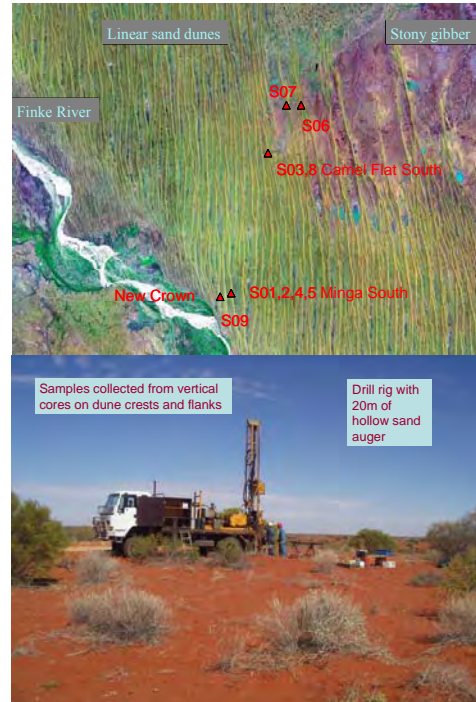
The age of the Simpson Desert, Australia

Ed Rhodes, John Chappell

Research School of Earth Sciences, The Australian National University, Canberra, ACT 0200, Australia

The results of 30 luminescence dates of sand cored from the centre of several large longitudinal sand dunes in the western Simpson Desert provide evidence that these significant geomorphological features are of a surprisingly great antiquity. The sediments were dated using optically stimulated luminescence (OSL) determinations of sand-sized quartz. This method provides an age estimate for the time of burial since the grains were last exposed to daylight, during the construction of the dune by aeolian processes.

The age estimates that we have derived from dune sediments in the Simpson Desert, near the community of Finke, NT, are in stark contrast to similar dates from the Stzelecki and Tirari Deserts. DEMS PhD student Kat Fitzsimmons has measured over 80 samples from dunes at locations throughout the Stzelecki and Tirari Deserts using a similar approach, and of these, fewer than 4% provide age estimates over 150,000 years (Rhodes et al. 2003). For the Simpson dataset, more than 50% provide age estimates of beyond 150,000 years. Of those that are younger, the majority were deposited before 60,000 years ago, again, providing a contrast to the age estimates from the Stzelecki and Tirari Deserts. Many of the older sediments from the Simpson are beyond the range of conventional OSL methods, and preliminary results from novel "slow component" OSL methods provide encouragement that this method will allow us to date deposition on time scales up to one million years.



We have also measured 12 paired $^{10}\text{Be}/^{26}\text{Al}$ cosmogenic nuclide concentrations in quartz from the Simpson dunes. This allows us to assess total burial time (possibly in multiple burial and erosion cycles) and approximate exposure time prior to burial for these bulk samples. The mean of the total burial age estimates is 850 ± 300 ka, while the mean of the pre-burial exposure ages is 210 ± 100 ka. We note that these exposure ages are similar to surface samples from the Macdonnell Ranges (which represents the source of sand in this region), suggesting that transport from the ranges into the desert was relatively rapid.

Rhodes E. J., Chappell, J. and Spooner N. A. 2003 Age and mobility of arid regolith: assessment by luminescence dating methods. In: Roach I. C. ed. *Advances in Regolith*, CRC LEME, 342-344.

Characterising southwest Australia's natural rainfall variability for the past 1000 years using speleothem records

Pauline C. Treble

¹Research School of Earth Sciences, The Australian National University, Canberra, ACT 0200, Australia

Speleothems (cave stalagmites) have the capacity to preserve high resolution proxy rainfall records extending from recent times to tens of thousands of years. Rainfall isotopes are preserved in the speleothem calcite, as are trace elements whose concentrations reflect the amount of soil and rock weathering and vegetation activity. These geochemical signals vary between wet and dry years.

Three papers from Earth Environment were published in 2005 that investigated the potential for reconstructing rainfall records from southern Australian speleothems. Treble et al. (2005a) showed that O isotopes ($\delta^{18}\text{O}$) in southern Australian rainfall vary inversely with rainfall amount and are primarily controlled by the strength and proximity of the mid-latitude low pressure systems that generate rainfall across this region. Analysing southern Australian speleothem $\delta^{18}\text{O}$ will allow us to reconstruct how wet it was in the past and potentially, how major atmospheric circulation features varied.

Using a modern speleothem that grew on a tourist cave boardwalk in southwest Western Australia, Treble et al. (2005b) confirmed that speleothem $\delta^{18}\text{O}$ can indeed be used to track rainfall history. Speleothem $\delta^{18}\text{O}$ rose 0.5‰ in response to the rainfall decrease that occurred from about 1970 onwards. Treble et al. (2005c) further contributed to the understanding of trace element incorporation in speleothems by mapping their concentrations over speleothem growth layers. The maps show that Ba, Sr, U and Na concentrations coherently follow annual growth layers but that complex crystal growth affects Mg incorporation as well as influencing the number of annual cycles, their amplitude and wavelengths. These results have clear



Stalagmite GL-S1 from Golgotha Cave, southwest Western Australia will be used to construct 1000 years of rainfall proxy data.

implications for studies that use annual trace element cycles as chronological markers, growth rate or seasonality proxies.

The study of southern Australian speleothems continues in Earth Environment with a new grant that began in May 2005. The aim of this latest project is to reconstruct 1000 years of rainfall history to determine natural variability for the region. This study will contribute significantly to our understanding of whether the drier conditions experienced from about 1970 onwards in southwest Western Australia are driven by natural variability or signal climate change.

Treble P. C., Budd W. F., Hope P. K. and Rustomji P.K. (2005a) Synoptic-scale climate patterns associated with rainfall $\delta^{18}\text{O}$ in southern Australia. *Journal of Hydrology* **302**, 270-282.

Treble P. C., Chappell J., Gagan M. K., McKean, K. D. and Harrison T. M. (2005b). In situ measurement of seasonal $\delta^{18}\text{O}$ variations and analysis of isotopic trends in a modern speleothem from southwest Australia. *Earth and Planetary Science Letters* **233**, 17-32.

Treble P. C., Chappell J. and Shelley, J. M. G. (2005c). Complex speleothem growth processes revealed by trace element mapping and scanning electron microscopy of annual layers. *Geochimica et Cosmochimica Acta* **69**, 4855-4863.

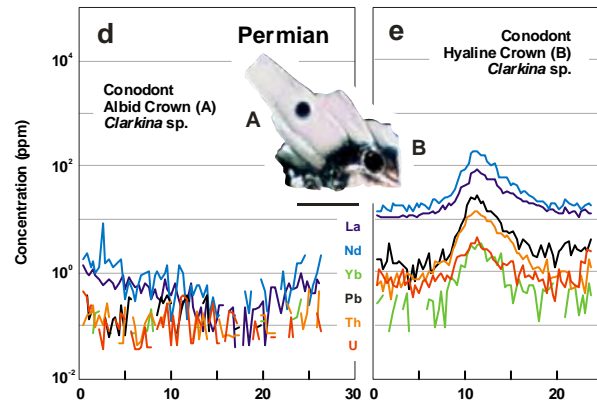
Chemical systematics of conodont apatite determined by laser-ablation ICPMS

Julie A Trotter^{1, 2} and Stephen M Eggin¹

¹Research School of Earth Sciences, Australian National University, Canberra, ACT 0200, Australia

²CSIRO Division of Petroleum Resources, North Ryde, NSW 2113, Australia

Major, minor, and trace element compositions of a suite of Ordovician, Silurian, and Permian conodonts have been characterised by laser ablation-inductively coupled plasma mass spectrometry. Continuous, high-resolution chemical profiles through individual conodont elements have revealed systematic compositional differences between the component histologies (albid, hyaline, and basal body tissues). Comparative analyses of contemporaneous bio-apatites (ichthyoliths and inarticulate brachiopods), as well as Late Holocene and modern fish material, show linear relationships between their respective rare earth element, yttrium, lead, thorium, and uranium compositions, which has implications for their relative permeability and susceptibility to diagenesis. Accordingly, LA-ICPMS profiles have been assessed in the context of histology, general morphological structure, and post-depositional chemical exchange, and suggest that albid crown may be the least permeable of the conodont mineralised tissues. These data have significant implications for the interpretation of conodont geochemistry and its application to palaeoceanography.



Submitted: Chemical Geology, Sept. 30th, 2005.

Ultrastructure, permeability, and integrity of conodont apatite determined by Transmission Electron Microscopy

Julie A Trotter^{1, 2}, John D Fitz Gerald¹, Harri Kokkonen¹ & Christopher R Barnes³

¹Research School of Earth Sciences, Australian National University, Canberra, ACT 0200, Australia

²CSIRO Division of Petroleum Resources, North Ryde, NSW 2113, Australia

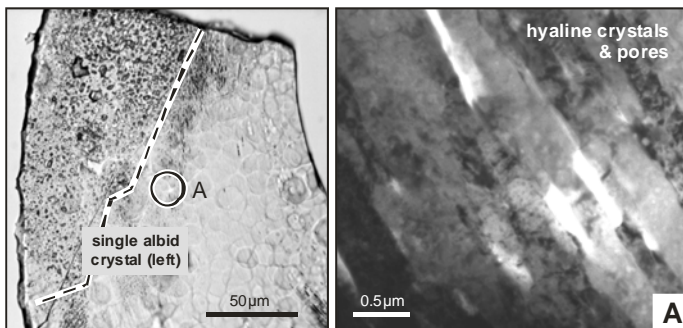
³School of Earth & Ocean Sciences, University of Victoria, British Columbia, Canada V8W 2Y2

Nanometre scale analysis of conodont apatite by Transmission Electron Microscopy has provided new insights into its crystalline structure, porosity, and inherent integrity. The component hard tissues are differentiated by crystal size, and inter- and intra-crystalline porosity. Basal body tissue typically comprises randomly oriented, isometric to elongate nanocrystals, which are commonly loosely packed causing significant intercrystalline porosity. Hyaline crown is also polycrystalline but characterised by elongate crystals typically of micron-scale that accommodate numerous spherical nanopores; the crystals are strongly aligned and typically tightly bound within a broader lamellar structure that lacks 'interlamellar spaces'. In contrast, albid crown comprises extraordinarily large crystals (100's μm) with nano- to micron-sized pores that are often irregularly shaped, forming a 'cancellate' microstructure.

Large pores ($\geq 0.5\mu\text{m}$) within crown tissues promote significant light scattering causing optical opacity ('albidity'), which may occur in both cancellate and polycrystalline lamellar crown. Cancellate albid and hyaline tissues are suggested to represent microstructural 'end-members' of conodont crown as some intermediate zones show 'hybrid' features and variable opacity. The range of histologies observed by TEM reveals the inadequacies of terms currently used to describe conodont crown, and are revised herein to accommodate some of these structural complexities.

The potential of conodont apatite to retain primary geochemical information

must depend upon crystal size and permeability. On this basis, cancellate albid crown probably offers the greatest potential for resisting post-mortem alteration and recording palaeomarine signatures.



Submitted: Lethaia, Oct. 21st, 2005.

Earth Materials, Introduction

The Experimental Petrology Group uses a laboratory-based experimental approach combined with field observations to study the Earth, its origin, evolution and mineral wealth. The group operates a wide range of experimental apparatuses for generating the high temperatures and pressures that are needed to reproduce the natural conditions within the Earth. The equipment includes: high temperature furnaces capable of reaching 1800°C, several of which are equipped for precise control of oxygen and sulfur fugacities by gas mixing; eleven solid-media piston-cylinder devices for generating pressures to 6 GPa and temperatures in excess of 2000°C, a multi-anvil apparatus, which can presently achieve pressures of 26 GPa; and, through collaboration with the Department of Earth and Marine Sciences, the Faculties, a well-equipped hydrothermal laboratory. These high-temperature, high-pressure apparatuses are complimented by an array of microbeam analytical techniques, including a Cameca SX100 electron microprobe; laser-ablation ICP-MS, which is now being used regularly to analyse trace-elements in experimental run products; FTIR spectroscopy for the determination of H₂O, CO₂ and other volatile species in minerals and glasses; and a STOE STADIP powder X-ray diffractometer.

As well as the conventional 1/2 inch and 5/8 inch apparatus for use to 4 GPa, the group's piston-cylinder laboratory also runs a high-pressure device that is now operating regularly at 6.5 GPa; the laboratory also has two large-capacity piston-cylinder devices that take 30 mm and 50 to 65 mm diameter pressure assemblies respectively, enabling pressure to be controlled extremely accurately, and which are capable of synthesising relatively large volumes of high pressure phases for detailed mineralogical studies. A novel diamond composite hard material, developed in these apparatuses and now under commercial production, offers promise as an anvil material to extend the pressure range of the multi-anvil apparatus above 26 GPa, thereby allowing detailed experimental exploration of the pressure-temperature regime of the Earth's lower mantle. To further this research the multi-anvil apparatus has now been refurbished and provided with full computer control of pressure and temperature. In recent years the group has become increasingly involved in developing methods to characterise geologic materials by X-ray absorption spectroscopy (XANES) and related techniques that use synchrotron radiation. Research in this area is presently concentrating on oxidation states in silicate melts, including in-situ measurements at temperatures to 1500°C, and speciation in ore-forming hydrothermal solutions.

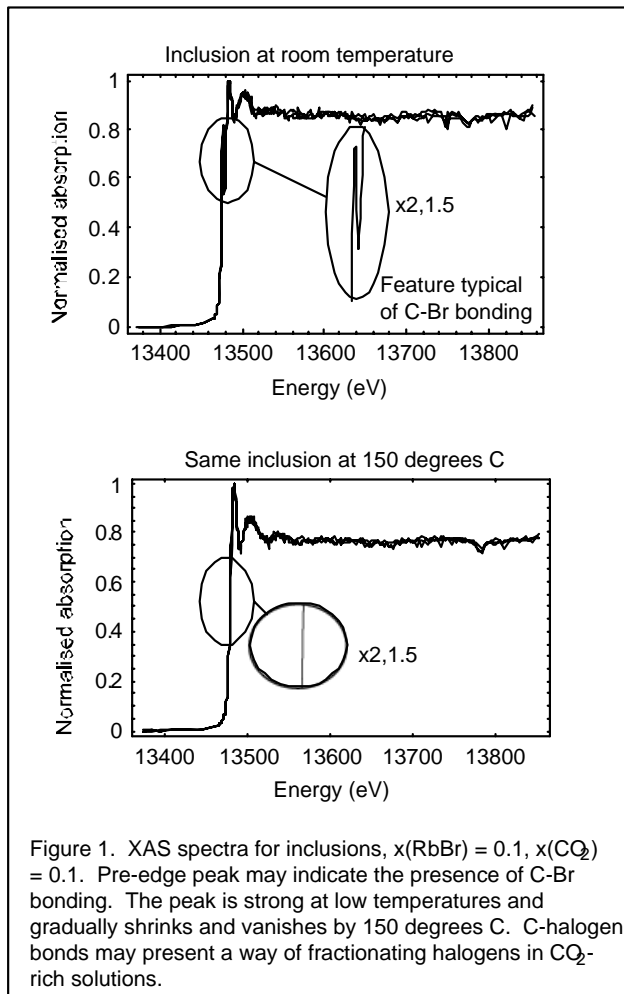
Members of the group continue to investigate conditions and processes in the Earth's upper mantle (Professors David Green and Hugh O'Neill), metamorphism in the continental crust (Drs Joerg Hermann, Chris McFarlane and Carl Spandler), as well as the physical chemistry of ore-forming solutions (Drs John Mavrogenes and Katy Evans).

The effect of CO₂ on supercritical fluids

Katy Evans¹ and John Mavrogenes¹

¹Research School of Earth Sciences, Australian National University, Canberra, ACT, 0200, Australia

CO₂ and dissolved salts such as NaCl are common components of supercritical solutions in the earth's crust. They are involved in ore deposit formation, magmatism and volcanism. The presence of CO₂ affects the relationships between solution and solutes at a molecular level, which changes the ability of solutions to dissolve minerals and metals, and solution properties such as viscosity.



Studies of CO₂-bearing fluids at elevated pressures and temperatures are very rare, largely because of the difficulty of containing and analysing solutions at the pressures and temperatures of interest. Synchrotron radiation is ideal for speciation studies because XAS studies can inform us of the environment around solute molecules. However, the salts commonly found in natural solutions have low atomic weights, and therefore (a) are inaccessible to the hard X-rays available on micro-spectroscopy beamlines and (b) have characteristic X-rays that are absorbed by most window materials capable of holding high pressure-temperature solutions. For this reason our work uses RbBr as an analogue for the 1:1 salts NaCl and KCl.

We have synthesised a series of artificial fluid inclusions (SFLINCS), which are tiny (20-40 micron diameter) samples of fluid trapped in a mineral host at high temperature and pressure. These fluid inclusions were then studied using synchrotron radiation at the APS to discover the effects that CO₂ had on

speciation in the fluids.

An exciting result from this work is the discovery of apparent C=Br bonding in the CO₂-bearing solutions (Figure 1). This has not been previously reported in geological solutions, although similar features are reported in the chemical literature at room temperature and pressure. One possible implication of this discovery is that CO₂-

bearing fluids could fractionate Br, and possibly Cl; quite the opposite to predictions based on our previous knowledge. Work continues on the interpretation of these results.

Redox Decoupling and Redox Budgets: Conceptual Tools for the Study of Earth Systems

Katy Evans¹

¹*Research School of Earth Sciences, Australian National University, Canberra, ACT, 0200, Australia*

Redox processes affect many aspects of geological systems. The Earth's evolution has included the development of planet-scale gradients in the distribution of redox pairs (e.g., Fe(3+)/Fe(2+)), which reflect gradients in redox potential (e.g., Kuramoto and Matsui, 1996). The mantle is significantly more reduced than the ocean and atmosphere (e.g., Arculus, 1985), and changes in the distribution of redox-sensitive elements during the Earth's early history have affected the composition of the atmosphere (e.g., Lowe and Tice, 2004). Redox-sensitive elements, particularly C, play a key role in global climate regulation (e.g., Wallman, 2001), and can limit the abundance of life (e.g., Petsch and Berner, 1998).

It is therefore useful to distinguish chemical processes that result in changes in the capacities of reservoirs to oxidise or reduce from those that do not. Two terms are proposed to make this distinction. The first is *redox decoupling*: the transport of redox-sensitive elements (e.g. H, C, S, Fe) such that reservoirs experience a change in their capacity to oxidise or reduce other material. The second is *electrochemical differentiation*: the effect of one or more redox decoupling processes that change existing gradients in redox potential.

Recognition of redox decoupling requires the use of an extensive rather than an intensive redox variable, because intensive variables do not provide information on fluxes. Redox budget, defined as the number of moles of negative charge that must be added to a sample to reach a reference state, is such a variable. Construction of redox budgets for mid-ocean ridge basalt (MORB) lavas and glasses reveals that redox decoupling occurs during crystallization at the Mid-Atlantic, Pacific and Red Sea ridges, with net oxidation of the crystallized lava.

The concepts of electrochemical differentiation, redox decoupling and redox budget may be useful for researchers studying global cycling, the formation of ore deposits, volcanism, evolution of the mantle, crust and core, redox-related environmental problems, and biotic systems.

Testing the Mantle Plume Hypothesis: Evaluation of Magmatic Temperatures at mid-ocean ridges, "Hot-spots", and other intraplate settings

David H. Green¹

¹*Research School of Earth Sciences, Australian National University, Canberra, ACT, 0200, Australia*

The deep mantle plume hypothesis postulates a large potential temperature difference ($\Delta T_p \sim 200\text{-}250^\circ\text{C}$) between the upwelling plume and normal ambient mantle as sampled by midocean ridge upwelling and by non-plume intra-plate basalts. This core tenet of the deep mantle plume hypothesis is testable by comparison of primitive "hot spot" magmas with intraplate magmas and particularly with primitive mid-ocean ridge basalts (MORB).

We have examined picrites and olivine phenocryst compositions from Hawaiian volcanoes and a large new data set of glass compositions from the Hawaiian Scientific Drilling Project, sampling deep into the main cone-building phase of Mauna Kea volcano. By incremental addition of olivine (reversing the crystallization of magmas saturated only in olivine + Cr-Al spinel) we infer the parental or primitive picrite magma compositions for distinctive compositional suites and individual volcanoes. We then calculate liquidus temperatures (1 Atm.) and infer conditions of melt separation from residual lherzolite (ol + opx + cpx \pm sp) or harzburgite (ol + opx + Cr-sp). The Hawaiian tholeiitic picrites of the main shield-building phase consistently indicate harzburgite residue and pressures of magma segregation around 1.5 to 2 GPa.

The petrological data base of glass compositions from mid-ocean ridge settings contains > 190 analyses of glass with more than 9.5% MgO. These quenched liquids were saturated in olivine ($Mg^\# = 86\text{-}89$) and Al-Cr spinel. Olivine addition calculations are used to estimate parental liquid compositions with liquidus olivine $Mg^\# = 90.5\text{-}91.5$. Further constraint is provided by the requirement that parental liquids lie on ol + opx \pm cpx + spinel saturation surfaces for a lherzolitic or harzburgitic residue. We infer primitive or parental MORB magmas to be picrites with 13-16% MgO, segregating from lherzolite to harzburgite residue for the most part at ~ 2 GPa but in some cases as low as 1 GPa. Our analysis of the compositions and liquidus temperatures of parental magmas at a "hot spot" (Hawaii) and at mid-ocean ridge settings finds that picritic magmas with >13% MgO are characteristic of both settings. Liquidus temperatures have the same range, to a maximum of 1380-1390°C if volatile-free, but up to 1335°C (Hawaii) and $\sim 1355^\circ\text{C}$ (mid-ocean ridges) if volatiles (C+H+O) are included.

The maximum temperatures of primitive magmas, and the inferences from the systematics of peridotite partial melting, are used to estimate mantle potential temperatures of $\sim 1430^\circ\text{C}$ at mid-ocean ridges and up to 1400°C beneath Hawaiian volcanoes. *The principal differences between "hot spot" and MORB primitive magmas are compositional and not thermal.* The "hot spot" source has geochemical signatures which suggest melting, depletion and re-fertilization processes in subduction settings, as well

as enrichment processes due to migration of incipient melt (carbonatite to olivine nephelinite) in the asthenosphere.

The melting and primary differentiation of the Earth's mantle observed at divergent plate boundaries and in intraplate settings, including "hot spots", is a consequence of the plate tectonics cycle acting on the modern Earth with $T_p \sim 1430^\circ\text{C}$. Plate tectonics introduces chemical inhomogeneity, including redox contrasts, into the Earth's upper mantle. Chemical heterogeneity within the asthenosphere and upper mantle (i.e. below the lithospheric plates), at $T_p \sim 1430^\circ\text{C}$ together with global degassing of (C+H+O) fluids, is responsible for the diverse intraplate, "hot spot" and MOR magmas. Mantle plumes or diapirs at "hot-spots" are inferred to result from compositional heterogeneity within the upper mantle, below the lithospheric plates. ¹ School of Earth Sciences, University of Tasmania, Hobart, Tasmania

Aqueous fluids and hydrous melts in high-pressure and ultra-high pressure rocks: implications for element transfer in subduction zones.

Jörg Hermann¹, Carl Spandler¹, Alistair Hack^{1,3}, Andrey V. Korsakov²

¹*Research School of Earth Sciences, Australian National University, Canberra, ACT, 0200, Australia*

²*Institute of Mineralogy and Petrography of Siberian Branch of Russian Academy of Sciences, Koptyug Pr. 3, Novosibirsk 630090, Russia*

³*Present address: Institute for Mineralogy and Petrography, ETH-Zürich, 8092 Zürich, Switzerland*

High-pressure (HP) and ultra-high pressure (UHP) terranes are excellent natural laboratories to study subduction-zone processes. The recognition that in felsic systems there is a second critical endpoint terminating the wet solidus at conditions that can be encountered by UHP rocks (Fig. 1) led to considerable confusion regarding the terminology for UHP-fluids. We argue that a fluid buffered by a solid residue is compositionally well defined and is either an aqueous fluid (total amount of dissolved solids < 30 wt.%) or a hydrous melt (H₂O < 35 wt.%). There is only a small temperature range of approximately 50-100 °C, where transitional solute-rich fluids exist (Fig. 1). Metasediments in the New-Caledonia HP terrain reached peak conditions of ~600 °C and ~20 kbar. This *P-T* region is clearly at lower temperatures than the wet solidus and at pressures lower than the second critical endpoint (Fig. 1). Hence an aqueous fluid must have been present at peak conditions. Higher pressures of up to 27 kbar have been documented in the metasediments of Lago di Cignana (Western Alps) where coesite has been found. Although it is expected that the amount of solutes in the fluid will be significantly larger than in New Caledonia, it plots still in the field where an aqueous fluid is stable. On the other hand, diamondiferous pelitic rocks such as the ones found in the Kokchetav massif experienced peak metamorphic conditions that are well within the stability field of hydrous melts (Fig. 1). Because the second critical endpoint in pelitic systems is likely to be at ~30 kbar, there is the potential that some UHP terrains will be situated in the region, where fluids are transitional. In fact, the *P-T* estimates for the Dora-Maira massif (Western Alps) are exactly in this region (Fig. 1).

The combined evidence from experiments and natural rocks indicates that aqueous fluids liberated at the blueschist to eclogite facies transition are dilute (Fig. 2). They contain only moderate amounts of LILE, Sr and Pb and do not transport significant amounts of key trace elements such as LREE, U and Th. This indicates that there is a decoupling of water and trace element release in subducted oceanic crust and that aqueous fluids are unable to enrich the mantle wedge significantly. Instead we propose that fluid-present melting in the sediments on top of the slab is required to transfer significant amounts of trace elements from the slab to the mantle wedge (Fig. 2). For such a process to be efficient, top slab temperature must be at least 700-750 °C at sub-arc depth. Slab melting is likely to be triggered by fluids that derive from dehydration of mafic and ultramafic rocks in colder (deeper) portions of the slab. A great amount of solutes will precipitate when the melts contacts the mantle wedge peridotite and the

trace elements are likely to be transported by an aqueous fluid within the sub-arc mantle wedge.

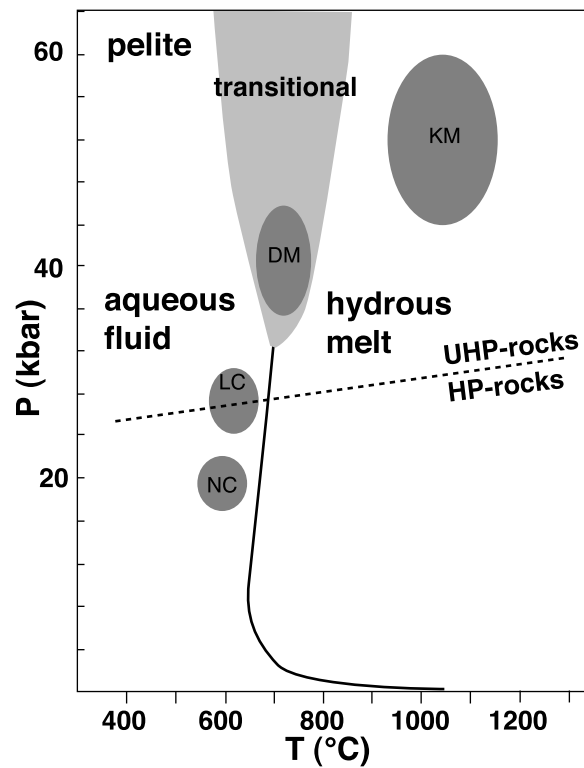


Fig. 1: The position of peak metamorphic conditions with respect to the wet solidus provides a first order information on the nature of the fluid phase present. a) Aqueous fluid must be present at eclogite facies metamorphism in the New Caledonia (NC) and the Lago di Cignana (LC) metapelites, whereas the felsic rocks from the Kokchetav massif (KM) are situated well within the field of hydrous melts. The pelitic rocks of the Dora Maira Massif (DM) plot in the field where the fluid phase is likely to be transitional between a hydrous felsic melt and an aqueous fluid.

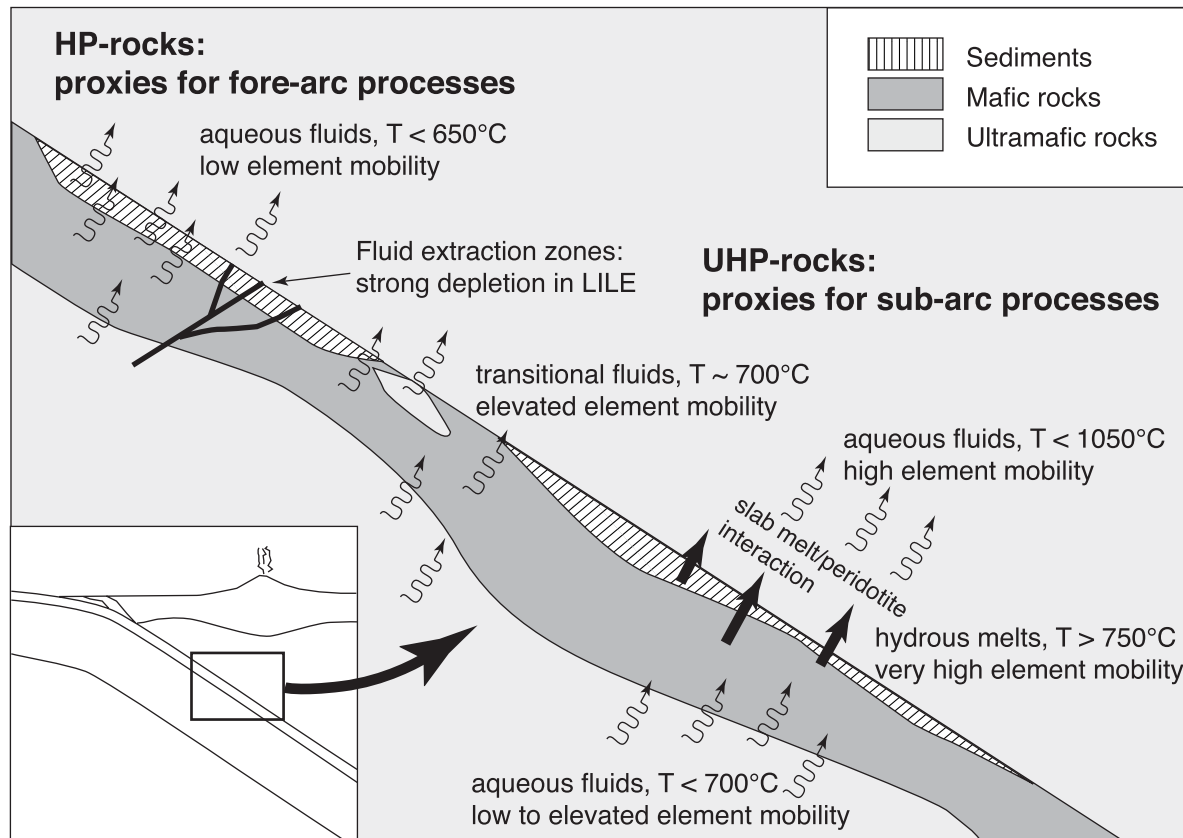


Fig. 2: Schematic occurrence of aqueous fluids and hydrous melts in a subduction zone setting. Natural high-pressure and ultra-high pressure rocks can be used to infer fore-arc and sub-arc processes, respectively

- Bolfan-Casanova, N., Keppler, H., and Rubie, D. C., 2000, Water partitioning between nominally anhydrous minerals in the $\text{MgO-SiO}_2\text{-H}_2\text{O}$ system up to 24 GPa: implications for the distribution of water in the Earth's mantle: *Earth And Planetary Science Letters*, v. 182, no. 3-4, p. 209-221.
- Koga, K., Hauri, E., Hirschmann, M., and Bell, D., 2003, Hydrogen concentration analyses using SIMS and FTIR: Comparison and calibration for nominally anhydrous minerals: *Geochemistry Geophysics Geosystems*, v. 4.
- Bell, D. R., Rossman, G. R., and Moore, R. O., 2004, Abundance and partitioning of OH in a high-pressure magmatic system: Megacrysts from the Monastery kimberlite, South Africa: *Journal Of Petrology*, v. 45, no. 8, p. 1539-1564.
- Lemaire, C., Kohn, S. C., and Brooker, R. A., 2004, The effect of silica activity on the incorporation mechanisms of water in synthetic forsterite: a polarised infrared spectroscopic study: *Contributions To Mineralogy And Petrology*, v. 147, no. 1, p. 48-57.
- Matsyuk, S. S., and Langer, K., 2004, Hydroxyl in olivines from mantle xenoliths in kimberlites of the Siberian platform: *Contributions To Mineralogy And Petrology*, v. 147, no. 4, p. 413-437.

The mechanism of H₂O incorporation as a function of P-T and bulk chemistry (Si-activity) in the MgO-SiO₂-H₂O system: a quantitative approach

Istvan Kovács,¹, Jörg Hermann¹, Hugh St. C. O'Neill¹

¹*Research School of Earth Sciences, Australian National University, Canberra, ACT, 0200, Australia*

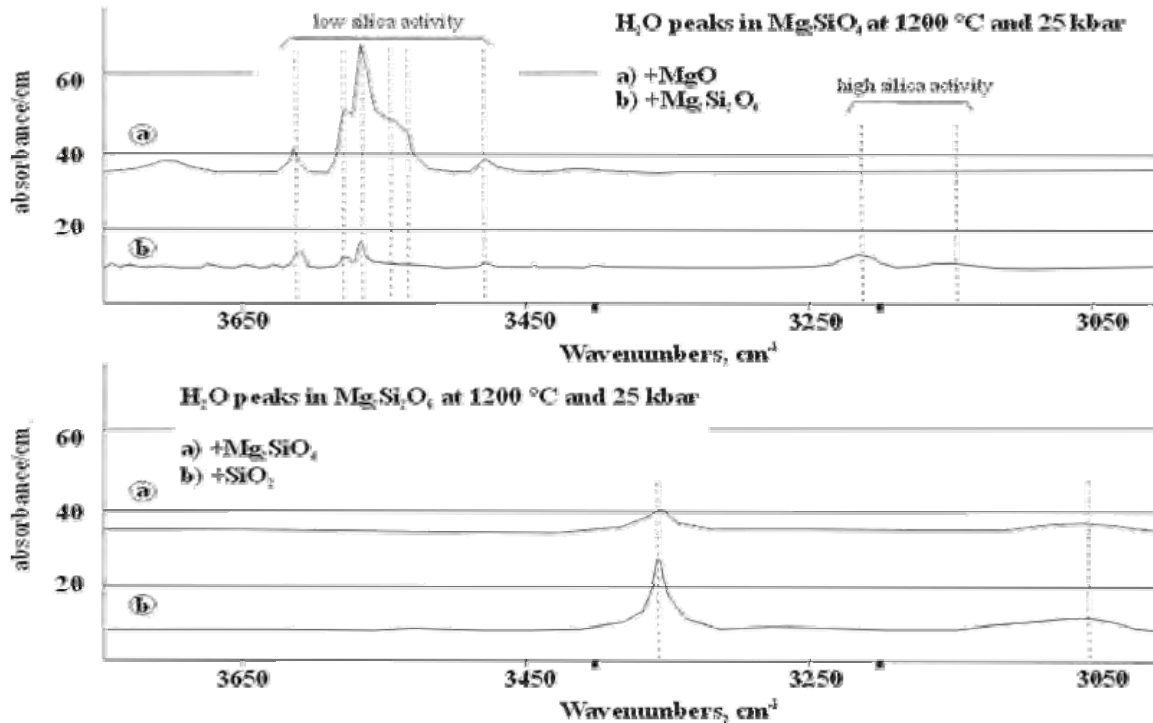
Although significant progress has been made in identifying major defect types responsible for hydrogen incorporation in olivine, only a few studies have dealt with the P-T dependence of water solubility. Similarly, with few exceptions (Bolfan-Casanova et al., 2000; Koga et al., 2003; Bell et al., 2004), the distribution of water among the main mantle minerals has not been addressed in previous experimental work. In order to shed light on these issues, we have carried out experiments using three different starting compositions in the MgO-SiO₂-H₂O system. The MgO (wt%):SiO₂ (wt%) ratios were 2:1, 1:1 and 1:2 respectively, which allowed us to study water incorporation in MgO (periclase)-buffered, Mg₂S₂iO₆ (enstatite)-buffered and SiO₂ (quartz)-systems.

All of the experiments were run at 25 kbar, with temperature varied from 1000 to 1400 °C, and the duration of the experiments was always longer than 24 hours. We found periclase+forsterite+fluid, forsterite+enstatite+fluid and enstatite+melt(?) +fluid in the respective systems. Recovered samples were examined for the type of H₂O substitution by FTIR spectroscopy. This analytical method can also give a quantitative assessment of the amount of H₂O if a calibration is available.

The position of main peaks in the FTIR spectrum for each bulk composition does not change significantly; nevertheless their normalized absorbance does change with temperature, indicating changing water solubility. In the MgO (periclase)-buffered experiments, peaks at 3612, 3589, 3566, 3555, 3533 and 3480 cm⁻¹ were found, in accordance with previous work (Lemaire et al., 2004; Matsyuk and Langer, 2004; Matveev et al., 2005). These peaks are related to silica vacancies due to low silica activity. In the enstatite-buffered experiments, where forsterite and enstatite coexist, the IR spectrum of forsterite shows two peaks at 3160 and 3220 cm⁻¹ in addition to those present in the MgO buffered experiments (Fig 1). These peaks indicate Mg vacancies in the forsterite structure. It seems that peak intensities decrease with increasing temperature in both MgO and enstatite buffered systems, which implies that water solubility is inversely proportional to temperature in olivine. For enstatite, in both forsterite and SiO₂ buffered experiments, two peaks at 3360 and 3060 cm⁻¹ are found (Fig 1). Peak intensities become stronger with increasing temperature in enstatite, indicating increased water solubility with temperature. Although the peak positions are the same in both the enstatite- and SiO₂ -buffered systems, the peak intensities tend to be higher at a given temperature in the SiO₂ buffered system. These peaks are close to those forsterite peaks (3220 and 3160 cm⁻¹) characteristic of higher silica activity: therefore, it is probable that H substitutes directly for Mg in enstatite.

Future work will address the calibration of the peak intensities as a function of H₂O content to develop a quantitative model for H₂O solubility in forsterite and enstatite.

Figure: OH stretching region of infrared absorption spectrum of forsterite and enstatite from our experiments (see text for more detail)



References

- Bolfan-Casanova, N., Keppler, H., and Rubie, D. C., 2000, Water partitioning between nominally anhydrous minerals in the MgO-SiO₂-H₂O system up to 24 GPa: implications for the distribution of water in the Earth's mantle: *Earth And Planetary Science Letters*, v. 182, no. 3-4, p. 209-221.
- Koga, K., Hauri, E., Hirschmann, M., and Bell, D., 2003, Hydrogen concentration analyses using SIMS and FTIR: Comparison and calibration for nominally anhydrous minerals: *Geochemistry Geophysics Geosystems*, v. 4.
- Bell, D. R., Rossman, G. R., and Moore, R. O., 2004, Abundance and partitioning of OH in a high-pressure magmatic system: Megacrysts from the Monastery kimberlite, South Africa: *Journal Of Petrology*, v. 45, no. 8, p. 1539-1564.
- Lemaire, C., Kohn, S. C., and Brooker, R. A., 2004, The effect of silica activity on the incorporation mechanisms of water in synthetic forsterite: a polarised infrared spectroscopic study: *Contributions To Mineralogy And Petrology*, v. 147, no. 1, p. 48-57.

- Matsyuk, S. S., and Langer, K., 2004, Hydroxyl in olivines from mantle xenoliths in kimberlites of the Siberian platform: *Contributions To Mineralogy And Petrology*, v. 147, no. 4, p. 413-437.
- Matveev, S., Portnyagin, M., Ballhaus, C., Brooker, R., and Geiger, C. A., 2005, FTIR spectrum of phenocryst olivine as an indicator of silica saturation in magmas: *Journal Of Petrology*, v. 46, no. 3, p. 603-614.

Crystal-silicate melt partitioning of rhenium during mantle melting and magma genesis

Guilherme Mallmann¹ and Hugh St.C. O'Neill¹

¹Research School of Earth Sciences, Australian National University, Canberra, ACT, 0200, Australia

The Re-Os isotopic system is a powerful and versatile geochemical/geochronological tool, yet its complete development is currently hindered by the poorly understood behaviour of Re and Os during mantle melting and magma genesis. We have experimentally studied the partitioning behaviour of Re between common upper mantle minerals (garnet, spinel, clinopyroxene, orthopyroxene, and olivine) and silicate melts under temperatures (1275 to 1450°C), pressures (1.5 to 3.2 GPa), and oxygen fugacities (QFM+5.6 to QFM-2.1) relevant for basaltic magma genesis. Calculated bulk crystal-silicate melt partition coefficients vary over 4 to 5 orders of magnitude, from compatible to highly incompatible, in all the studied mineral as a function of fO_2 , indicating a change in the oxidation state of Re and hence a strong redox control on the Re partitioning behaviour. Non-linear least squares fitting of the experimental data, assuming 4+ and 6+ as Re oxidation states, indicates that Re^{4+} is compatible and Re^{6+} highly incompatible. Re partition coefficients are thus expected to vary significantly during magma genesis according to the oxidation state of the source. For instance, assuming QFM-0.9 and QFM+1.1 as average oxygen fugacities for the sources of mid-ocean ridge and island arc basalts, respectively, a difference of one order of magnitude is expected for Re partition coefficients. Our results also demonstrate that silicate minerals, especially garnet and clinopyroxene, can accommodate significant amounts of Re, particularly in more reduced environments.

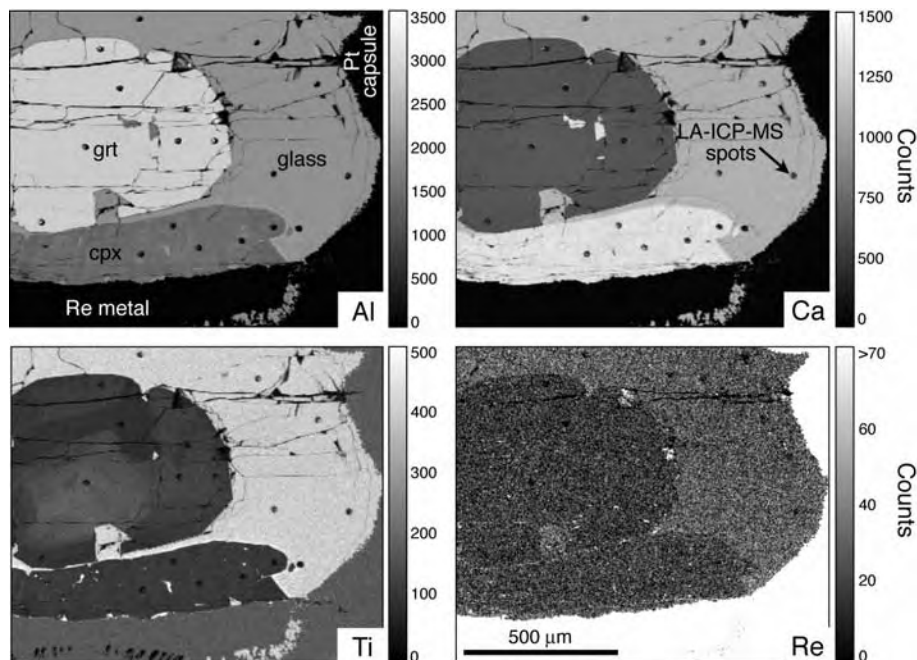


Fig. 1. X-ray electron microprobe maps showing the distribution of Al, Ca, Ti and Re among the experimental products in one of our high-*P*T runs (1425°C, 3.0GPa, QFM+0.88). Symbols: grt, garnet; cpx, clinopyroxene; glass, silicate glass. Also indicated LA-ICP-MS ablation pits. X-Ray map conditions: 15kV acceleration voltage, 40nA beam current, 0.5s dwell time.

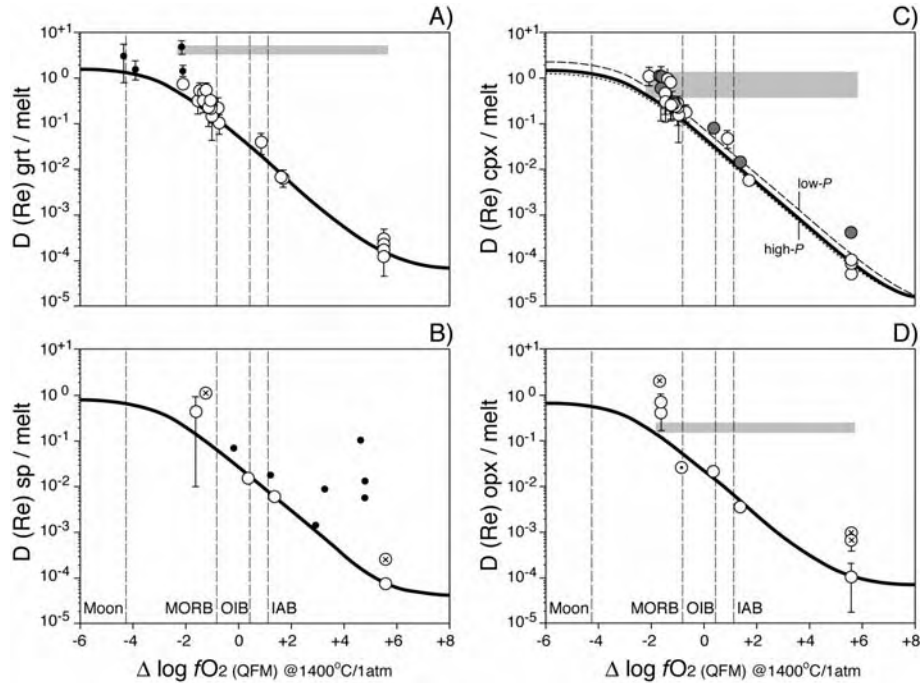


Fig. 2. Partitioning behaviour of Re between garnet, grt (A), spinel, sp (B), clinopyroxene, cpx (C), orthopyroxene, opx (D) and silicate melts as a function of oxygen fugacity (fO_2 , expressed relative to the quartz-fayalite-magnetite buffer (QFM) and normalized to 1400°C and 1atm). Also shown in grey the range of partition coefficients obtained for Yb in the same experimental charges. Vertical dashed lines correspond to values of fO_2 expected for basaltic magma genesis in the Moon (O'Neill et al., 1995), and averages obtained for mid-ocean ridge (MORB), ocean island (OIB) and island arc basalts (IAB). Solid lines are the results of non-linear least squares fitting of the experimental data to an equation describing both Re components (Re^{4+} and Re^{6+}) separately. Error bars for partition coefficients are 1σ standard deviation and generally smaller than the symbols, except when showed. Also plotted for comparison data from Righter and Hauri, 1998 and Righter et al., 2004 (\bullet), which probably represent micronugget-contaminated results. Symbols: grey circles in (C), low-*P* runs; crossed circles, maximum partition coefficients (not used in the data fitting); dotted circle in (D), high-*P* run.

References:

H.St.C. O'Neill, D.B. Dingwell, A. Borisov, B. Spettel, H. Palme, Experimental petrochemistry of some highly siderophile elements at high temperatures, and some implications for core formation and the mantle's early history, *Chem. Geol.* 120 (1995) 255-273.

K. Righter, E.H. Hauri, Compatibility of rhenium in garnet during mantle melting and magma genesis, *Science* 280 (1998) 1737-1741.

K. Righter, A.J. Campbell, M. Humayun, R.L. Herving, Partitioning of Ru, Rh, Pd, Re, Ir and Au between Cr-bearing spinel, olivine, pyroxene and silicate melts, *Geochim. Cosmochim. Acta* 68 (2004) 867-880.

Geochronological, geochemical, and isotopic studies of Au deposits in high-grade metamorphic terrains

Christopher R.M. McFarlane¹

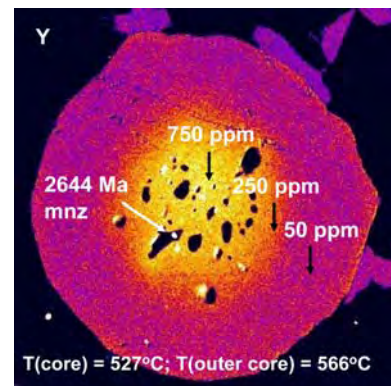
¹Research School of Earth Sciences/CSIRO Exploration, Australian National University, Canberra, ACT, 0200, Australia

Efforts to document the timing of Au mineralisation and the metamorphic evolution the Challenger Au deposit, South Australia, continued in 2005. A major initiative to use in-situ SHRIMP dating of monazite to reconstruct the Palaeoproterozoic evolution of the deposit was completed in July 2005. This research revealed that Challenger records a more complex high-grade metamorphic history than previously documented, and showed that Au deposition must have occurred prior to 2470 Ma. In October 2005, laser ablation ICP-MS studies of trace-elements in monazite separated from Au-bearing samples, revealed the presence of As-rich cores with ages between 2460-2470 Ma. Although it is impossible to determine whether high-As monazite precipitated at the same time as gold, this new data confirms the pre-peak metamorphic timing of Au deposition; high-As monazite cores are surrounded by low-As rims that formed in response to high-grade metamorphism during the Sleafordian Orogeny between 2450 and 2420 Ma.

Underground sampling at Challenger was undertaken in March and October 2005. A comprehensive suite of whole-rock geochemical data for each of the main lithologies present at Challenger is being used to document whether a geochemical signature of alteration survived high-grade metamorphism. Underground investigations have also confirmed the presence of relict mineralized quartz veins that were extensively deformed and variably contaminated with silicate partial melts.

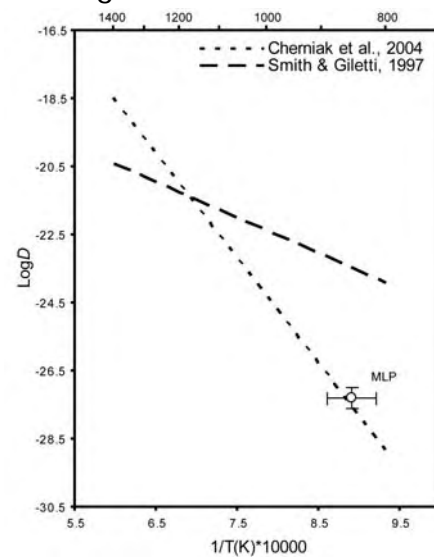
In March 2005, I had the opportunity to sample two Au deposits in the Southwest Yilgarn terrain, Western Australia, that are hosted in high-grade metamorphic rocks similar to those at Challenger. Griffin's Find and Badgebup are both undergoing renewed exploration to extend along strike mineralization. Like Challenger, both deposits contain mineralized quartz-rich veins intimately associated with anhydrous silicate minerals (pyroxenes, cordierite, K-feldspar) in granulite-facies gneisses.

Preliminary in-situ SHRIMP dating of monazite inclusions in garnet, and zircon and monazite in leucosomes in metatexite migmatites, indicate that prograde garnet growth occurred between 525 and 570°C (based on garnet-monzite thermometry) at ~2644 Ma (see figure) followed by partial melting above 800°C at ~2635 Ma. These and other deposits in the SW Yilgarn terrain have been cited as evidence for a continuum of gold deposition up to granulite-facies conditions. However, the lack of hydrous minerals in



'alteration' zones and the presence of inherited metamorphic zircon as old as 2800 Ma in gneisses surrounding these deposits (Wilde & Pidgeon, WAMPRI Rep. 30 1986) cast doubt on the validity of this model. For example, gold deposition at ~2800 Ma could have been subsequently reworked at 2635 Ma. Following the methodologies successfully applied at Challenger, it may again be possible to identify fabrics, vein assemblages, and accessory mineral compositions that retain a record of pre-2635 Ma Au deposition at Griffin's Find & Badgebup.

Understanding the temporal evolution of high-grade metamorphic rocks like those hosting these deposits is fundamentally dependent upon our confidence in the retentiveness or "closure" of radiogenic daughter products in chronometric minerals (U-Pb in zircon, monazite, and apatite, Ar-Ar in hornblende etc...). Unfortunately, most of the constraints on closure temperatures for widely-used chronometric minerals are based on experiments conducted at temperatures well in excess of those encountered in the crust. As a result, there remains a need to document evidence for diffusion in natural systems in order to assess whether high-temperature experimental data can be extrapolated to crustal conditions. In January 2005 I embarked upon a project funded through the ARC Discovery Project programme to investigate Pb-diffusion in natural monazite. In September 2005, a Cameca IMS1270 ion-microprobe (UCLA) was used to measure diffusion profiles in the rims of natural monazite that was reheated to >800°C in a well-documented contact aureole adjacent to the Makhavinekh Lake Pluton (MLP). This exercise revealed gradients in Pb/U and Pb/Th ages in the outermost 0.30 micron of the grains. The geometry of these profiles is consistent with one-dimensional concentration-independent diffusion. Estimated Pb-diffusion coefficients (D) range from 2.5×10^{-28} and $1.3 \times 10^{-27} \text{ m}^2/\text{s}$. This datum plots on the down-temperature extrapolation of experimental data obtained by Cherniak et al. (2004, *Geochim. Cosmochim.* 68, 829-840) and suggests that volume diffusion of Pb in natural monazite is likely to be negligible under thermal regimes and timescales attainable in the upper crust.



Towards the second critical end-point in the pelite-H₂O system: refining existing experimental techniques

Nicholas D. Tailby¹, John Mavrogenes^{1,2}, Joerg Hermann¹ and Hugh O'Neill¹

¹ *Research School of Earth Sciences, Australian National University, Canberra, ACT 2601, Australia*

² *Department of Earth and Marine Sciences, Australian National University, Canberra, ACT 2601, Australia*

The second critical end-point ($CP_{\text{Silicate-H}_2\text{O}}^2$) is a position in P-T-X space for any silicate-water system that is easy to define, difficult to conceptualize and extremely hard to determine experimentally. By definition the second critical end-point marks the position where the wet solidus and critical curve intercept. In short, this end-point marks the position in P-T space where the wet solidus terminates and silicate melts + aqueous "fluids" become completely miscible.

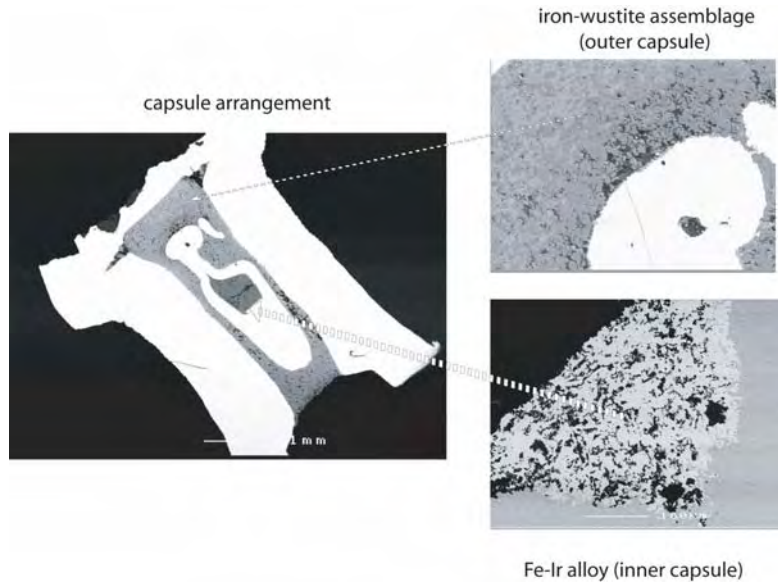
From a historical perspective, investigations into super- $CP_{\text{Silicate-H}_2\text{O}}^2$ behaviour have been hampered by experimental restrictions (particularly among end-loaded piston-cylinder experiments). Such restrictions include H₂O- and mass-loss during capsule welding, limited P-T working range among 5/8" pressure vessels, and retrograde solubility changes with experimental quenching. The research highlights of this year involve setting up experimental designs to overcome many of these problems. In essence, the aims of this project involve building on and combining recently developed experimental techniques in order to approach $CP_{\text{Silicate-H}_2\text{O}}^2$ conditions.

Cold-seal, large-volume, hydrothermal capsule designs established by Hack and Mavrogenes (2006) have shown it is possible to construct piston-cylinder experiments without welding. Such techniques avoid concerns related to volatilization of aqueous species on welding.

The workhorse of this cold-seal technique has been, till this point in time, a thick-walled 9mm Ag-/Au-/Cu-capsule suited to 5/8" pressure vessels. While this technique has been tried and tested for the various parameters crucial to hydrothermal experiments (e.g., inertness, temperature gradients, H-diffusion and P/T-calibrations), the capsule arrangement has a limited experimental range (~25kb/800C). In order to approach $CP_{\text{Silicate-H}_2\text{O}}^2$ conditions for the pelite-H₂O system, the working conditions must be extended to higher pressures (up to ~65Kb). To this end, a new thick-walled 6mm Ag-capsule, suitable for 1/2" pressure vessels, was designed.

A major milestone of the last 8 months was H-diffusion and P-T calibration experiments which have demonstrated that the scaled down capsule arrangement can successfully be run at high P-T conditions.

Additional developments include the use of sliding noble metal alloy H-sensors. These sensors, when combined with an external fO_2 buffer, allow one to monitor a_{H_2O} . This has a number of advantages over traditional silicate- H_2O solubility experiments by virtue of the fact that the experiment does not attempt to determine solubility relationships by direct analysis of silicate-fluid quench products. Rather, the technique involves directly sensing water activity.



Gold and metal enrichment in natural granitic melts during fractional crystallization

Roger Mustard², Thomas Ulrich¹, Vadim S. Kamenetsky³, and Terrence Mernagh⁴

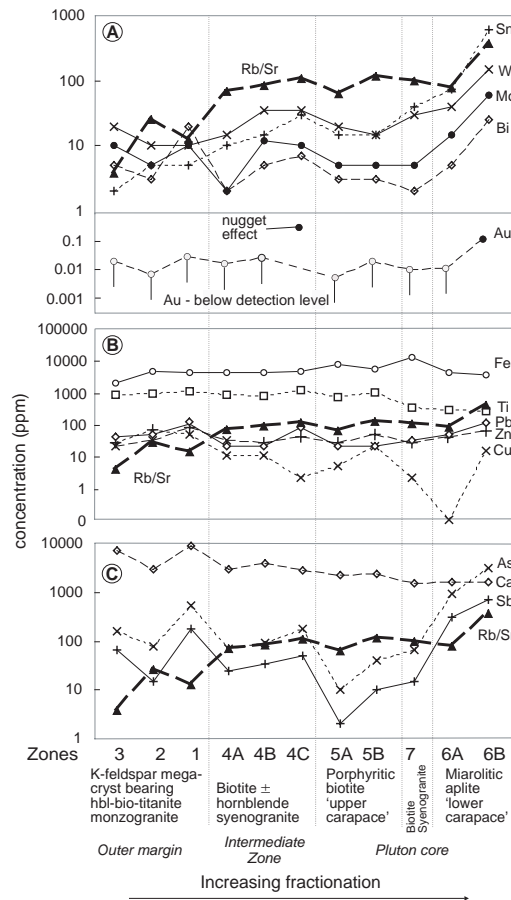
¹Research School of Earth Sciences, Australian National University, Canberra, ACT, 0200, Australia

²Predictive Mineral Discovery Cooperative Research Centre (pmdCRC*), Economic Geology Research Unit, School of Earth Sciences, James Cook University, Townsville, QLD 4811, Australia, *current address: Auzex Resources Limited, Townsville, Queensland, 4810, Australia.

³School of Earth Sciences and Centre for Ore Deposit Research, University of Tasmania, Hobart TAS 7001, Australia

⁴Geoscience Australia, Canberra, ACT 0200, Australia

The formation of magmatic-hydrothermal an ore deposit, and in particular the metal enrichment in the magmatic stage, was investigated at the Timbarra gold deposit in NSW, Australia [Mustard, et al., 2006].



Detailed mapping and petrography revealed different granite types that represent consecutive fractionation products of an unexposed larger magma chamber. This series of increasingly fractionated granite batches was used to look at the metal behaviour during the process of magma differentiation.

Melt inclusions in quartz were studied from each of the granite zones by laser ablation inductively-coupled mass spectrometry (LA ICPMS). In figure 1 the different behaviour of several elements during fractionation processes is shown and an increase of up to 300 times (e.g., Sn) in concentration in the most fractionated zone. Similarly, Au was enriched during fractionation. It seems that in the case where sulfides are absent in the magmatic stage and no early fluid exsolution occurs, that would sequester metals from the melt, fractionation processes can enrich metals in melts to economic concentrations

Mustard, R., T. Ulrich, V. Kamenetsky, and T. P. Mernagh, (2006), Gold and metal enrichment in natural granitic melt during fractional crystallization, *Geology*, 34, 85-88.

Sulfur solubility in felsic melts at different oxygen fugacities

Thomas Ulrich¹, Hugh O'Neill¹, John Mavrogenes¹

¹*Research School of Earth Sciences, Australian National University, Canberra, ACT, 0200, Australia*

The sulfur solubility in felsic melt compositions is of interest because many volcanic eruptions are of andesitic to rhyolitic nature and associated with large amounts of sulfur gas emissions from fluids and vapors (e.g. Mt Pinatubo eruption 1991). The knowledge of the solubility of S in melts can then aid to estimate the S budget in these systems.

Furthermore, at present it is quite well understood how much sulfur can be stored in mafic melts at different oxygen fugacities, but it is unknown how much the solubility changes when more primitive basaltic melts fractionate into more differentiated melt compositions. In order to look at this problem double capsule experiments are carried out at conditions of 1000°C and 3kbars and different oxygen fugacities by using different buffer assemblages (NNO, MnMnO, ReReO₂, RuRuO₂, HM, QFM). The starting assemblage consists of anhydrite, H₂O and an andesitic melt composition.

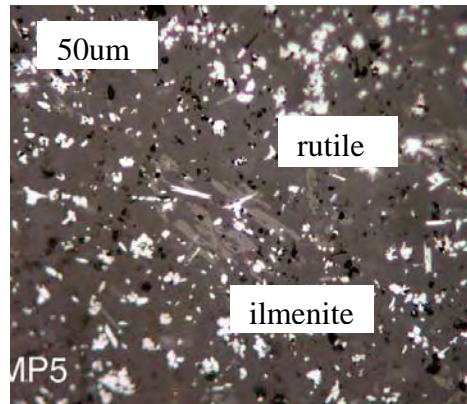
The quenched glasses are analyzed on the SX100 electron microprobe with a new routine developed by A. Norris.

Preliminary results show that tens to several 100ppms of S can be dissolved in these melts at different oxygen fugacities. The work is ongoing and refinements to the experiments as well as to the analytical procedure are in progress.

Metal partitioning in magmatic-hydrothermal systems

Thomas Ulrich¹

¹Research School of Earth Sciences, Australian National University, Canberra, ACT, 0200, Australia



The partitioning of metals during early magmatic stages is influential to the formation of magmatic-hydrothermal ore deposits. To better understand which mineral phases sequester potential ore-forming metals, experiments are carried out in a piston cylinder apparatus. A hydrous andesitic melt composition is doped with metals and powders of ilmenite and/or pyrrhotite and run at 850°C and 3kbars. At this stage only very small crystals formed during the experiments (Fig) and preliminary SEM results show the partitioning of Mo and Zn into ilmenite and Sn into rutile. More experiments will be carried out to distinguish between the effect of sulfides and oxides on the metal partitioning.

Earth Materials, Rock Physics Introduction

Geological and geophysical observations of the response of the Earth to naturally applied stresses, which vary widely in intensity and timescale, provide much of the motivation for the Rock Physics Group's work. In the laboratory, ultrasonic wave propagation and lower frequency forced-oscillation methods are used to probe the elastic/anelastic behaviour which determines seismic wave speeds and attenuation. On longer time scales and at higher stresses, the mechanical behaviour of synthetic faults and fault gouge is studied with particular interest in the complex interaction between chemical reaction, crustal deformation and fluid flow. The fact that all but the simplest elastic behaviour of geological materials is controlled by microscopic defects such as dislocations and processes operative at grain boundaries, places a premium on the complementary microstructural studies involving light and electron microscopy.

Members of Rock Physics collaborate widely within RSES and beyond. Within the Earth Materials area of RSES, the preparation and characterisation of synthetic rock specimens and their precursors, and the study of water-related crystal defects involves intensive collaboration between the Rock Physics and Experimental Petrology Groups. The interest in the structures and microstructures in naturally deformed rocks and related fluid-chemical studies is similarly widely shared – especially with members of the Structure/Tectonics group and the Thermochronology laboratories and the Department of Earth and Marine Sciences, Faculty of Science. Natural links with the Seismology Group, Earth Physics are based on a common interest in the interpretation of seismological models for the Earth's interior.

The group's current research, led by Professors Ian Jackson and Stephen Cox, has three main themes: seismic properties and interpretation, high-temperature rheology and deformation fabrics, and the coupling between fluid flow, deformation processes and reaction. Vital contributions to the group's research effort are provided by postdoctoral/research fellows Drs Yoshitaka Aizawa, Auke Barnhoorn, Ulrich Faul, Stephen Micklethwaite, Eric Tenthorey and Andrew Walker, and Ph. D. students Shaun Barker and Silvio Giger. The capacity to operate novel equipment, and the further development and timely exploitation of associated experimental techniques, depend heavily upon the skill and commitment of research support staff Messrs Harri Kokkonen and Craig Saint and Ms. Lara Weston along with the staff of the School's Engineering and Electronics Workshops. Mrs Kay Provins, Administrator, Earth Materials provides critical support for the Group in purchasing and in website development and maintenance. The Group pursues this ambitious research agenda using core funding from RSES boosted by several grants from the Australian Research Council.

Within the wider ANU community, the influence of the Rock Physics Group is felt in a variety of forums. For example, the ANU's flagship TEM which serves the needs of the campus materials science community is housed within the School and operated by Dr. John Fitz Gerald, the RSES leader in microstructural studies, and Mr. David Llewellyn on behalf of the ANU Electron Microscope Unit.

The group also is committed to undergraduate and graduate teaching, and for many years has participated in the CSIRO Student Research Scheme with students from Canberra secondary colleges.

Seismic properties and high-temperature viscoelastic relaxation

High-temperature rheology and deformation fabrics

Coupling between fluid flow, deformation processes and reaction

Seismic properties and high-temperature viscoelastic relaxation

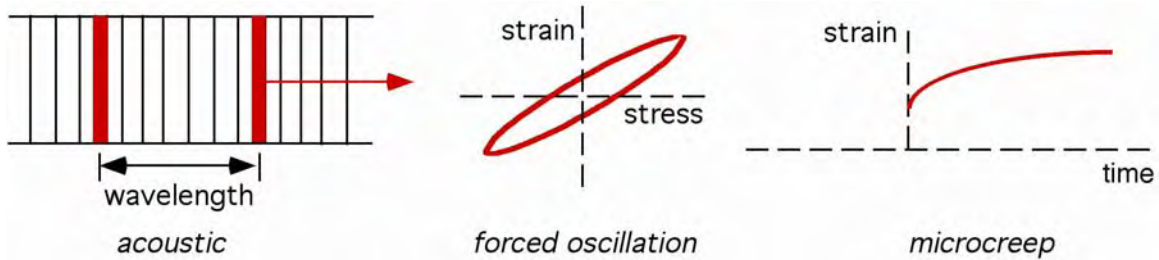
The structure of the Earth's mantle interpreted through laboratory measurements of seismic properties: background and experimental techniques

Seismic wave speeds typically increase with increasing depth in the Earth's mantle – the generally smooth variation evident in global average models being punctuated by discontinuous increases of 5-10% at depths near 410 and 660 km. Superimposed upon this radial variation is substantial lateral variability especially in the uppermost 300 km of the mantle and near the core-mantle boundary.

Are the discontinuities near 410 and 660 km depth simply the result of known pressure-induced changes in crystal structure or is the mantle sharply stratified in chemical composition? What causes the marked lateral variability of the shear wave speed and attenuation in the upper mantle? Variations in temperature? Compositional heterogeneity? Partial melting?

These questions are central to an understanding of the internal dynamical processes represented at the Earth's surface by continental drift and plate tectonics. Answers require measurements on appropriate materials performed under controlled laboratory conditions of pressure and temperature.

The variation of elastic wave speeds with pressure and temperature, like thermal expansion, arises from asymmetry of the interatomic potential energy. Such 'anharmonic' variations of elastic wave speeds can be conveniently measured in the laboratory on mineral or rock specimens of ~0.1 mm – cm size at sufficiently high frequencies (MHz-GHz) by acoustic techniques (ultrasonic interferometry and opto-acoustic methods). During the past decade, both single-crystal and coherent polycrystalline specimens of most of the major mantle minerals (including high-pressure phases) have been characterised with these high-frequency methods. Much has been learned about the pressure, and more recently temperature, dependence of their elastic wave speeds. However, substantial uncertainties remain – especially as regards the combined influence of pressure and temperature.



At the much lower frequencies of teleseismic wave propagation (< 1 Hz) the shear modulus and hence both shear and compressional wave speeds may be profoundly altered at high temperature, and in the presence of fluids, by viscoelastic relaxation. The stress-induced migration of crystal defects (vacancies, dislocations and grain boundaries) and/or redistribution of interstitial melt result in additional strain and hence lower wave speeds accompanied by attenuation.

These effects have only recently become amenable to laboratory study through the testing of cm-sized cylindrical specimens at mHz-Hz frequencies with sub-resonant torsional forced-oscillation methods. Creep methods probing microstrain deformations in torsion distinguish recoverable (anelastic) from permanent (viscous) strains, whereas axially compressive creep tests constrain the rheology at larger strains ($\sim 20\%$).

The following links provide access to selected 2005 highlights of our progress in the development and application of ultrasonic and forced-oscillation/microcreep methods.

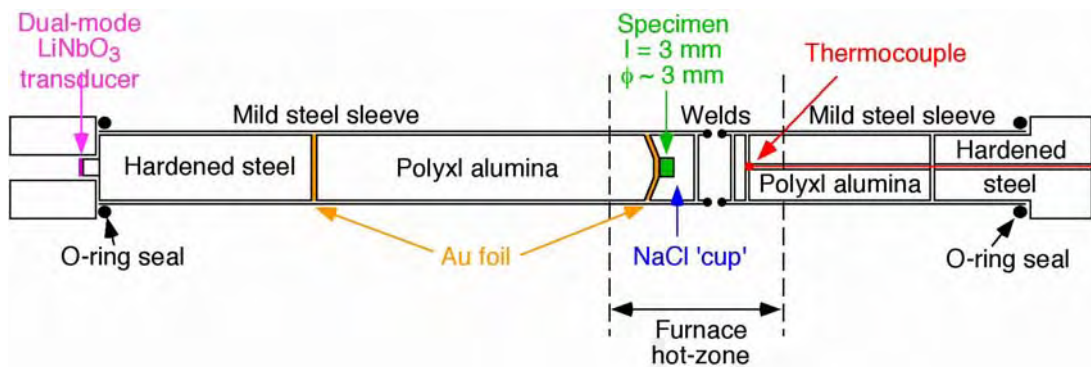
High-temperature ultrasonic interferometry: applications to ScAlO_3 perovskite, orthoenstatite and magnesioferrite

Lara Weston¹, Jennifer Kung², S. M. Antao², Craig Saint¹, Ian Jackson¹, John Fitz Gerald¹, Robert Liebermann² and John Parise²

¹Research School of Earth Sciences, Australian National University, Canberra, ACT, 0200, Australia

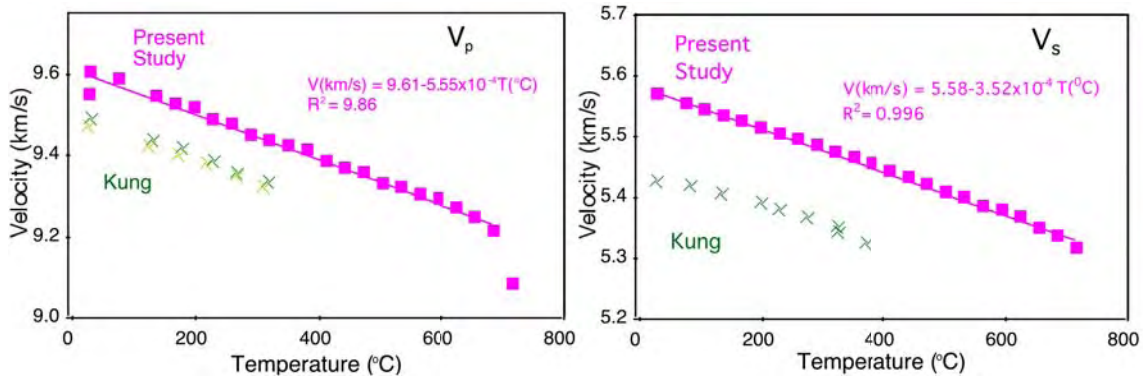
²Department of Geosciences, Stony Brook University, Stony Brook, New York, USA

Elastic wave speeds are precisely measured by ultrasonic interferometry at high temperature and moderate pressure (300 MPa) in gas-medium high-pressure apparatus:



For small specimens and temperatures < 1000 K an alumina buffer-rod tapered to roughly match the specimen diameter and an NaCl pressure-transmitting 'cup' are used. For higher temperatures (to 1600 K), a simple cylindrical buffer-rod and soft Fe cup are employed as in our recently published study of Fo90 olivine (Jackson, Webb, Weston & Boness, *Phys. Earth Planet. Interiors*, 2005).

The former assembly has recently been used to extend a previous study of the elastic wavespeeds in polycrystalline ScAlO_3 – a close structural analogue for MgSiO_3 perovskite, the dominant mineral of the Earth's lower mantle. The newly measured wavespeeds, though systematically higher than those previously measured as the result of intrusion of metallic Fe into the pore space, reveal a temperature dependence that is broadly consistent with the previous measurements but now much better constrained.



The next step will be to fit the temperature dependence of the bulk and shear moduli calculated from the measured wavespeeds and known temperature-dependent density to the comprehensive, internally consistent finite-strain model of Stixrude and Lithgow-Bertelloni (*Geophys. J. Int.*, 2005) and extract values for key thermoelastic parameters to provide guidance in modelling the behaviour of MgSiO₃ perovskite in the Earth's lower mantle.

Visitors Jennifer Kung and Sytle Antao performed measurements this year on polycrystalline samples of MgSiO₃ orthoenstatite, CaTiO₃ perovskite, and MgFe₂O₄ spinel, elucidating the influence of phase transformations and temperature-dependent cation disorder on elastic properties (Kung et al., Antao et al., *AGU Fall Annual Meeting*, 2005).

High-temperature viscoelastic relaxation in upper-mantle materials and its seismological implications

Yoshitaka Aizawa², Uli Faul¹, John Fitz Gerald¹, Stephen Morris³, Ian Jackson¹, Auke Barnhoorn¹, Harri Kokkonen¹ and Craig Saint¹

1Research School of Earth Sciences, Australian National University, Canberra, ACT, 0200, Australia

2Institute for Study of the Earth's Interior, Okayama University, Misasa, Japan

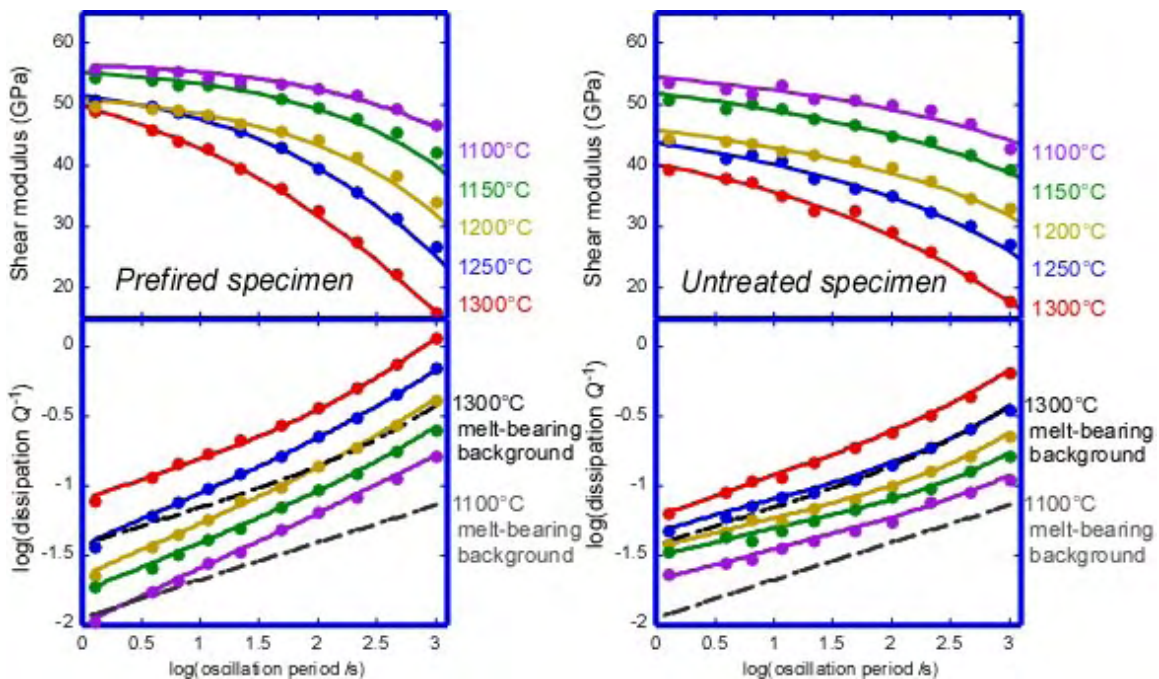
3Department of Mechanical Engineering, University of California, Berkeley, California, USA

In recent years we have applied torsional forced-oscillation and microcreep methods in seismic-frequency studies of the high-temperature viscoelastic behaviour of fine-grained materials based on the dominant upper-mantle mineral olivine. Initially we fabricated and tested a suite of dense, high-purity olivine polycrystals – establishing the ‘base-line’ behaviour in the absence of melt. The variations of both shear modulus G and strain-energy dissipation $1/Q$ with oscillation period, temperature and mean grain size were quantified. The behaviour is of the type commonly referred to as ‘high-temperature background’ in which $1/Q$ varies smoothly and monotonically with period and temperature without any resolvable dissipation peak. Qualitatively different behaviour has been observed for a second suite of olivine specimens containing basaltic melt fractions ranging between 0.01 and 4%. For these specimens, a broad dissipation peak superimposed upon a melt-enhanced background is consistently observed. The high-temperature dissipation background and associated modulus dispersion are attributed to grain-boundary sliding with diffusional accommodation, whereas the peak seen only in the melt-bearing materials is thought to be caused by elastically accommodated sliding facilitated by the rounding of olivine grain edges at triple-junction melt tubules (Jackson et al., *Mat. Sci. Eng. A*, in press).

Motivated by such findings, we have begun a collaboration led by Stephen Morris in the micromechanical modelling of the role of grain boundaries in high-temperature viscoelastic behaviour. A phenomenological study has already elucidated the conditions under which a dissipation peak associated with elastically accommodated sliding is to be expected (Morris and Jackson, *AGU Fall Annual Meeting*, 2005). The next step is to extend the classic work of Raj and Ashby into more realistic regimes – allowing sliding accommodated by a mixture of elastic and diffusional accommodation and clarifying the role of rounding of grain edges at triple-junction melt tubules.

Both the experimental techniques for mechanical testing by torsional forced-oscillation and microcreep methods and the associated procedures for data analysis have been significantly improved during 2005 with particular attention to:

- ◆ the mechanical impact of the foil-bearing interfaces between specimen and torsion rods
- ◆ use of welded Pt capsules to facilitate retention of water
- ◆ more thorough documentation of the viscoelastic behaviour of the steel jacket material
- ◆ allowance for drift in displacement transducer calibration.



Shear modulus and strain-energy dissipation as functions of oscillation period and temperature for untreated and prefired specimens of Anita Bay dunite. The dissipation data are compared at 1100 and 1300°C with the predictions for 100 μm grain size (dashed lines) of a background-only model based on a previous study of fine-grained synthetic melt-bearing olivine polycrystals.

A study of the Anita Bay (NZ) dunite mylonite of ~100 mm average olivine grain size was undertaken this year to complement the ongoing work on synthetic olivine polycrystals. Untreated and prefired specimens, wrapped in Ni₇₀Fe₃₀ foil were tested with torsional forced-oscillation/microcreep methods at temperatures of 20-1300°C, oscillation periods of 1-1000 s, and shear strain amplitudes < 3 × 10⁻⁵. Our intention to explore the influence of water on seismic wave attenuation and dispersion was compromised by the escape of most of the water (0.2 wt %)

initially contained in hydrous minerals such as talc and amphibole in the untreated specimen. On recovery after sustained high-temperature testing, neither specimen contained more than 10 ppm water. The two specimens display generally similar absorption-band behaviour without obvious indications of the broad dissipation peaks characteristic of melt-bearing synthetic olivine polycrystals tested in our laboratory. The new forced-oscillation data for the two specimens are most different at short periods, but are broadly consistent with the background component of dissipation for melt-bearing synthetic olivine polycrystals extrapolated to 100 μm grain size. The absence of an obvious dissipation peak is tentatively attributed to strong heterogeneity in the melt distribution whereby most of the melt is localised in restricted regions of high melt fraction where it has less impact on the mechanical behaviour than in pervasively distributed grain-edge tubules. (Aizawa et al., *AGU Fall Annual Meeting*, 2005).

Grain-boundary sliding in high-temperature ceramics: mechanical spectroscopy of high-purity MgO

Auke Barnhoorn¹, Ian Jackson¹, John Fitz Gerald¹, Yoshitaka Aizawa², Harri Kokkonen¹, Craig Saint¹, Lara Weston¹

¹Research School of Earth Sciences, Australian National University, Canberra, ACT, 0200, Australia

²Institute for Study of the Earth's Interior, Okayama University, Misasa, Japan

This year we started to perform torsional forced oscillation experiments on high-purity magnesium oxide (MgO) samples to investigate the role of grain boundary sliding in viscoelastic deformation across the range of seismic frequencies.

Samples have been fabricated from MgO – Ube powders with an initial grain size of 45-50 nm and > 99.98% wt. % of MgO. Fabrication of dense MgO samples suitable for torsional forced-oscillation experiments involved a four-stage process: 1) Cold isostatic pressing of the powder at 200 MPa confining pressure followed by 2) firing at 1100 °C for 2 hours to eliminate atmospheric contamination, 3) hot-isostatic pressing of the fired pellets at 1100 °C for 24 h decreasing the porosity to < 1%, 4) subsequent hot-isostatic pressing at 1300 °C for another 24 hours enhancing grain growth of the MgO grains and producing a texturally equilibrated microstructure with a mean grain size of 10 μm. This four-stage fabrication process is the only procedure which results in sample of high enough quality and large enough dimensions to be suitable for torsional forced-oscillation experiments. So far we have produced samples with

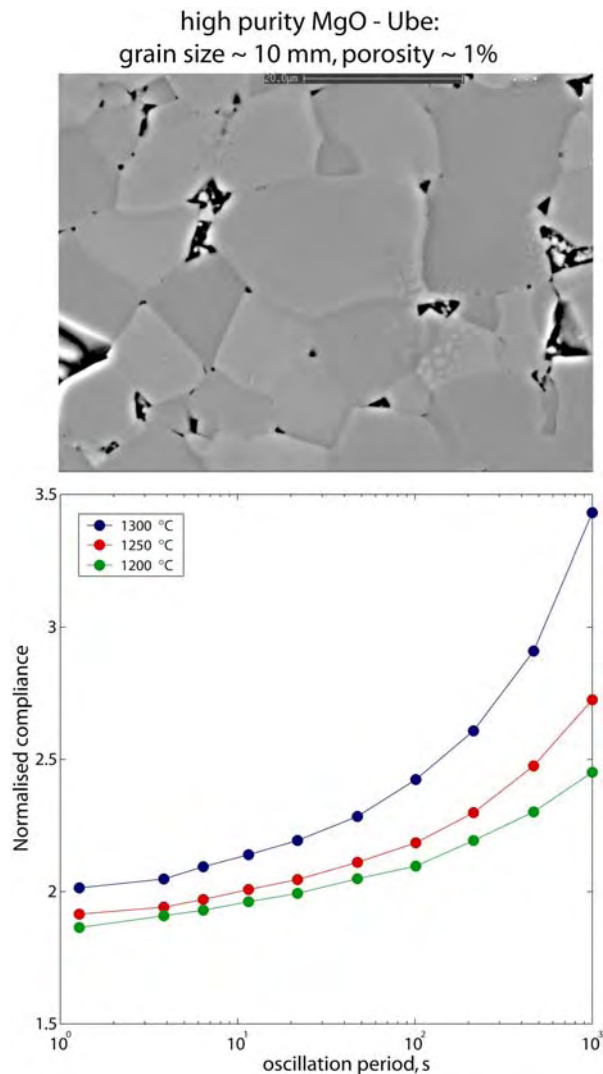


Fig. 1 BSE image of MgO-Ube sample hot isostatically pressed at 1100 °C for 24 hours followed by 1300 °C for 24 hours. Forced oscillation results of normalised compliance at 1300-1200 °C of the same sample.

different grain sizes (mean grain size of 1 μm and 10 μm), which are currently being measured in forced oscillation.

First results of the torsional forced-oscillation experiments show that there is significant anelastic and viscous behaviour during deformation of MgO. The temperature- and frequency-dependence of the shear modulus (G) and dissipation (Q^{-1}) of the two samples with different grain sizes will contribute to the understanding of the influence of the grain boundary sliding processes on the deformation of ceramics and geological materials at frequencies similar to seismic frequencies. This study is aimed to determine whether a revision of the widely used Raj and Ashby model (Raj and Ashby, *Metall. Trans.*, 1971) for grain boundary sliding is needed, as previously suggested by our group (Faul et al., *J. geophys. Res.*, 2004).

High-temperature rheology and deformation fabrics

Research activities in this field during 2005 involved a multidisciplinary mix of fieldwork, experimental studies and computer modelling.

The incorporation of water into titaniferous olivine was studied with ab initio computational methods and infrared and X-ray spectroscopy whereas a robust baseline for the rheology of upper-mantle materials was established through experimental deformation of a new class of genuinely melt-free polycrystalline olivine. Fabrics resulting from deformation by dislocation creep were also a major focus. A study of the statistical significance of crystallographic preferred orientation was undertaken – based on random sampling of synthetic datasets. Meanwhile lattice preferred orientations preserved in rocks dredged from the mid-Atlantic ocean floor were examined to provide constraints on the pattern on flow in the underlying mantle.

The rheology of dry, genuinely melt-free polycrystalline Fo₉₀ olivine

Ulrich Faul¹, Ian Jackson¹, Craig Saint¹ and Harri Kokkonen¹

¹*Research School of Earth Sciences, Australian National University, Canberra, ACT, 0200, Australia*

We have recently measured the seismic properties on a new class of fully synthetically derived rocks of a simplified upper mantle composition (Jackson et al., 2002). The key advantage of these materials is that the occurrence of small amounts of melt can be suppressed at the relatively low pressures typical for experiments in a gas-medium apparatus. Because properties such as diffusivity and viscosity are many orders of magnitude different in a melt relative to a fully crystalline rock, even small amounts of melt will substantially affect the bulk properties of rocks. Samples derived from reconstituted natural rocks invariably contain small amounts of melt at upper mantle temperatures but relatively low experimental pressures due to inclusions, secondary phases on grain boundaries or the trace element inventory established at the conditions of last equilibration in the mantle.

Because the micro-strains generated during the measurements of seismic properties do not fully constrain the (long term) viscous creep behavior we have begun a series of large strain deformation experiments in a Paterson type gas-medium apparatus with the fully synthetic rocks. The materials are prepared by a solution-gelation procedure as for the seismic property measurements, where we continue to improve the homogeneity of the material and reduce its porosity prior to hot-pressing. Preliminary triaxial compression experiments were conducted at a confining pressure of 300 MPa and temperatures in the range from 1200 - 1250 °C. Each experiment is conducted at one temperature in a series of steps of increasing load. At each step the load is held constant with the aim to determine the steady-state strain rate for a given stress before stepping up to the next load segment. Initial results show that strain rates at a given stress of these genuinely melt-free polycrystals are up to 2 orders of magnitude lower than those observed by Hirth and Kohlstedt (JGR, 1995) for nominally melt-free polycrystals, which contain between 0.5 and 1% melt

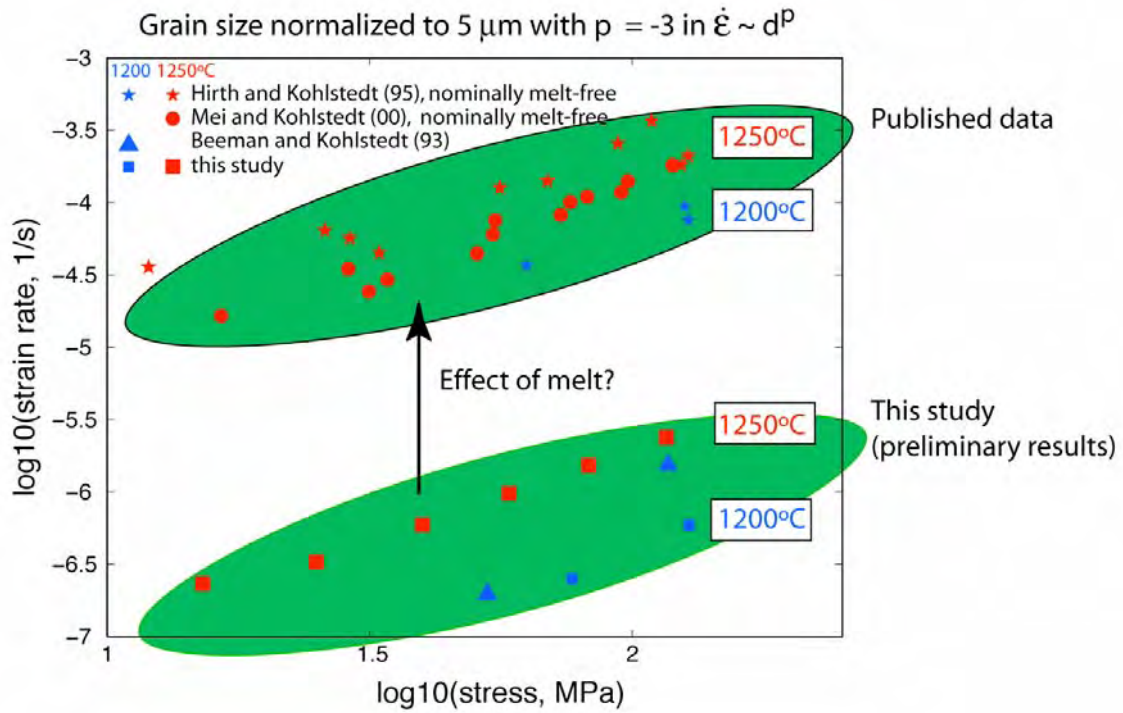


(Figure 1). If confirmed this means that the effect of even small amounts of melt are comparable to a change in temperature by more than 200°C.

References

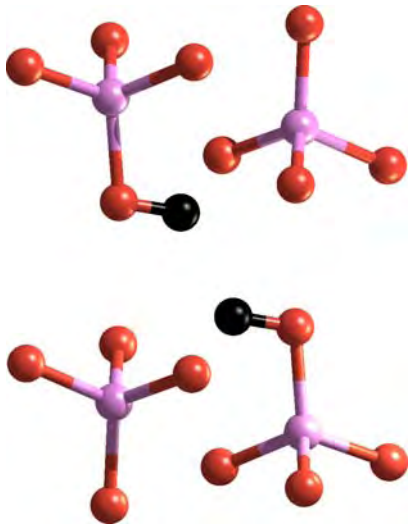
- Beeman, M.L., and D.L. Kohlstedt, JGR, 1993.
 Hirth, G., and D.L. Kohlstedt, JGR, 1995.
 Jackson, I., J. Fitz Gerald, U.H. Faul, and B.H. Tan, JGR, 2002.
 Mei, S., and D. Kohlstedt, JGR 2000.

A new model for the water weakening of Earth's mantle

Andrew M. Walker¹

¹Research School of Earth Sciences, Australian National University, Canberra, ACT, 0200, Australia

The dramatic difference in the planetary scale tectonics operative on Earth and Venus was the major result of the radar mapping of Venus's surface undertaken by NASA's Magellan mission in the early 1990s. The terrestrial landscape is controlled by the motion of a handful of ridged plates with deformation mostly limited to comparatively narrow zones around the plate margins. Despite its similar size and composition, Venus has no plate like features and no ring of fire. It has a surface that is 300–500 million years old and is peppered with impact craters and volcanic features. One plausible reason for these differences is that the upper part of Earth's mantle is weaker than the upper mantle of Venus. Indeed, numerical modeling of the initiation of subduction of oceanic lithosphere shows that a weak mantle is needed to permit the onset of subduction along passive margins and one way to create such a weak mantle is to use a rheology appropriate for wet, rather than dry, olivine [1,2].

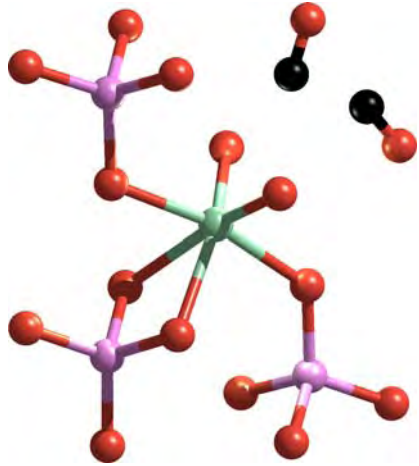


The fact that a small amount of water dissolved into olivine crystals dramatically lowers their resistance to deformation has long been established by work at RSES and elsewhere [3-6]. However, the way that water causes this weakening has remained enigmatic. Using a combination of first principles calculation and infrared and x-ray spectroscopy a new mechanism for water incorporation into olivine has been elucidated. This process relies upon the presence of titanium, but results in the formation of partially

Figure 1: model fragment showing a hydrated cation vacancy formed when water dissolves in forsterite in equilibrium with orthopyroxene. Oxygen atoms are shown in red, silicon in pink and hydrogen in black.

hydrated silicon vacancies. Because silicon is the most slowly diffusion species in olivine, increasing the concentration of vacancies on this sublattice will lead directly to more rapid deformation in the diffusion creep and dislocation climb regimes that are believed to be operative when the mantle deforms.

Figure 2: model fragment showing the titanium - hydrogen defect formed when water dissolves in titanium-bearing forsterite in equilibrium with orthopyroxene. Oxygen atoms are shown in red, silicon in pink and hydrogen in black and titanium ions are shown in green.



The calculations, which involve the solution of an approximation of the Schrödinger equation, yield the energy and structure of single defects in otherwise perfect crystals of forsterite and require only atomic numbers and fundamental physical constants as input. The calculation show that in hydrogen free olivine the lowest energy mechanism for the incorporation of titanium(IV) is direct substitution onto the silicon site and the resulting structure agrees with Ti – O bond lengths derive from EXAFS spectroscopy of titanium bearing olivine. The results

also show that, in equilibrium with orthopyroxene, water is incorporated into forsterite by the replacement of magnesium for two hydrogen ions (Figure 1) and that the magnesium and left over oxygen react with orthopyroxene to form more olivine. However, the situation is dramatically different when titanium and hydrogen enter olivine together (or when hydrogen enters titanium-bearing olivine). In this case the titanium occupies a 6 co-ordinate magnesium site leaving a silicon vacancy which is occupied by two hydrogen ions (Figure 2). The resulting defect has a distinct infrared fingerprint which is observed in recovered olivine from mantle sources [7] and the change in titanium co-ordination on hydration has been observed using XANES spectroscopy. The proposed defect will act to weaken olivine and thus provides an atomic scale view of the planetary scale differences between the two most similar planets in our solar system.

[1] Regenauer-Lieb, K., Yuen, D. A., and Branlund, J. (2001). The initiation of subduction: criticality by addition of water? *Science* **294**, 578 – 580.

[2] Regenauer-Lieb, K., Hohl, T. (2003). Water and diffusivity in olivine: its role in planetary tectonics. *Mineralogical Magazine* **67**, 697 - 715.

[3] Regenauer-Lieb, K., Yuen, D. A., and Branlund, J. (2001). The initiation of subduction: criticality by addition of water? *Science* **294**, 578 – 580.

[4] Mei, S. and Kohlstedt, D. L. (2000). Influence of water on plastic deformation of olivine aggregates, 1. diffusion creep regime. *Journal of Geophysical Research* **105** (B5), 21457 – 21469.

[5] Mei, S. and Kohlstedt, D. L. (2000). Influence of water on plastic deformation of olivine aggregates, 2. dislocation creep regime. *Journal of Geophysical Research* **105** (B5), 21471 – 21481.

[6] Karato, S. I., Paterson, M. S. and Fitz Gerald, J. D. (1986). Rheology of synthetic olivine aggregates: Influence of grain size and water. *Journal of Geophysical Research* **91**, 8151 - 8176.

[7] Berry, A. J., Hermann, J., O'Neill, H. S.C, and Foran, G. L. (2005). Fingerprinting the water site in mantle olivine. *Geology* 33, 869 - 872.

Statistical significance of the strength of discrete crystallographic preferred orientation data

Auke Barnhoorn¹ and Andrew M. Walker¹

¹Research School of Earth Sciences, Australian National University, Canberra, ACT, 0200, Australia

The type, presence and/or asymmetry of crystallographic preferred orientations (CPOs) observed in rocks are frequently used for the interpretation of the deformation history (e.g. stress field, shear sense, post-deformational annealing), the deformation conditions (e.g. temperature, pressure, presence of water) or the activity of certain deformation mechanisms. These interpretations contribute to the interpretation of crustal and mantle-related deformation processes (in both experiment and nature).

Recent advances in the acquisition of crystallographic preferred orientation data by electron backscatter diffraction (EBSD) analyses has increased the interest in the use of CPOs for the interpretation of the deformation history of the material. Methods have been proposed for the quantification of the strength of the CPO, e.g. the J-index by Bunge (*Texture analysis in materials science: mathematical methods*, Butterworths, 1982) and recently the M-index by Skemer et al. (*Tectonophys.*, in press). Both methods have the complication that the value J or M is dependent on the number of measurements in the dataset. Therefore, comparing different datasets with varying number of measurements becomes difficult.

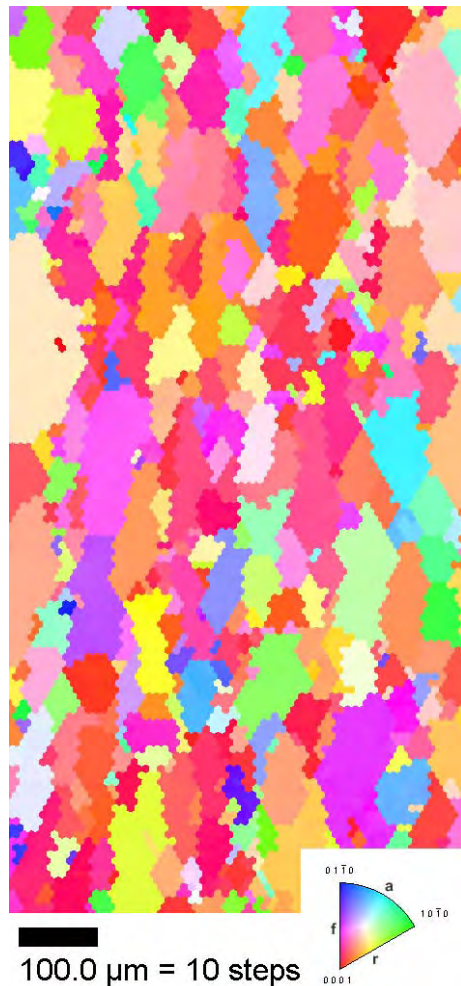


Fig. 1 Colour-coded EBSD map of naturally deformed Carrara marble. Is there significant crystallographic preferred orientation?

This dependence of J and M on number of measurements becomes especially important when one wants to determine whether a dataset with a relatively small number of measurements (<10000) has a random or non-random crystallographic preferred orientation.

To investigate this, we have generated large numbers of datasets (typically 400) with random crystallographic preferred orientations, sampled with varying numbers of simulated measurements in order to determine the strength of the CPO (J and M) for each dataset. The variation in resulting CPO strengths reflects the under-representation of the orientation space by the datasets with limited number of measurements. The standard deviation from the mean of the CPO strength distribution can be used to distinguish whether a dataset obtained by EBSD can be regarded as random or as non-random. The relationships between strength of the CPO and number of measurements can be used for the interpretation of e.g. active deformation mechanisms in rocks and provides a tool to compare different datasets of orientation measurements in a statistically more rigorous manner.

Mantle Flow at Slow Spreading Ridges: Constraints from ODP Leg 209, Mid-Atlantic Ridge

Kay Achenbach², Ulrich Faul¹ and Mike Cheadle²

1Research School of Earth Sciences, Australian National University, Canberra, ACT, 0200, Australia

2Department of Geology and Geophysics, University of Wyoming, Laramie, WY 82071 USA

Owing to the scarcity of oriented mantle peridotite samples, few microstructural and crystallographic data are currently available to constrain models of mantle upwelling and deformation beneath slow-spreading ridges. We have collected quantitative data regarding the shape- and lattice-preferred orientations (SPO and LPO) of olivine and orthopyroxene in peridotites from Hole 1274A, drilled to a depth of 156 mbsf, on the western flank of the rift valley wall at 15° 39' N on the Mid-Atlantic Ridge during ODP Leg 209. With as little as 50% alteration in places, our samples are the freshest peridotites recovered during Leg 209.

The rocks are protogranular harzburgites with 75-82% olivine, 17-22% orthopyroxene, 0.8-1.4% clinopyroxene, and 0.9-2.4% spinel, and one dunite with 96.3% olivine, 0.1% opx, 1.7% clinopyroxene, and 1.9% spinel. The samples preserve evidence of melt-rock interaction and weak lithospheric deformation, but the primary asthenospheric SPO is preserved. Olivine and orthopyroxene exhibit a weak but consistently measurable foliation; no spinel lineation is readily apparent.

Crystallographic data, collected using Electron Backscatter Diffraction (EBSD), are based on measurements of as many as 1100 olivine crystals and 530 orthopyroxene crystals per sample in rocks from ten sections of core (recovered from depths ranging from 20 - 150 mbsf). Olivine crystals show a strong [010] maximum sub-perpendicular to foliation, with a less strongly developed [100] maximum and diffuse clusters of [001] axes roughly parallel to the foliation plane. This fabric is consistent with dislocation creep operating at ~1200° C predominantly on the olivine (010)[100] slip system.

Rotation of the SPO and LPO to a common magnetic declination, using shipboard paleomagnetic data, shows a consistent down-hole olivine foliation dipping at ~80°, with sub-horizontal olivine [100] and [010] axes. The orthopyroxene foliation is less well constrained, but, dipping at ~50°, is discordant to the olivine foliation. Removing the effects of tectonic rotation, we find that at the time of the onset of magnetization in these rocks, olivine [100] axes were subparallel to the ridge axis, and olivine [010] axes were subvertical (resulting in a subhorizontal foliation).

Although the fabrics are relatively weak and there is large uncertainty in the amount and direction of tectonic rotation, this sample reorientation suggests that the direction of mantle flow in this portion of the slow-spreading Mid-Atlantic Ridge was most likely parallel to the ridge axis.

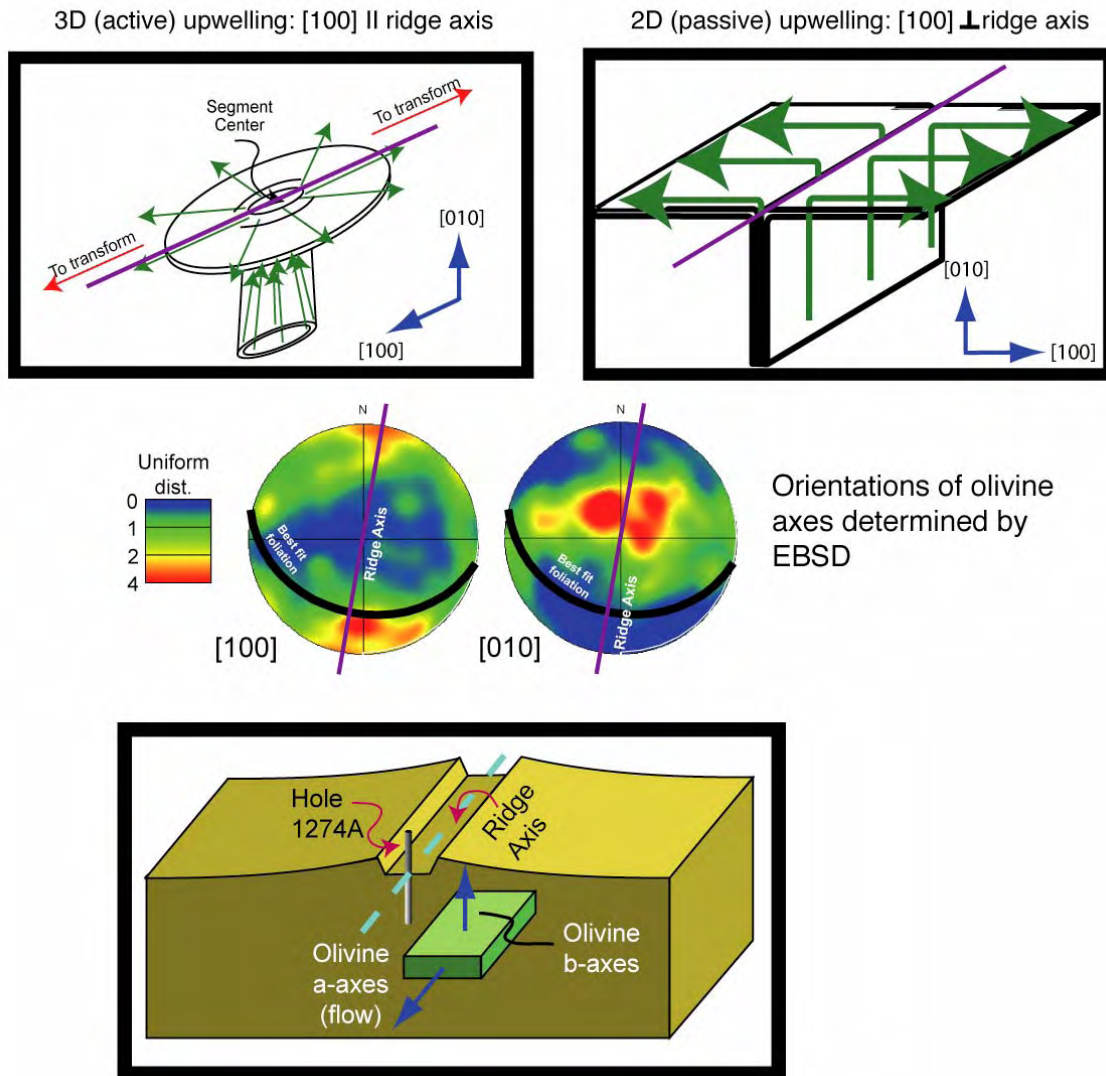


(Figure 1). Models of mantle flow indicate that this requires a component of active (buoyancy induced) upwelling at least locally, as passive upwelling in response to spreading results in an alignment of olivine $[100]$ perpendicular to the ridge axis

Coupling Between Fluid Flow, Deformation Processes and Reaction

Experimental, field-based, microstructural and numerical modelling approaches are being used to explore several aspects of coupling between deformation processes, fluid transport, reactions and the strength of earth materials, especially in fault regimes.

Experimental studies have focussed on measuring changes in permeability and mechanical behaviour of simulated fault rocks in hydrothermally-active regimes. In high temperature hydrothermal environments, the permeability evolution of simulated quartz gouge is found to be strongly dependent on both temperature and grainsize of the materials. During hydrothermal hot-pressing, both permeability and porosity decrease in response to grain-crushing and dissolution-precipitation processes. Permeability reduction occurs at rates which suggest that quartz-rich gouges can become essentially impermeable near the base the crustal seismogenic regime on timescales comparable to the repeat time of major earthquakes. Severe fluctuation in permeability in fault zones during the seismic cycle is likely to be associated with fluctuation in fluid pressures and effective stress states, which in turn impact on processes governing the nucleation and recurrence of earthquakes.

In a separate study, recovery of cohesive strength in quartz sandstone in the presence of reactive pore fluid is being explored. Very rapid crack healing and compaction of cataclasite in laboratory-scale fault damage zones is fostered by strongly temperature-dependent dissolution-precipitation processes. The measured rates and temperature dependences of interseismic fault healing indicate that, in fluid-active environments, faults can largely recover to pre-failure cohesive strengths on timescales comparable to earthquake recurrence at mid-crustal depths in plate boundary regions. Overall, the experimental studies are providing quantitative constraints on the evolution of strength and fluid transport properties of fault zones during the seismic cycle.

Both *field-based and numerical modelling studies* are being used to further test a new model that mesothermal lode gold systems can develop in faults and related fracture arrays that are repeatedly reactivated during aftershocks following major slip events on nearby crustal-scale faults. New field and modelling case studies, in several well-explored areas in the Eastern Goldfields province of WA, have provided further support for the concept that co-seismic static stress changes associated with mainshocks and large aftershocks on high displacement faults provide a first order control on the distribution of gold deposits in fault systems. In a new project, we are testing the application of these models to other types of fault-related mineral systems, such as precious metal epithermal systems and Carlin-type gold systems.

Field-based studies are also using high spatial resolution LA-ICPMS Sr isotope analyses in calcite veins to explore the evolution of fluid-rock reaction and fluid chemistry during vein growth in a fracture-controlled hydrothermal system. The system being studied was dominated by upflow of low $d^{18}\text{O}$ fluids through a limestone sequence at approximately 200°C. Veins developed throughout a protracted period of folding and faulting in the upper crust. In combination with high spatial resolution C/O isotope studies and trace element analyses, this work is providing unprecedented insights about changes in fluid chemistry during the growth of individual veins. Sr isotopic compositions, C/O isotopic compositions, trace elements, and oxidation states all exhibit a complex evolution during vein growth. The work is beginning to provide a new understanding of processes controlling the dynamics of fluid-rock interaction during discontinuous flow in fracture-controlled hydrothermal systems.

Fluid flow changes recorded in syntectonic veins – the use of high-spatial resolution, *in situ* Sr isotope ($^{87}\text{Sr}/^{86}\text{Sr}$) measurements

Shaun Barker¹, Stephen Eggins¹ and Stephen Cox¹

¹*Research School of Earth Sciences, Australian National University, Canberra, ACT, 0200, Australia*

Syntectonic veins provide evidence for fluid redistribution and transport during crustal deformation. Calcite veins contain a valuable trace element (e.g. Mn, Sr, Fe, Mg, REEs) and isotopic record (C, O, Sr), which allow constraints to be placed on the physical (e.g. P, T) and chemical conditions (e.g. fluid composition, pH, oxidation state) at the time of vein formation (*Barker and Cox, 2005*). The veins described here are found within a regionally extensive (> 20 km²) fault-fracture network, which is hosted within a deformed limestone-shale sequence of one-kilometer thickness in the Taemas area of the Lachlan Fold Belt.

Our previous work examining stable C and O isotope ratios in veins throughout this deformed sequence demonstrates that fluid flow was localized to fold and fold-related fracture networks of high-permeability. Systematic vertical variations in the O isotope composition of veins is related to the upward migration of externally-derived, low $\delta^{18}\text{O}$ fluids. In this study, high-spatial resolution *in situ* measurements of $^{87}\text{Sr}/^{86}\text{Sr}$ are used to determine how fluid reservoirs and fluid flow pathways (influencing the nature of fluid-rock reaction) change during the growth of an individual vein (*Barker et al 2005a, 2005b*). *In situ* analyses allow?? The vein examined here is a fibrous, antitaxial growth calcite vein (Durney, 1973; Oliver and Bons, 2001). The vein has 5 distinct textural zones, which are sub-parallel to the vein-wallrock contact. These zones are characterized by variations in calcite fibre orientation and thickness, and changes in cathodoluminescence intensity.

Strontium isotope analyses were conducted using a HelEx ArF excimer laser ablation system, interfaced to a Finnigan MAT Neptune Multicollector ICPMS. Spot sizes of 137 to 233 μm were used, with spot size chosen to optimise the ICPMS signal (Eggins et al, 1998). Analyses were carried out for 200 seconds. Eighteen spot analyses were carried out across the vein, parallel to fibre long axes. Additionally, a lower precision, continuous survey of Sr isotope ratio variations was carried out across the vein, by moving the sample slowly (10 $\mu\text{m s}^{-1}$) beneath the laser. The spot analyses sample are but the narrowest of the textural zones.

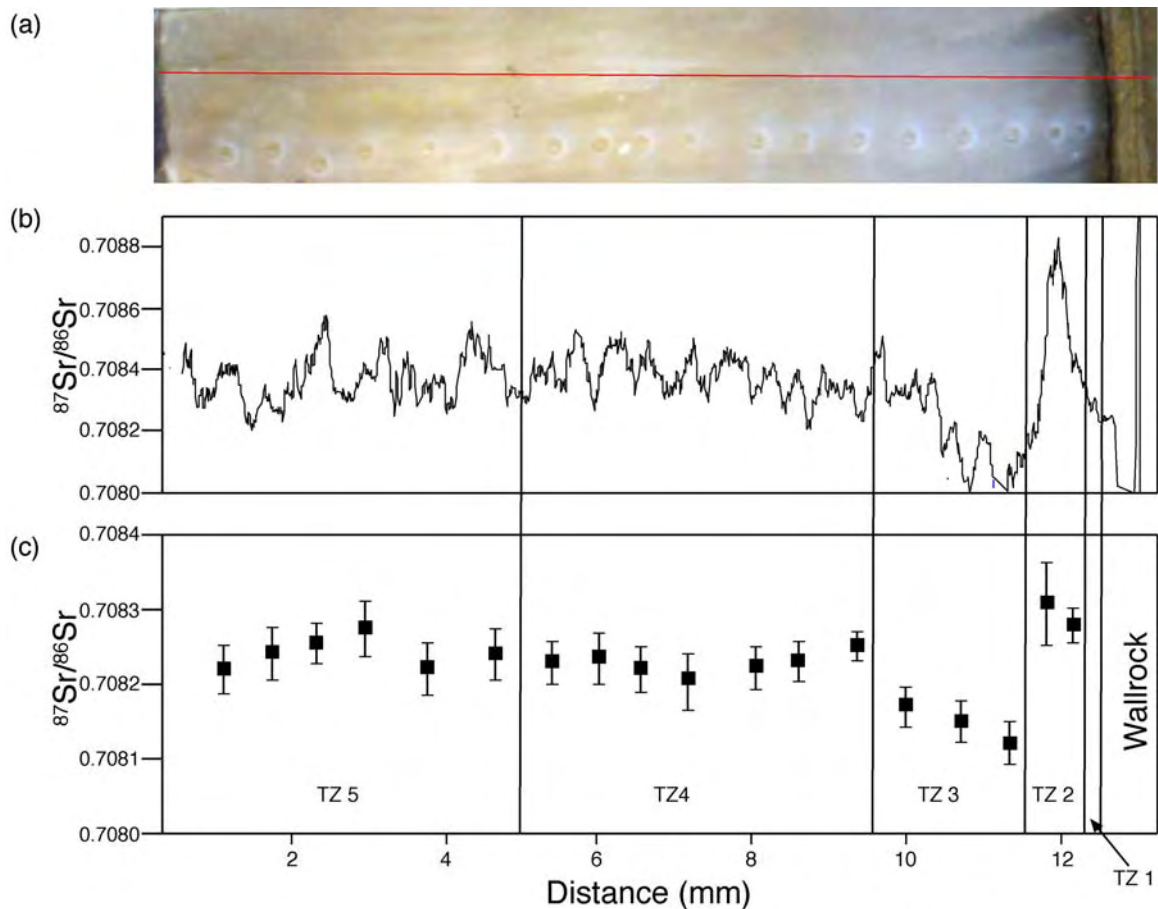


Figure 1: (a) Polished thick section on which Sr isotope analyses were conducted. Red line marks the location of the line profile. The locations of the different textural zones (TZ) are shown. (b) Low-precision Sr isotope variations measured along line profile. (c) High-precision spot Sr isotope ratios. Error bars are analytical 2 s.e.

Strontium isotope ratios through the vein are shown in Figure 1. Strontium isotope ratios are constant within analytical error in each textural zone; significant differences (at the 2σ level) are observed between textural zones 2 and 3, and 3 and 4. Strontium isotopes are not believed to undergo significant mass fractionation in most geological situations. Hence, the Sr isotope ratio of a calcite vein will reflect the parent fluid isotope signature, and will not vary as a function of pressure or temperature (as opposed to O isotopes). Our results indicate that the Sr isotope signature of the fluid from which this vein grew changed with time. These changes are directly linked to variations in vein growth. This implies that changes in growth character are directly linked to changes in the fluid reservoir, or fluid flow pathway (*Barker et al, 2005b*). This implies that fluid flow pathways (and hence crustal permeability) may vary significantly with time, and may be linked to variations in permeability which are believed to occur during the seismic cycle (*Sibson, 2001*).

By combining the Sr isotope results, with fluid inclusion studies, high-resolution records of C and O isotopes, and trace and REE variations, it will be possible to make inferences about variations in pressure, temperature, fluid oxidation state, pH, fluid composition, fluid source and fluid flow pathway during the growth of a single vein.

- Barker, S.L.L. and Cox, S.F. (2005) Chemical evidence for incremental opening and episodic fluid flow during the formation of crack-seal veins. Structure, tectonics and ore mineralisation processes meeting, Townsville, Queensland
- Barker, S.L.L., Cox, S.F. and Gagan, M.K. (2005a) Formation of fibrous and crustiform textured veins – trace element and stable isotope evidence. Structure, Tectonics and Ore Mineralisation Processes meeting, Townsville, Queensland
- Barker, S.L.L., Cox, S.F. and Gagan, M.K. (2005b) Chemical evidence for episodic growth of a fibrous antitaxial calcite vein from externally derived fluid. American Geophysical Union Fall meeting, San Francisco,
- Barker, S.L.L., Cox, S.F. and Gagan, M.K. (2005b) Formation of fibrous and crustiform textured veins – trace element and stable isotope evidence. Structure, Tectonics and Ore Mineralisation Processes meeting, Townsville
- Durney, D.W. and Ramsay, J.G. (1973) Incremental strains measured by syntectonic crystal growths In: De Jong, K.A. and Scholten, R. (Eds.) *Gravity and Tectonics*, Wiley, New York 67-96
- Eggins, S.M., Kinsley, L.P.J. and Shelley, J.M.G. (1998) Deposition and element fractionation processes during atmospheric pressure laser sampling for analysis by ICP-MS. *Applied Surface Science* 127-129 278-286
- Oliver, N.H.S. and Bons, P.D. (2001) Mechanisms of fluid flow and fluid-rock interaction in fossil metamorphic hydrothermal systems inferred from vein-wall rock patterns, geometry and microstructure *Geofluids* 1 137-162
- Sibson, R.H. (2001) Seismogenic framework for hydrothermal transport and ore deposition. *Reviews in Economic Geology* 14 25-50

Time dependent permeability evolution and the development of percolation thresholds in quartz fault gouges in hydrothermal environments

Silvio Giger¹, Stephen Cox¹, Eric Tenthorey¹ and Craig Saint¹

¹*Research School of Earth Sciences, Australian National University, Canberra, ACT, 0200, Australia*

At elevated temperatures in fluid-active environments, the permeability (k) of fault damage zones is expected to evolve with time in the interseismic interval following rupture events. This time-dependent permeability evolution can impact on fluid flow rates within and across fault zones. It also influences the evolution of fluid pressures in fault zones. Rupture recurrence intervals and the distribution of sites of rupture nucleation can be particularly sensitive to fluid pressure evolution. Additionally, cycling of permeability in fault zones between high permeability states and low permeability states during the seismic cycle can establish episodic flow regimes which have implications for the development of fault-related ore systems, such as mesothermal gold systems.

Permeability evolution depends on numerous parameters such as pore size and shape, stress states, pore pressure and fluid type. In granular aggregates, there seems to be a remarkably simple power-law relationship between k and porosity (f) down to a certain critical porosity f_c at which connectivity between pores is lost and flow is no longer possible. This critical porosity is known as the percolation threshold. At high porosities, permeability scales with the cube of porosity. However, as the percolation threshold is approached, pore connectivity decreases and k becomes much more sensitive to changes in f . Understanding porosity-permeability relationships in fault damage products is of fundamental importance to understanding fluid pressure evolution and factors influencing rupture nucleation and recurrence in the mid-crust where most shallow large earthquakes nucleate.

To examine the evolution of permeability in fault gouges during interseismic fault healing, we have measured time-dependent changes in porosity and permeability in granular quartz-aggregates hot-pressed at hydrothermal conditions at temperatures in the range of 700-850°C, confining pressure of 250 MPa and fluid pressure of 150 MPa. Both k and f gradually decreased during hot-pressing in response to mechanical and chemical processes. We analysed f using a variety of techniques; these included high-precision gravimetry, helium pycnometer techniques, and scanning electron microscopy. To our knowledge, the results (Figure 1) represent the first-ever k - f relationship established for a quartzitic fault gouge analogue at low porosities.

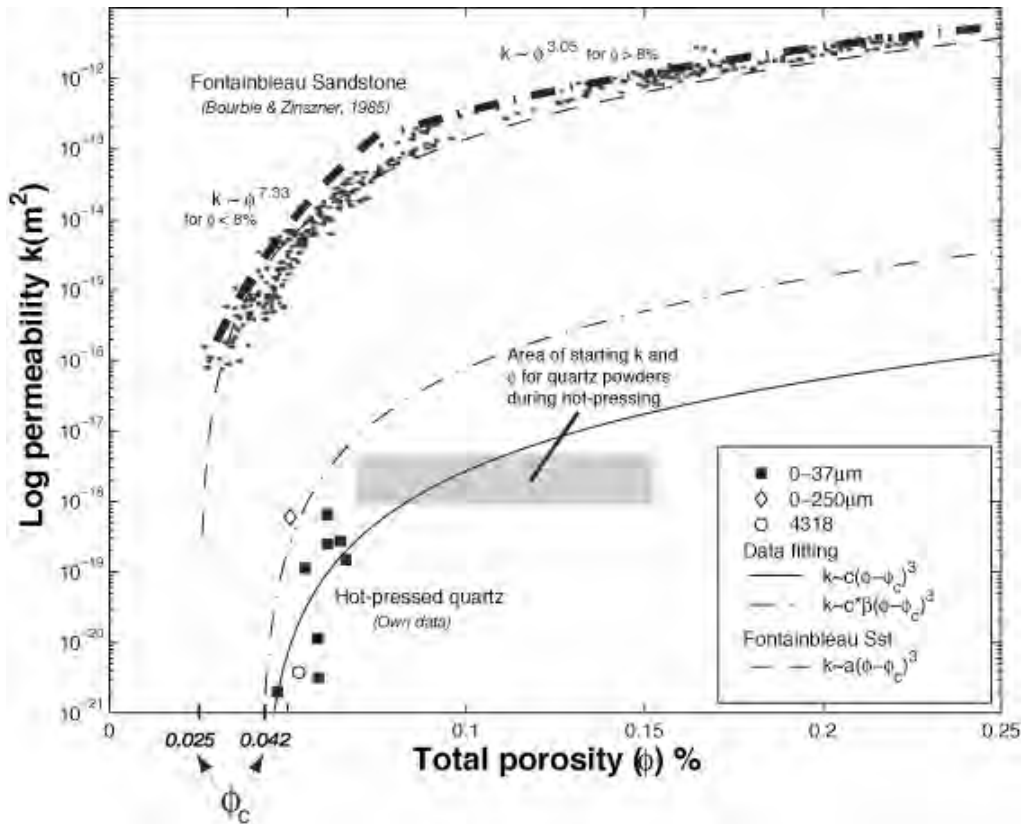


Fig.1. Permeability - porosity relationship for hot-pressed quartz powder compared with Fontainbleau sandstone (Bourbié and Zinszner, 1985). The grain size of the powders was 0-37 μm (with an average of 8.4 μm) and 0-250 μm (45 μm). Run #4318 also had a grain size 0-37 μm , but was performed at considerably higher differential stress.

Our new data on simulated quartz gouges indicate that a percolation threshold occurs at $f_c = 4.2\%$, and that near the percolation threshold the porosity-permeability evolution can be described by a relationship of the form, $k = c \cdot (f - f_c)^3$, where c is mainly a function of grain size (Mavko and Nur (1997); Fig. 1). In order to test the validity of this relationship, we also performed one experiment with a coarser-grained powder (0-250 μm ; average $\approx 45\ \mu\text{m}$) in addition to the fine powders of the other experiments (0-37 μm ; average $\approx 8.4\ \mu\text{m}$). Using a grain-size scaling factor $b \approx 29$, which corresponds to the square of the ratio of the mean grain sizes of the two powders used in our hot-pressing experiments, we can reasonably fit the same equation to our measurement of the 0-250 μm grain size data (Fig.1).

The recognition of a percolation threshold in an experimentally deformed, granular quartz-aggregate has implications for understanding the fluid transport properties and mechanical behaviour of fault zones. In the continental seismogenic regime, co-seismic slip is expected to dramatically enhance permeability in fault zones. In the subsequent interseismic period, mechanical

and fluid-activated compaction and fault healing processes rapidly destroy permeability, especially where fault ruptures tap into high temperature, overpressured fluid reservoirs. Cycling of fault zones between high permeability and low permeability states leads to episodic flow through faults, and potentially to fluid pressure build-up beneath rapidly sealing domains in faults. As they are zones of least normal stress, these high fluid pressure zones potentially provide nucleation sites for the next rupture event. Ongoing work is focussing on measuring rates of permeability destruction, as well as modelling the evolution of fluid pressure and stress states, and their impacts on rupture nucleation and recurrence in fluid-active regimes where major earthquakes nucleate in the mid-crust.

Bourbie T., Zinszner B. (1985), Hydraulic and acoustic properties as function of porosity in Fontainebleau sandstone, *J. Geophys. Res.*, 90, 11524-11532.

Mavko G., Nur A. (1997), The effect of a percolation threshold in the Kozeny-Carman relation : *Geophysics*, 62, 1480-1482.

Exploration potential of stress transfer modelling in fault-related mineral deposits

Steven Micklethwaite¹ and Stephen Cox¹

¹Research School of Earth Sciences, Australian National University, Canberra, ACT, 0200, Australia

We are concerned with the dynamics of seismogenic fault zones, their effect on fluid migration in mid to upper crustal conditions and the implications for fault-related ore mineralisation. Using a combination of field observations and stress transfer modeling (STM), we are carrying out case studies on well-constrained, fault-related mineral deposits from around the world.

The basis of our approach is the common observation that fault-related mineralisation occurs when those fault systems were active. It is well known from experimental and geophysical observations that fault rupture enhances permeability, particularly in low porosity rocks. Over the lifespan of regional fault systems, moderate to large magnitude earthquakes consistently arrest at linkage zones between fault segments (e.g. fault jogs or bends). These linkage zones where main shocks arrest can be contractional or dilational, and clustered domains of aftershocks are triggered over broad areas adjacent to the arrest points. The distribution of resulting aftershocks, or triggering of subsequent large earthquakes, can be successfully predicted by simulating fault ruptures and calculating changes in the static Coulomb failure stress around the ruptures (STM).

The main focus of research in 2005 has been the New Celebration-Jubilee goldfield, located adjacent to a prominent double-bend along the Boulder-Lefroy Shear Zone, Kalgoorlie, Western Australia. Gold deposits in the Kalgoorlie greenstone terrane are often clustered and hosted on small-displacement faults. These small-displacement fault networks are adjacent to and kinematically related to regional-scale fault systems, such as the Boulder-Lefroy Shear Zone. The New Celebration-Jubilee goldfield differs in that its high-tonnage gold deposits are located directly on the Boulder-Lefroy Shear Zone, and a range of lower-tonnage deposits are hosted on smaller displacement faults within a 10×10 km area of the double-bend. The exposure and aeromagnetic data from this goldfield is excellent, providing an unparalleled opportunity to study and understand a broad range of faults, in a major fault system associated with mineralisation. Observations on the fault architecture, geometry and kinematics allow for us to identify some important components of fault system dynamics; for instance geometric barriers to rupture propagation, rupture slip directions and the likely far-field principal stress orientations during deformation and mineralisation. In this case study we are using such information with simple 3D stress transfer modelling, in order match the distribution of known

mineralisation, identify aftershock-related fluid migration pathways and predict potential exploration targets. Similar approaches have already proven very successful in other goldfields (Cox & Ruming 2004, Micklethwaite & Cox 2004), and demonstrated that long-term rupture arrest sites enable aftershocks and transiently high permeability in predictable areas. STM is proving to be powerful for both blind exploration, for brownfields targeting and for our fundamental understanding of faulting and fluid flow.

During the coming year we will begin to apply STM to other types of mineral deposit around the world, including Carlin and Epithermal. Software development is also a high priority, with the aim of incorporating changing fluid pressures as aftershock triggering occurs.

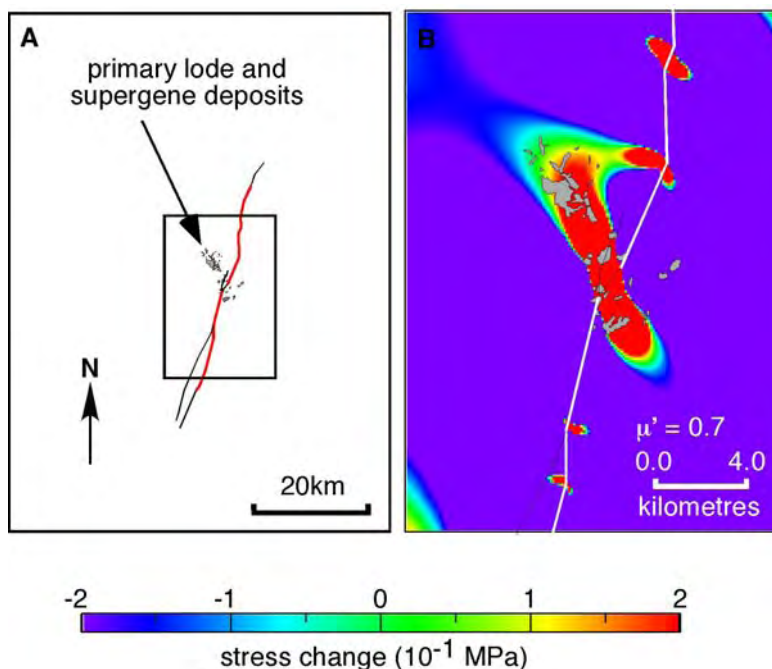


Figure 1: Example of STM results from the Mt Pleasant goldfield, Kalgoorlie, WA. A) plan view of the Black Flag fault system. Fault segments (red) generated large earthquakes, which arrested in the vicinity of the Mt Pleasant gold deposits (black polygons), at a jog on the Black Flag fault system. B) STM results. Areas of positive stress change are proxies for concentrations of aftershocks resulting from the modelled earthquakes on the Black Flag fault. The predicted aftershock distribution matches the distribution of gold deposits hosted on small-displacement faults associated with the larger Black Flag fault.

S.F. Cox, K. Ruming, The St Ives mesothermal gold system, Western Australia—A case of golden aftershocks? *J. Struct. Geol.* 26 (2004) 1109–1125.

S. Micklethwaite, S.F. Cox, Fault-segment rupture, aftershock-zone fluid flow, and mineralization, *Geology*, 32 (2004) 813-816.

Thermal history of an orogen-scale tectonic shuffle zone: K-feldspar $^{40}\text{Ar}/^{39}\text{Ar}$ geochronology transects through the Western and Central Alps of Austria, Switzerland, France and Italy

Jim Dunlap¹, Marnie Forster¹, Marco Beltrando¹, and Gordon Lister¹

*¹Research School of Earth Sciences, Australian National University, Canberra,
ACT, 0200, Australia*

Research into the evolution of the Central and Western European Alps, funded by an ARC Discovery Grant, has been aided by the completion of several traverses (Figure 1) designed to elucidate the thermal evolution of this important orogen using $^{40}\text{Ar}/^{39}\text{Ar}$ step-heating experiments on K-feldspar. This technique has never before been systematically applied to the European theatre, principally as the result of scepticism as to the validity of the method, repeatedly expressed by influential antagonists.

The method we have used is the approach worked out in detail by the UCLA group some fifteen year ago, using the updated modelling programs available on their website. The method assumes that the argon system in K-feldspar is diffusion limited, at length scales typical of the microstructure of K-feldspars. Typical closure temperatures are in the window of ~350-150 °C. The method predicts that K-feldspars are likely to record thermal signatures equivalent to ages between those of the $^{40}\text{Ar}/^{39}\text{Ar}$ system in micas (~300-450 °C), and that of fission track ages of zircon and apatite (~240°C and ~110°C, respectively). We first concentrate K-feldspar from samples of granitoid or granitic gneiss, using conventional density and magnetic separation. The sample is then checked for purity using oil immersion microscopy. The samples that we typically analyze are >99% pure K-feldspar. Microstructural study of each sample is done to make sure that each K-feldspar preserves a "high temperature" microstructure, so that modification of the domain size by grain size reduction, for example, has not occurred during closure to argon diffusion, which would obviously complicate our results. This ensures that the diffusion domains that were actively closing in nature, through the ~350-150 °C window, are still likely to be present in the sample when we undertake laboratory measurements. Each sample is stepwise heated using a schedule of isothermal duplicate steps, to drive off unwanted trapped argon, which is more often than not correlated with chlorine release. These measurements allow us to plot an Arrhenius diagram, from which we can gain an idea of the activation energy for diffusive loss of argon. The Arrhenius information is then modelled using the Lovera programs, the results of which are a domain distribution, their associated volume fractions, and a set of frequency factors. This information is then used to forward model the thermal history, to produce theoretical age spectra that match the laboratory spectra.

We are able to report that the initial results of this study are of considerable interest and significance in the interpretation of Alpine tectonic evolution, because: a) the $^{40}\text{Ar}/^{39}\text{Ar}$ spectra (e.g. Figure 2) show continuity between ages determined using fission track methods and the least retentive domain of K-feldspar (young ages at left side of Figure 2); and b) the $^{40}\text{Ar}/^{39}\text{Ar}$

spectra show continuity between ages determined using phengitic white mica, crystallized in shear zones, and the ages determined using the more retentive domains of K-feldspar (ages at right side of Figure 2, the high temperature portion of the gas release). This allows thermal modelling over the principal temperature range through which most ductile deformation has taken place. Highlights of the research so far include: a) demonstrating that parts of the Sesia zone ceased ductile behaviour in the Oligocene, prior to the indentation of Adria; b) potential evidence for thermal pulses can be recognized associated with the Lepontine event, both in the Western Alps (e.g., in the Gran Paradiso massif), and in Val Calanca, in the heart of the Lepontine culmination. Short-lived thermal events have been recognized previously in Barrovian terranes in the Aegean. This is thus the second classical Barrovian terrane in which such phenomena have been discovered. In these and other areas we are undertaking a numerical modelling study to determine and extent and nature (amplitude and frequency) of thermal pulses using the K-feldspar data as constraints (Figure 3).

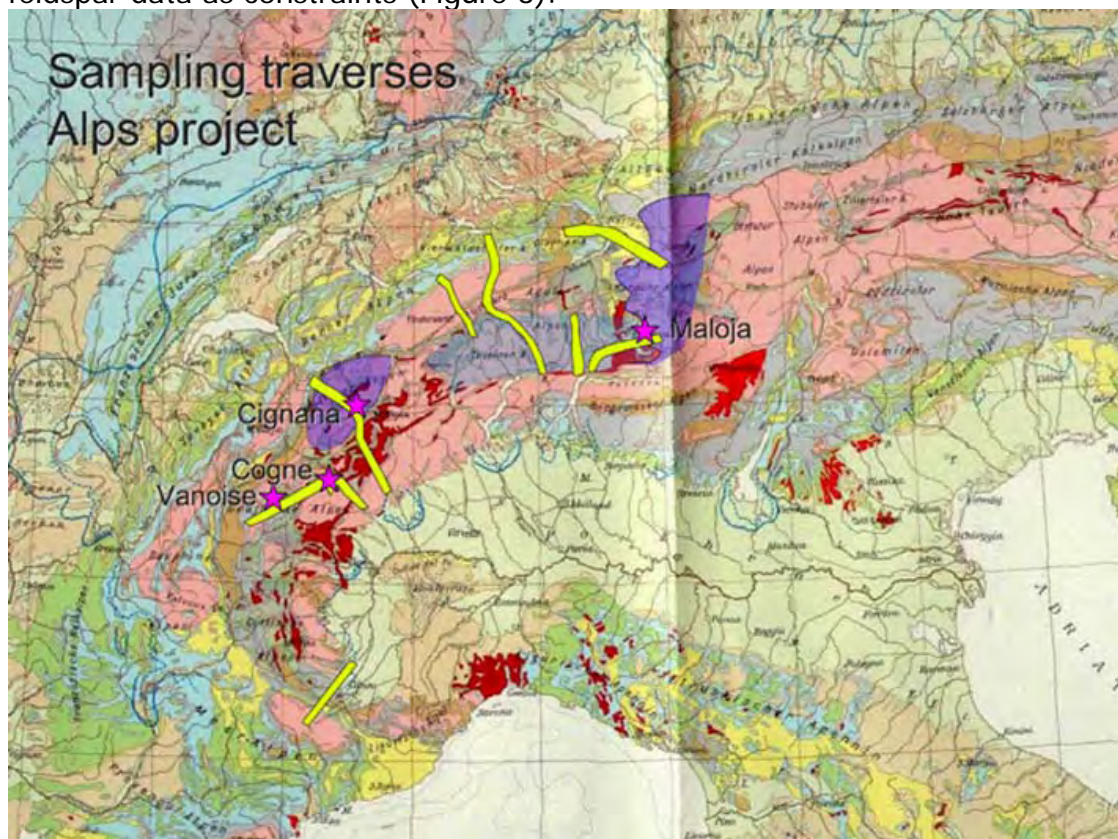


Figure 1. A map of the Central and Western Alps of Austria, Switzerland, France and Italy shows the extent of sampling traverses now completed as part of this research project (in collaboration with Professor Roberto Compagnoni at Torino University, and Professor Jean-Pierre Brun at ETH, Zurich). Traverses (clockwise around the orogen) are: 1) Dora Maira; 2) Northern Gran Paradiso and Vanoise; 3) Monte Rosa, Lago di Cignana and Dent Blanche nappe; 4) a-b-c Lepontine Culmination and Aar massif; 5) a-b across the lower Austro-Alpine nappe boundary.

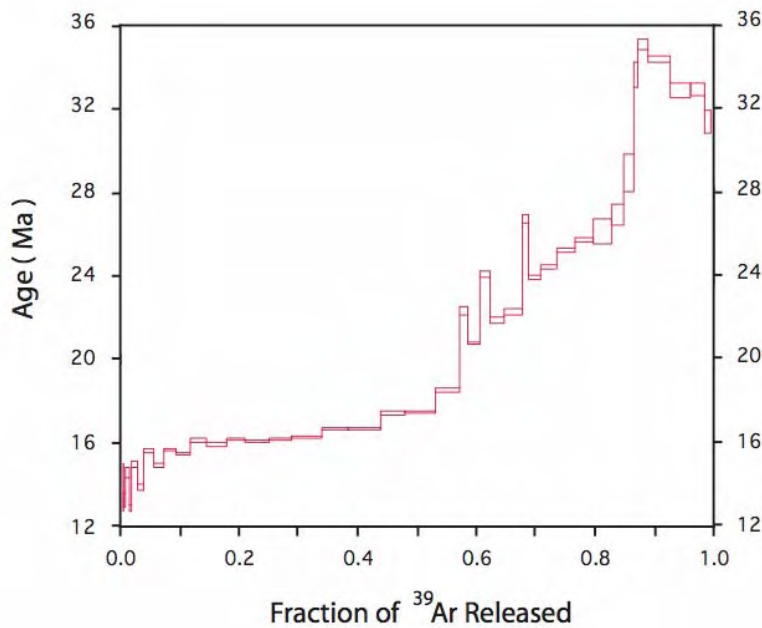


Figure 2. A typical $^{40}\text{Ar}/^{39}\text{Ar}$ apparent age spectrum obtained from step heating K-feldspar from one of the transects (Glarus Thrust region). Due to the multi-domain nature of the K-feldspar microtexture it is reasonable to assume that variable length scales for diffusion are responsible for the range of apparent ages. Two steps at each temperature are analyzed. This allows degassing in the first step of fluid inclusions, as indicated by high Cl/K ratios (not shown), and elevated ages. These relatively high ages are a mixture of both argon trapped in fluid inclusions and argon derived from diffusive loss through the K-feldspar lattice. The second step presents a more accurate approximation to the true age of the sample, as most of the trapped argon was released in the first isothermal heating step.

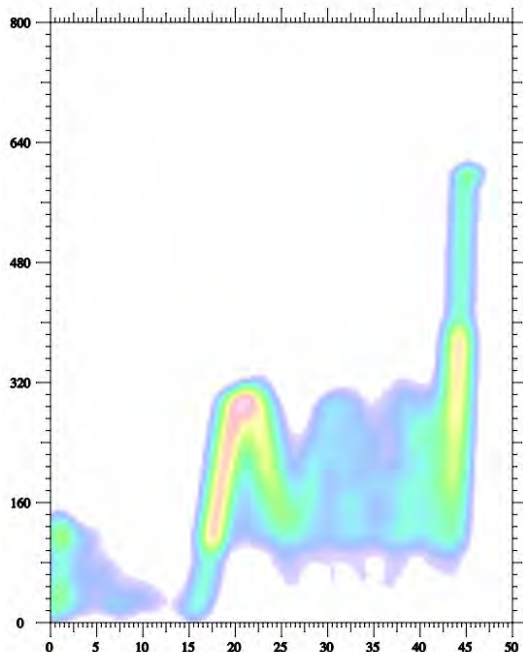


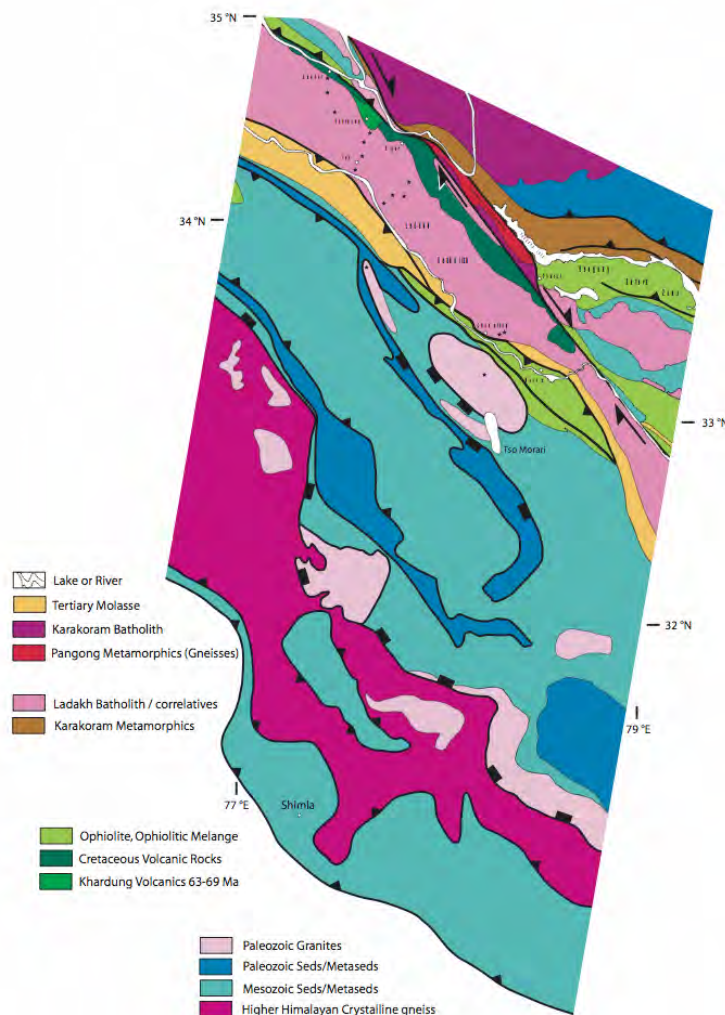
Figure 3. Temperature (y-axis) – Time (x-axis, Ma) diagram obtained by using the Multi-Diffusion-Domain program of Lovera (1989) to calculate a set of non-interacting domains that are able to reproduce the Arrhenius and Log R/R₀ for the sample. The calculated domain distribution is used to forward model the thermal history, to find a match between the laboratory-derived age spectrum and the model age spectrum. These results are for a freely oscillating thermal history, to help understand how thermal spikes might play a role in producing the age gradients we see in the K-feldspars.

Post-Collisional Ramping of the TransHimalayan Batholith and the Ancestral Course of the Indus River: A Tale of a Mountain, Ten Feldspars and a Dam (and a Lion, a Witch, and a Wardrobe).

Jim Dunlap¹

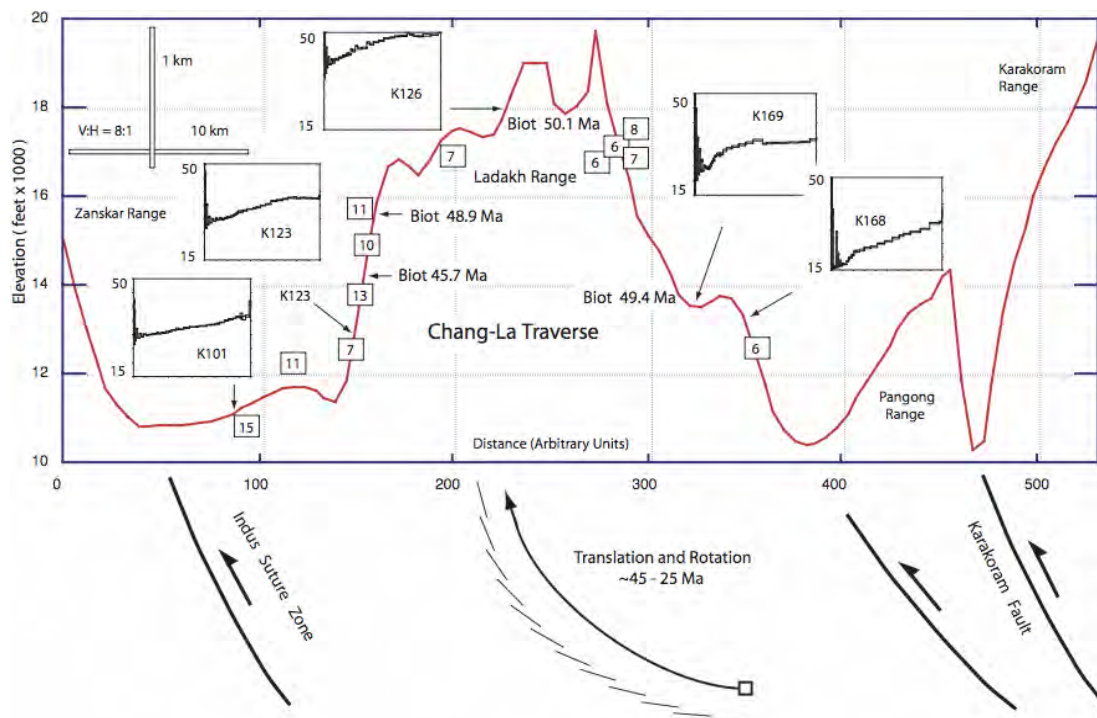
¹Research School of Earth Sciences, Australian National University, Canberra, ACT, 0200 Australia

The Ladakh Batholith is the western section of the ~2000 km long TranHimalayan Batholith in Kashmir, northwestern India. The batholith is bounded by a pair of sutures along most of its length, to the south by the Indus-Tsangbo suture, and to the north by the Shyok-Shiquanhe suture (Figure 1). For most of its length the batholith appears from the geological evidence to be upright, or tilted to the north, with only a few sections thinned or stretched parallel to the arc due to deformation during and after collision. In Ladakh the batholith reaches its maximum width of ~45 km, but near the Chinese border to the east, at the precise point where the Indus River crosses the arc, the batholith is locally at its thinnest in map view (Figure 1). The exhumation history of the batholith in the Ladakhi sector has been revealed through ⁴⁰Ar/³⁹Ar analysis of K-feldspars (stars on Figure 1). The multi-diffusion-domain method of Lovera has been applied to laboratory step heating data, to determine a distribution of diffusion domains appropriate to each sample. The Arrhenius results from the laboratory have been simulated using the Lovera approach and model thermal histories that match the laboratory results have been calculated.

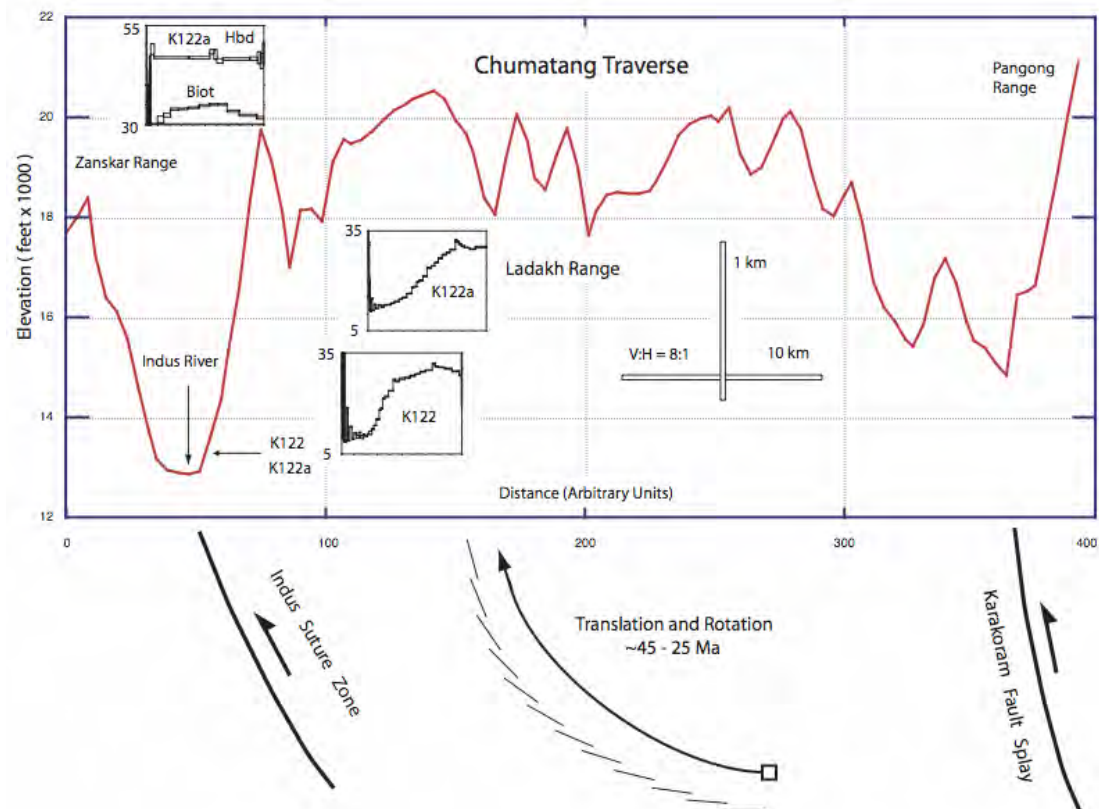


The bulk of the granitoid rocks in the Ladakh Batholith appear to have been emplaced in the period between about 75 Ma and 55 Ma, based upon a still small number of dated zircons (e.g., Weinberg and Dunlap, 1999). This suggests that the batholith was mostly built in the fifteen or twenty million years immediately prior to collision, during subduction of the last few thousand kilometres of Tethyan oceanic lithosphere. Aside from the obduction of small slices of ophiolite (Nidar and Spontang), accretion of material along the southern margin of the Ladakh batholith in this period prior to collision appears to be minimal. The Nidar ophiolite is suspected of being a basaltic oceanic island, which would clearly have been an “asperity” that clogged the subduction zone. The nearby Tso Moriri continental, domal crustal slice to the south appears to have gone down to some 90 km depth before making its way back to the surface, probably via extensional processes, cutting its way through the overlying accreted material.

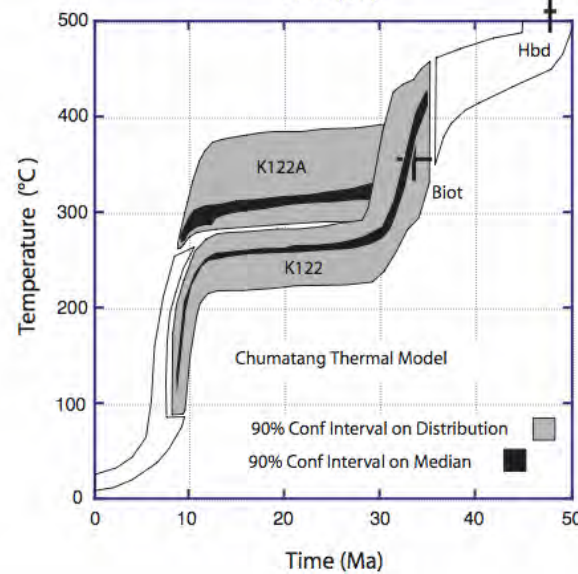
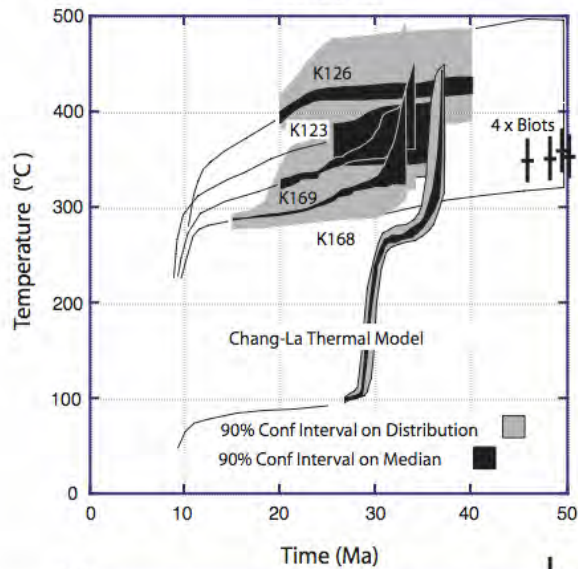
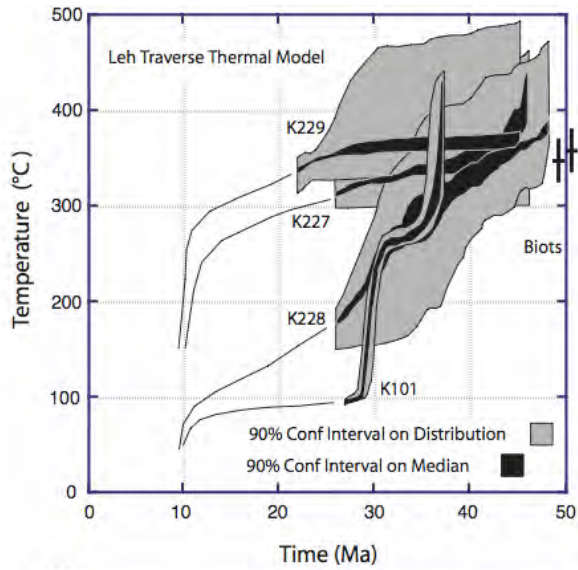
The Ladakh Batholith in the area of study between Leh and Chumatang is (at least in part) tilted to the north at about 35°, as evidenced by remnants of the 63-69 Ma Khardung Volcanics (Figure 1) which were deposited as a ten kilometre thick pile along its northern margin (Dunlap and Wysoczanski, 2002). Aside from the Khardung Volcanics the preservation of sediments and volcanic rocks deposited upon the arc is limited to a few localities in the Ladakhi sector (Honnegger, 1981, Roland, 1999). These occurrences are important in that they establish both paleohorizontal and depth of exhumation subsequent to collision. Volcanic rocks and sediments preserved in western Ladakh in the thickest section of the batholith, near Kargil, dip gently to the south, indicating that exhumation since deposition is limited. Sediments and volcanics directly to the north of this locality show that the northern margin of the batholith is tilted to the north (Brookfield, 1983). In general the Ladakh Batholith in the study area between Leh and Chumatang is tilted to the north up to 35°. Exposures of pre-collision marine deposits along the southern side of the batholith between Leh and Chumatang are strongly disturbed by post-collisional tectonism, and cannot be used to estimate paleohorizontal or depth of exhumation. On the other hand, the Eocene Indus Molasse (Clift, 2003) in



in places undisturbed, standing directly on eroded Ladakh Batholith. At such sites paleohorizontal dips gently to the south. Excursions across the Ladakh Batholith via the passes of Lasirmu, Khardung, Wuri and Chang (e.g., Weinberg and Dunlap, 1999), encountered little in the way of major internal structures such as faults or shear zones. In fact the granitoids within the batholith are virtually undisturbed except for tilting which was accomplished by movement along the bounding sutures to the north and south. The one exception worth noting is the right-lateral Tanglasgo shear zone, which formed in response to regional right-lateral ductile deformation prior to 22 Ma (Weinberg and Dunlap, 2000). Nevertheless, this structure is minor and localised. Moreover, post-collisional uplift and exhumation appears to have been accomplished almost exclusively by movement on the shear zones bounding the batholith, rather than through internal structures. This then begs the question of how the tilting was achieved. Was the batholith in our study area tilted as a largely coherent unit? Do the bounding shear zones become asymptotic at depth and join to form a crustal detachment?



This question and others have spurred on research into the cooling history of the Ladakh Batholith (Figures 2, 3). Samples of undeformed granitic rock were taken along the starred sections indicated in Figure 1, with a view to determining a post-collisional thermal path using $^{40}\text{Ar}/^{39}\text{Ar}$ thermochronology of K-feldspars (Figure 2), micas and amphiboles. The data is used to compare and contrast the exhumation history of the batholith in the section from Leh to Chumatang. The results also bear on the subject of the ancestral course of the Indus River.



The thermal history results, shown in Figure 3, indicate that samples from each of the four traverses in the Ladakh Batholith yield different portions of what appears to be a common cooling path. Remarkably, sample 95212 from the Lasirmu-La traverse appears to date a rapid cooling event associated with the impact of collision, at 53 Ma. As a whole the thermal models show that samples from the northern side of the batholith, or from high elevations, have cooled slowly since collision at about 53 Ma. There are broad similarities between the more northerly thermal models for each traverse, particularly those from the Lasirmu-La, Khardung-La and Chang-La traverses. In contrast, the sample K101 from the southern side of the batholith cooled more rapidly, during a pulse of exhumation at ~30 Ma. The Chang-La and Chumatang traverses also show evidence of a pulse of exhumation at 30 Ma, to varying degrees, with this event reflected more prominently near Chumatang.

It would appear that the 30 Ma event is related to tilting of the batholith to the north, thus allowing southerly samples

to be rotated upward quickly and cooled quickly, and northerly samples to remain relatively less affected by exhumation and cooling. For tilting of the batholith on a horizontal axis, at a depth of about 10 km one would expect to see northerly samples cool less, and less rapidly (or even heat up due to burial), and southerly samples cool by a greater amount and more rapidly. In addition, much more material must have been eroded from the southern side of the divide, which is expected due to the prevailing and pronounced orographic precipitation.

Tectonic and thermochronological studies by our group on the northern side of the Ladakh Batholith (Dunlap et al., 1998), along the active Karakoram Fault Zone, within the extruded lower crustal gneisses, have allowed us to track the uplift and exhumation history of these rocks. The past and active movement on the Karakoram Fault has helped to form a major valley system that includes portions of the Nubra and Shyok Rivers. These rivers drain a large section of the high Karakoram Mountains, the largest area of extreme elevation and relief on the planet. Near Tangtse, transpression on the Karakoram Fault's northern strand has resulted in damming of the northwesterly outlet of the Pangong Lake (Searle, 1996). Previous evidence for damming of the northwestward flow of these rivers also includes the large thickness of Tertiary lake sediments near Agham. It is likely that the ancestral Indus River flowed to the northwest, through the Pangong Lake region, or through the valley to the south adjacent the Ladakh Batholith, rather than across the Ladakh batholith near Nyoma, as it does today. The northwesterly route would have been the easiest path for the Indus River to take, instead of cutting across the Ladakh Batholith, which was presumably high ground relative to the bounding valleys.

The transpressional deformation that likely dammed the northwestward flow of the Indus River and outlets from Panong Lake most likely developed either in the period from ~14-11 Ma or from 8.5 Ma to less than ~4 Ma, when tranpressional deformation and uplift of the Pangong metamorphic rocks resulted in their dramatic cooling. During the 8.5-11 Ma period of strike slip deformation on the Karakoram Fault (little or no cooling of Pangong metamorphics), proposed by Dunlap et al. (1998), it seems likely that the Ladakh Batholith was stretched parallel to its length, failing by tensional fracturing and extensional faulting in the area northeast of Nyoma. It is noted that the Indus River cuts across the Ladakh Batholith in this region, following a series of north-south and east-west striking linear segments. The north-south segments are in an orientation preferred by tensional fractures (Y-Z plan) in a right-lateral shear system. The east-west segment would have been activated as right-lateral Riedel shears. Although no field evidence from these gorges is available, it would not be hard to prove the proposed scenario where the Indus River was captured along the thinned and fractured section of the batholith near the 90° bend just upstream from Nyoma. If the northwesterly outlet for the Indus along the Panong Lake route, and down

the Shyok River was dammed starting about 8 Ma, then it seems likely that the Indus exploited the low ground, underlain by extended crust, near Nyoma, and cut a new path along the southern side of the batholith, following the linear belt of easily eroded rocks along the Indus suture zone between Nyoma and Leh.

We believe that there is thermal evidence in the models made from the K-feldspar results that the Indus river traversed the Ladakh Batholith at ~8.5 Ma. With such a large source of water coursing down a catchment that had prior to 8.5 Ma been relatively small, one would expect enhanced erosion in the Nyoma-Leh sector to follow, as large volumes of easily eroded sediment were removed. The relatively steep river bed gradient in the Nyoma to Chumatang sector is remanant feature of river capture and diversion along this section. Indeed, this seems to be the easiest way to explain the dramatic cooling event recorded in the K-feldspars from Chumatang at ~8.5 Ma, as the Tso Morari metamorphics had already been exhumed to fission track closure temperatures (Schlup et al., 2003). As the K-feldspars from the Leh and Chang-La traverses had already cooled to below their lower recording limit of about 150°C, these K-feldspars were not able to record a transition to more rapid cooling at ~8.5 Ma. The damming of northwesterly flow of the Indus along the Karakoram Fault, due to transpression, the thinning and failure of the Ladakh Batholith by tensional and shear fracturing northeast of Nyoma, and the previously developed linear drainage along the Indus suture between Nyoma and Leh, all conspired to reset the course of the Indus River from ~8.5 Ma, leading to a change toward more rapid cooling of the K-feldspars at Chumatang.

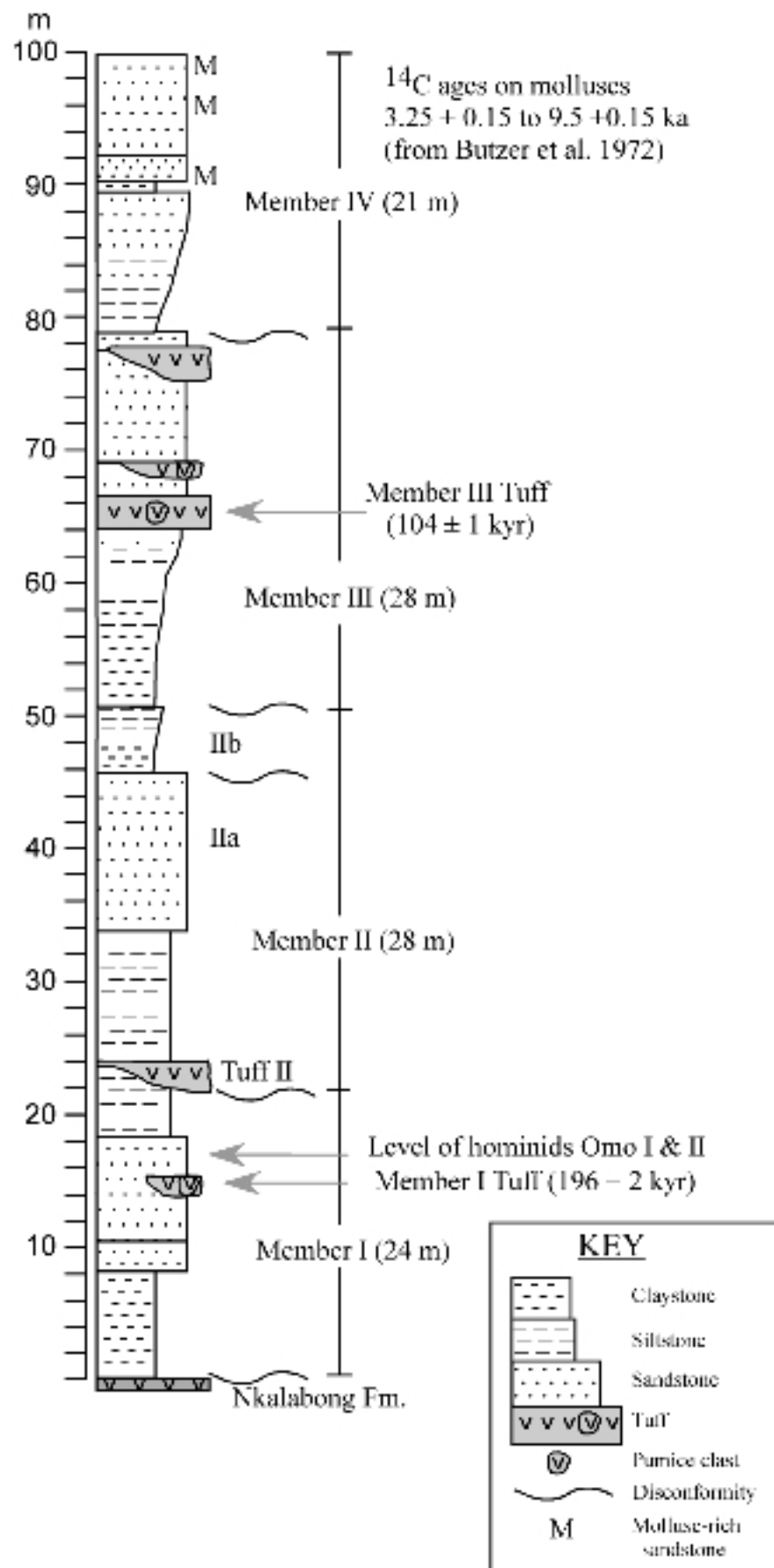
Geochronology of the Nabwal Hills: a record of earliest magmatism in the northern Kenyan Rift Valley

Ian McDougall¹ and Ronald T. Watkins²

¹ *Research School of Earth Sciences, Australian National University, Canberra ACT 0200
Australia*

² *Department of Applied Geology, Curtin University of Technology, PO Box U1987, Perth WA
6845*

The Nabwal Hills, NE of Lake Turkana, contain a record of magmatism associated with the initiation and early development of the East African Rift System in northernmost Kenya. The predominantly volcanic Asille Group, 1400 m thick, directly overlies metamorphic basement and comprises a sequence of basaltic lava flows with significant intervals of rhyolitic pyroclastic units, and minor intercalations of fluviatile sediments. The basement gneisses yield K-Ar cooling ages on biotite of 510 and 522 Ma, typically Pan-African. The ⁴⁰Ar-³⁹Ar ages on alkali feldspar crystals from the rhyolitic units are concordant and show that the Asille Group spans the interval from at least 34.3 to 15.8 Ma, continuing to younger than 13 Ma from previous measurements. Vertebrate fossil sites, containing primate remains, at Irile and Nabwal are shown to be 17 ± 2 Ma old, Early Miocene, based upon K-Ar age measurements on immediately overlying basalts. Variably reliable whole rock K-Ar ages, determined on basalt samples from low in the sequence, indicate that volcanism commenced as early as 34.8 Ma ago. The overall geochronological results show that magmatism in the Nabwal Hills began about 35 Ma ago in the Late Eocene, interpreted as the time of initiation of crustal extension that lead to the development of this segment of the East African Rift System. The Asille Group is tilted about 6° to the SSW. This tilting occurred subsequent to 13 Ma ago, and prior to the eruption of the flat-lying Gombe Group basalts. These basalts may have begun erupting about 6 Ma ago in the Late Miocene, although much of this volcanism occurred between about 3.9 and 4.2 Ma ago in the Pliocene. It is suggested that the main rifting, which continues today, commenced in the Middle Miocene, less than 13 Ma ago, and is partly reflected in the tilting of the Asille Group.



Successful microstructural analysis of K-feldspar using the electron backscatter diffraction method and its application to understanding the link between microstructure and $^{40}\text{Ar}/^{39}\text{Ar}$ age

Sandra McLaren¹ and Steve Reddy²

¹ *Research School of Earth Sciences, Australian National University, Canberra ACT 0200 Australia*

² *Department of Applied Geology, Curtin University of Technology, WA*

K-feldspars are one of the most common rock forming minerals, occurring in a wide variety of terrestrial rocks. The mineralogy of K-feldspars has been extensively studied and their use in thermometry and argon thermochronology is well established. However, their abundance in many lithotypes means they are also potentially very useful for understanding rock deformation mechanisms and strain kinematics. Obtaining quantitative crystallographic orientation data from K-feldspars is essential if their role in understanding the formation processes is to be fully met.

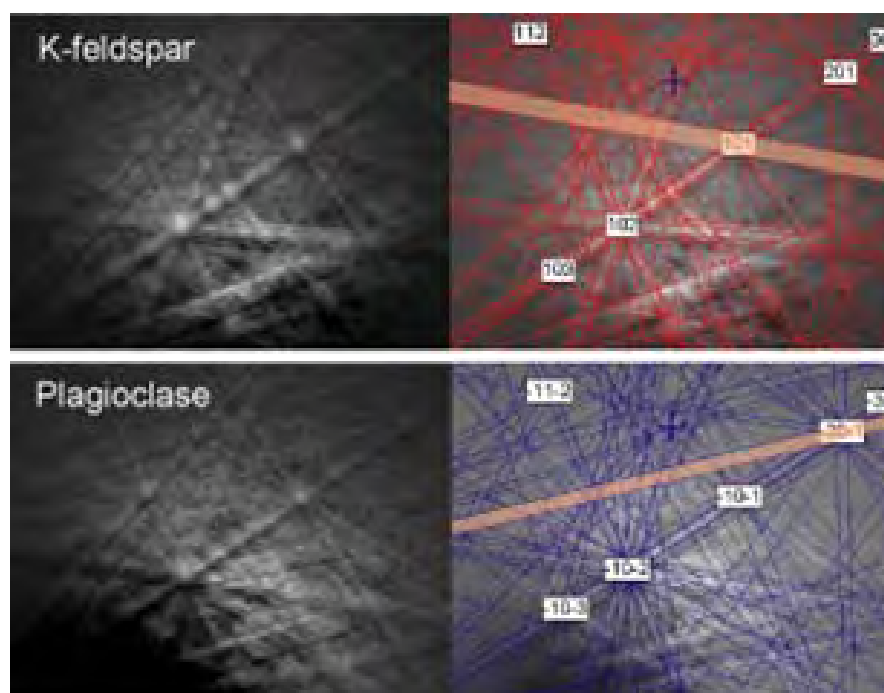


Figure 1. Examples of raw electron backscatter patterns (EBSPs) together with the automated fit produced by the processing software CHANNEL5 for K-feldspar and Plagioclase. The bands that discriminate the patterns from one another are indicated in orange.

The electron backscatter diffraction (EBSD) method allows for rapid quantitative analysis of microstructure. In high symmetry phases such as olivine, garnet, calcite and galena, the method has yielded useful insights into the microstructural behaviour of these minerals during recrystallization, deformation and/or grain growth (e.g., Prior et al. 2002). However, EBSD analysis of lower symmetry phases such as feldspars, has proven difficult. In particular, the similarity of the electron backscatter patterns from different feldspars (Figure 1) has previously resulted in significant mis-indexing,

particularly when EBSD mapping is automated. In this study, the EBSD method for the quantitative analysis of microstructure has been successfully applied to a number of granitic K-feldspars. Automated mapping using HKL Technology CHANNEL5 software successfully discriminates K-feldspar and plagioclase (Figure 2), and allows orientation contrasts within K-feldspar grains to be quantified. These results represent the first automated quantitative analysis of microstructure in K-feldspar.

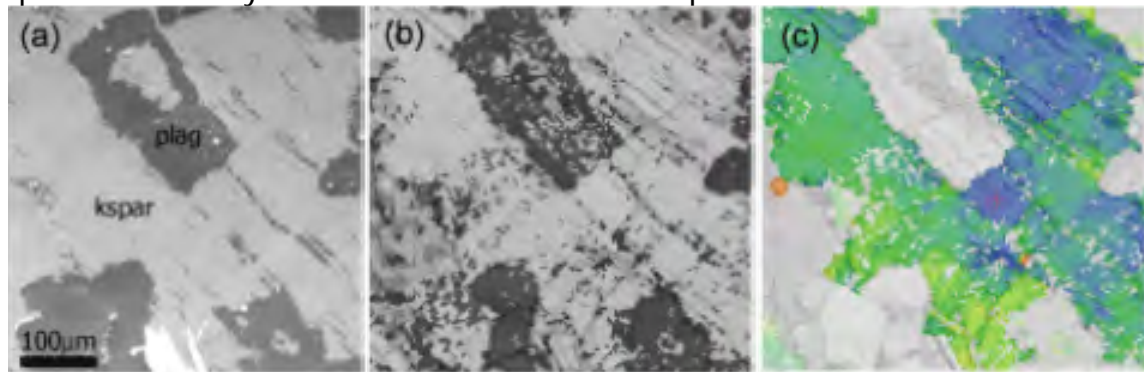
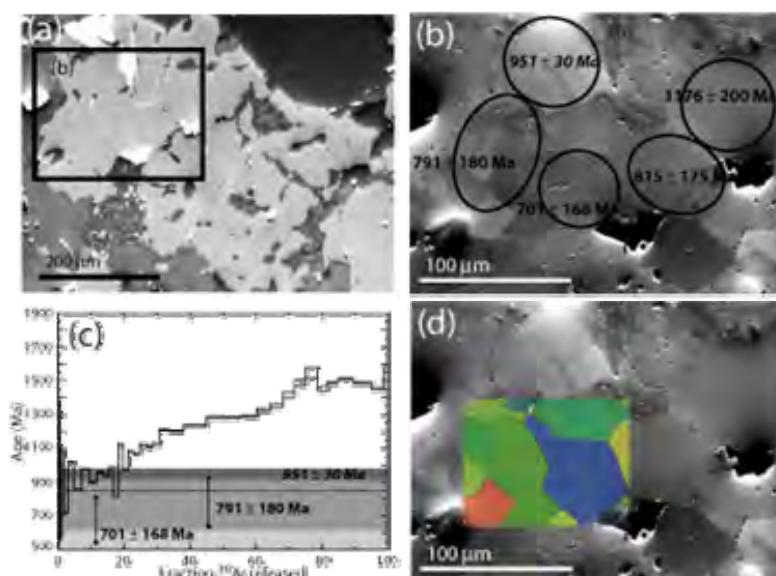


Figure 2. Example of the successful discrimination of plagioclase and K-feldspar using automatic EBSD mapping. (a) grey scale back scattered electron image; (b) electron backscatter diffraction map, coloured for phase (dark grey = plagioclase, light grey = K-feldspar). Some apparent mis-indexing reflects micron scale exsolution not visible at the scale of this image. (c) texture component map, coloured from blue to red for a 10° misorientation from the red cross. Maximum misorientation in other areas of this grain is 16 degrees.

We have applied the EBSD method to the problem of linking microstructure and $^{40}\text{Ar}/^{39}\text{Ar}$ age in K-feldspar using examples from the Dead Fox Granite from central Australia. The multiple-diffusion-domain model (Lovera et al. 1989) attests that typical K-feldspars contain a distribution of different sized diffusion domains that have variable closure temperature to argon loss. This characteristic allows temperature-time histories to be calculated by inversion. Although the model has been applied to a wide variety of rocks in different tectonic settings, there is ongoing debate about its validity (e.g. Parsons et al. 1999) and the relationship between argon loss and microtexture remains unresolved. Our EBSD observations suggest the presence of two main microstructural regions with the Dead Fox Granite K-feldspar: (1) large homogeneous regions of K-feldspar (around 300-800 µm in diameter) that show very little, if any, internal orientation contrast and (2) small coherent



grain-mosaic textured K-feldspars (around 20-50 µm in diameter) that show significant orientation contrasts.

Figure 3. Dead Fox Granite K-feldspar (a) back scattered electron image showing atomic

number contrast; note disrupted microstructure associated with myrmekitic intergrowths of K-feldspar, quartz and plagioclase; (b) Orientation Contrast Image showing coherent subgrain K-feldspar, subgrains range in size from ~ 15 to 60 μm and show little internal orientation contrast. Also shown are the location of UV laser ablation pits and corresponding $^{40}\text{Ar}/^{39}\text{Ar}$ ages; (c) age spectrum from grain separate showing actual ages recorded by the three youngest spot analyses; (d) Orientation Contrast Image with EBSD map overlain. EBSD map shows texture component and is shaded red-blue to represent a 60° orientation contrast from pixel indicated by the red cross.

In-situ ultraviolet laser microprobe $^{40}\text{Ar}/^{39}\text{Ar}$ analysis (undertaken at the Western Australian Argon Isotope Facility in Perth, operated by a consortium consisting of Curtin University and the University of Western Australia) show that the small sub-grain mosaic textured K-feldspars record ages corresponding to the youngest ages recorded in the age spectrum of the bulk sample (Figure 3). Large regions of homogeneous K-feldspar record ages corresponding to the oldest ages in the age spectrum. The calculated domain distribution from the MDD modelling predicts 5 different sized domains. The largest domain (relative size = 1) and an intermediate sized domain (relative size = 0.61) account for > 60% of the gas released. The relative sizes of these two main domains appear to correlate well with the relative size of the two main microstructural regions observed. The smallest predicted domain size (relative size = 0.0006) probably corresponds with sub-micron sized structures not discernible using the EBSD method. Although these observations suggest some relationship between microstructure and $^{40}\text{Ar}/^{39}\text{Ar}$ age, we are still yet to identify obvious candidates for intermediate sized domains (relative size ~ 0.25).

- Lovera OM, Richter FM, Harrison TM (1989) The $^{40}\text{Ar}/^{39}\text{Ar}$ thermochronometry for slowly cooled samples having a distribution of diffusion domain sizes. *J Geophys Res* 94: 17917-17935.
- Parsons I, Brown WL, Smith JV (1999) $^{40}\text{Ar}/^{39}\text{Ar}$ thermochronology using alkali feldspars: real thermal history or mathematical mirage of microtexture? *Contrib Mineral Petrol* 136: 92-110
- Prior DJ, Wheeler J, Peruzzo L, Spiess R, Storey C (2002) Some garnet microstructures; an illustration of the potential of orientation maps and misorientation analysis in microstructural studies. *J Struct Geo* 24: 999-1011.

Orogen-scale extensional shear zones in the Alps: towards a new model of orogeny?

Marco Beltrando¹, Marnie Forster¹ and Gordon Lister¹

¹Research School of Earth Sciences, Australian National University, Canberra, ACT, 0200, Australia

The joint application of structural geology, petrology and geochronology at the scale of the mountain belt has resulted in the recognition of an orogen-scale extensional shear zone in the Western Alps (Figure 1). This result has been possible through simultaneous study of different transects (Figure 1) with the collaboration of Prof. Roberto Compagnoni, Prof. Marco Gattiglio and Dr. Bruno Lombardo. The extensional shear zone puts in contact eclogite facies rock units in the footwall with blueschist facies rocks in the hangingwall (Figure 1 and 2). Its presence is often marked by slices of exotic rock units. The shear zone is deformed by later folding and then cut by younger extensional shear zones and faults (Figure 2). The structural evolution that has been detected indicates that the entire orogen experienced deformation mode switches from shortening to extension several times during its evolution. Compositional studies of amphiboles have revealed that periods of extensional deformation culminated in the exhumation of rock units to near-surface conditions, while shortening episodes resulted in re-burial (Figure 3 and 4). Further research is being currently undertaken aiming to understand the tectonic setting in which these deformation mode switches took place. They may be related to strain partitioning within an orogenic wedge which is undergoing bulk shortening or they may be a consequence of tectonic mode switches, with extension periodically disrupting a mountain belt that has been constructed during the shortening phase.

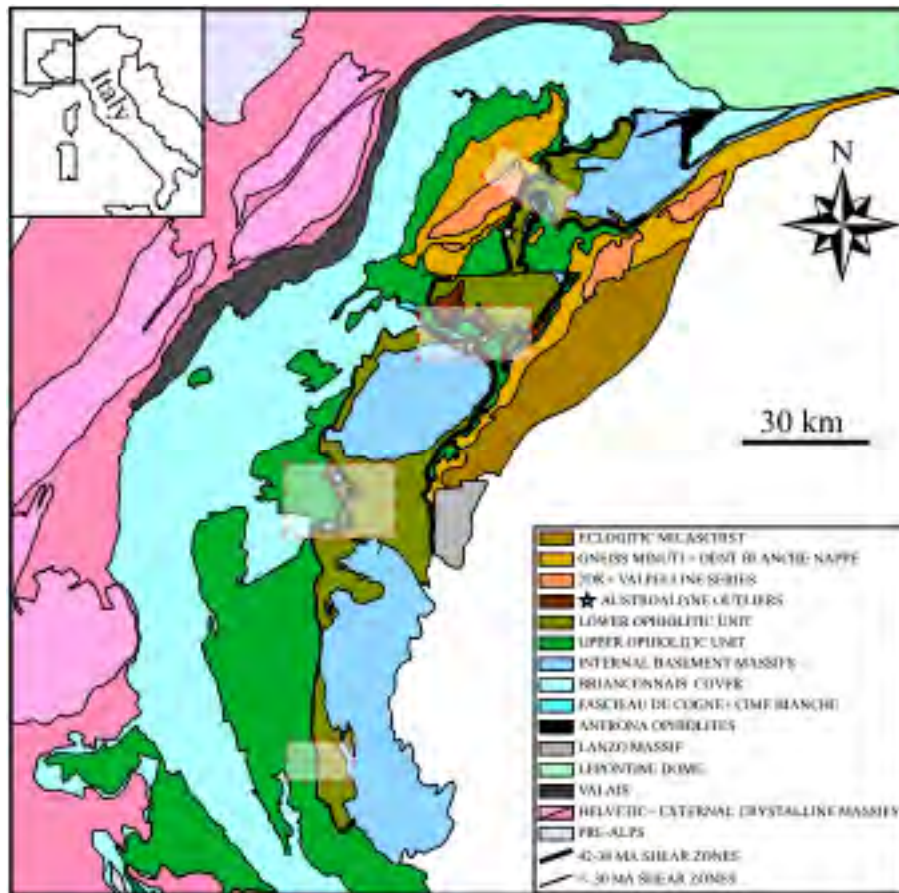


Figure 1. Simplified tectonic map of the Western Alps. Thick black lines indicate extensional shear zones. Dashed squares indicate the study areas (see also Figure 2)

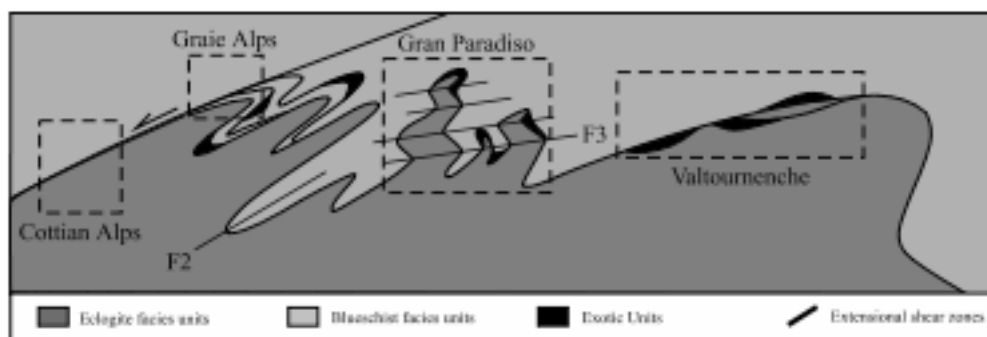


Figure 2. Idealized cross section of the western Alps designed to show the geometry of the orogen-scale extensional shear zones. Notice the presence of several exotic rock slices along it.



Figure 3. Photograph of a retrogressed eclogite under crossed polarizers. The oldest amphibole (1) breaks down in an albite+actinolite simplectite (2). Both (1) and (2) are then included in a large younger amphibole (3)

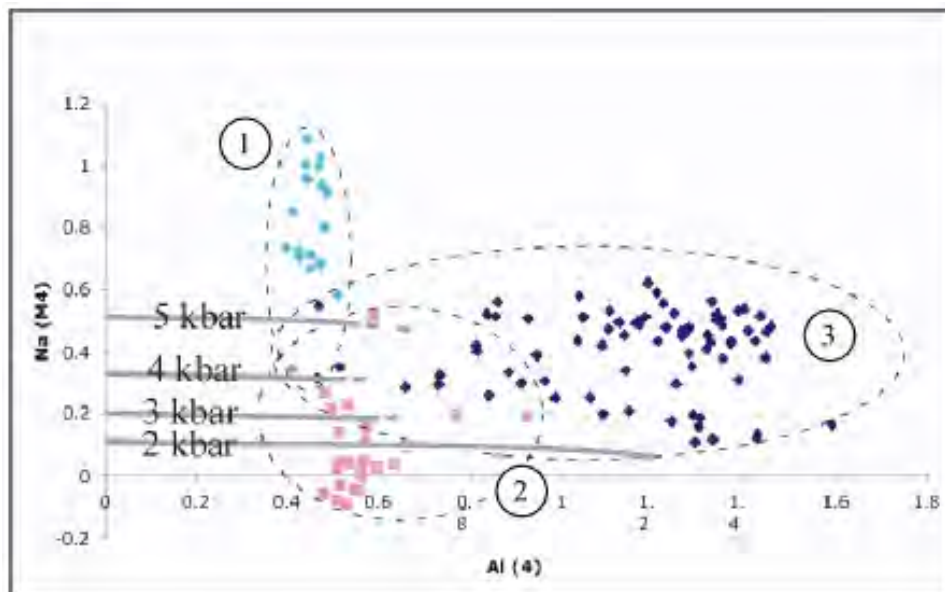


Figure 4. Amphibole compositions from a retrogressed eclogite. The Na content in the M4 site increases with increasing pressure of crystallization (Brown, 1977, Okamoto and Toriumi, 2004). The first (1) and the third (3) generation of amphiboles are characterized by a higher content of Na in M4 that the second generation (2). This is taken as an indication of a decrease in pressure between 1 and 2 and a renewed P-increase between 2 and 3

Pplates – Interactive plate tectonic reconstruction tool

Joe Kurtz¹, Gordon Lister¹ and Simon Richards¹

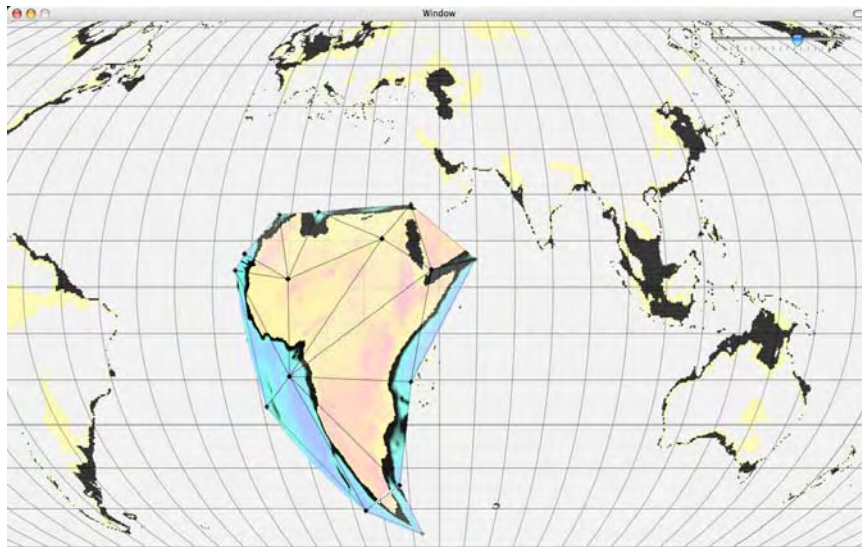
¹*Research School of Earth Sciences, Australian National University, Canberra, ACT, 0200, Australia*

Pplates is a MacIntosh-based reconstruction program that aids in plate and continental tectonic reconstructions by providing a tool for visualisation of movements of continents and plates. A unique feature of Pplates is that it can provide a visual reference for plate boundary processes that generate/allow for movement of plates (i.e. ocean opening and subduction) that are contiguous over the earth's surface. In 2005, Pplates was also used to visualise the location of kimberlite pipes and correlate their "birth" (emplacement dates as given by geochemical analyses) to continental movements.

In late 2005, intensive development of Pplates has focused on creating a version that will allow a user to deform plate crust while conserving crustal mass and imposing isostasy. Such manipulations can aid in reconstructing continental collisions, for example, by visually un-building mountains as the clock is moved back. The first official release with this capability is expected in early 2006.

Current capabilities include the facility for users to:

- (1) Create a mesh and add topography to it from a NOAA terrain data set, and/or set crust depth and terrain elevation at mesh nodes
- (2) Save the map image to a PDF file at any time
- (3) Save a mesh to an XML-style text file and read a mesh from a file



(4) Read in and display Platyplus-style boundary data and apply Platyplus-style motion data to them

(5) Click and drag meshes/nodes to move/distort crust with the option of conserving crustal mass and imposing isostasy

(6) Add an ocean ridge and use it to move plate images.

Mountain belts: The Alpine paradigm

Gordon S. Lister, W. Jim Dunlap and Marnie A. Forster

¹Research School of Earth Sciences, Australian National University, Canberra, ACT, 0200, Australia

Research on orogenic-scale structures in the European Alps, funded by an ARC grant, has now been extended into the Central Alps (Figure 1). Structural mapping has been undertaken on a region immediately above the Turbo Mylonite zone in Switzerland where major tectonic contacts and regional-scale shear zones between Cretaceous and Tertiary rocks occur (Figure 2). A correlation of large-scale structures across the Alps is underway, analysis is based on micro- to macro-scale structural analysis linked with detailed geochronology and thermo-chronological modelling.

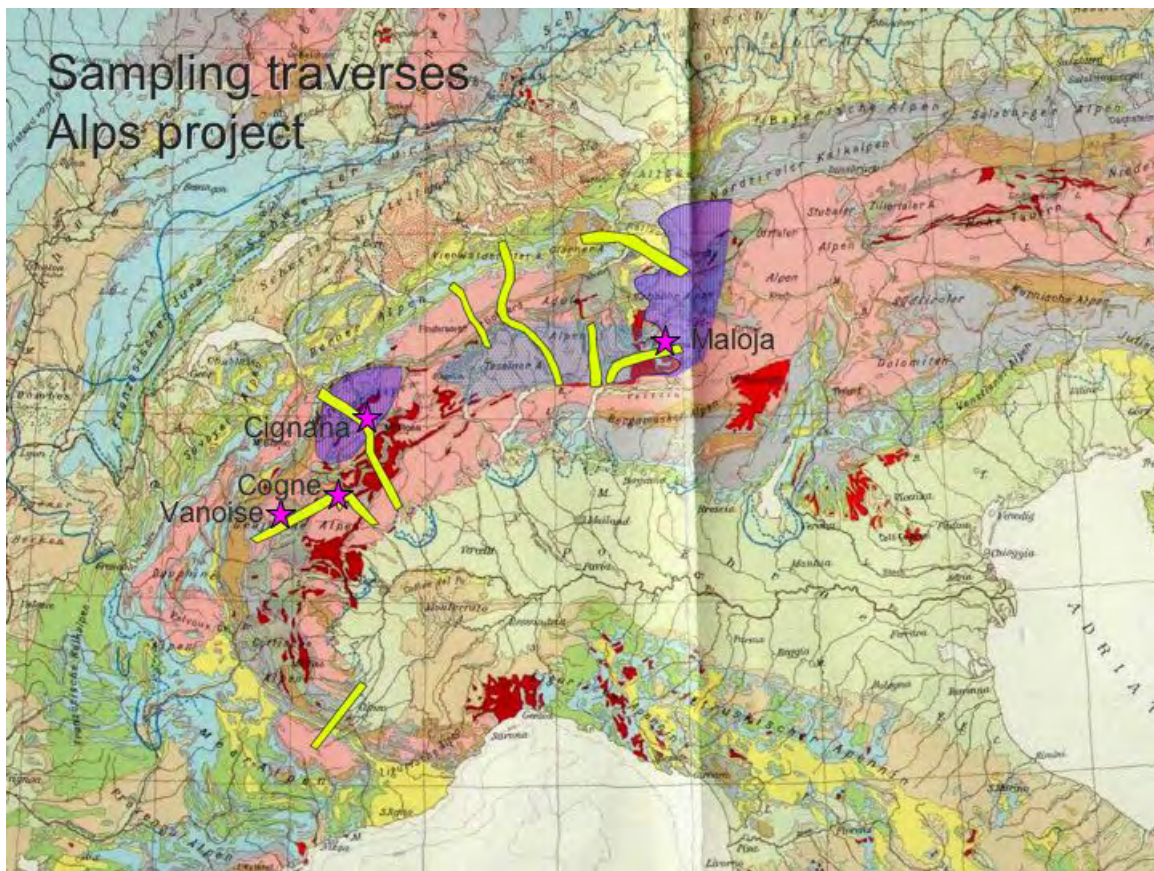


Figure 1. Regions where research on orogenic-scale structures have been undertaken or are presently being analysed. Maloja, Switzerland, is the latest region of study in the Central Alps region. Major shuffle zone trending approximately E-W and cut by the Engadine Line in the south-east region of.

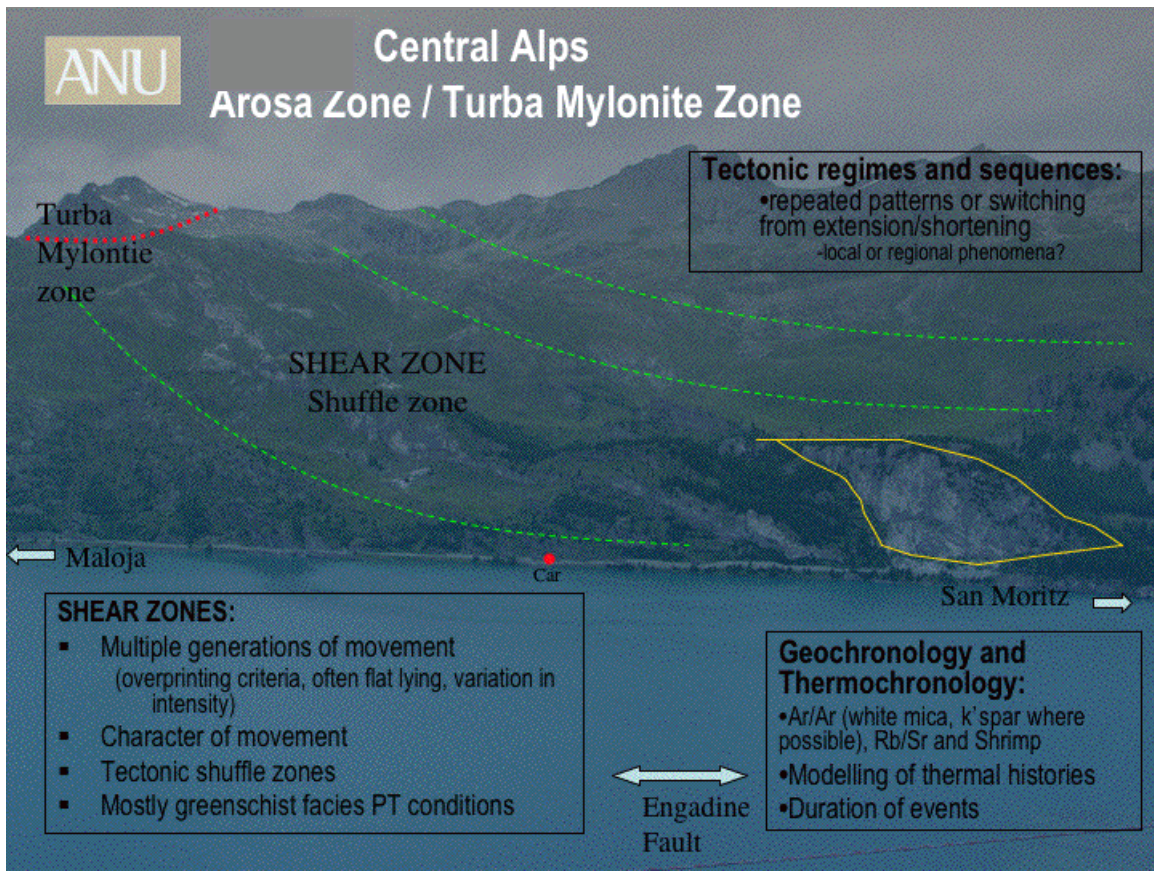


Figure 2. Major shuffle zone immediately west of the Engadine Line in the south-east region of Switzerland.

The Aroza shear zone, north of Maloja, has the same structural character as that observed in the Western Alps. For example, the shear zone preserves a complex geological history within boudins that are remnants of layers that have undergone boudinage during extension. Both boudins and tectonic contacts within this shear zone have been folded during later compressional events. Thermochronology is presently being undertaken to understand both the structural and cooling history of this shear zone.

Several distinct tectono-metamorphic slices in the Cyclades eclogite-blueschist belt, Greece

Marnie A. Forster¹ and Gordon S. Lister¹

¹Research School of Earth Sciences, Australian National University, Canberra, ACT, 0200, Australia

Many years of research across the Aegean Blueschist Belt have been summarized in a paper accepted to Contributions to Mineralogy and Petrology this year. Multiple tectono-metamorphic slices have been recognized with tectonic contacts that operated pre-Oligocene, Oligocene and in the Miocene that juxtapose slices with dominantly different metamorphic histories (Figure 1). Multiple HP-LT events have been recognized (Figure 4) and timing of these slices have been constrained using the 'method of asymptotes and limits' on argon geochronology (Table 1).

Eclogite metamorphic event	53-49 Ma
Blueschist metamorphic event	44-38 Ma
Transitional Blueschist event	35-30 Ma

Table 1. HP-LT metamorphic events in the Aegean Blueschist Belt

Tectono-metamorphic slices are juxtaposed and overprinted by regional-scale shear zones that operated at different times and at different PT conditions (Figure 1).

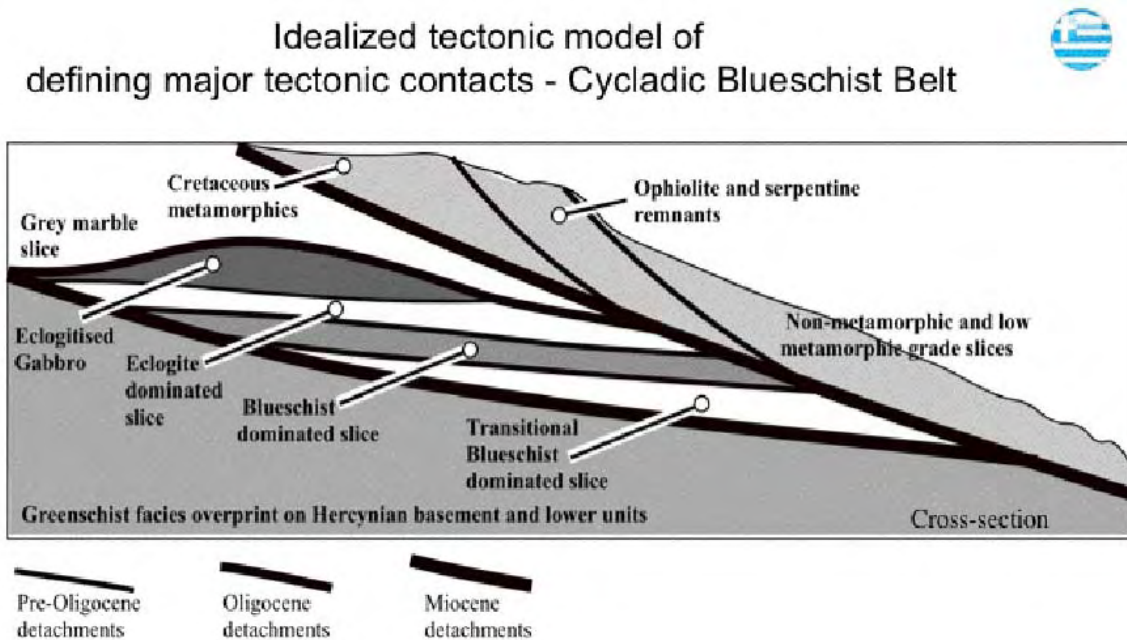


Figure 1. Faults and shear zones that operated at different stages in the history of the Blueschist belt.

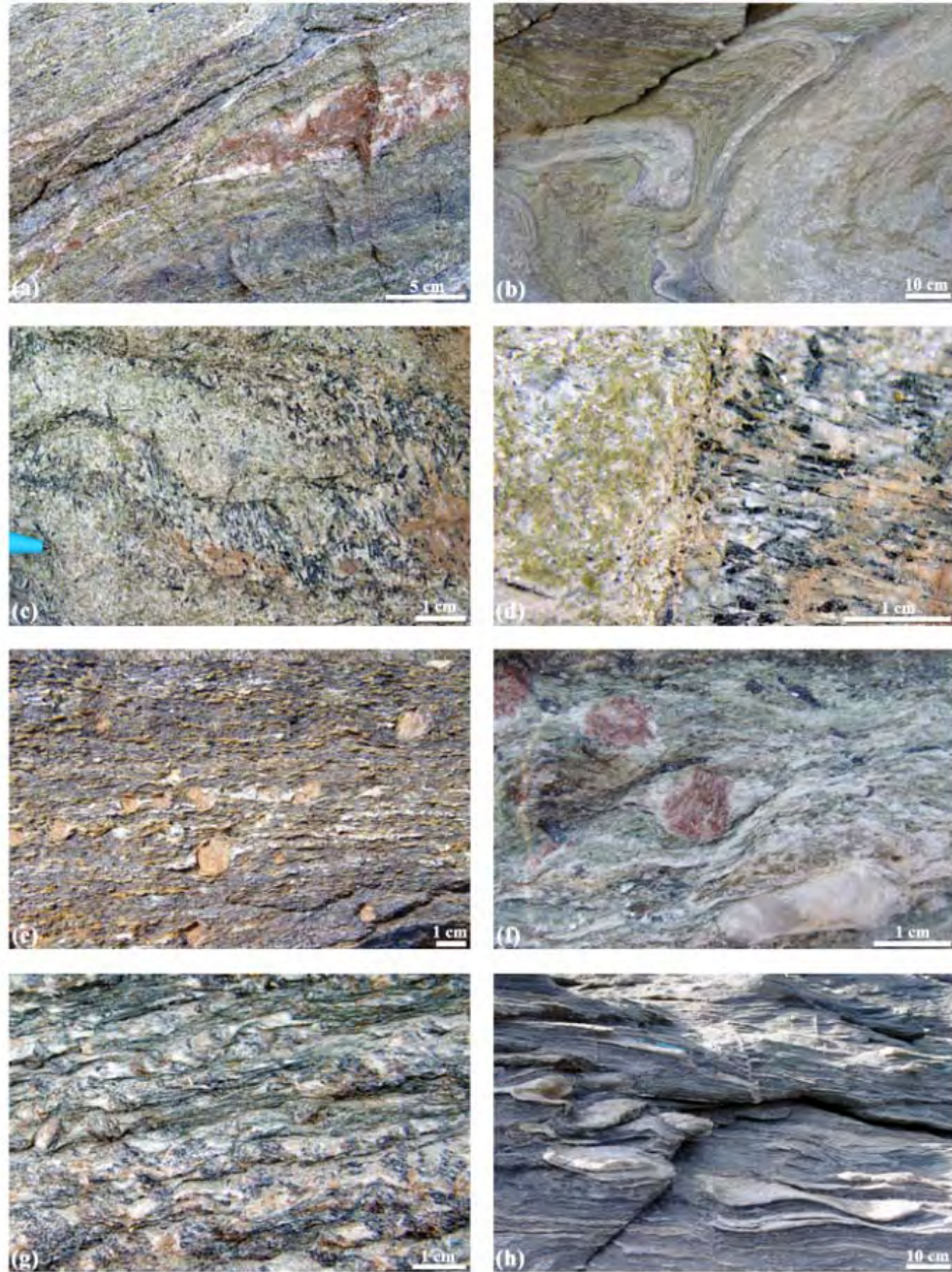


Figure 2. Deformation in the Cyclades Blueschist can be associated with multiple episodes of HP-LT metamorphism: a) M1D shear zone with ankerite and glaucophane veins; b) these veins are recumbently folded in kilometer-scale axial zones; c) and d) quartz and glaucophane veins in M1D event; e) and f) M1C garnet porphyroblastic event in a major extensional shear zone with asymmetric pressure shadows; g) rotated M1D albite porphyroblasts in S-C crenulations in a post M1D shear zone; h) mylonitized quartz vein in a post M1D shear zone is locally overprinted by recumbent folds.

One of the fundamental findings from the research in the Blueschist Belt is the complex exhumation path of the different tectono-metamorphic slices across the belt (Figure 5). The simple burial then peak metamorphic mineral growth followed by exhumation with a small increase in temperature at greenschist facies is not what is observed in the rocks from this region.

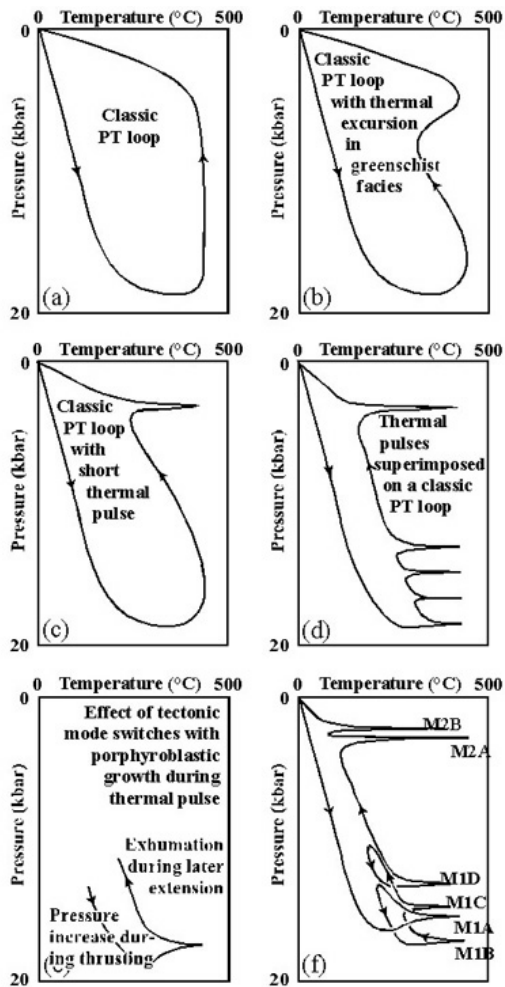


Figure 3. Schematics of PT-t paths inferred for the eclogite-blueschist belt of the Cyclades. The recognition of multiple tectonic slices in the Cycladic blueschist belt has led to the recognition that PT-t paths in this region can be complex and varied. PT-t histories vary from slice to slice and complexity can occur as slices are partially exhumed and then thrust deeper into the crust. Porphyroblastic metamorphic mineral growth events overprint more ambient pervasive metamorphic slices producing thermal 'excursions' onto the PT-t histories. For example a) is not observed; b) the PT is too simple due to the variation observed, but theoretically possible; c) a possible scenario with a short greenschist event; d) an example of short metamorphic events overprinting the basic burial and exhumation; e) shows that each tectono-metamorphic slice can have an independent history; and f) the most realistic scenario with repeated extension and shortening of tectonic slices.

Forster M. A. and Lister G. S. (2005) Several distinct tectono-metamorphic slices in the Cyclades eclogite-blueschist belt, Greece. *Contributions to Mineralogy and Petrology*, DOI 10.1007/s00410-005-0032-9.

Timing of extension in the Aegean Blueschist Belt older than previously recorded

Marnie A. Forster¹ and Gordon S. Lister¹

¹Research School of Earth Sciences, Australian National University, Canberra, ACT, 0200, Australia

The Aegean micro-plate is accepted to have undergone extension in the Miocene due to the roll-back of the subducting slab (Figure 1). I have just completed a geochronology in the argon Thermochronology Laboratory at RSES, ANU, that has shown extension in the central Cyclades occurred earlier than previously thought.

Aegean Blueschist Belt

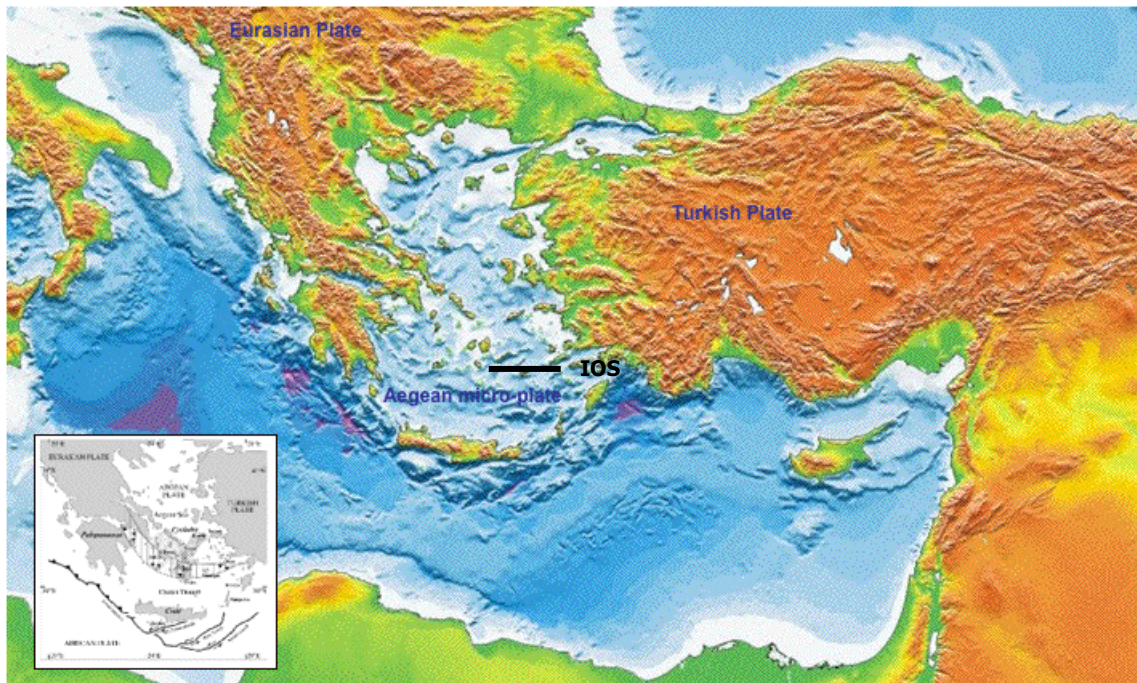


Figure 1. Map of the Aegean micro-plate with Ios, the metamorphic core complex with the most intense extension in the central Cyclades.

Extension in the Cyclades is accepted to have occurred during the Miocene and is defined by greenschist facies PT conditions. The metamorphic core complex of Ios, has the lower plate is capped by the South Cyclades Shear Zone. This shear zone is crustal-scale top-to-the-south ductile zone (Figures 2 and 3).

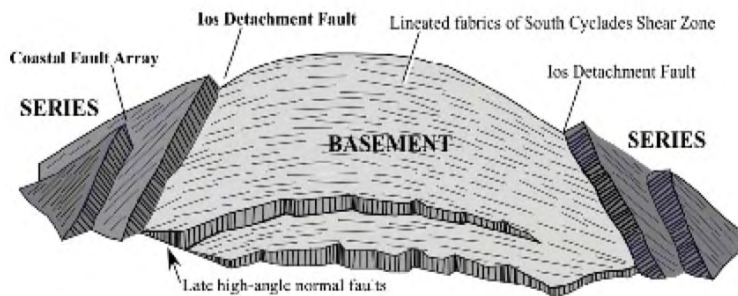


Figure 2. Schematic drawing of the of Ios, showing the upper and lower plates with the South Cyclades Shear Zone being a carapace to the lower plate

The timing of operation of this shear zone has been done in detail (Figure 4. Our research shows that an Ar^{40}/Ar^{39} geochronology on both white micas and K-feldspars and microstructural analysis on the South Cyclades Shear Zone on Ios shows that extension occurred prior to the Miocene. White mica preserves the older history except except in the most intense top-to-the-north shear zone where deformation occurred at 25 Ma. In contrast the K-feldspars preserved older histories at 25 Ma, 30 Ma and 44 Ma, with distinct event occurring at 12-14 Ma suggested to have occurred at $\sim 200^{\circ}C$).

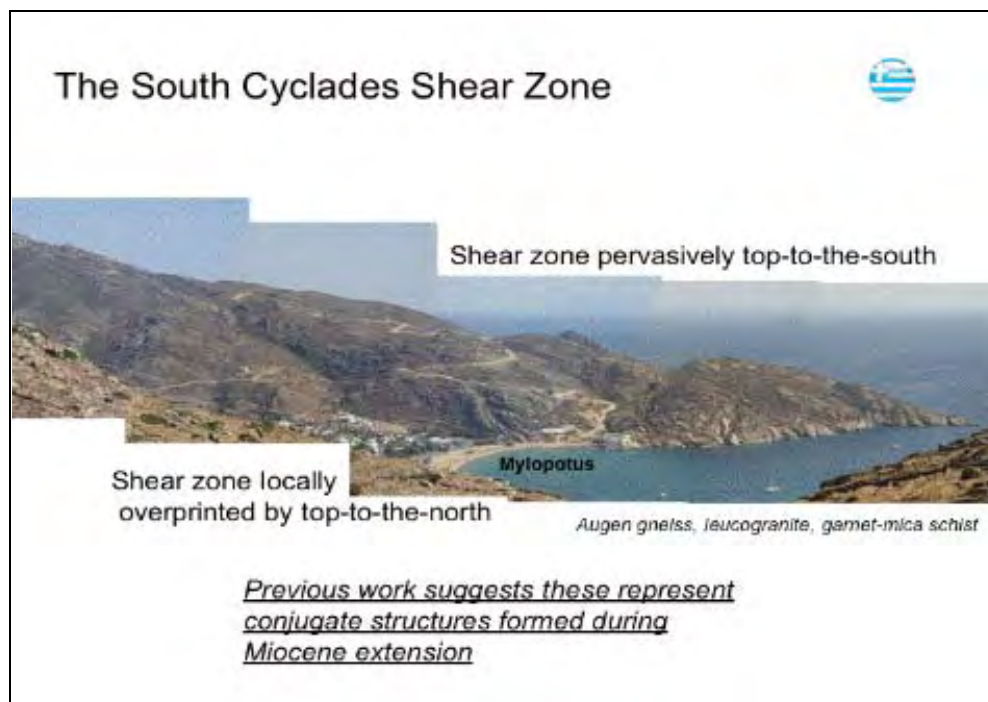


Figure 3. The South Cyclades Shear Zone on the island of Ios is dominantly top-to-the-south with narrow shear zones overprinting with top-to-the-north.

These two shear zones, top-to-the-north and top-to-the-south, have been explained as being synchronous, however this study shows that they operated at quite different times in the history of extension. Only the very last stage of operation of the narrow top-to-the-north shear zones are Miocene in age and have undertaken only a minor amount of exhumation that occurred on this shear zone.

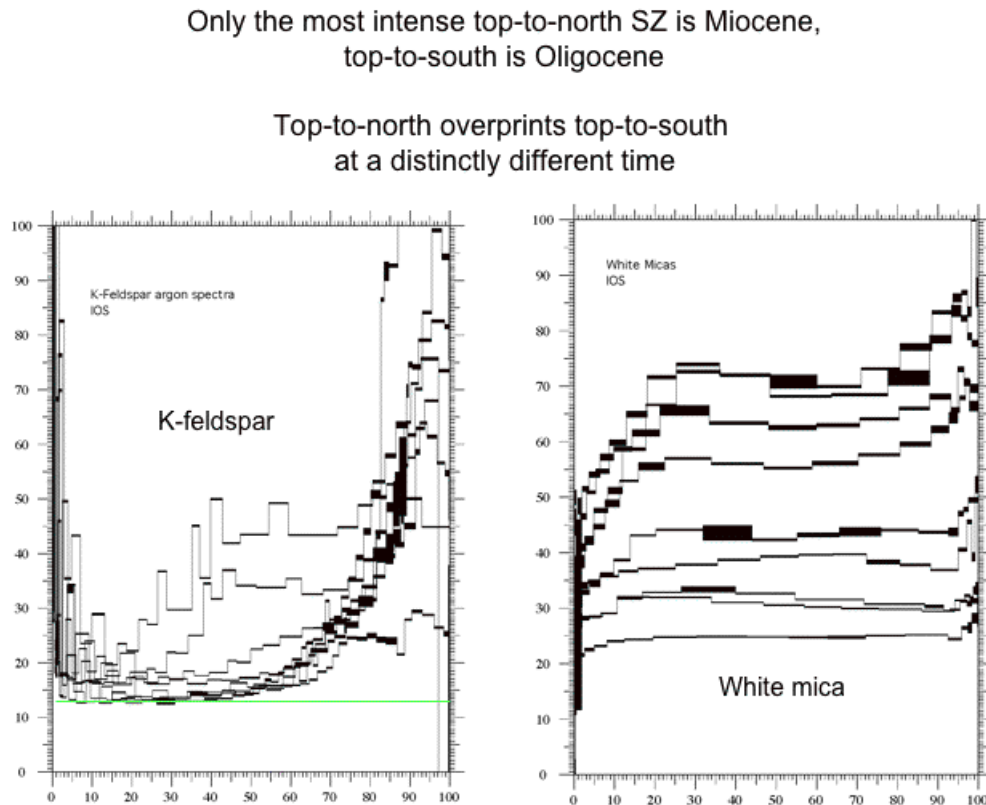


Figure 4. $\text{Ar}^{40}/\text{Ar}^{39}$ apparentage spectra for K-feldspar and white mica from the island of Ios.

Plate tectonic reconstructions, kimberlite emplacement and exploration

Simon Richards¹

¹Research School of Earth Sciences, Australian National University, Canberra, ACT, 0200, Australia

Tectonics and resources formed a focal point of the ACcESS funded ANU project P14. The project also involved the development and application of plate tectonic reconstructions in conjunction with Joe Kurtz. Research resulted in the generation of a global-scale tectonic model for the emplacement of kimberlite magmas. Recent research in the field of kimberlites and related rocks (especially those bearing diamonds) has focused on detailed studies on individual pipes, their internal structure and geochemistry. A number of studies have also looked at the role of localized structural geometries in controlling the emplacement of these specific mantle-derived rocks. Such studies have revealed that trends in kimberlite dykes and clusters of kimberlite pipes are intimately related to the orientation of small and large-scale faults and shear zones. The project is focused on regional (global) – scale orogenic and plate-tectonic processes with particular attention to analyzing the large-scale trends, in both space and time, of kimberlite emplacement.

A database containing information including location, age, continent, associated craton (if applicable) and dating method has been constructed. The database contains the ages of well over 800 pipes and also contains the location and some relative ages on over 4500 pipes. The expansion of this database over 2005 has led to a dramatic change in the way that we should view the timing of emplacement of kimberlite magmas and their relationship to the formation of large-scale (lithospheric) structures and the role of plate tectonics and continental (supercontinent) fragmentation and breakup.

The results have shown that transfer faults that are linked to large transform faults on the adjacent oceanic crust are the major controlling structures for the emplacement of these magmas; an idea that was discounted in the early 80's due to an apparent discontinuity between the timing of emplacement and the formation of these structures. These results were achieved using the Pplates program and supported by funding from the ACcESS MNRF. The project was also undertaken with the support from the DeBeers group.

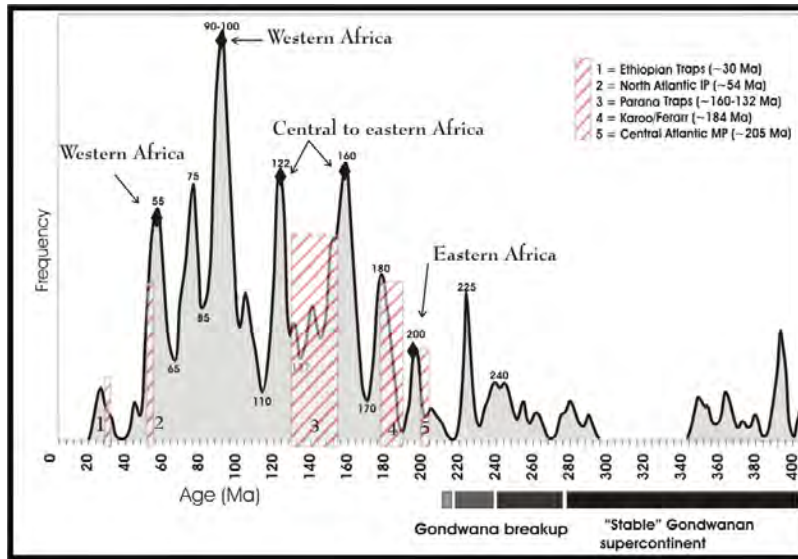


Figure 1. This figure shows the accumulated frequency of kimberlites at times between 0 and 400 Ma. The figure illustrates distinct periods of abundant kimberlite activity separated by periods of quiescence. Highlighted in red are periods of major flood basalt magmatism. Also shown is the period of Gondwana stability and breakup corresponding to a period of quiescence.

Figure 1 illustrates a compilation of information from the latest dataset but the data set presented here is restricted to an age range of between 0 and 400 Ma. The figure shows two main characteristics of kimberlite magmatism: (1) the occurrence of distinct eruption events throughout time both on a short timescale (e.g. 10 Ma) and on a longer timescale (100's of Ma). Some events are synchronous on a global scale and also appear to be intrinsically related to global-scale tectonic processes. (2) There is a close temporal and in some cases spatial (the latter not shown here) relationship between the timing of kimberlite magmatism and the formation of large igneous provinces (LIPs). We have explored this relationship in a model of kimberlite emplacement.

Kimberlites also exhibit a preferred orientation of hypabyssal dyke orientations, which are almost exclusively parallel to the overall trend of kimberlite fields that contain these dykes. Such preferred orientations also imply a tectonic control on their emplacement. Based on these results, that the timing and location of kimberlite magmatism is intimately linked to major periods of plate reorganisation, particularly periods of incipient supercontinent fragmentation and continent dispersal.

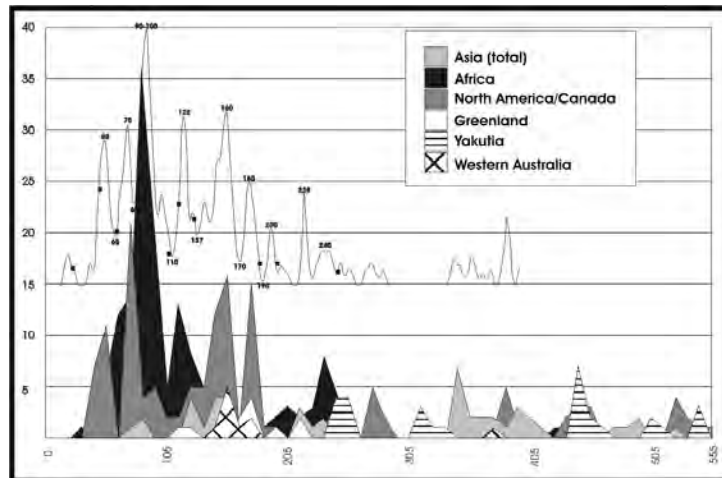


Figure 2. This figure is similar to figure 1 but “flare-ups” in kimberlite magmatism are broken down according to their respective continents. It highlights that kimberlite magmatism is not just a localised phenomenon, rather, specific times in the Earth’s history are characterised by these “flare-ups” at particular times, e.g. at 440 Ma when kimberlite magmatism occurred in Siberia, North America and Africa.

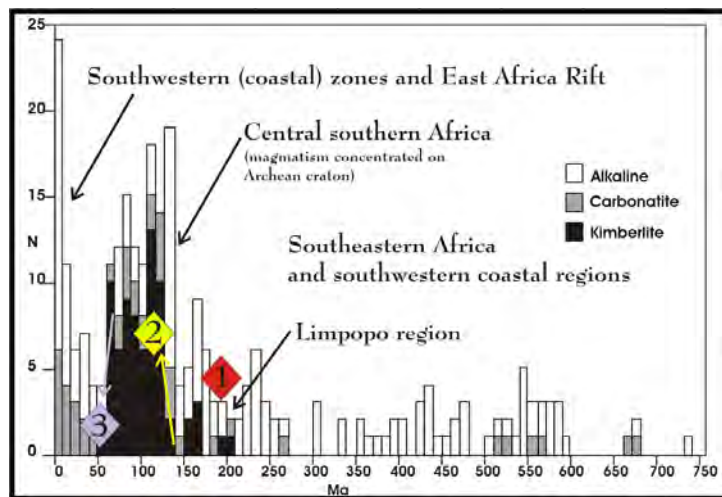


Figure 3. This diagram is similar to Fig. 2 but the dykes and pipes are broken down according to composition. Between 200 and 750 Ma, alkali-type magmatism is dominant, however, kimberlites become a major component between 200 Ma and 50 Ma during the period of Gondwanan breakup and continent dispersal. The change in composition is attributed to the tapping of different source regions by lithosphere-scale plumbing structures (faults) along which the magmas are emplaced. Modified from Woolley, 2001.

Figure 1 also illustrates that a paucity in kimberlite eruption occurred during stability of the Gondwanan supercontinent between ~250 and 340 Ma. Conversely, continental fragmentation and breakup at ~250 Ma coincides with the onset of “recent” periods of voluminous kimberlite eruption. Specifically, rifting at ~95 and ~122 Ma is closely associated with the formation of the south Atlantic and also corresponds with some of the most voluminous and economic

kimberlites in South Africa. The dominant structural trend of the kimberlite fields in Africa (NE-SW) and South America (SE-NW) reflect structures that developed during incipient rifting at this time.

Large oceanic transforms begin their existence as continental transfer faults during the period of lithosphere-scale extension that preceded breakup. Asymmetry of detachment-related structures (both brittle and ductile) leads to stretching of the lithosphere beneath adjacent cratonic regions. The locus of maximum sub-cratonic stretching is progressively offset oceanward as extension continues. If the continental lithosphere is thick, such as the lithospheric roots below old, cold Archean cratons, then the transforms must, therefore, propagate to the base of this thick lithosphere and intersect the field where diamond is a stable phase and kimberlite magmas are generated. I envisage that this is the reason why transfer faults and transforms are the dominant structures controlling the location of kimberlite generation in the mantle and also controlling the location where kimberlites are emplaced at the surface of the Earth.

Model proposed for the formation of a large (continental)-scale detachment fault between southern South America (SA) and southern Africa (Af)

The model we have developed diverges from the classical "passive-rifting" model proposed for continental breakup. In the rifting scenario shown in figure 4b, the continental crust is "torn" apart symmetrically and new oceanic crust is developed; the lithosphere and overlying crust is approximately the same thickness on either side of the rift. Transforms and transfer structures (between rift segments) are only developed during and soon after new oceanic crust is developed. The model proposed here involves the formation of a lithosphere-scale detachment whereby continental and lithospheric extension occurs well before oceanic crust is developed (Fig. 4a). Accordingly, transfer structures must develop in continental crust to accommodate different rates of spreading as the distance from the associated pole of rotation (Euler pole) changes. These structures must also link to the base of the lithosphere as it is coupled to the overlying and extending crust. As continental extension continues, these sub-vertical transfer faults (which intersect the lithosphere) propagate toward the continental (away from "rift axis") interior where they source deeper lithosphere (and asthenosphere) and hence magmas generated at different pressures. This model explains a clear progressive change in magma composition from the continental margin to the interior from high-K alkaline basalts to carbonatites and finally kimberlite magmas.

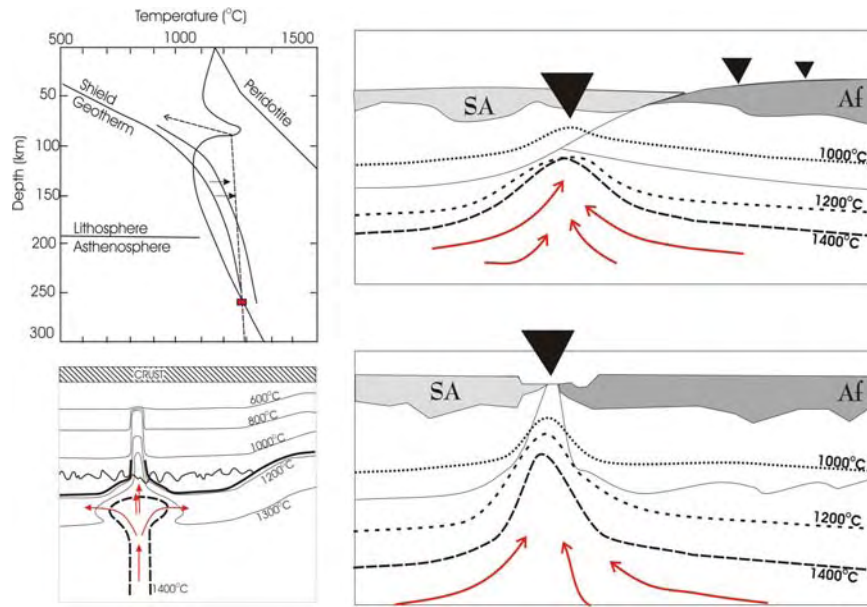


Figure 4. (a) The model proposed for continental rifting and kimberlite emplacement involving the formation of deeply penetrating listric faults. The formation of these structures results in an asymmetry of rifting. (b) This differs from the classical "passive", pure shear-dominated" model often envisaged for continental rifting. (a) and (b) Large triangle indicates location of potential flood basalts. Smaller triangles show regions where kimberlites might be found.

(P-T diagram from Wyllie, 1989)

The asymmetry of the sub-continental stretching and the progressive offset during extension (shown above) provides a physical model that explains the temporal and spatial sequence of magma types observed as well as the translation of the locus of magmatism as the rift phase develops into continental breakup.

African kimberlites in a reconstruction framework: Application of Pplates

Simon Richards¹ and Joe Kurtz¹

¹Research School of Earth Sciences, Australian National University, Canberra, ACT, 0200, Australia

Development of the Pplates reconstruction program in 2005 focussed on providing reconstructions applicable to the Kimberlites project. Below are some of the reconstructions of South America and Africa. Some kimberlite data was added (approximately) after the reconstruction was performed using Pplates. The reconstructions helped decipher trends in kimberlitic magmatism and the relationship between these trends and the motion of plates.

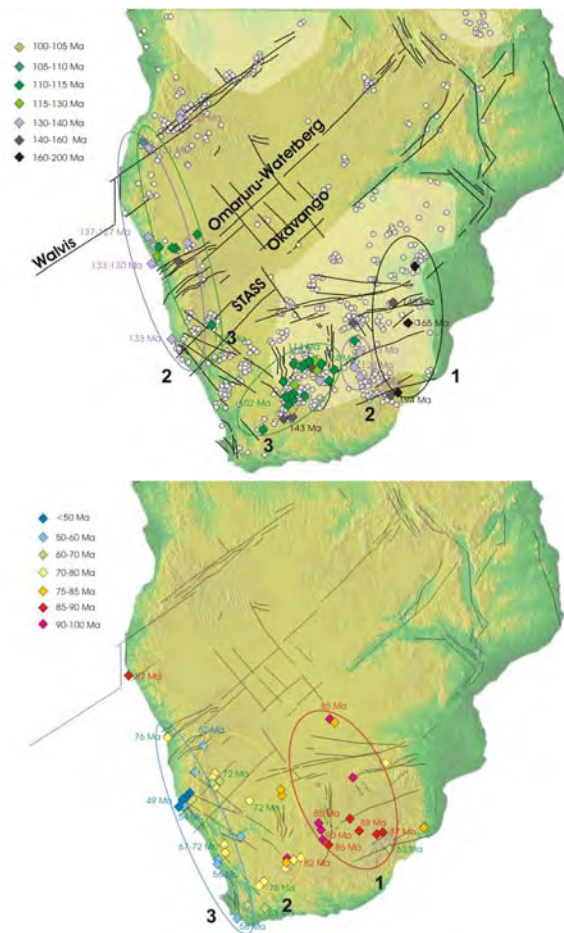


Figure 5. Kimberlite locations in southern Africa colour coded according to their age of emplacement. a) Kimberlites emplaced between 100 and 200 Ma showing general inland progression of magmatic centers. b) Kimberlites emplaced between 0 and 100 Ma showing a general seaward progression of magmatic centers.

Between 180 and 100 Ma there were several regions of active kimberlite magmatism (Fig. 5a). In eastern Africa, the earliest phase occurred between 195 Ma and 165 Ma. Here, magmatism is interpreted to have been associated with the initial breakup of Gondwana, specifically the NE motion of Madagascar, India as well as the eastward motion of Antarctica relative to Africa. This period of extension was coupled to the formation of lithosphere-scale ENE-trending faults, which in turn, triggered kimberlite generation and magma emplacement in discrete locations along these faults. We would suggest that Continued extension along this margin resulted in thinning of the lithosphere, upwelling, and decompression melting which culminated in the eruption of the Karoo (stage 1) continental flood basalts (CFB's) immediately postdating emplacement of the kimberlites.



Figure 6a. 180 Ma Semi-schematic reconstruction of South America and Africa highlighting transform orientations, KRM locations and CFB's.

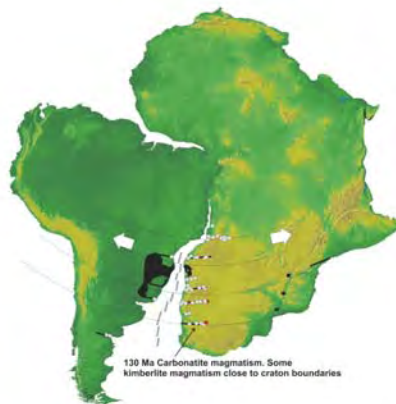


Figure 6b. 130 Ma Semi-schematic reconstruction of South America and Africa highlighting transform orientations, KRM locations and CFB's.



Figure 6c. 110 Ma Semi-schematic reconstruction of South America and Africa highlighting transform orientations, KRM locations and CFB's



Figure 6d. 100 Ma Semi-schematic reconstruction of South America and Africa highlighting transform orientations, KRM locations and CFB's.

At around 140 Ma, rifting between South America and Africa initiated (Figures 6a-6b and 7a). Extension created NW-trending rift-parallel normal faults as well as NE-trending, rift-perpendicular transforms and transfer faults. Additionally, extension triggered CFB- and carbonatite-dominated magmatism (Figures 6a and 7a), but only along the rift margin. Emplacement was focussed on NE and NW trending faults and fractures (Figures 6c, 7b and 7c).

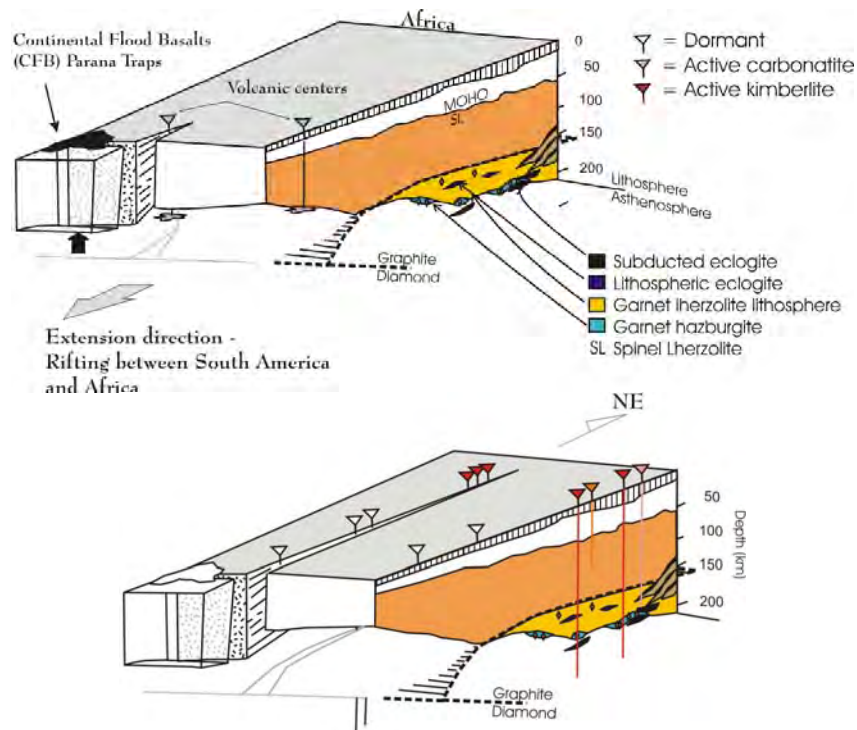


Figure 7. This figure is designed to illustrate simply the proposed progressive landward propagation of transfer faults from the rift axis between South America and southern Africa. As the structures propagate inward, they intersect lithosphere, which thickens progressively toward the cratonic regions of southern Africa. During the initial stages of rifting (7a), the structures intersect thin lithosphere but as rifting continues, the structures intersect thick lithosphere (7b) where diamonds are stable and kimberlite magmas are sourced.

Between 120 and 100 Ma, extension between the continents continued. At this time, transforms propagated inland toward the Archean craton where they intersected thick continental lithosphere. Continued fault propagation facilitated melting by focussing volatiles as well as providing a conduit for magma emplacement. The intersection between these structures and the thickened lithosphere resulted in predominantly kimberlite magmatism and emplacement of diamond-bearing magmas (Figures 5b, 6c and 7c).

Between 55 and 100 Ma, kimberlite magmatism was centered entirely within the cratonic regions of southern Africa, but the volume and intensity of magmatism had subsided due to the increasing distance between the active rift center (Mid-Atlantic Ridge - focus for transforms) and the continental interior.

Between 70 and 60 Ma, magmatism retreated to the west, toward the continental margin, and was again dominated by carbonatite and alkali magmatism (Fig. 5b).

Southeastern Lachlan Fold Belt: Field trip to the base of a batholith in the southeastern Lachlan Fold Belt (LFB).

Simon Richards¹

¹*Research School of Earth Sciences, Australian National University, Canberra, ACT, 0200, Australia*

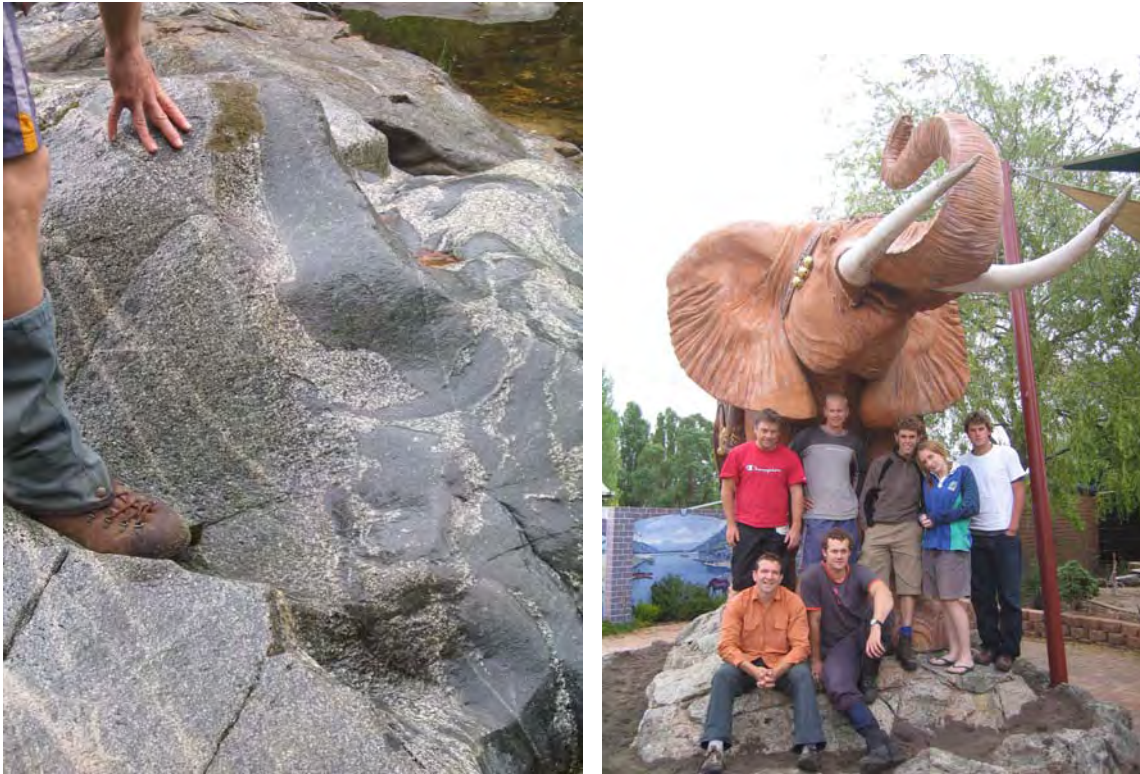


Figure 1. Photo highlighting a typical sharp contact between granite containing a dense accumulation of microgranitoid enclaves and enclave poor granite. Such structures can be used to determine stratigraphy within a pluton.

Figure 2. Participants of the Lachlan Fold Belt field trip.

Plutons form significant components to many orogens, including the eastern LFB. The primary aim of the trip was to examine structural and magmatic processes associated with crustal growth and orogenesis and to examine how we can use plutons, much like folds and faults, as tectonic indicators. The two-day trip focused on a cross-section through one of the largest plutons of the Bega Batholith, the Kameruka Granodiorite and associated phases. We had the chance to examine internal magmatic features of the pluton that can be used like sedimentary structures to determine a 'stratigraphy'. The stratigraphy and internal structure can be used to suggest a mode of magma emplacement and

pluton construction. Country rocks were also examined in detail. Migmatites formed below the pluton and coeval with its emplacement have a well-developed, shallow-dipping shear fabric and show that pluton emplacement occurred coeval with extension. This idea is supported by the contemporaneous eruption of co-magmatic volcanics in extensional basins overlying the Bega Batholith. A comprehensive 45-page field guide was produced to accompany the trip.

Wyangala Batholith Structural Shortcourse

Simon Richards¹

¹*Research School of Earth Sciences, Australian National University, Canberra, ACT, 0200, Australia*

In March 2005 a weeklong structural short course to the northern Wyangala Batholith in central eastern NSW was conducted as part of an academic, field-oriented development scheme for PhD students at RSES. The Wyangala Batholith forms one of the largest and laterally extensive batholiths in the Paleozoic Lachlan Fold Belt. The fieldtrip focused on teaching students to identify, using field relations, the relationship between large, orogen-scale shear zones and the emplacement of granite plutons. Work by Paul Lennox and others has shown that several plutons of the batholith exhibit shear zones that are aligned parallel the plutons margin. They also show syn-magmatic mineral fabrics indicative of syntectonic (with respect to shearing) emplacement. Detailed structural analysis and mapping of a single pluton showed that the fabric exhibited by some phases of the pluton is entirely magmatic with very little evidence for major solid-state deformation. However, the fabric locally graded into a fabric that was a transitional magmatic to tectonic fabric revealed by the alignment of magmatic minerals plagioclase and K-feldspar but also the alignment of recrystallised biotite. This evidence was interpreted to represent progressive cooling of the pluton during compressive deformation. The fabric was locally shallow dipping to the west but typically steeply dipping. The field trip was a great success and highlights some of the opportunities geologists have at RSES.



Figure 1. This photo illustrates the style of fabric commonly observed within the granite plutons of the Wyangala Batholith in the region where the field course was run. The granite exhibits prominent S and C foliation planes indicating a top to the left. The fabric is interpreted as a high-T mylonitic fabric. Base of photo is approximately 80cm.

Structural evolution of the Scottish Barrovian sequences: implications for the Barrovian heat source

Daniel Viète¹, Simon Richards¹ and Gordon Lister¹

¹*Research School of Earth Sciences, Australian National University, Canberra, ACT, 0200, Australia*

A field-based study was commenced in 2005 into the structure of the classic Barrovian localities of the Scottish Highlands and the influence of structure on the development of the Barrovian metamorphic sequences for which the region is famous. We have found that in the region north of Stonehaven, on the Scottish east coast, the rocks show that an early, near isoclinal folding is followed by a period of localised isoclinal folding and associated(?), pervasive, top to the SE shearing (Fig. 1). A later, shear fabric is best developed in the northern part of the transect. This shearing is also associated with localised shear folding. Finally, a less intense deformation folds structures formed during earlier deformation events, forming a regional scale monoformal downbend that separates the steeply dipping units that crop out adjacent to the Highland Boundary Fault (HBF) in the south from the flat-lying units of the north. An association between the top to the SE shearing and the preservation of Barrovian assemblages was recognised in the biotite through sillimanite isograds.



Figure 1. Large scale top to the SE shear zone

Early models for regional metamorphism (i.e. England and Thompson 1984) invoked crustal thickening during shortening for the origin of the metamorphic event. According to this model, any fabric associated with Barrovian-type metamorphism has generally been viewed as a fabric formed during shortening and vertical thickening of the crustal pile. Though the exact nature of the fabric is uncertain, it is possible that the SE shearing event was responsible for unroofing of the Barrovian series and that, as suggested by Harte and Hudson (1979), a major extensional tectonic boundary exists near to the current location of the HBF. The Southern Uplands could represent the low-grade lid to the Grampian

terrane (Fig. 2). According to our model, elevated geothermal gradients caused by lithospheric scale extension during collapse of the overthickened Grampian crust, possibly coupled with shear-related internal heat production, was responsible for the Barrovian event.



Figure 2. Simplified tectonic map of the UK and Ireland (modified from Reverdatto and Polyansky 2004)

Crustal Heat Flow Modeling

Justin Freeman¹, Daniel Viete¹, and Gordon Lister¹.

¹Research School of Earth Sciences, Australian National University, Canberra, ACT, 0200, Australia

We have developed a series of computational tools that extend the capabilities of the ACcESS MNRF supported geodynamics codes. These tools cater for the inclusion of non-linear feedback terms in the energy equation. Specifically, we are exploring the role of crustal heat sources on the tectonic evolution of a region. Additional energy equation terms include radiogenic heating, shear heating and basal heating through either a constant or episodically varying heat flux. Figure 1 below shows two views of the same extensional model which includes frictional heating along the fault (or weak zone) and the dramatic effect this has on the temperature field.

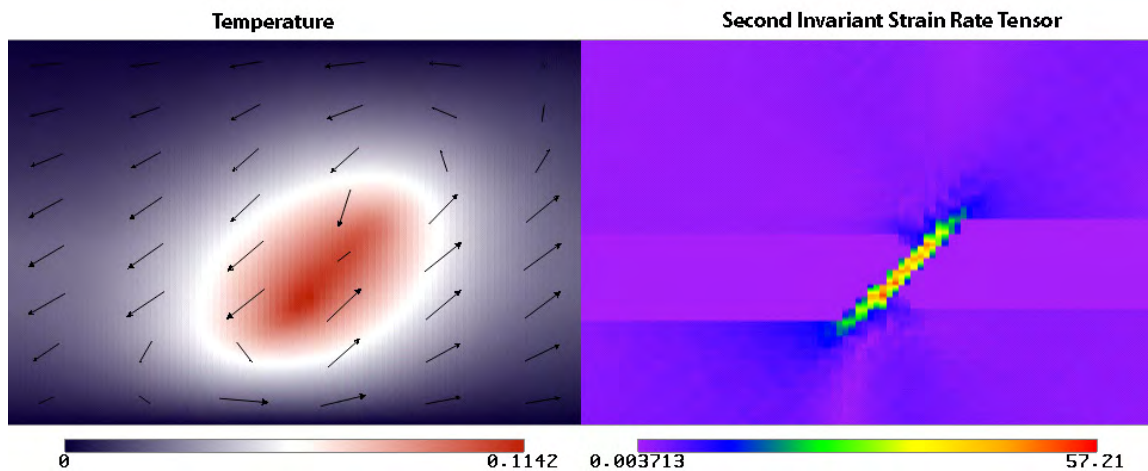


Figure 1 2D crustal extension model including the effect of shear heating along a weak zone. This model consists of a brittle upper layer and a ductile lower layer. Left figure is the temperature anomaly due to shear heating with velocity vectors whilst the right figure shows the second invariant of the deviatoric strain rate tensor. The fault is clearly seen in the middle of the image in red colours in the strain rate invariant field.

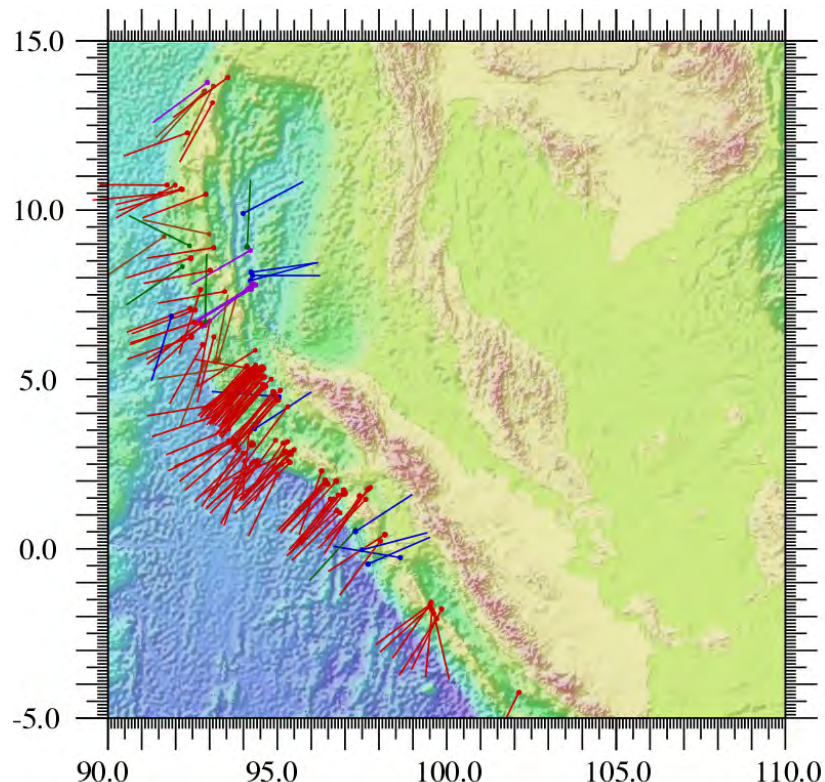
Geodynamics of the Great Sumatran Earthquake: structural analysis of aftershock sequences

Gordon Lister¹, Marnie Forster¹, Brian Kennett¹ and Joe Kurtz¹

¹Research School of Earth Sciences, Australian National University, Canberra, ACT, 0200, Australia

Research into reconstruction of the evolution of the Alpine-Himalayan chain, funded by an ARC Discovery Grant, has now been extended into the Indonesian region focussed on the geodynamics of the Great Sumatran earthquake. A C++ program has been developed (called Quakes II) to analyse and classify aftershock sequences in the Harvard CMT database. Figure 1 shows slip directions for 138 thrusts (red) and strike-slip faults with an up-dip component of movement (blue and green). Figure 2 shows slip directions for 72 normal faults (red) and strike-slip faults with a down-dip component of movement. Figure 3 shows poles to thrust faults in the aftershock sequence, plotted on an upper hemisphere stereographic projection. Figure 4 shows the corresponding slip lines. There is a high degree of kinematic coordination, towards 220° , which is coincidentally also the direction of slip reported for both the Sumatra I and Sumatra II Great Earthquakes. Since the primary events involved relatively gently inclined slip lines ($\sim 7-8^\circ$) in general these aftershock sequences are breaking new faults, with slip lines clustered around a $\sim 27^\circ$ dip (close to the theoretical Mohr-Coulomb angle for failure if the σ_1 axis after the main event was oriented with a $220^\circ-40^\circ$ trend.

Figure 1. Thrust faults in the aftershock sequence (in red) show a high degree of kinematic coordination. They cluster in the south.



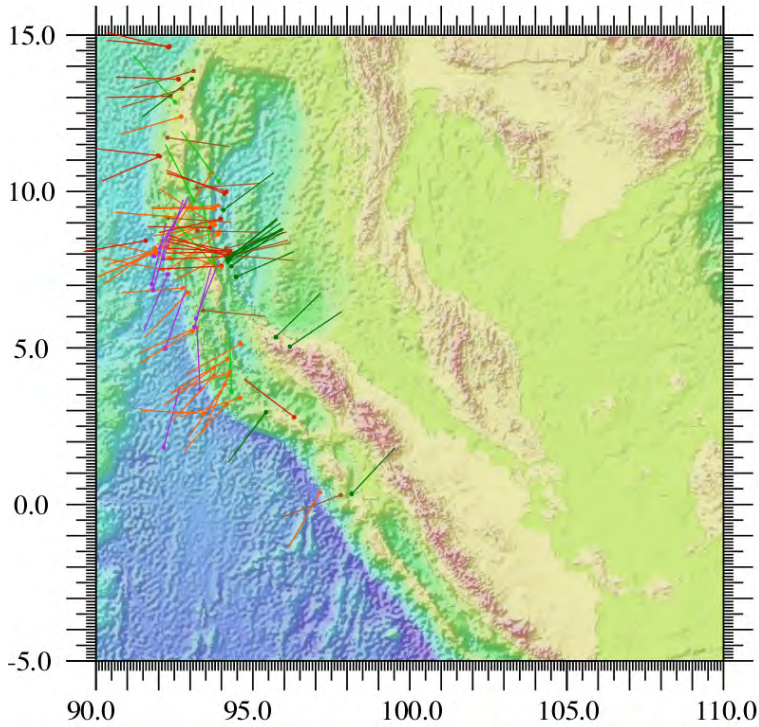


Figure 2. Normal faults in the aftershock sequence (in red) show a lesser degree of kinematic coordination. They cluster in the north of the earthquake zone. Many of these aftershocks formed on normal faults with a common slip line dipping $\sim 40^\circ$ W.

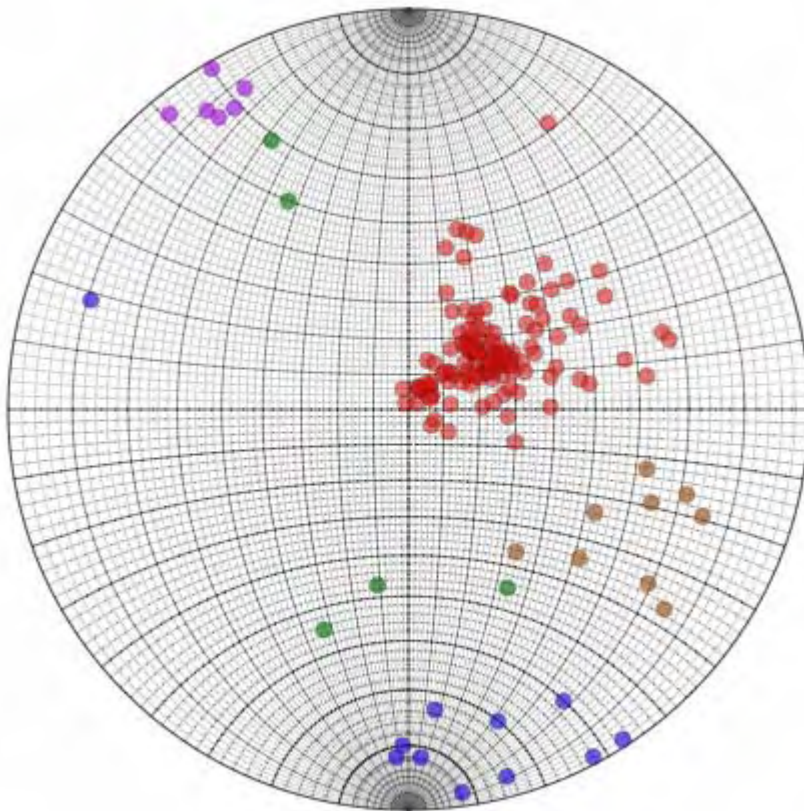


Figure 3. Poles to thrust faults (red) in the aftershock sequence plotted on an upper hemisphere stereographic projection. Poles to strike-slip faults are violet and blue.

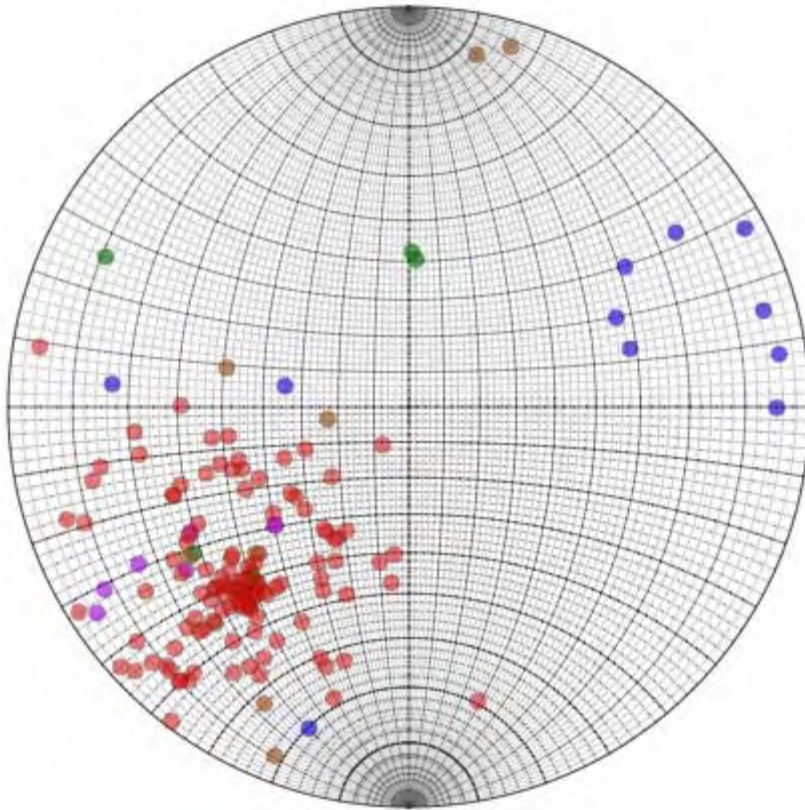


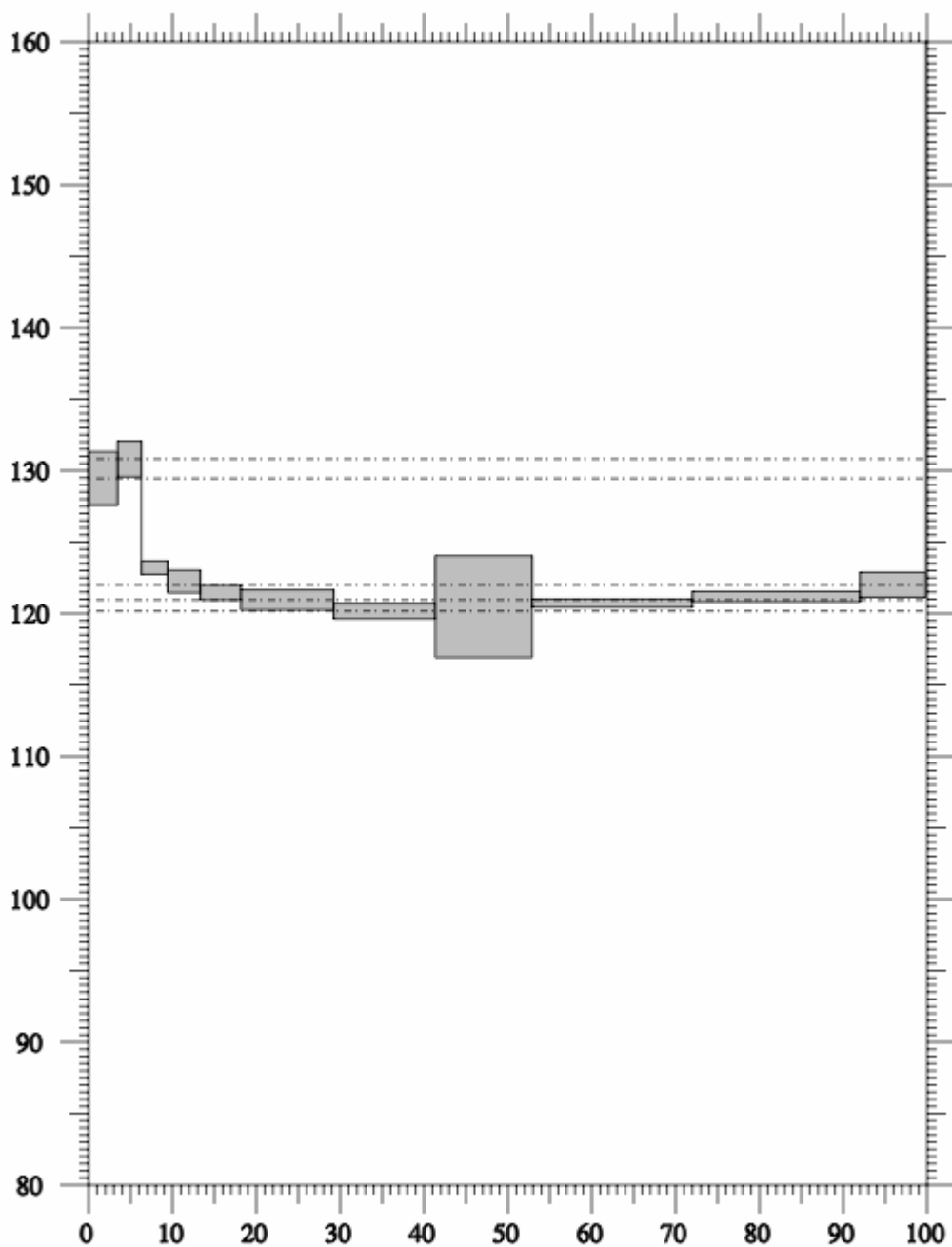
Figure 4. Slip lines for thrust faults (red) in the aftershock sequence plotted on an upper hemisphere stereographic projection. Slip lines for strike-slip faults are violet and blue.

Automatization of the method of asymptotes and limits for the analysis of $^{40}\text{Ar}/^{39}\text{Ar}$ step-heating experiments

Gordon Lister¹, Marnie Forster¹, Jim Dunlap¹ and Joe Kurtz¹

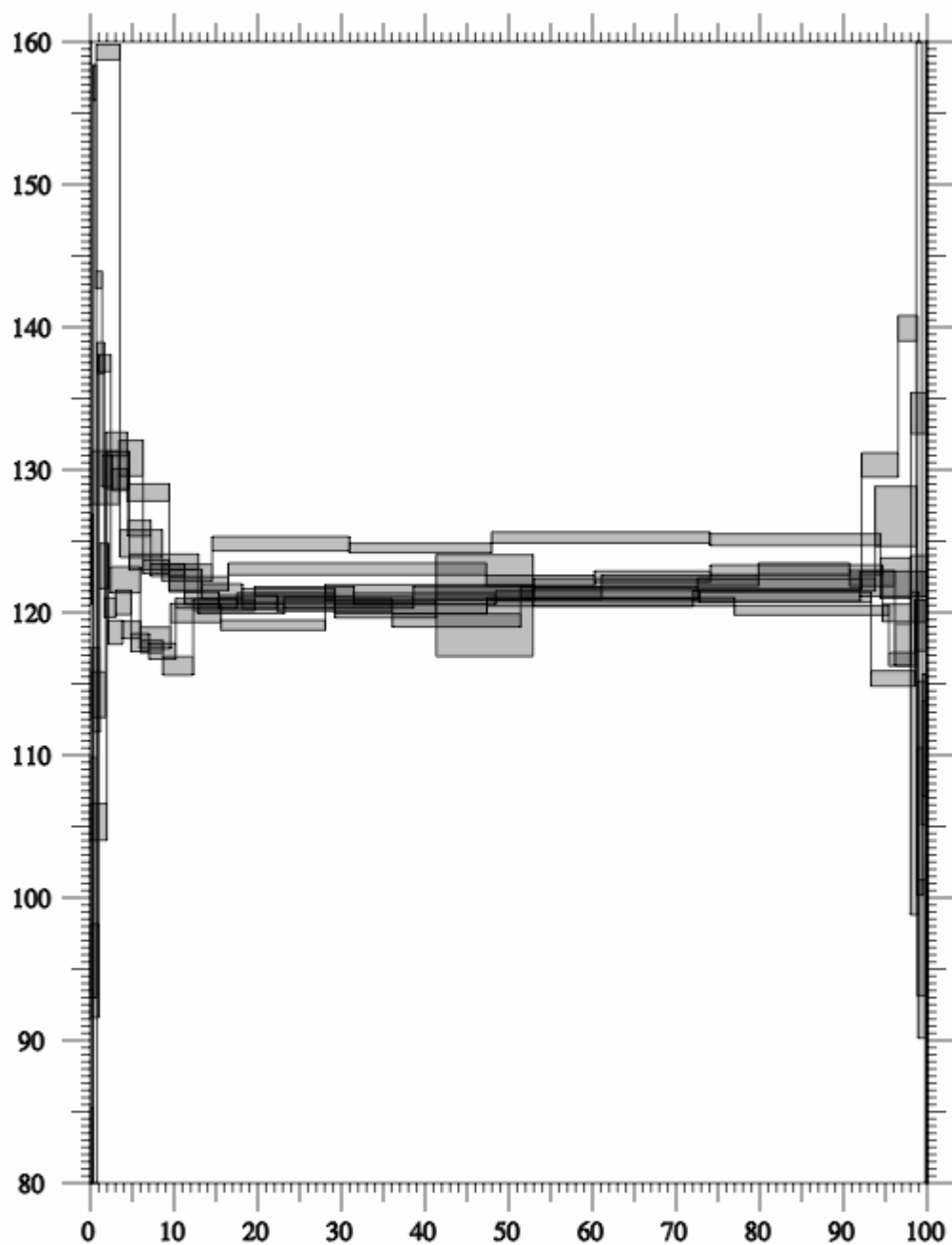
¹Research School of Earth Sciences, Australian National University, Canberra, ACT, 0200, Australia

Research into analysis of the timing of movement during the evolution of the Alpine-Himalayan chain, funded by an ARC Discovery Grant, has been aided by the development of a C++ program to automatically recognize asymptotes and limits in data from $^{40}\text{Ar}/^{39}\text{Ar}$ step heating experiments. Figure 1 shows a typical apparent age spectrum with asymptotes and limits recognized by the program. Figure 2 shows the cumulated apparent age plots. Figure 3 shows the cumulated Gaussian curves for each asymptote and limit recognized in the dataset. These are individually weighted by the percentage gas released in the defining step, with each Gaussian curve determined by the standard deviation for the same defining step. The cumulated Gaussian allows definition of the age of white mica in the km-scale extensional ductile shear zone that separates the Caples and Torlesse tectonic slices in the Otago schist.



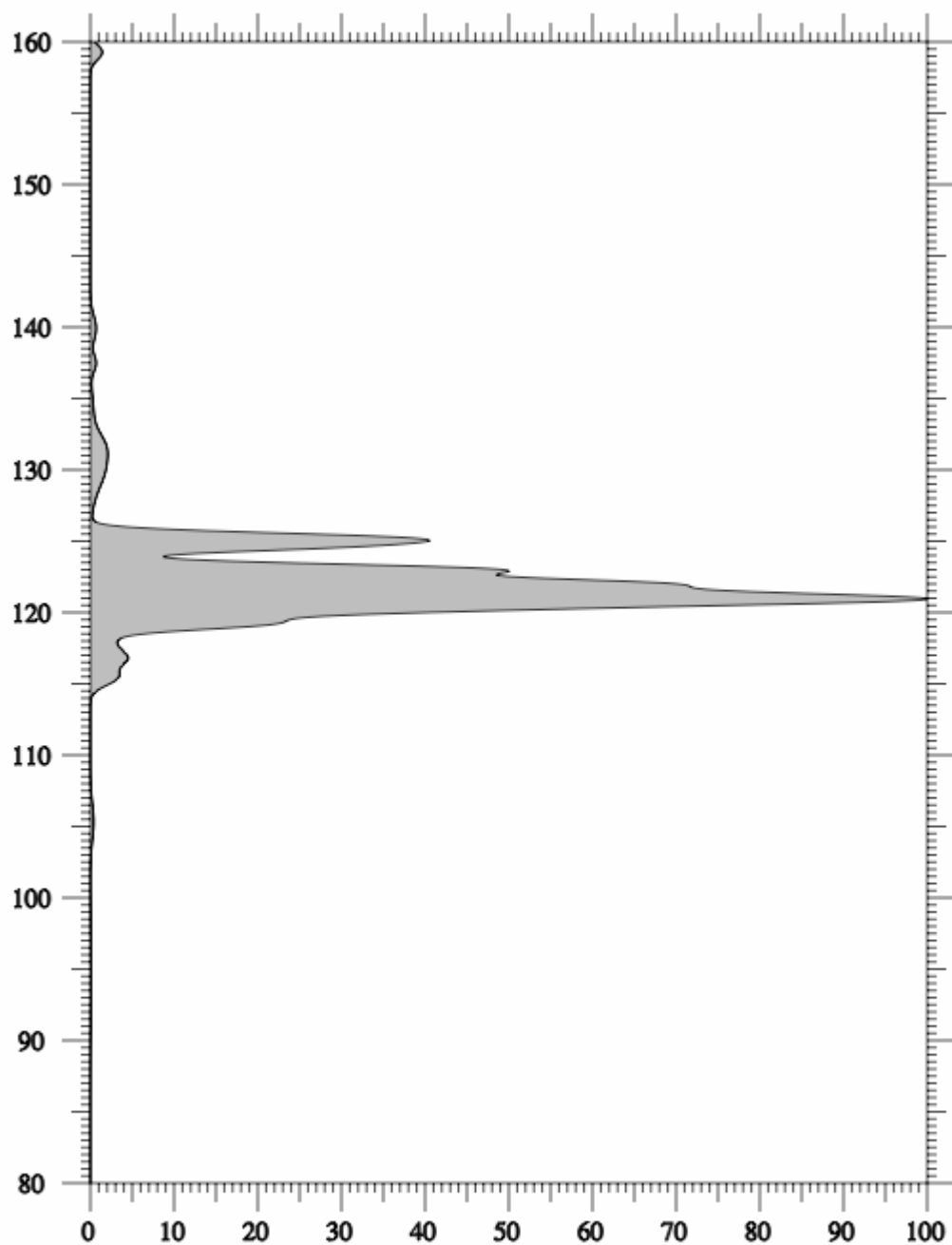
Name = APERS/ProgramAsymptote/Marnie3600 NZ 2003/MF98-02:M5/TableNZ98-02, number=1
 Program Asymptote - based on Forster & Lister 2004

Figure 1. Asymptotes and limits recognized by the computer program in data obtained in an $^{40}\text{Ar}/^{39}\text{Ar}$ step-heating experiment performed on white mica from the Caples-Torlesse shear zone.



Cumulated Apparent Age Plots Cumulated NZ plots (June 2005) Marnie3600 NZ 2003
 Program Asymptote - based on Forster & Lister 2004

Figure 2. Cumulated apparent age plots produced by the computer program, here illustrated using data produced during $^{40}\text{Ar}/^{39}\text{Ar}$ step heating experiments on white mica from the Caples-Torlesse extensional ductile shear zone in the Otago Schist, New Zealand.



Cumulated Gaussian Plots Cumulated NZ plots (June 2005) Marnie3600 NZ 2003
 Program Asymptote - based on Forster & Lister 2004

Figure 3. Cumulated Gaussian plots for asymptotes and limits recognized in the dataset by the computer program. These allow accurate definition of the age of the mica in the Caples-Torlesse extensional ductile shear zone.

Gold mineralisation in the Anakie Inlier, Clermont region

David Wood¹

¹*Research School of Earth Sciences, Australian National University, Canberra, ACT, 0200, Australia*

The Anakie Inlier is the only basement outcrop in an area of extensive basin development in central and south east Queensland that includes the Drummond, Bowen and Galilee Basins (Figure 1). Outcrop occurs in the southern part of the inlier and comprises polydeformed and metamorphosed basement of The Anakie Metamorphic Group (pre-Ordovician), sedimentary and volcanic rocks of the Fork Lagoons Beds (Upper Ordovician), intrusive rocks of the Retreat Batholith and the related Theresa Creek Volcanics (Mid Devonian), and volcanic rocks of the Drummond Basin sequence (Devonian-Carboniferous). These have been described in detail by Withnall et al. (1995).

Gold mineralisation in the Anakie Inlier, Clermont region occurs in four distinct settings:

1. Shear zone hosted quartz vein and siliceous lodes, with pyrite, arsenopyrite, galena and sphalerite as accessory minerals. These lodes typically form close to greenstone layers in the Bathampton Metamorphics, and are formed during D4 compressional deformation, concentrated around the Oaky Ck Antiform (Figure 2).
2. Quartz-gold veins and reefs that truncate schistosity and form tension-gash style structures. These veins typically form at the intersection of D4 and later shear zones, and contain coarse nuggety gold. Structural corridors up to 500m wide in the map area contain these veins, with the highest gold concentrations found at fault intersections.
3. A basal conglomerate sequence in Permian basins contains water-worn gold nuggets derived from erosion of quartz-gold reefs. Gold is concentrated in the first 20 to 50cm above the unconformity, however has also been found in false bottoms within the sequence. This horizon has been the target of most of the mining activities, both historical and recent in the region.
4. Fault and fracture systems close to the base of Permian basins host rich hydrothermal mineralization. The host structures transect the unconformity, have negligible to little offset and are defined by centimeter-scale zones of pug comprising fractured and clay altered sediment. Gold in these structures is intimately related to quartz, marcasite and siderite veining, often forming spectacular aggregates or 'specimens'. Secondary overgrowths of hydrothermal gold 'wings' form on the surface of water-worn nuggets in the basal conglomerate where fracturing occurs.

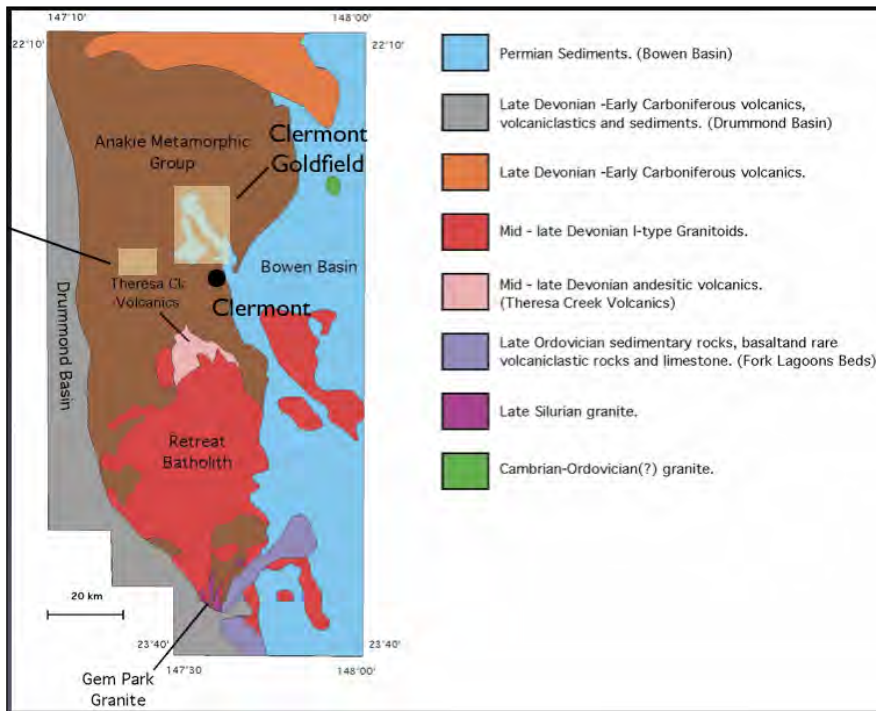
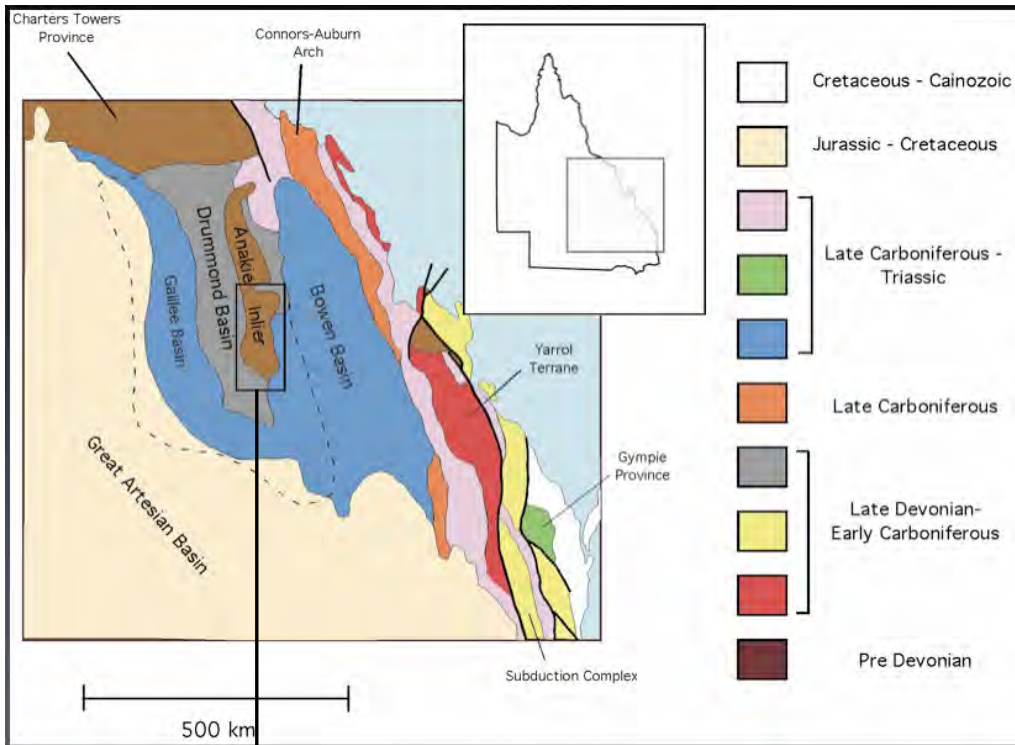


Figure 1. Location of the Anakie Inlier, map area and gold field near Clermont.

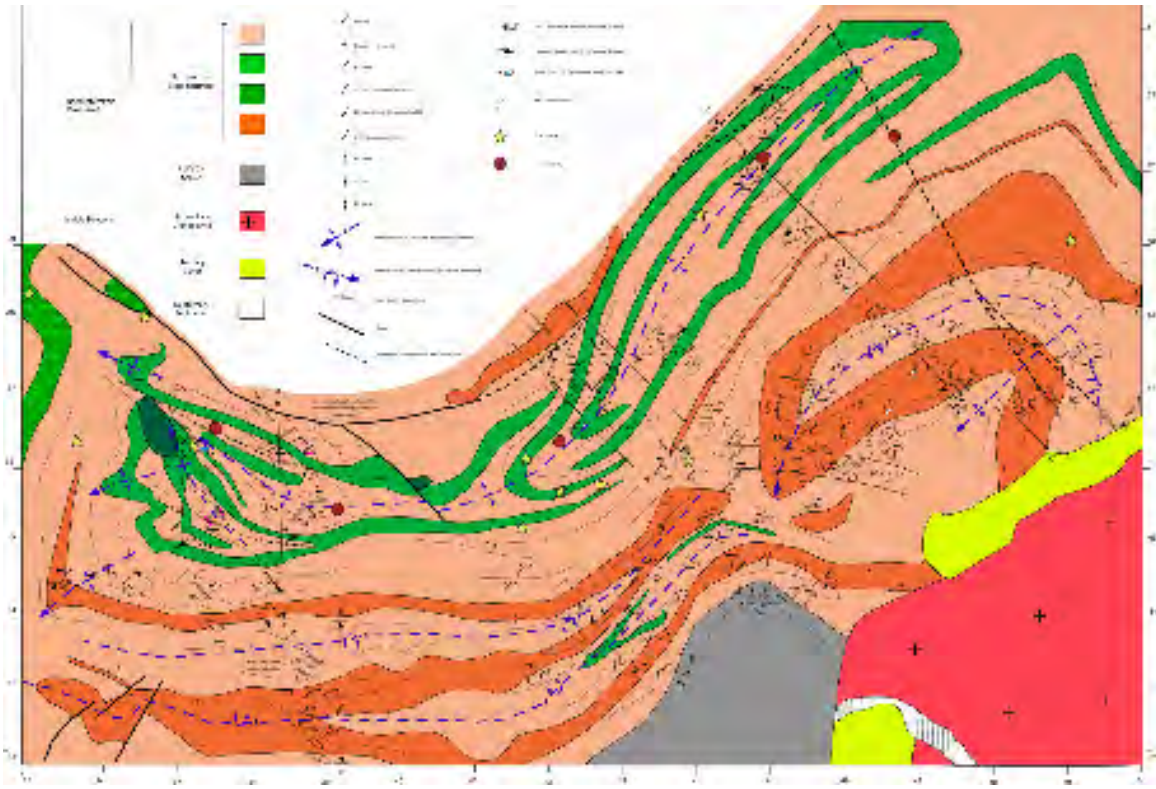


Figure 2. Geologic map of the Oaky Ck Antiform, west of Clermont.

Withnall, I. W., Blake, P. R., Crouch, S. B. S., Tenison Woods, K., Grimes, K. G., Hayward, M. A., Lam, J. S., Garrad, P.D. and Rees, I. D. (1995). Geology of The Southern Part of The Anakie Inlier. *Queensland Geology*.7.

Extra Information for Structure Tectonics

Lidena Carr

¹Research School of Earth Sciences, Australian National University, Canberra, ACT, 0200, Australia

Monday 11am Seminars

Each Monday throughout 2005 the structure and tectonics team has met at 11am for a seminar from a member of the group or an invited visitor. These meetings are an opportunity to bring the group together and inform each other of the various directions that research is taking. The seminars are informal and are a valuable source of critique on ideas or instruction. This year we have been lucky to have speakers from Geoscience Australia, the Department of Earth and Marine Science from ANU, Frogtec as well as from interstate. A full list of this year's speakers is shown at:

<http://tectonics.anu.edu.au/2005/seminars/>

Other Meetings

In 2005 the Structure and Tectonics team have hosted two major meetings. The 'Day on Diamonds' on August 25 and 'Earth Dynamics 2005' on the 24 and 25th of November.

The 'Day on Diamonds' was an informal day of talks all on the subject of diamonds and incorporated the weekly RSES 4pm seminar that was given by Simon Richards also on diamonds and titled: "The role of plate tectonics in controlling the emplacement of diamond-bearing kimberlites and related magmas". Due to the popularity of this day it was moved before the first talk began to the larger Jaeger seminar room. The schedule for the 'Day on Diamonds' is below in table 1.

Earth Dynamics 2005 took place on November 24 and 25 and bringing speakers and guests from as far a field as the University of Queensland, the University of Melbourne and Geoscience Australia. The focus of the talks on Thursday and Friday being 'Episodes' and 'Tectonics, Risk and Resources' respectively and as with the 'Day on Diamonds' incorporated the weekly RSES seminar which was presented by Paulo Vasconcelos from the University of Queensland. The relaxed nature of the presentations provided valuable discussion and much interest in Earth Dynamics 2006. A full list of the talks presented at Earth Dynamics 2005 is below in table 2.

Visitors

This Year Structure and Tectonics has been privileged to have several visitors including Professor Roberto Compagnoni from University of Turino Italy, who is a co-supervisor of PhD student Marco Beltrando. His visit was spent working with Marco and other members of the team.

Scott McTaggart, ACcESS CEO from the University of Queensland, has visited us several times to help us complete administrative tasks associated with ACcESS setup and reporting commitments, as well as inspecting progress on ACcESS MNRF projects.

Dr Guiting Hou from Peking University in China is visiting us for twelve months and is working with Professor Gordon Lister on the Gold in China project, and on reconstruction of the Palaeo Proterozoic Supercontinent.

Table 1.

SCHEDULE FOR A DAY ON DIAMONDS

Thursday, August 25th

10:00 Greg Yaxley	Diamond indicator minerals – novel techniques for advancing diamond exploration
10:45 Masahiko Honda	Diamonds - a window into the ancient mantle: the origin of the Earth's atmosphere and outgassing of the mantle.
11:30 Stewart Fishwick	Tomography and diamonds: what we can see.
LUNCH (12:30 - 13:30)	
13:45 Uli Faul	Translating tomographic images into a physical state of the upper mantle.
14:30 Joerg Hermann	Diamonds in subducted continental crust.
15:15 Lynton Jaques	Controls on the distribution of Australian diamond pipes.
16:00 Simon Richards (RSES seminar in Jaeger Room)	The role of plate tectonics in controlling the emplacement of diamond-bearing kimberlites and related magmas.

Table 2.

24th November 2005		
Coffee will be available from 9:30am		
☐ Episodes		
10:00 - 10:45	Marnie Forster, The Australian National University	Episodes and the Structural Geologist
10:45 - 11:30	Daniela Rubatto and Joerg Hermann, The Australian National University	Episodic (?) subduction in the western Alps
11:30 - 12:15	Brian Kennett, The Australian National University	Subduction zones and their properties
12:15 - 13:30 LUNCH in the Fellows Garden		
13:30 - 14:00	Geoff Davies, The Australian National University	Dynamics of the early mantle: depletion, reservoirs and plates
14:00 - 14:30	David Giles, The University of Adelaide	Is there order in the chaos of Proterozoic plate motions?
14:30 - 15:00 Hans Mühlhaus, ACcESS MNRF and The University of Queensland Computational simulation of planet scale episodicity in mantle convection and plate tectonics		
15:00 - 15:30	Mark Quigley, The University of Melbourne	Tectonic and climatic episodicity in landscape evolution
15:30 - 16:00 Afternoon Tea		
16:00 - 17:00	RSES Seminar Paulo Vasconcelos, The University of Queensland	Weathering and Landscape Evolution: Episodicity at Local, Regional, Continental, and Global Scales
17:00 - 18:30 Beer and Nibbles		
19:00 Conference Dinner		
25th November 2005		
☐ Tectonics, Risk and Resources		
9:15 - 9:50	Rod Holcombe, The University of Queensland	Exploration kinematics: linked faults, corner flow, and crustal plumbing.
9:50 - 10:30 Barry Köhn and Andrew Gleadow, The University of Melbourne Thermochronology and landscape evolution in the basin hinterland-		

understanding basin supply and deep basin sediments.

10:30 - 11:00 ☐ Coffee Break

11:00 - 11:40 Mike Sandiford, The University of Melbourne **Timor**

11:40 - 12:30 Gordon Lister and Brian Kennett ANSIR and ACcESS MNRFs and The Australian National University **Geodynamics of the Great Sumatran Earthquake**

12:30 - 13:30 **LUNCH in the Fellows Garden**

13:30- 14:15 Dan Clark and David Burbidge, Geoscience Australia **Quaternary crustal deformation in Australia: ☐ stirrings of life in the dead continent**

14:15 - 15:00 Steve Roberts, The Australian National University Ole Nielsen, Geoscience Australia **Inundation modelling and tsunami risk** t.b.a.

15:00 - 15:45 Minghai Jia, Phil Cummins, Spiro Spiliopoulos and Barry Drummond Geoscience Australia **The Australian Tsunami Warning System**

15:45 - 16:15 Post-Conference Discussion

16:15 Continued discussion in the Fellows Garden

The End

Earth Physics Introduction

Research into the structure and dynamics of the Earth uses a range of modern physical and mathematical techniques grouped into four themes of Geodynamics, Geophysical Fluid Dynamics and the Centre for Advanced Data Inference (CADI). Work in the Earth Physics area spans observational, theoretical, computational, and data oriented studies that are all directed towards understanding the structure and processes in the solid and fluid Earth, and their environmental consequences. The four themes in Earth Physics have considerable cross-interaction, particularly through a common use of computational methods.

Prof B.L.N. Kennett, the Area Coordinator, was awarded the Jaeger Medal for Australian Earth Science from the Australian Academy of Sciences in May 2005 and at the end of the same month was elected as a Fellow of the Royal Society of London.

Work in geophysical fluid dynamics this year includes a new theoretical model for the thermohaline overturning circulation of the oceans, based on insight from laboratory experiments on turbulent entrainment. Experimental runs in the GFD laboratory have been linked to major computational simulations, e.g. in understanding the amount of mixing that takes place in density-driven exchange flow through constrictions, such as ocean straits. Other classes of laboratory investigations include studies of lava flow dynamics, particularly in pre-existing channels and three-dimensional simulations of subduction to understand the flow around subducting plates.

Studies of the interaction of mantle dynamics with mantle chemistry, with the aid of numerical models, suggest that early plate tectonics is a more viable concept than previously thought, which would change the expected cooling history of the mantle. Further the age of mantle trace components depends little on the viscosity structure but mainly on the rate of processing through zones of melting.

In seismology, the long running Tasman Line experiment was completed this year and all 20 stations have been recovered. This data has made significant contributions to the resolution of structure in the neighbourhood of the transition from Precambrian to Phanerozoic Australia, both from surface wave tomography and in the mapping of crustal structure using receiver functions. The improved resolution of lithospheric structure suggest the presence of three steps in lithosphere thickness in the transition from the cratonic core in the west to the eastern seaboard of the continent.

A deployment of short-period instruments in the Murray Basin has provided important tomographic constraints on structures beneath the basin. A further major deployment has been made in Eastern Victoria that will run to mid 2006, and when linked with previous data should provide high density of

station coverage across the whole of Victoria. Waveform correlations methods have been successfully employed on data from the Tasman Line experiment to provide new constraints on crustal and upper mantle structure from surface wave analysis.

In the Centre for Advanced Data Inference projects have been conducted in geomorphology, probability theory, statistical inference techniques, structural seismology, airborne geophysics, earthquake seismology, computational mineral physics and geodesy. This year saw continued development of the CADI inversion toolkit whereby CADI visitors and project participants have a simple interface to both software and hardware facilities including the Terrawulf parallel cluster.

The focus of the glacial rebound work in 2005 has focussed on Arctic Eurasia from the time of the penultimate glacial maximum (MIS 6 or the Late Saalian at ~145,000 years ago) up to the present with the goal of establishing constraints on the ice thickness and ice margins for some of the major phases of the last glacial cycle. A major compilation of field evidence for the ice margin locations and shoreline elevations and sea levels across the region has been completed and the inversion of which has led to new ice models from 140,000 years to 60,000 years ago, including the time of the renewed initiation of the ice sheets after the last interglacial.

Geodetic research during 2005 produced significant improvements in the accuracy of the analysis of GPS, primarily through software developments made at RSES in modelling geophysical phenomena such as atmospheric pressure loading, ocean tide loading and atmospheric propagation effects. A successful GPS field observation program was carried out in Papua New Guinea on a transect of sites along the western border, in the Schouten Islands, central Highlands and the Papuan Peninsula region.

GEOPHYSICAL FLUID DYNAMICS INTRODUCTION

Geophysical Fluid Dynamics is the study of fluid flows and their roles in transporting heat, mass and momentum in the oceans, atmosphere and Earth's deep interior. In RSES, the research in this field focuses on the exploration of physical processes of importance in three different areas:

- convection, mixing and circulation in the oceans, with implications for climate,
- magmatic and volcanic processes, and
- convection of the solid silicate mantle, with its implications for plate tectonics and the evolution of our planet.

Geophysical Fluid Dynamics (GFD) emphasises the importance of dynamical modelling. At the ANU our research program is anchored strongly in experimental fluid dynamics and benefits from the excellent facilities of a purpose-built 400 sq. m laboratory and workshop area, opened in 2000. This is one of the premier GFD laboratories in the world, and one of only two such labs in Australia. It is well known around the world for its contributions across fluid dynamics, oceanography and 'solid earth' geophysics. A second crucial strand of our research lies in advanced computing, and this work benefits from a range of computing facilities within the Research School and in the Australian Partnership for Advanced Computing (APAC) located at ANU.

SUMMARY OF DEVELOPMENTS IN 2005

This year, an exciting new theoretical model for the [thermohaline overturning circulation](#) of the oceans was completed and published in *Ocean Modelling* (by Dr Hughes and Prof Griffiths). Growing out of insights from their laboratory experiments published in the previous year, this model expresses the role of turbulent entrainment into the major sinking regions of the oceans, which take the form of overflows from marginal seas and dense slope currents falling to large depths in the oceans. It turns out that entrainment, a previously neglected process in this global context but one that has long been known to cause large dilutions of the dense sinking water with surrounding waters, can have a substantial effect on the global density distribution in the oceans and on the rate of overturning of bottom and surface waters. Once this effect is included, the model indicates that the globally averaged vertical mixing rates in the oceans as measured by oceanographers, are consistent with observed overturning rates, top-to-bottom density difference and surface thermal forcing, without any need to call for the much larger mixing rates previously indicated by the simpler one-dimensional (Munk) advection-diffusion balance.

Other work on ocean processes includes a very successful attempt to measure the amount of mixing that takes place in [density-driven exchange flow](#) through constrictions, such as ocean straits (figure A), [the interaction of headland wakes](#) in coastal waters with disturbances carried from upstream by a mean flow, and a study of low-frequency variability, induced by the effects of baroclinic eddy instability and interaction of flow with bottom topography in

the oceans, using a high-resolution quasi-geostrophic coupled [ocean-atmosphere model](#)

Studies of the interaction of [mantle dynamics](#) with mantle chemistry, using numerical models, also have yielded some important findings. First, a possible explanation has emerged for a well-documented strong depletion of incompatible trace elements prior to 4 billion years ago, due to enhanced sinking of subducted basaltic crust through the early upper mantle, whose viscosity was relatively low at the time. This would make early plate tectonics more viable than previously thought and change the expected cooling history of the mantle. A second finding is that the age of mantle trace components depends little on the viscosity structure and other details of models, even whether they are in two or three dimensions. Rather, the age depends mainly on the rate of processing through zones of melting. Since this is more predictable it opens the way for a clearer understanding of the chemical evolution of the mantle.

In other work, a re-examination of the [heat flowing from the core into the mantle](#) suggests that radioactivity is not required in the core to help drive the dynamo that generates Earth's magnetic field, and an extensive review of the mantle plume hypothesis concludes that it is a viable and useful hypothesis, though it is unlikely to explain all volcanism that is not related to plate tectonics. Experimental work continued on three-dimensional laboratory [simulations of subduction](#), involving a dense high-viscosity plate, which sinks into the lower density low-viscosity mantle. The experiments reveal the influence of the lithosphere-mantle viscosity contrast on the process of subduction and the induced flows in the surrounding mantle.

Studies of volcanic processes have progressed through a thorough theoretical and experimental investigation of the 'run-out' of rapidly released volumes of lava in pre-existing channels or valleys, which has revealed the conditions under which the [lava flows](#) are stopped by yield strength or when they are stopped by cooling. Flows from continuous vents on a slope and the way in which flows form their own channel have also been examined. A novel theoretical prediction of channel width compares well with the results from laboratory experiments.

The group continued to benefit from the presence of Emeritus Professor J.S. Turner. Prof. Griffiths and Drs Hughes and Hogg taught the "Ocean Dynamics" unit in the RSES Physics of the Earth Honours program. Prof. Griffiths again taught a 3rd year undergraduate course on fluid dynamics and ocean-atmosphere dynamics in the Department of Physics and Theoretical Physics, ANU. The staff, students and visitors all acknowledge the vital contributions of our technical support staff, A.R. Beasley and C.J. Morgan, to our research program. A new ARC Discovery grant was awarded to Prof. R.W. Griffiths for studies of the fundamental dynamics of the oceans' meridional overturning circulation.

The dynamics of the ocean thermohaline circulation, and 'horizontal convection'

R.W. Griffiths, G.O. Hughes, M.A. Coman and J.C. Mullaney

The meridional overturning circulation of the oceans is an example of "horizontal convection", a flow forced by heating and cooling at the same horizontal surface. In studying horizontal convection we aim to provide insight into the dynamics that underpin the complex overturning circulation in the oceans. In recent years we have conducted both laboratory experiments and numerical simulations of horizontal convection, in cases of either thermal or thermohaline forcing (figure 1). This work has progressed during 2005 on a number of fronts.

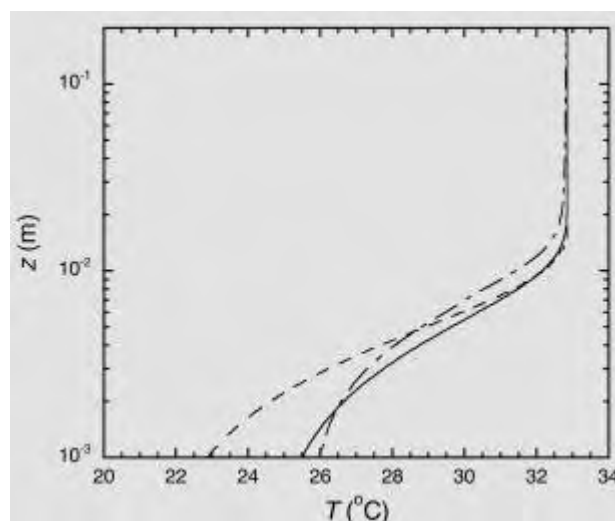


Figure 1: A photograph of dye tracer in the convective circulation in a long box of water which is cooled through the right hand half of the base and heated through the left hand half of the base. The box interior is 1.25 m long and 0.2 m high, but only the left 1/2 of the length is shown. Features include small-scale convection above the heated base of the tank, with a narrow plume ascending on the left hand wall.

We have developed a theoretical model that successfully describes many aspects of horizontal convection including the vertical density structure (figure 2), the thermal boundary layer thickness adjacent to the differentially heated boundary, and the dependence of the heat transfer upon the Rayleigh number and other quantities.

Figure 2: Theoretical prediction (solid line) of the temperature profile and a comparison with laboratory data (long-short dashed line) from a horizontal convection experiment (Mullaney *et al.* 2004).

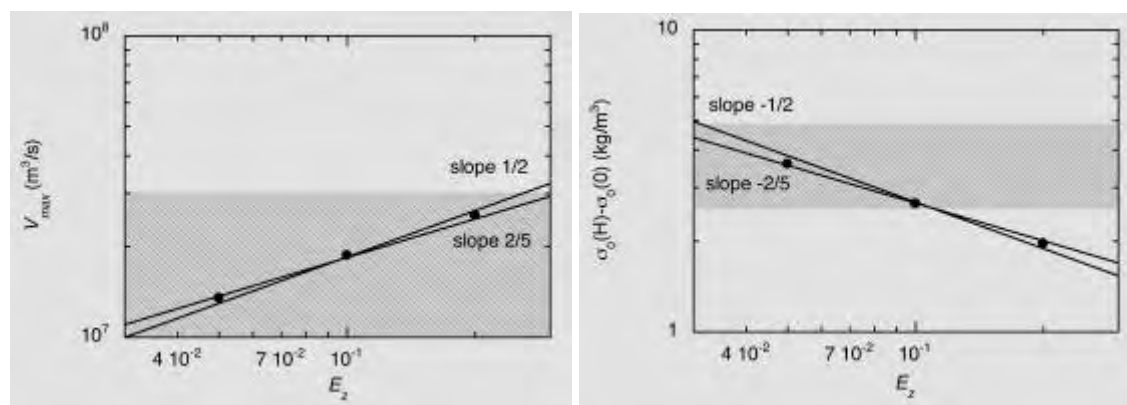
The prediction is based upon the properties of water at the average temperature in the box. The additional curve (dashed line) is a prediction based on



water properties at the coldest temperature in the flow (16 °C) and indicates the robust nature of the results.

The application of horizontal convection to the meridional overturning circulation in the global oceans has been controversial. Early experimental work by Sandstrom (1908, 1916) is frequently cited as evidence that heating and cooling at the ocean surface cannot lead to the observed vigorous overturning circulation. In particular, that work is cited as showing that heating and cooling sources at the same level (as is the case at the ocean surface) cannot drive a significant circulation. However, Sandstrom's conclusions are at odds with modern experiments on horizontal convection. Hence we have revisited Sandstrom's original experiments and find that some of his original conclusions require revision. In recreating his experiments we observe strong flows irrespective of the relative level of heating and cooling, and these are consistent the results of modern experiments in which heating and cooling are distributed over a planar horizontal surface. We conclude that heating and cooling at the same level can force strong a circulation penetrating through the full depth of a basin.

We have continued the development of a simple mathematical model for the ocean circulation that gives predictions consistent with a variety of field estimates. Entrainment of ambient water laterally into dense localized sinking currents is predicted to be an important mechanism of vertical heat transport in the global oceans. We have also examined the dependence of the results upon the amount of entrainment into the sinking currents (characterized by a mathematical constant Ez , Figure 3) and the vertical mixing rate averaged over the interior of the oceans (characterized by the diffusivity k^* , Figure 4). These results show that failure to allow for entrainment into highly localized sinking regions in models can be partially offset by artificially increasing the vertical diffusivity in those models. However, we find that approximate parameterisation of entrainment in this manner leads to model predictions that are flawed in other respects. As most climate and ocean numerical models are unable to resolve the sinking regions, our results illustrate the imperative for the development of better entrainment parameterisations for use in computations.



(a)

(b)

Figure 3: The theoretical dependence of (a) overturning volume flux and (b) top-to-bottom density difference predicted by our model for entrainment constant $Ez = 0.05, 0.1$ and 0.2 , and other parameters appropriate to the global oceans ($Ez = 0.1$ is the normally accepted value). The hatched band indicates the uncertainty of the measured globally-averaged ocean value in each case. Lines indicate the power law slopes predicted by previous non-rotating and geostrophic scaling theories.

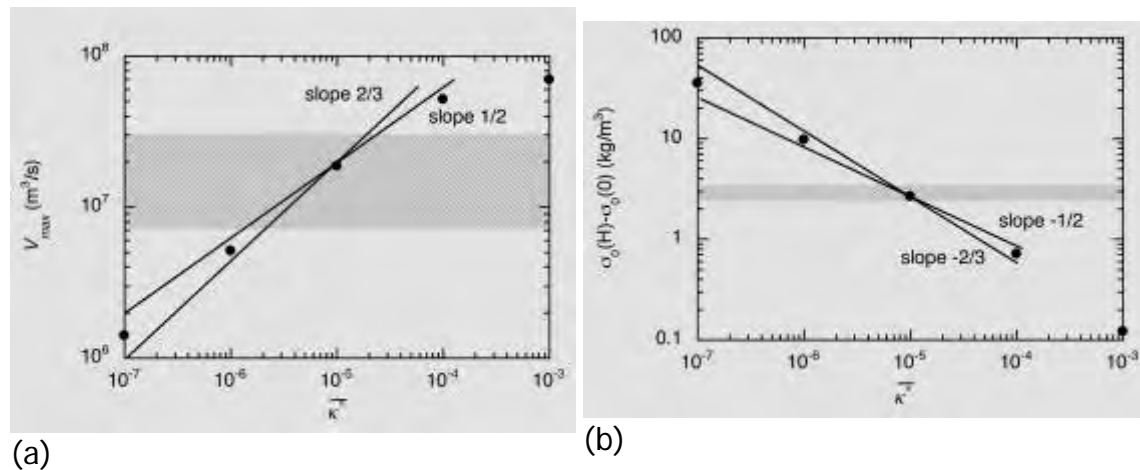


Figure 4: The theoretical dependence of (a) overturning flux and (b) top-to-bottom density difference predicted by our model for the vertical diffusivity $k^* = 10^{-6}, 10^{-5}$ and 10^{-4} m²/s, and other parameters appropriate to the global oceans ($k^* = 10^{-5}$ m²/s is the observed value in the oceans). The hatched band indicates the uncertainty of the measured globally-averaged ocean value in each case. Lines indicate the power law slopes predicted by non-rotating and geostrophic scaling theories.

We have also examined numerically the effect on horizontal convection of a small additional heat input at the top boundary in figure 1. This system is a simple thermally-driven representation of the ocean's meridional overturning circulation (again inverted for comparison with laboratory experiments) with a small amount of geothermal heating at the ocean bottom. A more vigorous overturning circulation is observed when the additional heat input is destabilizing (as for geothermal heating), whereas a stabilizing flux (heating at the top of the box) results in a slower circulation and a plume that no longer penetrates through the full depth of the box (Figure 5). Our results suggest that the geothermal heating in the oceans (about 1% of the heat supplied at the surface) could enhance the overturning by about 10%.

Additional aspects of horizontal convection are being investigated in studies commenced this year, in order to better understand the fundamental dynamics as well as oceanic complexities. These aspects include the nature of transient adjustment to perturbed boundary conditions, the case of (nearly) symmetric boundary heating such that there is a plume at both ends of the basin (mimicking the slightly unequal North Atlantic and Southern Ocean sinking), and the effects of planetary rotation.

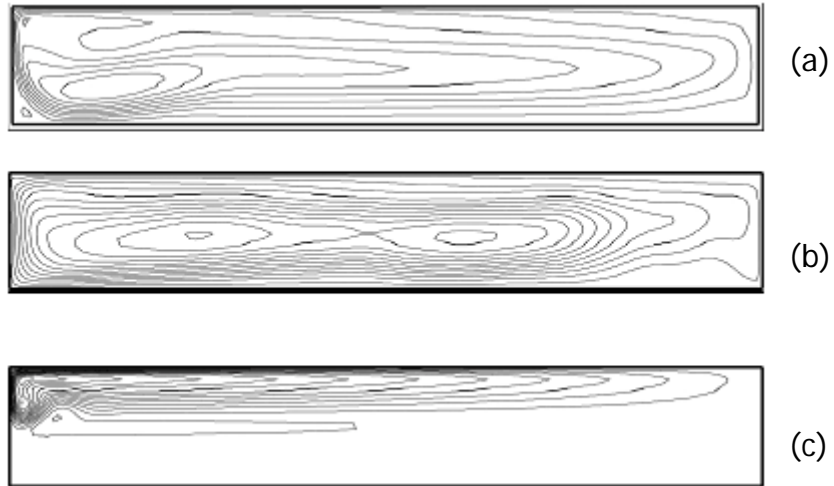


Figure 5: Two-dimensional numerical solutions (showing streamfunction contours) for the convective circulation in a long box of water which is (a) cooled through the right hand half of the top and heated through the left hand half of the top; (b) as for (a), but with heating at the base equal to 10% of the heating at the top; and (c) as for (a), but with cooling at the base equal to 2% of the cooling at the top.

Dynamics of ocean straits and overflows

Straits and sills commonly exercise control over the rates of water transport out of estuaries and marginal seas, and between abyssal ocean basins. Analytical methods are frequently used to estimate flow through these constrictions; our approach focuses on extending the simple analytical solutions to more realistic cases.

T.J. Prastowo, R.W. Griffiths, G.O. Hughes and A.McC. Hogg

We have continued a study of the amounts of mixing that occur in two-layer density-driven exchange flows. The flow involves a strong velocity gradient between layers flowing in different directions, and this flow can become critical (i.e. reach the speed of gravity waves on the density interface), so that there is a hydraulic control point in the strait or above the sill. The mass flux through the constriction is also influenced by the mixing between the layers. This year we have continued a series of experiments in a long channel (figure 6), from which both the amount of mixing and the effect of the mixing on the exchange rates is determined (as a function of the density difference and constriction width). The exchange rate is found to be a constant $82\pm 1\%$ of the exchange rate predicted by inviscid hydraulic theory. The mixing can be described in terms of an efficiency - the proportion of the available potential energy (released by the flow over a given time) that goes into raising the density field by vertical mixing. We find that exchange flows driven by density differences in excess of 2% have efficiencies of $11\pm 1\%$ (figure 7). We have also developed scaling theories that predict both the observed exchange rate and the measured mixing efficiency. Ongoing work is aimed at understanding a measured decrease in mixing efficiency at density differences less than 2%.

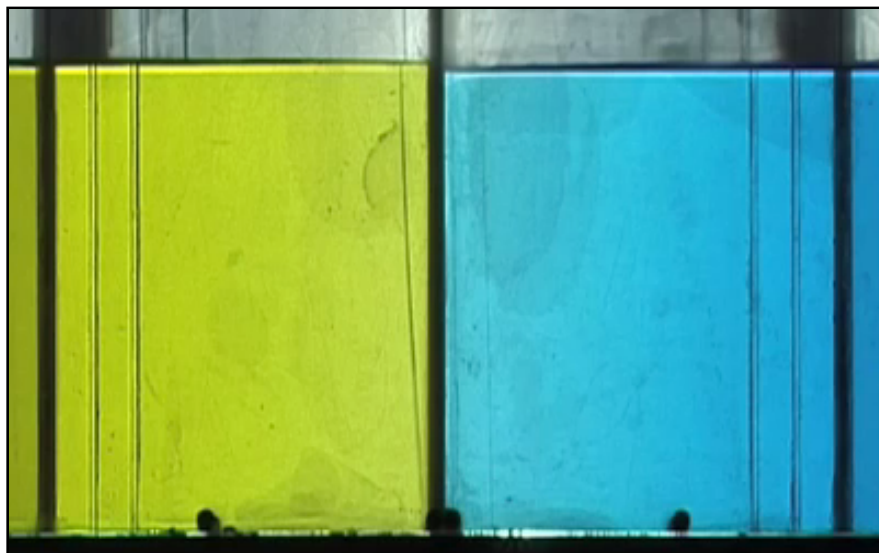


Figure 6: A movie of the exchange flow through a horizontal constriction in a laboratory water channel, showing the shear instability and subsequent turbulent mixing.

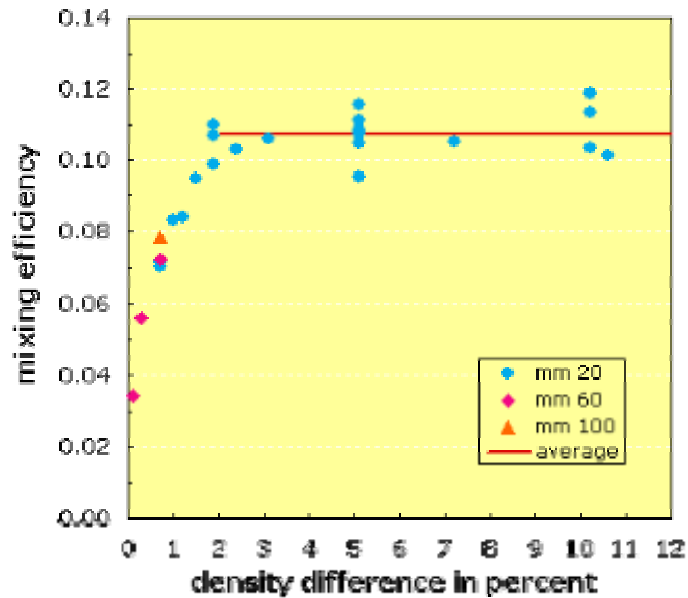


Figure 7: Mixing efficiency as a function of density difference

L.M. Frankcombe and A.McC. Hogg

Motivated by observations that tidal oscillations can modify the density-driven flow through straits we have attempted to characterise the response of sill and strait flows to time-dependence. The approach is to simulate the time-dependent flow with an idealised numerical model, using a new set of open boundary conditions developed for use in ocean models (in collaboration with Dr J. Nycander of Stockholm University).

The model is computationally efficient, allowing the simulation of time-dependent flows over a wide parameter space. The results are compared with a theoretical prediction (the black curve in figure 8). The simulations demonstrate that, contrary to previous investigations, the effect of tidal period may be offset by reflections and nonlinearity. Thus there is a strong dependence of flux upon tidal amplitude, but not period, as seen in figure 8.

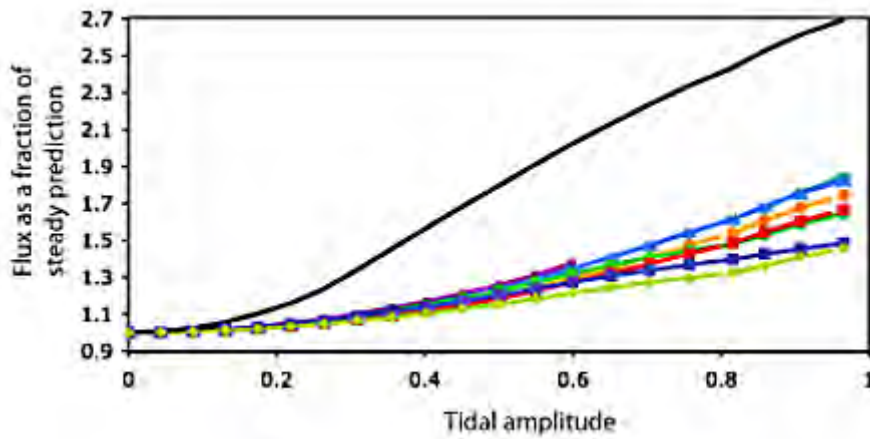


Figure 8: Simulated flux as a function of tidal amplitude. The black line shows a theoretical prediction, while the coloured lines showed the flux for a number of cases with different tidal period.

A.McC. Hogg and G.O. Hughes

The extension of analytical hydraulic solutions to fluids with viscosity (whether a molecular viscosity or a parameterised turbulent eddy viscosity) is a difficult problem that remains unsolved. In this work we propose that such a solution is only possible numerically, and construct a numerical algorithm for solving such flows. A sample solution for hydraulically controlled viscous one-layer flow over a sill is shown in figure 9.

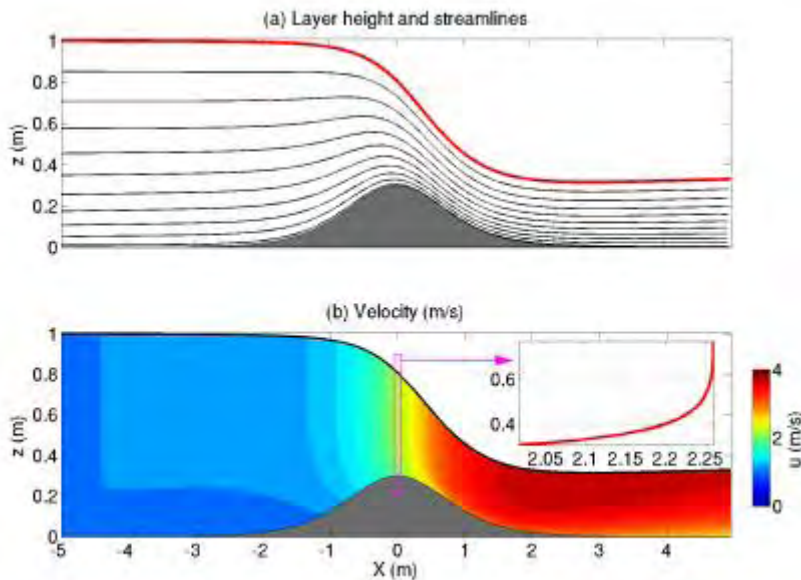
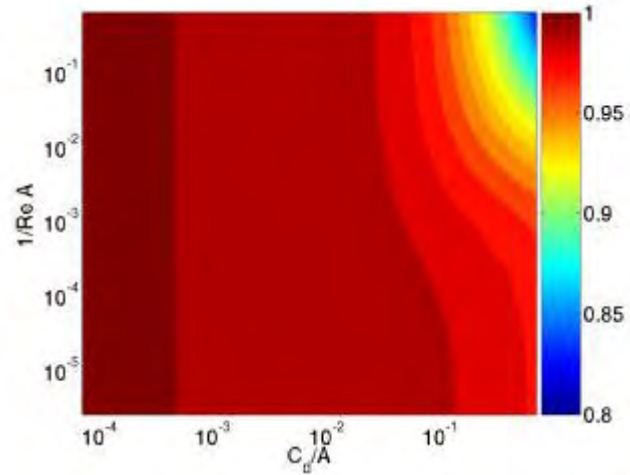


Figure 9: Solution of viscous hydraulically controlled flow over a sill showing (a) layer height and streamlines; and (b) fluid velocity (colour scale), with inset showing the velocity profile at the sill crest.

The numerical solution method is used to demonstrate that flux decreases with both bottom drag and viscosity, as shown in figure 10. Furthermore, we demonstrate that the effect of internal viscosity is greatest at intermediate values of viscosity, contrary to previous theoretical predictions.

Figure 10: Flux as a function of dimensionless bottom drag, C_d/A and dimensionless viscosity $1/ReA$.



The role of ocean eddies in the ocean circulation and climate

A.McC. Hogg

This study is part of a long-term project to determine whether ocean eddies need to be resolved by climate models to correctly simulate present and future climates. In previous years, this project concentrated on the variability of the double gyre circulation in the ocean (relevant to the North Atlantic and North Pacific Oceans). The study, which was a collaborative effort between ANU, Florida State University and the National Oceanography Centre, Southampton, identified a new mode of ocean variability which is only present when eddies are explicitly included in the simulation. Furthermore, it was shown that this ocean variability might contribute to climate variability.

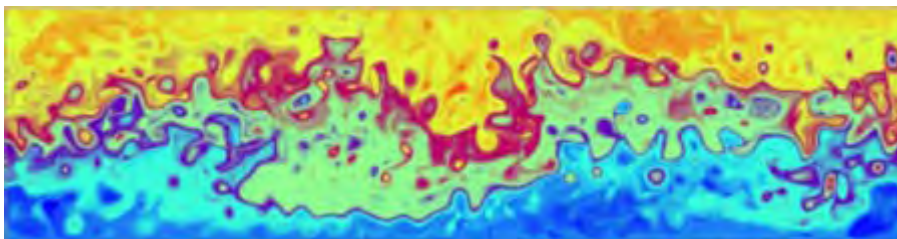


Figure 11: Potential vorticity field of the upper ocean for an idealised, eddy resolving ocean simulation. Flow in this re-entrant channel is from left to right.

In 2005 this work was extended to the mid-latitude flow of the Southern Ocean (see figure 11 for a sample image of the vorticity distribution in the eddy-resolving model, and figure B for sea surface temperature and pressure). The model displays a robust mode of inter-decadal variability, as shown by the energy time-series in figure 12, that is not observed in standard ocean models. This suggests that ocean models cannot correctly simulate ocean variability.

Resolution of this problem is part of an ongoing project.

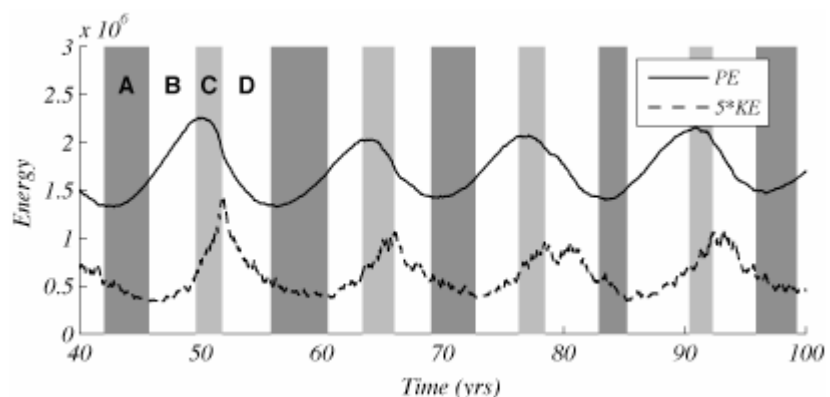


Figure 12: Illustration of the variability observed in the Southern Ocean model. The variability is characterised by large variations in both potential energy (PE; solid line) and kinetic energy (KE; dashed line), and the time-series is divided into four dynamical regimes for analysis. This variability only occurs when ocean eddies are fully resolved.

The melting of ice in the Arctic Ocean: double-diffusive transport of heat from below

J.S. Turner

This study has been motivated by two oceanographic observations: an increase in the rate of melting of sea ice in the Arctic Ocean, and the advance of an anomalously warm tongue of Atlantic water across the Arctic below the halocline over the last few decades. These raise the question: are these two observations related? The results of previously reported laboratory experiments have shown that, in principle, an increased rate of melting can be produced by vertical double-diffusive transports, but the aim now is to assess whether this mechanism is quantitatively sufficient to explain the observations.

There is certainly enough heat in the intruding tongue to melt all the sea ice in about a year. But a careful assessment of the purely vertical transport, based on the results of laboratory experiments and associated theories, shows that this can account for only about 5% of the flux required to melt all the surface ice in this time. An alternative source of heat is the solar input to the surface mixed layer. In particular years when detailed measurements and calculations have been made, this input from the atmosphere could explain both the seasonal cyclic behaviour of the ice and the increased melting rate.

However, given the large heat content in the advancing tongue of Atlantic water it is worth exploring other advective mechanisms that could bring this heat to the surface. For example, a strong downflow of salty water, formed by freezing on the shelves round the Arctic basin, could penetrate through the halocline into the warm layer and mix this up to the surface. This mechanism is currently being investigated in the laboratory and theoretically by Mathew Wells, a former PhD student in the GFD group and presently at Yale University.

Effects of upstream disturbances on coastal wake flows

M.J. O'Byrne R.W. Griffiths and J.H. Middleton

Laboratory investigations are addressing the effect of upstream disturbances on the flow around islands and headlands in coastal waters, as part of an ARC-funded collaboration between the University of New South Wales, the University of Colorado at Boulder and the Australian National University.

Our first experiments on this problem were carried out in a one-metre diameter cylindrical tank, with a model headland drawn through initially stationary water. While simple and convenient, these experiments had the disadvantage of not having a bottom or sidewall boundary layer in the oncoming flow. In a new arrangement, the same tank is placed on a rotating table, so that the headland, base and sidewall can be impulsively set in motion relative to the water, thus providing physically more realistic boundary layers.

Results indicate that at a Reynolds number of 1000 or less, the unperturbed wake of a semi-cylindrical headland is almost stable. Adding a perturbation generated by flow past a small cylinder placed upstream of the headland leads to instability with a frequency given by the incident disturbance. When the wake is naturally unstable, conditions are found under which the wake frequency is changed owing to a frequency 'lock-on' effect to the frequency of the upstream disturbance (figure 13). We observe a periodic dipole vortex formation.



Figure 13: Still images of an experiment with a headland Reynolds number of 1000, indicating pairing of incident vortices with an induced vortex of opposite sign in the wake. The image on the right was extracted 4s after the left-hand image, during consecutive dipole formation events. Flow is from left to right. The coastline, a vertical wall, is at the bottom of the images.

Convection in complex geometries

Convection drives flows throughout the atmosphere and oceans, and in many engineering and industrial applications. Such flows are driven by buoyancy forces that arise from locally destabilising variations in temperature and/or chemical composition within a fluid. These convective flows are the primary mechanism by which heat, mass and chemicals are transferred between parts of the fluid domain. In many practical situations the confining geometry is complex and has a dramatic influence on the flow.

M. A. Coman, G. O. Hughes, R. C. Kerr and R. W. Griffiths

This year we have completed a study of the convection in a two-chamber cavity that is heated and cooled on opposite vertical endwalls (Figure 14). This flow is forced to pass through a relatively small gap connecting the chambers, a geometry that is relevant to the flow over a sill between ocean basins, or through doorways in buildings. The introduction of the barrier between the two chambers severely disrupts the flow. Recent measurements have shown that both the flow structure and the heat transfer through the gap are almost independent of the lateral position of the barrier. However, the mass exchanged between the chambers increases with the relative width RL of the hot chamber.

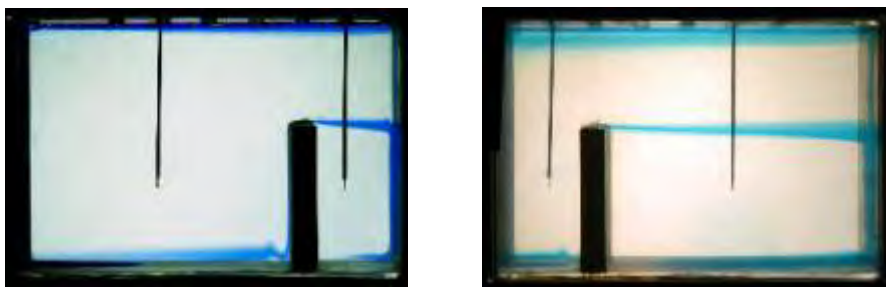


Figure 14. Dye visualization of the convective exchange flow between two connected chambers driven by heating and cooling of the left and right endwalls, respectively. The relative size of the hot and cold chambers has little effect on the flow structure and heat transfer between the chambers.

K.C. Yeh, G.O. Hughes and K. Lovegrove

We have studied convective flows inside an inclined cavity that was open at one end (Figure 15). This geometry models a 'cavity receiver', which is used to harness thermal energy at the focus of a concentrating solar paraboloidal dish. The dish system can be inclined to track the sun and the cavity temperature is typically increased by several hundred degrees Celsius. An understanding of the ensuing convective flow inside the cavity receiver is important for providing design pointers to minimise convective heat losses and hence improving the efficiency of solar collection. However, visualisation of airflows in a high-temperature cavity receiver is impractical. Instead, we have simulated such flows using convection driven by salinity differences in

water. By matching the Grashof number of convective flows in the laboratory to those typical of solar cavity receivers, we have found that the circulation inside the cavity is generally laminar (figure 15). However, at marginally higher Grashof numbers the cavity circulation was observed to become turbulent, corresponding to a significant increase in convective losses. Convective losses are reduced when the cavity axis is closer to vertical and the geometry can trap a larger volume of the buoyant fluid.

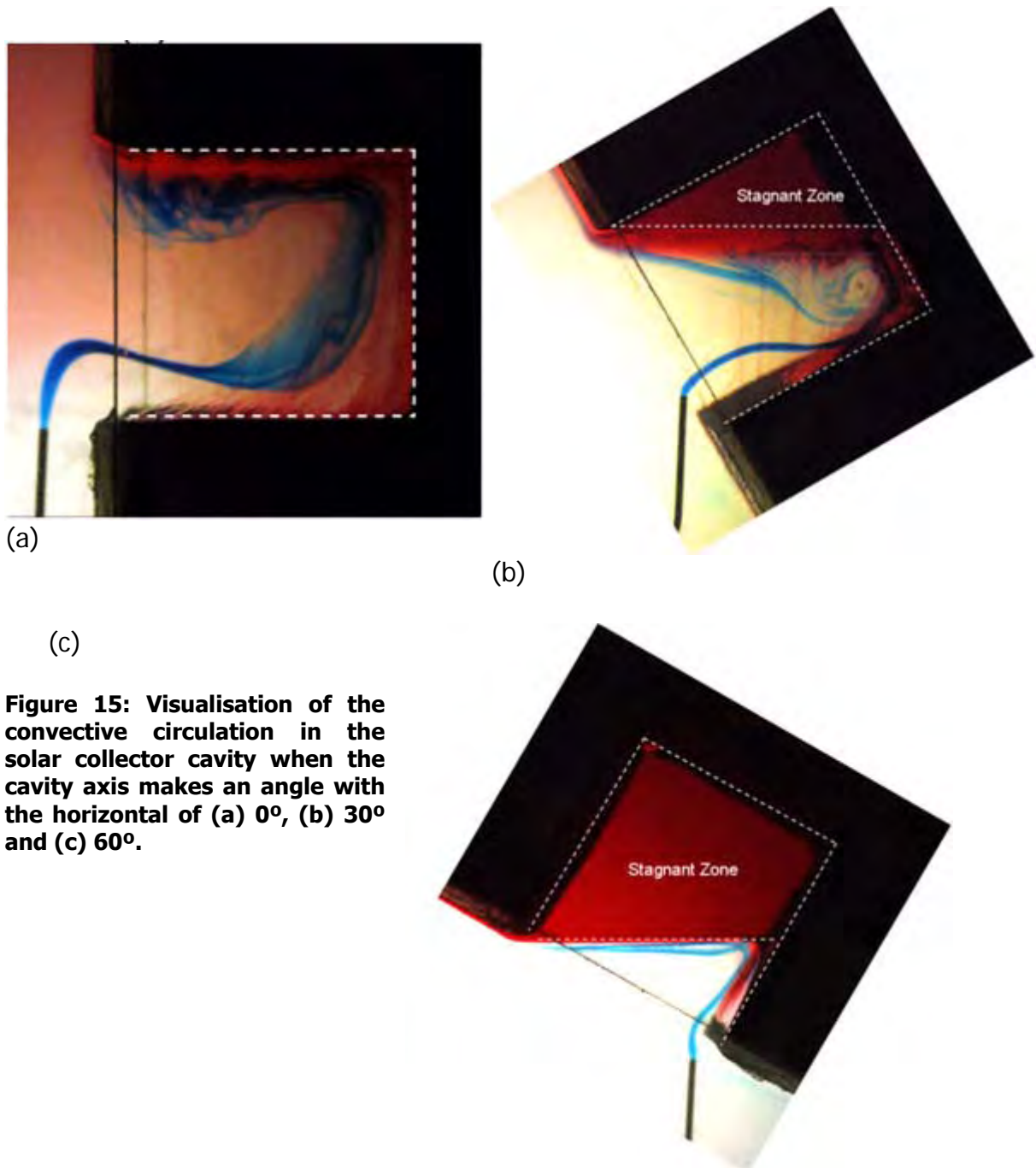


Figure 15: Visualisation of the convective circulation in the solar collector cavity when the cavity axis makes an angle with the horizontal of (a) 0°, (b) 30° and (c) 60°.

The formation of channelized lava flows and their final runout length

In continuing studies of lava flow dynamics and the behaviour of flows with cooling and solidification, we have examined channel formation on slopes as well as the factors controlling the final length of flows produced by the rapid release of a volume of melt in an existing channel or valley.

R.C. Kerr, R.W. Griffiths and K.V. Cashman



Figure 16: Photograph of a Hawaiian lava channel, whose surface is a combination of incandescent melt (red) and broken solid surface crust (dark material).

In a collaborative project with volcanologist Professor K.V. Cashman of the University of Oregon, and funded by both the ARC and the National Science Foundation, we have explored the formation of basaltic lava channels (Figure 16), with the aim of understanding the factors controlling the channel width and the resulting flow behaviour. To model the lava flows, we use laboratory experiments in which molten polyethylene glycol (PEG) wax flows under cold water along the base of a wide sloping tank (Figure 17). When the wax is released at a constant flow rate from a point source, it flows both down and across the slope at the same rate in an early-time regime, before undergoing a transition to a long-time regime where downslope flow is faster than lateral flow. Eventually, the lateral flow is stopped by the strength of the growing surface crust, and the flow then travels downslope in a channel of constant width.

Using scaling analysis, we have derived expressions for the final channel width in both the early-time and long-time flow regimes, as a function of the flow rate, the slope, the density difference driving the flow, the lava viscosity, the thermal diffusivity, and the yield strength of the crust. We also found a dimensionless flow morphology parameter that controls whether the subsequent channel flow occurs in a 'mobile crust' regime (involving lots of

exposed melt and consequent heat loss) or in a 'tube' regime (involving a complete solid roof and relatively small heat loss from the melt).

The theory has been successfully applied to understand the formation of a basaltic sheet flow lobe in Hawaii, for which we estimated a crust yield strength of order 6×10^4 Pa. Our results provide important insight into conditions that promote lava tube formation, which is in turn responsible for greatly increasing the length of individual flows. Flows may change from mobile crust to tube regime (or vice versa) at a constant flux, simply from local changes in the slope.

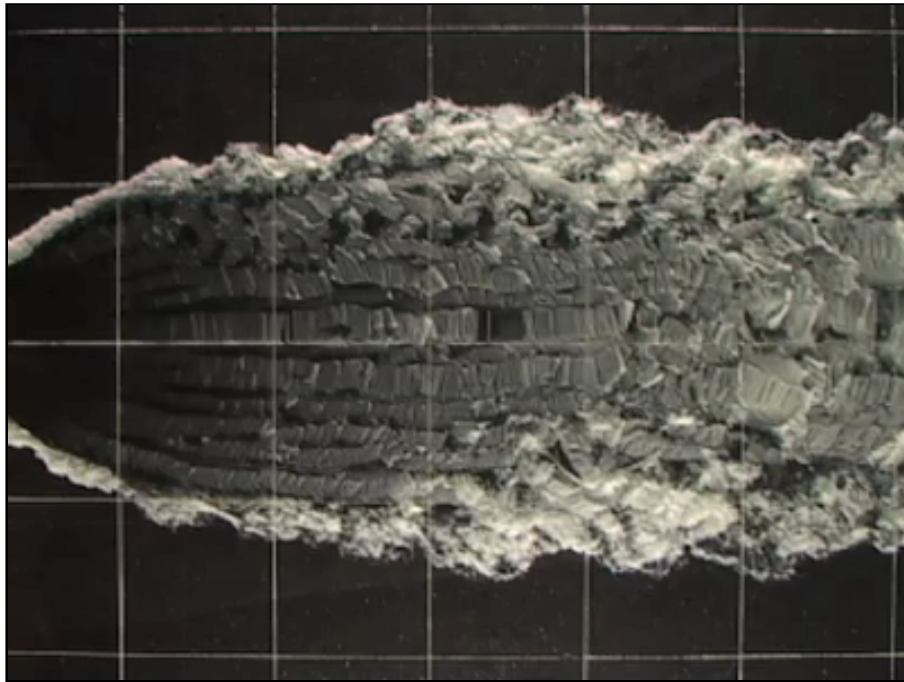


Figure 17: Time-lapse video movie of molten PEG wax flowing down a wide uniform slope and cooled from above. The flow is viewed from above, and the tank is 90 cm wide. Solid wax is white, liquid PEG is transparent and the base of the tank is black.

A.W. Lyman and R.C. Kerr

Over the past three years, we have modeled the emplacement dynamics of lava flows using a combination of theoretical scaling analyses and laboratory experiments (Figure 18), for the case when a fixed volume of lava is rapidly released and propagates as a two-dimensional flow. When the lava has no internal yield strength, we have identified four dynamical flow regimes that can arise: an inertial slumping regime, a horizontal viscous regime, a sloping viscous regime, and a crust yield strength regime that finally stops the flow. When the lava has an internal yield strength, it can also flow in a sloping viscoplastic regime, which is accurately predicted by a simple box model that we have developed.

Our results have been applied to predict the propagation downhill of various volumes of two typical lavas: a Hawaiian lava with no internal yield strength and a Mt. Etna lava with an internal yield strength. In particular, we show that sloping flows of the Mt. Etna lava are stopped by the surface crust strength rather than the internal yield strength. Our work will be helpful both in predicting the advance of flows from future volcanic eruptions, and in placing bounds on the durations of eruptions of large prehistoric flows.

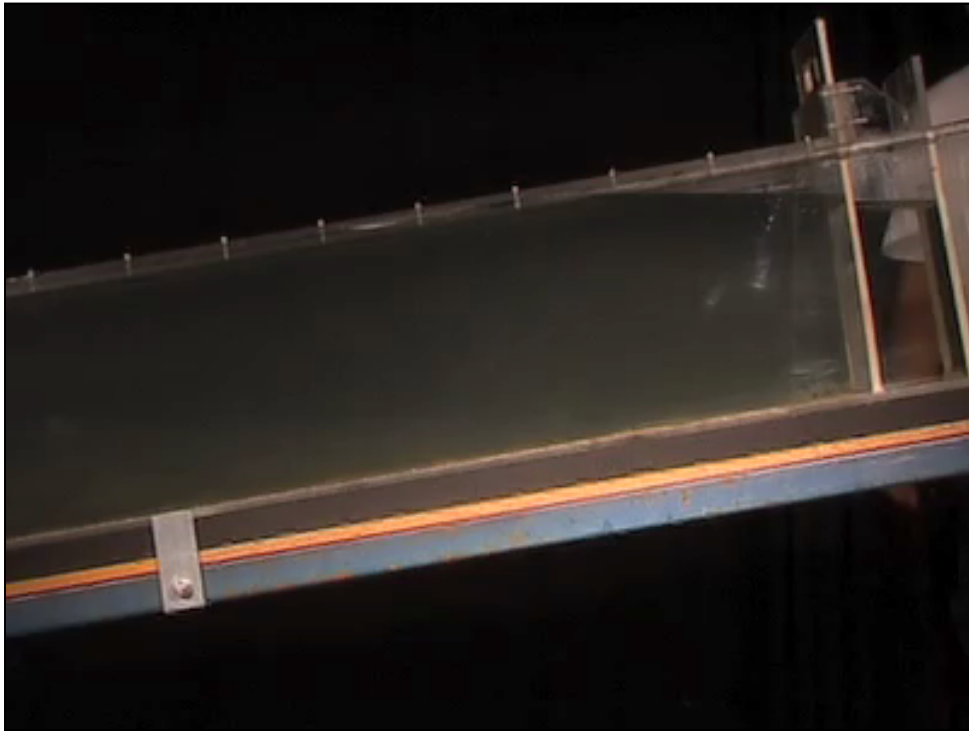


Figure 18: Time-lapse video movie of the release of a fixed volume of molten PEG wax down a sloping channel underneath cold water.

Dynamics and Chemical Evolution of the Earth's Early Mantle

G. Davies and J. Huang

Isotopes and trace elements have been used by geochemists to document a range of source types in the mantle whose apparent ages approach two billion years. Numerical modelling of mantle dynamics is used in this project to explore and exploit this information. It extends previous modelling in two ways: into the past, hotter mantle and into three dimensions at present Earth conditions. Some significant results have been obtained and more are imminent.

The 2D modelling has extended the previous models to the more extreme conditions of the early mantle, which was hotter, had lower viscosity, and convected faster. The upper mantle becomes quite depleted of a denser, basaltic component when the mantle is hotter than about 1500°C. This provides a plausible explanation for a very strong and early depletion of the mantle sources of the earliest preserved materials (ancient rocks and zircon crystals) documented by geochemists.

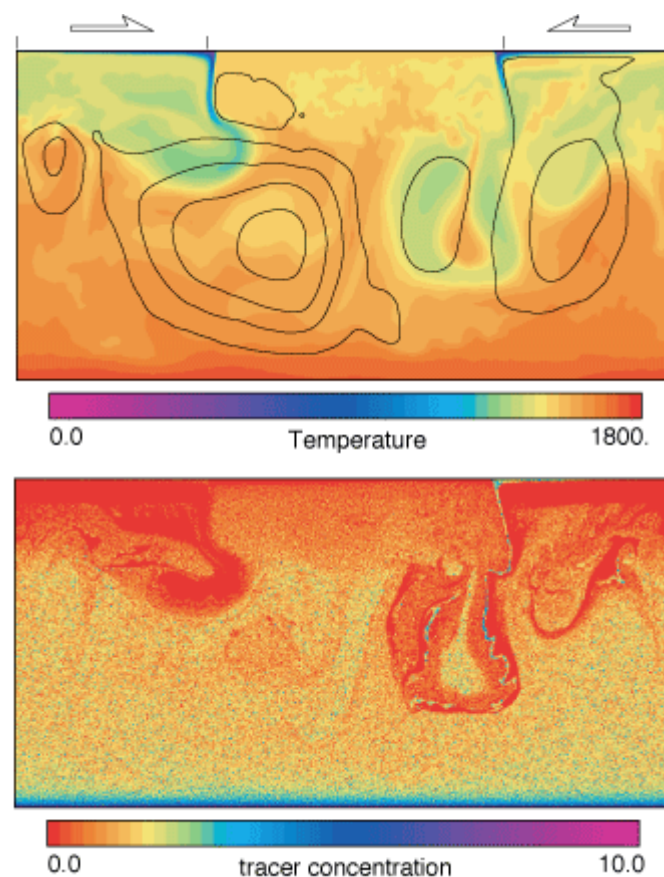
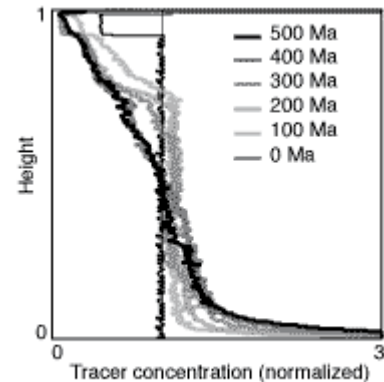


Figure 19. Temperature and stream lines (upper) and tracer concentration (lower) after 500 Ma of subduction and convective stirring in the mantle. The model features two "oceanic" plates converging towards and subducting under a central "continental" region.

The tracers represent the basaltic component of the mantle composition, and simulate both its melting near the surface and its excess density in the mantle. Melting concentrates the tracers into an oceanic “crust”, and because of their greater density after subduction they settle out of the lower-viscosity upper mantle (the upper 30% of the model). Some tracers also accumulate at the base of the model, although many remain suspended in the lower mantle, which is 30 times more viscous than the upper mantle.

Figure 20. Progressive depletion of basaltic components in the early upper mantle. The plot shows vertical profiles of horizontally averaged tracer concentration at various times in the model shown in Fig. 1, revealing a rapid depletion of the upper mantle, a slight enrichment of the lower mantle and a strongly enriched thin layer at the base.



This early depletion has other potentially important implications. Oceanic crust formed in these conditions would be quite thin, and this would enhance the viability of plate tectonics, which in turn would provide a mechanism for cooling the mantle. Such a mechanism has been lacking, as the previously expected thick oceanic crust would tend to inhibit plate tectonics and mantle cooling.

A further possible implication is that the mantle ‘hangs’ in this hot state until radioactive heating declines enough to allow it to drop into the present, cooler state. Such a transition might correspond to a well-documented major geological transition around 2.5 Ga ago.

The 3D modelling has been carried out by Research Associate Jinshui Huang, who arrived early in 2005. This work uses the 3D-spherical code “Terra” obtained from Professor P. Bunge (Munich) and Dr. J. Baumgardner (Los Alamos). The code has required considerable adaptation and testing. Although it turned out to be not as robust as hoped, this is less important than expected and clear results have already been obtained.

We have found that the main control on the residence time of previously melted components is the rate of processing through the melting zones. The geometry, viscosity structure and excess density of subducted oceanic crust have only secondary effects. The residence times are predicted quite well with a very simple theory based on the rate of reprocessing of material relative to the total volume of the mantle. Since the rate of reprocessing depends only on plate velocities and melting depths, which are relatively predictable, these results promise a substantially improved understanding of the chemical evolution of the mantle.

The Viability of Mantle Plume Theory

G. Davies

Mantle plumes were proposed in the 1970s as an explanation for age-progressive volcanic 'hotspot tracks' and for large flood basalt eruptions. Recently the plume theory has come under criticism. Some maintain that plumes have been disproven or that there is little evidence for plumes and the plume theory is unquantified and infinitely malleable, and so is not a scientific theory. A quite heated controversy has been underway. Others merely point out that there is much volcanism that does not obviously accord with plume theory, without implying there are no plumes at all. A substantial review of the subject was therefore undertaken to clarify the status of the theory.

The review points out that plumes can be inferred from well-known observations with few assumptions and no theory, that a well-quantified physical theory of plumes exists, that plumes are to be expected in the silicate mantles of planets and that a number of important questions about plumes have been quantitatively resolved. The review notes there are indeed observations that do not obviously accord with plume theory and that other mechanisms may need to be considered. Some recent numerical modelling is noted in which compositional density considerably complicates plume dynamics, and this may explain some hitherto puzzling volcanism. The review concludes that plumes are a quite viable theory, but plumes probably do not explain all volcanism that is not related to plate tectonics.

Thermal Evolution of the Core and Mantle

G. Davies

The thermal budget of the core is a key quantity relating the generation of the magnetic field, the growth of the solid inner core and the generation of plumes in the mantle. Recently modellers of the core dynamo responsible for generating the magnetic field have appealed to the possibility of radioactivity in the core to accommodate all of these phenomena, but new results indicate this may not be necessary.

Estimates of the conductivity of the core have been revised upwards. This implies the core is cooling faster and hence that the solid inner core is younger than previously thought, only about 1 Ga. However, solidification of the inner core makes the dynamo mechanism more efficient, so before the inner core began to crystallise a higher heat flow would have been required to maintain the dynamo, which is documented via magnetised rocks as far back as 3.5 Ga. Some recent calculations have yielded early core and mantle temperatures that seem unreasonably high, and core radioactivity has been proposed to resolve the problem, as this would allow a higher heat flow without requiring the core temperature to have declined as much. However there are strong geochemical arguments against core radioactivity.

It turns out that an inappropriate formula has been used by others for the heat carried into the mantle from the core-mantle boundary. Using a more appropriate formula that yields lower core heat flow in the past, I find that a non-radioactive core is less problematic than previously concluded. More detailed consideration of the complicated interactions and the considerable uncertainties is underway.

Rollback subduction – insights from laboratory experiments

W. Schellart

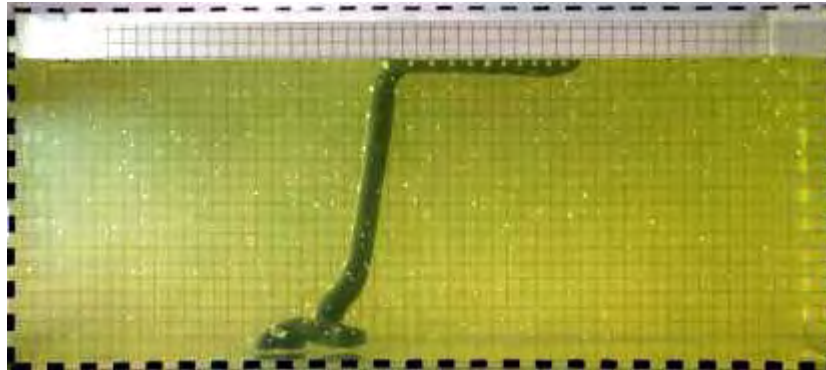


Figure 21. The photograph shows a laboratory experiment with subduction of a relatively high-viscosity slab. The slab was initially horizontal on the surface of the tank of corn syrup. One end begins to sink once it is slightly disturbed, and the rest of the slab follows, with a degree of migration of the point of sinking (the trench).

Three-dimensional laboratory simulations of subduction, involving a dense high-viscosity plate that sinks into a mantle of lower density and viscosity, have been used to develop insights into the nature of lithosphere subduction and trench motion. In the simulations, the mantle reservoir represents the entire mantle (from the surface to 2900 km depth) and is homogeneous throughout. The experiments are specifically designed to investigate the influence of the plate-to-mantle viscosity ratio on the style of subduction and on the pattern of subduction-induced mantle flow. In particular, the relative importance of trench-ward plate velocity versus trench velocity, as well as the flux associated with poloidal and toroidal flow were investigated. The viscosity ratio was varied by altering the temperature (from 4 degrees C up to 28 degrees C), noting that the viscosity of the experimental plate material is much less temperature dependent than that of the experimental mantle material. This resulted in a variation of the viscosity ratio from ~60 to ~1400. Such a range of viscosity ratios covers the predicted range of effective viscosity ratios in nature. We conclude from the observations that, in facilitating roll-back of the slab (trench migration), quasi-horizontal mantle flow around the edges of the descending slab is much more significant than flow around the leading edge of the plate.

GEODYNAMICS 2005

The glacial rebound work in 2005 has focussed on Arctic Eurasia from the time of the penultimate glacial maximum (MIS 6 or the Late Saalian at ~145,000 years ago) up to the present with the goal of establishing constraints on the ice thickness and ice margins for some of the major phases of the last glacial cycle. A major compilation of field evidence for the ice margin locations and shoreline elevations and sea levels across the region has been completed and the inversion of which has led to new ice models from 140,000 years to 60,000 years ago, including the time of the renewed initiation of the ice sheets after the last interglacial.

Developments in both modelling and dating techniques have contributed to the study of sea-level fluctuations in the Mediterranean during the last interglacial. The Mediterranean lies on the forebulge of the Late Saalian ice sheets and the present elevations of MIS 5e shorelines reflect the effects of the Stage 6 and subsequent ice sheets. The study of speleothems from submerged caves and dating of molluscan shells hold the promise of refining the sea level curve, providing constraints on the extent of these ice sheets. A laser ablation system coupled to a MC-ICP-MS has been used to explore the potential for more precise and accurate U-series dating of these shells.

Another application of the glacial rebound work has been to assess stress evolution in the crust through a glacial cycle. Specific questions about the stability of the crust during and after major glaciations have been addressed for sites in Sweden. This has shown that fault stability is strongly dependent on location relative to the ice sheets and that the glacial-load stress is an important factor to be considered in decisions on waste repository locations.

During 2005, research continued into understanding error sources within geodetic analysis and modelling the deformation of the Earth caused by geophysical processes such as solid Earth tides, atmospheric pressure loading, ocean tide loading as well as atmospheric propagation effects. A successful GPS observing program was undertaken again in Papua New Guinea, adding important observations on many sites to those made over the past decade. John Dawson (Geoscience Australia) commenced a PhD investigating the use of Interferometric Synthetic Aperture Radar (InSAR) to measure crustal deformation in the Australian region.

Early in the year, the Superconducting Gravimeter operated by RSES at Mt Stromlo recorded a long episode of free oscillations of the Earth after the M_w 9.3 Sumatra-Andaman earthquake. The Earth continued to oscillate measurably for over three months after the earthquake and tsunami that devastated large areas of Asia on Boxing Day 2004, and the Mt Stromlo gravity station monitored the faint changes in gravity that accompanied the oscillations. The observations at this and other stations around the world has produced the highest resolution spectrum of Earth's free oscillations so far

recorded, providing improved constraints on the internal structure of the Earth.

TECTONIC STUDIES IN PAPUA NEW GUINEA GPS MONITORING OF PLATE MOTION AND CRUSTAL DEFORMATION

Paul Tregoning¹, Richard Decrevel¹, Suvenia Hasiata², Sylvester Tiki², Steve Saunders³, Herb McQueen¹, Kurt Lambeck¹

1. Research School of Earth Sciences, The Australian National University, Canberra, Australia

2. Department of Surveying and Land Studies, Papua New Guinea University of Technology, Lae, Papua New Guinea

3. Rabaul Volcano Observatory, Rabaul, Papua New Guinea

The GPS program to measure crustal deformation in Papua New Guinea continued during 2005. The transect of sites along the western border was reobserved, spanning from Kiunga in the south to the northern coast at Vanimo. Sites at Telefomin, Tabubil, Green River and Bewani were all reobserved. The network of sites spanning the triple junction and the Schouten Islands was reobserved (thanks to Richard Decrevel and staff and students from Unitech for their involvement in organising and conducting the field program!). A second occupation was made at Tufi (first observed in 2004) and a reoccupation at Misima (not observed since 1996). Also, staff from the National Mapping Bureau (NMB) reobserved at Kora and commenced observations at a new site at Kokoda. In addition, observations were continued by staff at the Rabaul Volcano Observatory of sites on the Gazelle Peninsula in eastern New Britain. Figure 1 shows the sites observed during 2005.

Fieldwork Conducted in 2005

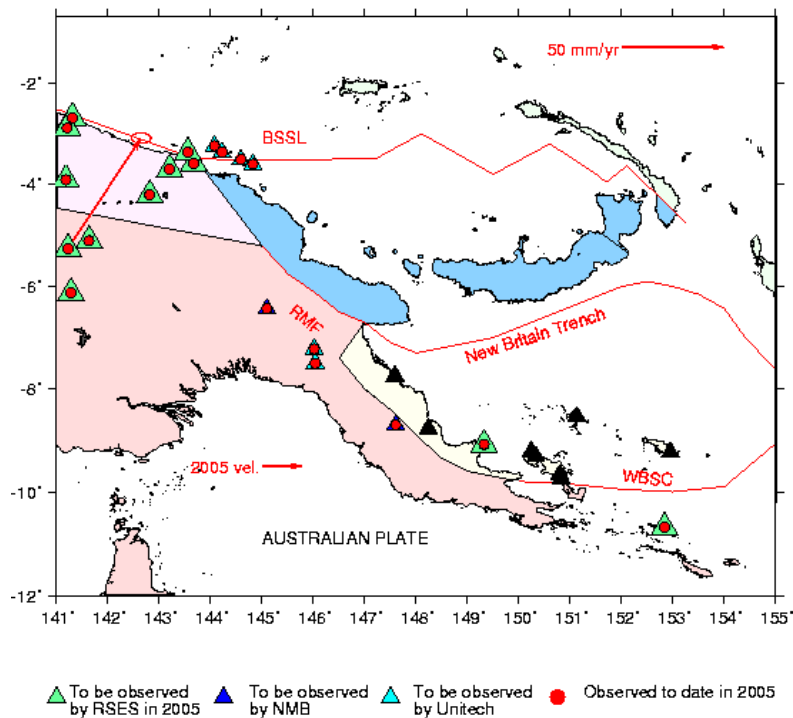


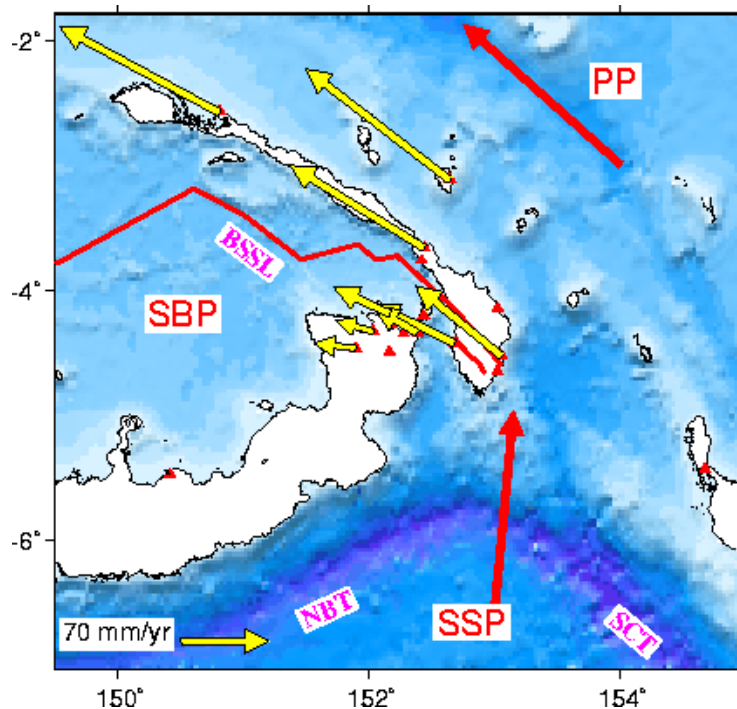
Figure 1: Sites observed in PNG during the 2005 field program (red dots) and sites observed during 2004 (black triangles).

Results

Schouten Islands/Wewak

The analysis of the GPS data observed in the Wewak area and at sites in the Schouten Islands was undertaken as an Honours Project in 2005 by Ryan Ruddick. The aim of the study was to:

- Estimate site coordinates from all available data
- Estimate inter-seismic site velocities
- Estimate co-seismic displacements caused by the 8 September 2002 Wewak Earthquake
- Resolve the inconsistency between uplift/tsunami runup studies and GPS co-seismic displacements



The conclusions of the study were that inter-seismic strain accumulation was affecting the motion of the sites at Bam and Mut Mut Islands, as well as at Wewak, Ambunti and Maprik. Also, the sites located on the mainland are most likely not moving as part of the rigid Australian Plate nor Highlands Plate (proposed by *Wallace et al.*, 2004). The observed horizontal co-seismic displacements are not consistent with the "classic thrust" interpretation of the earthquake as proposed by *Borrero et al.* (2003). Ryan also discovered that post-seismic relaxation is occurring at Kairuru Island (GPS site XAVI) and also at Wewak (WEWK).

A copy of his honours thesis can be found at

http://rses.anu.edu.au/geodynamics/gps/papers/ryan_honours05.pdf.

New Ireland/New Britain

The GPS monitoring of post-seismic relaxation of the Gazelle Peninsula continued during 2005, with Steve Saunders and his team observing several sites. Non-linear motion of the sites is ongoing.

The aftershocks following the November 2000 Mw=8.0 strike-slip and two Mw=7.8 thrust events have been relocated using the Arrival Pattern method (*Tregoning et al., 2005*). Analysis is continuing to separate the co- and post-seismic components of deformation so that the former can be inverted to solve for the distribution of slip on the Weitin Fault as a result of the left-lateral earthquake. Preliminary results are encouraging.

The inter-seismic velocities (with respect to the South Bismarck Plate) are shown in the figure to the right.

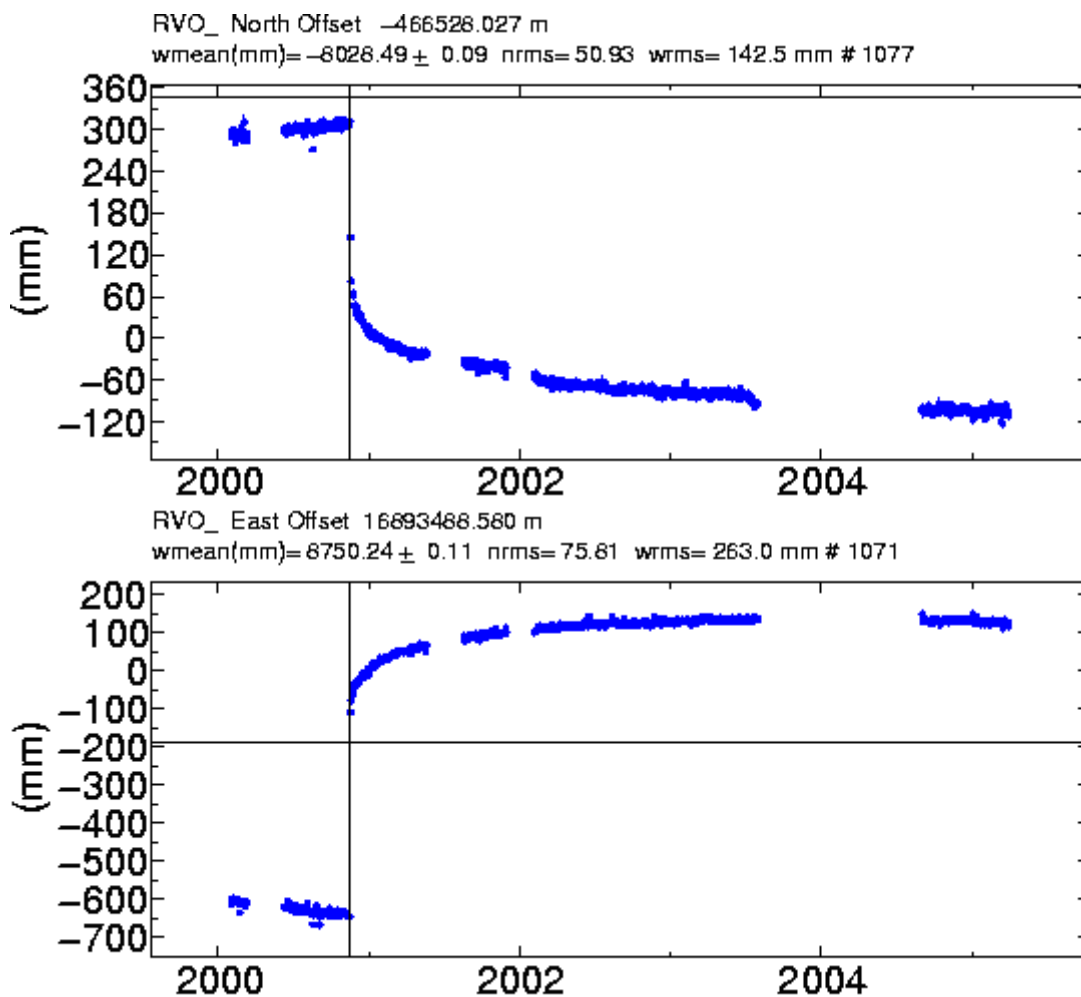


Figure 2: Position of permanently operating GPS receiver at Rabaul Volcano Observatory relative to the rigid South Bismarck Plate.

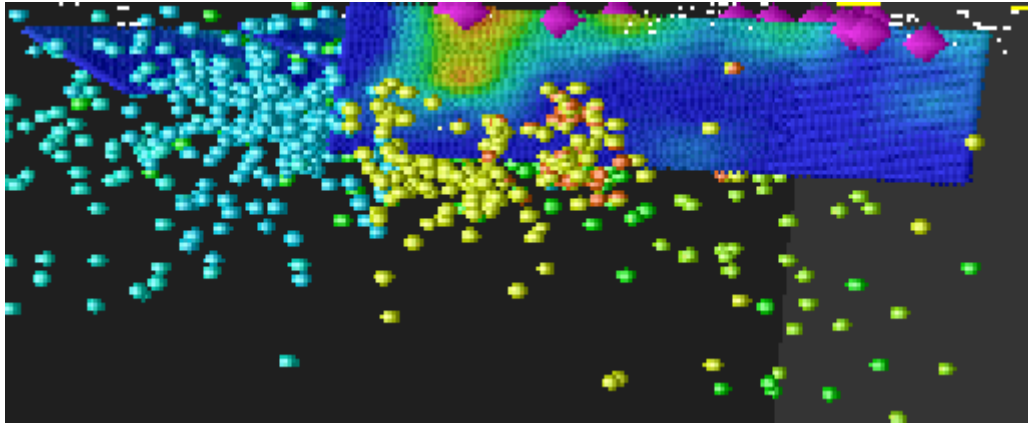


Figure 3: Distribution of slip on the Weitin Fault, viewed looking to the southwest. Location of aftershocks from *Tregoning et al (2005)* are also plotted.

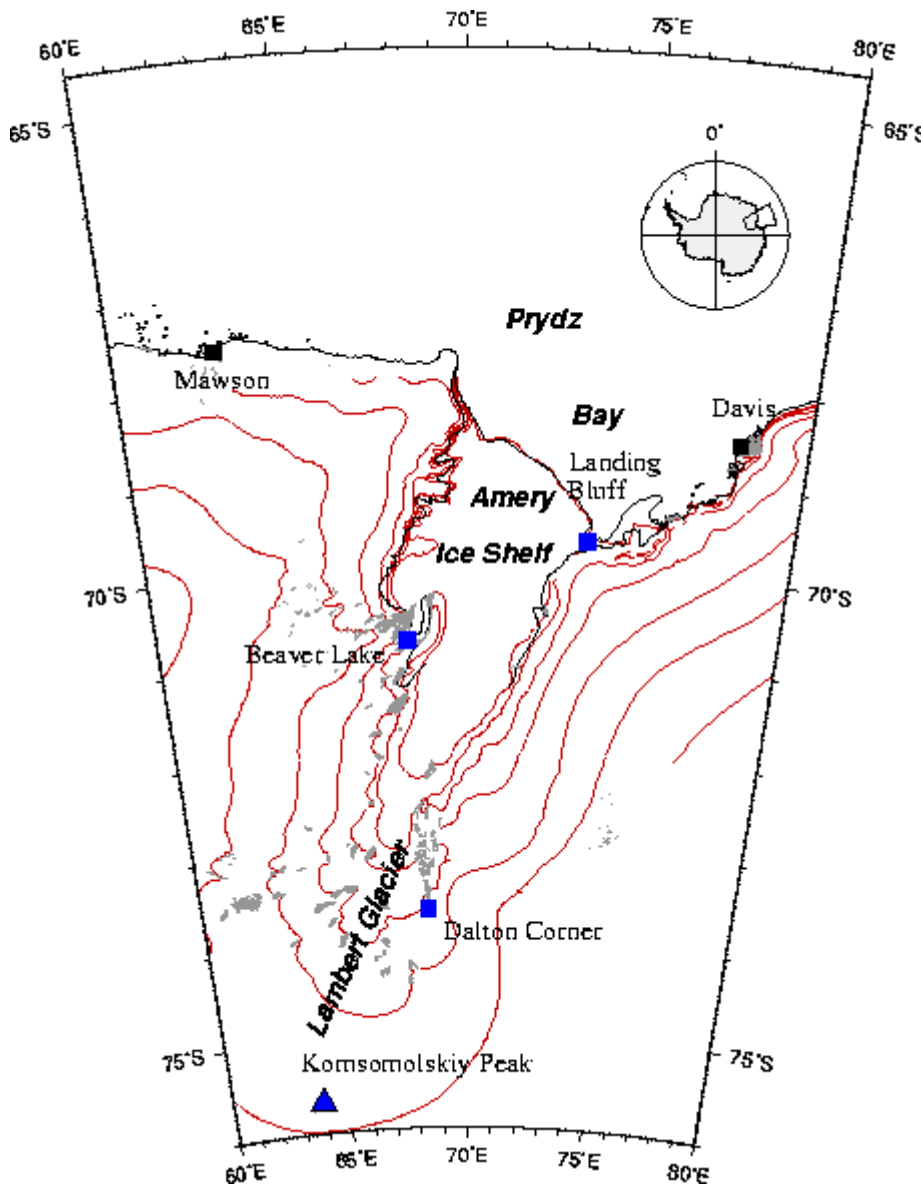
Publications in 2005 relating to this work

Tectonic interpretation of aftershock relocations in eastern Papua New Guinea using teleseismic data and the Arrival Pattern method. Tregoning, P., M. Sambridge, H. McQueen, S. Toulmin and T. Nicholson. *Geophys. J. Int.*, **160(3)**, 1103-1111, 2005.

GLACIAL ISOSTATIC ADJUSTMENT IN ANTARCTICA GPS MONITORING OF UPLIFT

Paul Tregoning¹, Richard Decrevel¹, Herb McQueen¹, Kurt Lambeck¹

Research School of Earth Sciences, The Australian National University, Canberra, Australia



Using GPS to monitor present-day uplift rates in the Lambert Glacier Drainage Basin continued during 2005. Owing to lack of logistical support from the Australian Antarctic Division, two of the four sites (Dalton Corner and Komsomolskiy Peak) were not visited in the 2004/05 summer season. The satellite phone at Beaver Lake was removed and only the site at Landing Bluff transmitted data during the summer/autumn period. By now the computer disks at Dalton Corner and Komsomolskiy Peak will be full; unfortunately, no access to these sites will be provided during the 2005/06 season either.

The focus of the research in 2005 was in the improvement of the analysis of the GPS data

recorded to date. Significant enhancements have been made to the GAMIT software, which have brought about dramatic increases in the accuracy of height estimates:

- IERS 2003 solid Earth Tide model
- Atmospheric pressure loading corrections
- Absolute satellite and ground antenna phase centre variations and offsets
- Weather-based mapping functions
- Improved ocean tide loading models

Figure 1 shows the improvement seen in the height estimates at Mawson between analysis computed in 2004 and that of 2005.

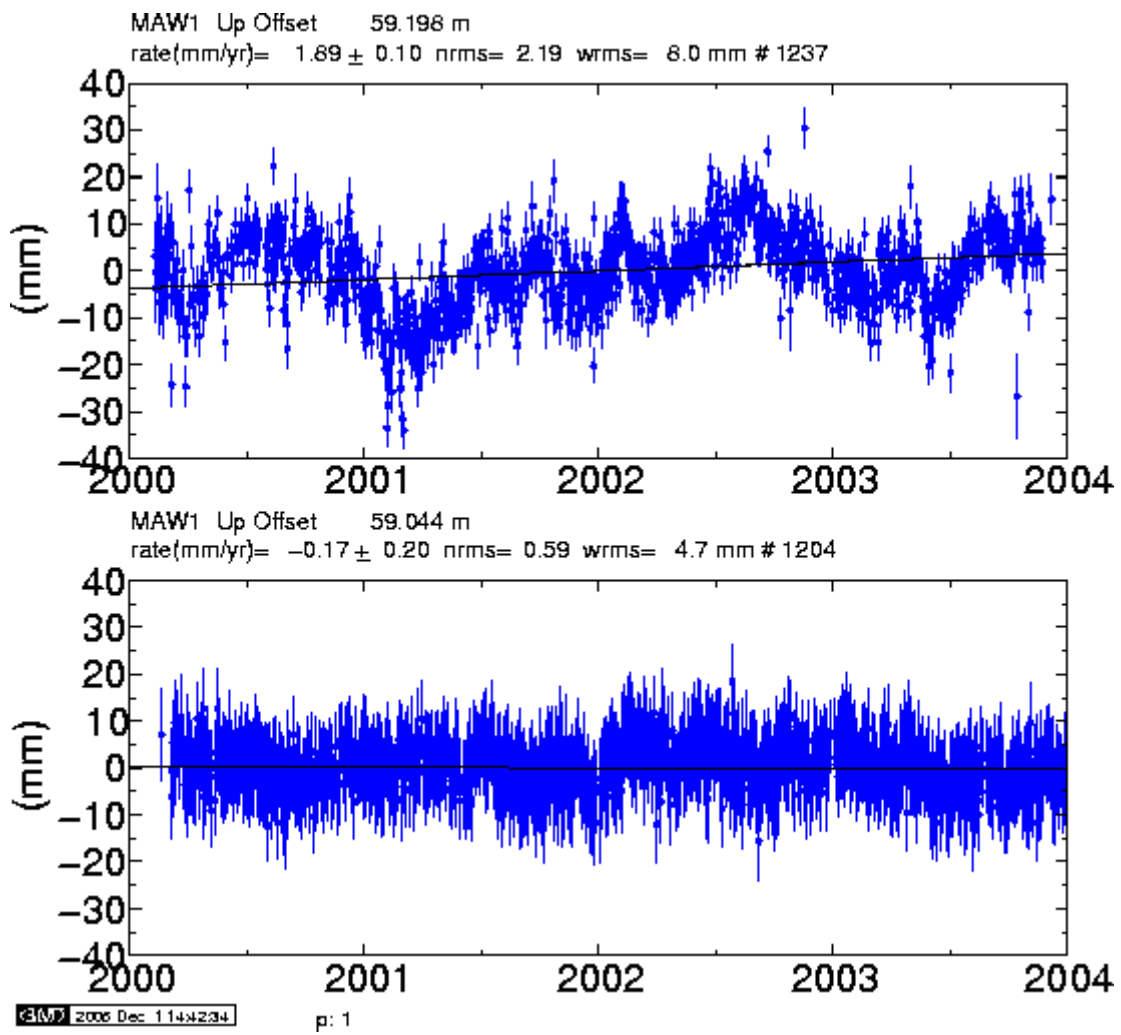


Figure 1: Improvement in height estimates at Mawson brought about by improvements in analysis techniques.

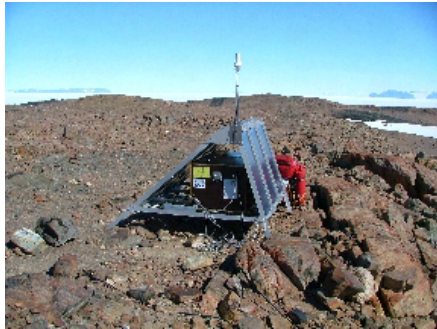
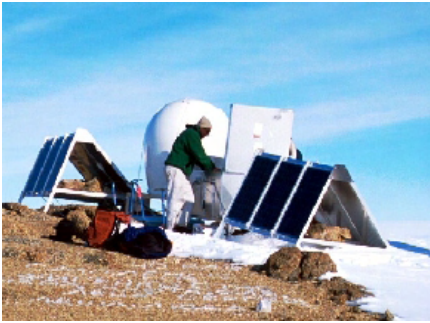


Figure 2: The GPS sites. Top (left to right) - Landing Bluff, Dalton Corner, Komsomolskiy Peak, and (left) Beaver Lake

GEODETTIC ANALYSES AT RSES

IMPROVEMENTS OF GPS DATA PROCESSING

Paul Tregoning¹ Chris Watson², Tonie van Dam³, Bob King⁴

1. Research School of Earth Sciences, The Australian National University, Canberra, Australia

2. Centre for Spatial Information Systems, The University of Tasmania, Hobart.

3. European Centre for Geodynamics and Seismology, Luxembourg.

4. Department of Earth, Atmospheric and Planetary Sciences, Massachusetts Institute of Technology, Cambridge, MA, U.S.A.

During 2005 considerable improvements were made to the modelling of the theoretical range from site to satellite in an attempt to improve the accuracy of the analysis. Significant enhancements have been made to the GAMIT software, which have brought about dramatic increases in the accuracy of coordinate - in particular height - estimates:

- IERS 2003 solid Earth Tide model
- Atmospheric pressure loading corrections
- Absolute satellite and ground antenna phase centre variations and offsets
- Weather-based mapping functions
- Improved ocean tide loading models

Solid Earth tide model

In conjunction with Dr Christopher Watson, The University of Tasmania, the IERS 2003 solid Earth tide model was implemented and tested within the GAMIT software. Five years of data at over 140 globally distributed sites were computed using the old IERS92 model, then again with the IERS 2003 model. Computations were done on the Terrawulf facility at RSES.

The results showed that the improved solid Earth tide model reduced the amplitude of the annual periodic signal in height estimates, with a maximum reduction occurring at mid-latitudes. Also, the errors in the earlier solid Earth tide model were shown to be aliasing into zenith tropospheric delay estimates at sub-daily frequencies.

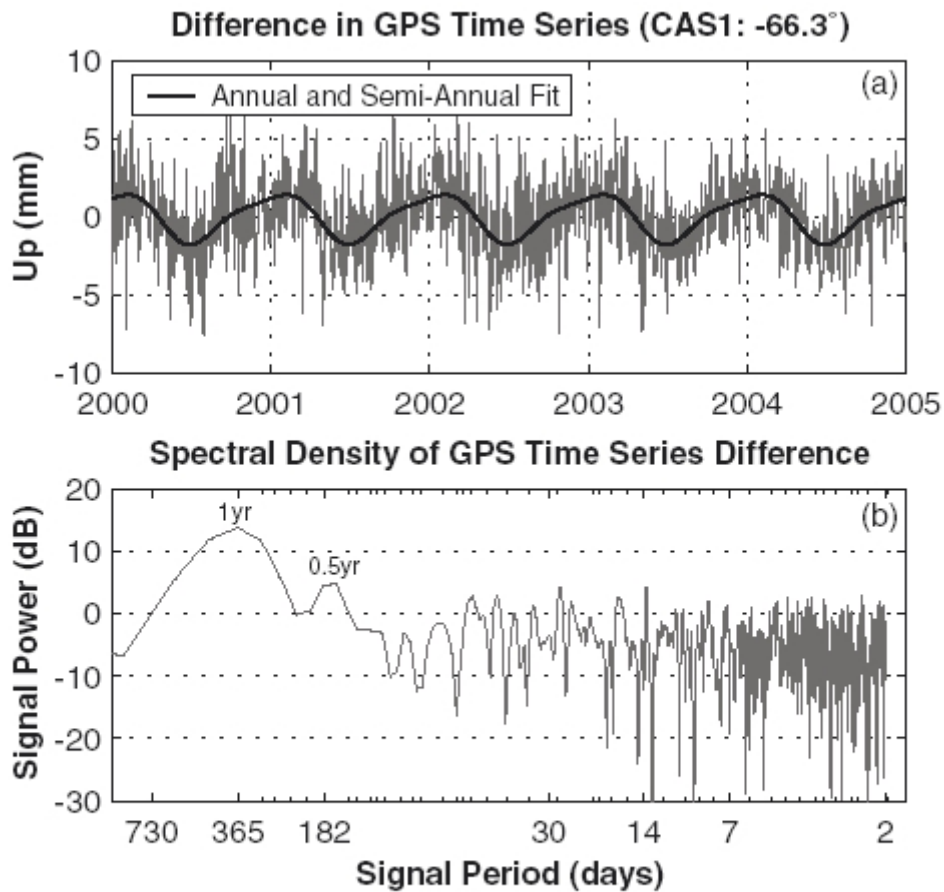


Figure 2 a) Difference in the vertical component of the GPS time series (IERS 2003 – IERS 1992 solution) at CAS1. b) Power spectral density of the difference time series.

From *Watson et al (2005)*.

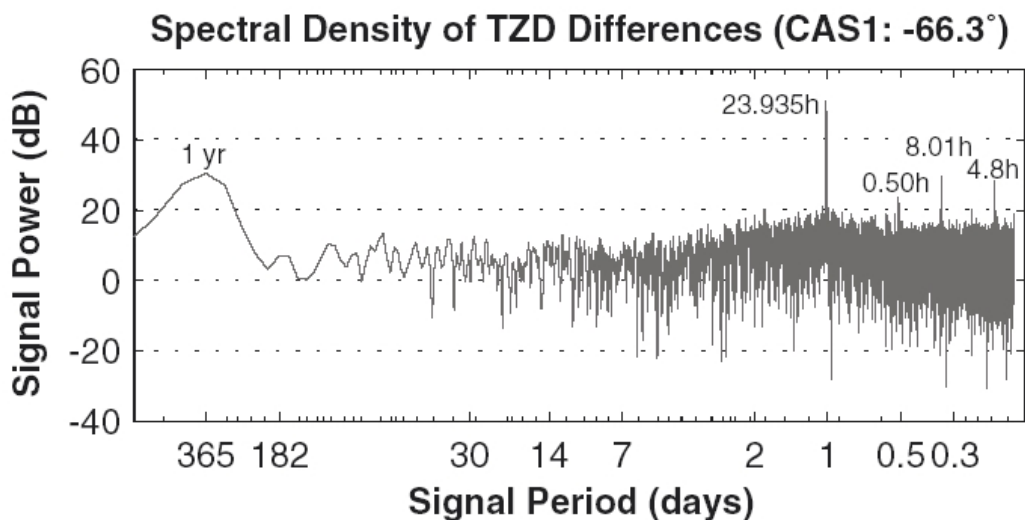


Figure 6. Power spectral density of the TZD differences at the CAS1 site.

Atmospheric Pressure Loading Corrections

Assessments were made as to whether site coordinates should be adjusted for atmospheric pressure loading at the observation level or whether it would suffice to apply daily-averaged values once the GPS phase observations were analysed. One year of global GPS data were processed - again using the Terrawulf facility at RSES - using various strategies for modelling of the atmospheric diurnal and semi-diurnal tides as well as the "non-tidal" component of the loading that is related to weather systems.

The results of this study can be found in

Atmospheric pressure loading corrections applied to GPS data at the observation level, Tregoning, P. and T. van Dam, *Geophys. Res. Lett.*, **32**, L22310, doi:10.1029/2005GL024104, 2005.

See also web pages related to ATM loading at

- The effects of atmospheric pressure loading (<http://rses.anu.edu.au/geodynamics/gps/atm/index.html>)
- Applying atmospheric pressure loading at the observation level in GPS analysis (http://rses.anu.edu.au/geodynamics/gps/atm_gamit/index.html)

Mapping Functions

The new weather-based mapping functions VMF, VMF1 and GMF, were implemented in the GAMIT software and tested extensively. Global GPS data from July 2004 to August 2005 were processed using the Terrawulf Facility to compare the height time series using different mapping functions.

Comparisons of the VMF1 and the routinely-used Niell Mapping Function (NMF) showed that the VMF1 produces height estimates with smaller annual periodic amplitudes and with a smaller precision than solutions of the same data using the NMF.

See <http://rses.anu.edu.au/geodynamics/gps/VMF/index.html> for more details.

Publications relating to this work

The effects of atmospheric pressure loading and 7-parameter transformations on estimates of geocenter motion and station heights from space-geodetic observations, Tregoning, P. and T. van Dam, *J. Geophys. Res.*, **110**, B03408, doi:10.1029/2004JB003334, 2005.

Atmospheric pressure loading corrections applied to GPS data at the observation level Tregoning, P. and T. van Dam *Geophys. Res. Lett.*, **32**, L22310, doi:10.1029/2005GL024104, 2005.

<http://rses.anu.edu.au/geodynamics/gps/papers/2005GL024104.pdf>

The impact of tropospheric mapping functions based on numerical weather models on the determination of geodetic parameters, Boehm, J., P.J. Mendes Cerveira, H. Schuh, P. Tregoning *IAG Proceedings, Cairns, Aug. 2005, in press*

The GMF: A new empirical mapping function based on numerical weather model data, Boehm, J., A. Niell, P. Tregoning, H. Schuh *Geophys. Res. Lett., in press.*

The impact of solid Earth tide models on GPS time series analysis, C. Watson, P. Tregoning, R. Coleman *Geophys. Res. Lett. In press*

Interferometric Synthetic Aperture Radar (InSAR)

John Dawson, Paul Tregoning

Research School of Earth Sciences, The Australian National University, Canberra, Australia

The focus of the research in 2005 was to investigate the applicability of Synthetic Aperture Radar (SAR) as a tool for the study of deformation caused by earthquakes within Australia. Satellite SAR observations of the Australian continent have been made since 1991 from various multi-year, temporally overlapping satellite missions, including ERS-1, ERS-2, JERS-1, RADARSAT and ENVISAT. SAR data can provide a highly accurate, spatially comprehensive datasets over large areas of surface deformations that result from large earthquakes.

Using data from ERS1/2 and ENVISAT we have characterised the typical spatial noise structure of InSAR observations made in Australia. Using this noise characterisation and catalogued Australian Earthquakes we have undertaken a simulation study, including geophysical inversion, to learn how InSAR may contribute to the investigation of earthquake deformation processes in Australia.

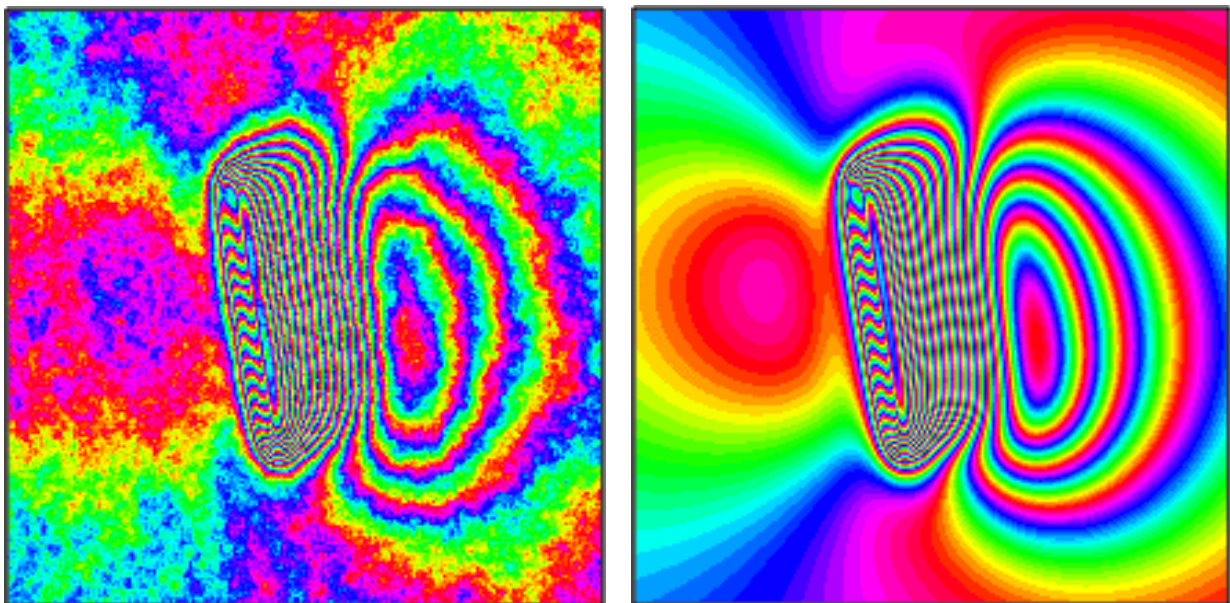


Figure 1a) Simulated interferogram (60 x 60 km) of surface displacement as seen by the ENVISAT satellite (each colour fringe represents 28.3 mm of displacement in the satellite view direction). The earthquake simulated is the $M_w=6.6$ 1968 Meckering event. **1b)** Simulated interferogram (60 x 60 km) including characteristic synthetic noise.

Publications relating to this work

Investigation of Australian earthquakes using InSAR J. Dawson, P. Tregoning and H. McQueen *in preparation*.

MOUNTAIN GLACIERS

CONTRIBUTION TO SEA LEVEL CHANGE

Gisela Estermann

Research School of Earth Sciences, The Australian National University, Canberra, Australia

Compared to the total area of ice on land of $16 \times 10^6 \text{ km}^2$ the area covered by mountain glaciers (excluding Antarctica and Greenland) is small. Nevertheless this area of almost $528 \times 10^3 \text{ km}^2$ has been retreating since the 19th century in most parts of the world. According to the IPCC report 2001 (Church et al. 2001) sea level has been rising at a rate of 0.2 to 0.4mm per year water equivalent (w.e.) due to the melting of mountain glaciers since the end of the 19th century. The aim in 2005 was to establish a global model to calculate the change in ice volume of mountain glaciers for a range of different parameter values. The approach for estimating the change in ice-volume of mountain glaciers has been taken and adopted from Zuo & Oerlemans (1997). The changes in ice-volume (melting rates) are based on the following parameters:

- the area of the glaciated region
- the temperature and
- mass balance sensitivity, which is controlled by the annual precipitation

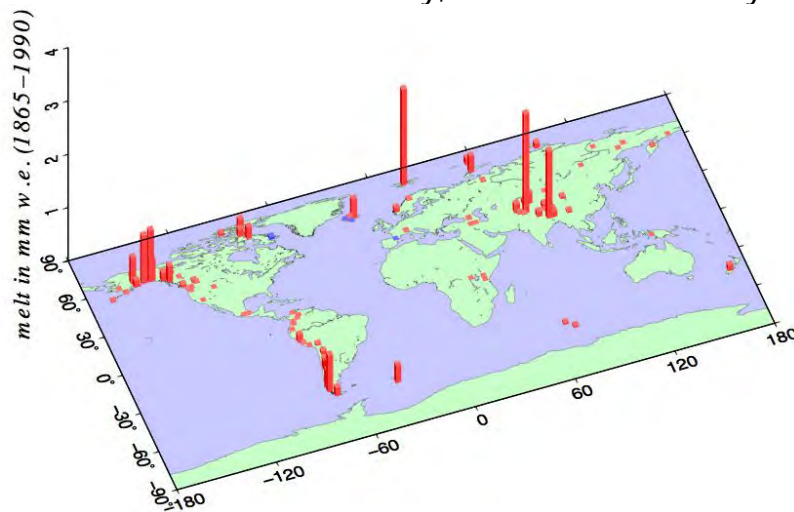


Figure 1: Total change in ice volume for period 1865-1990 for 100 glaciated regions in mm w.e. Red bars indicate an decrease and blue bars an increase in ice-volume.

For sensitivity studies different parameter sets of temperature and precipitation have been used and the resolution necessary when modelling the areas of the glaciers has been analysed. The calculation of changes in ice-volume starts in 1865. An initial imbalance between glacier and climate state has been allowed for to account for the fact that the glaciers in general were too big for the climate up to 1900. Other studies also show the imbalance, resulting in glacier retreat (or advance) in that period and that is probably not uniform over the world. Using a set of input parameters matching the one given in Zuo & Oerlemans (1997) as closely as possible results in a total

change in ice-volume for the period 1865-1990 of 22mm w.e. (Zuo & Oerlemans obtain a rate of 27mm w.e. for the same period).

In order to calculate changes in relative sea level and vertical deformation of the Earth's crust due to loading or unloading the Earth, two major assumptions have to be made:

- description of the response of the earth due to changes in surface loads
- the history of the surface loads, e.g. rates of mountain deglaciation

With known melting rates in glaciated regions and the Earth response due to these changes, the effect on relative sea level and the Earth's surface itself has been calculated. The spatial pattern of relative sea-level changes due to mountain deglaciation shows a strong spatial variability, with both the surface deformation and change in sea level being much larger in areas close to the glaciated region. Of the mountain glaciers, those in Patagonia, Alaska and Canada, and the Arctic Sea (Iceland, Spitsbergen and Franz-Josef Land) make the most significant contribution to modern sea-level change, while significant vertical uplift also takes place in central Asia. Tide gauge, VLBI and GPS records are expected to include this effect of deglaciation. The contribution might be at a measurable level if the geodetic site is located close to the receding glacier.

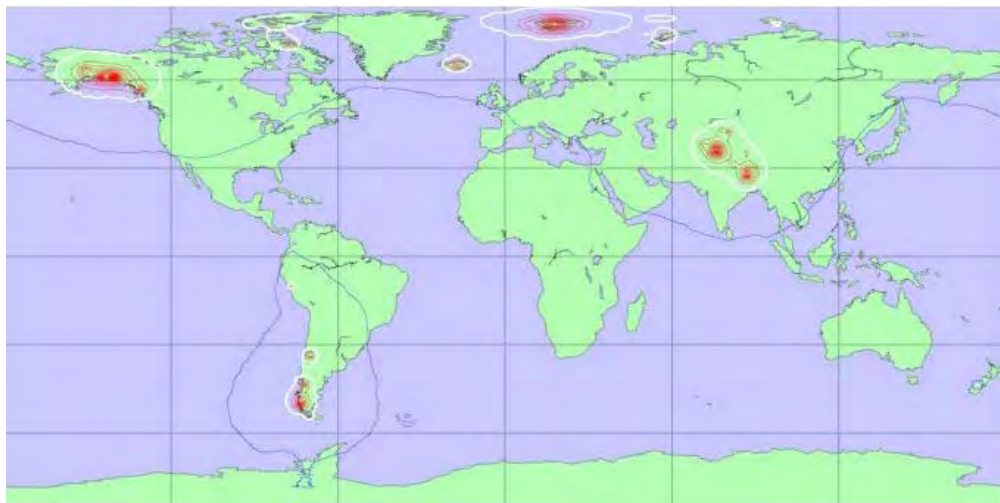


Figure 2: Spatial distribution of relative sea level changes applying recent mountain deglaciation. The contour interval is 0.1mm/year. Red contour lines indicate relative sea-level fall, blue indicate relative sea-level rise.

The initial analysis was performed using a generalised data set defining the glaciated regions over a relatively coarse grid. The results for this model give a reasonably good estimate of the pattern of relative sea-level change and vertical deformation across the globe. In order to determine whether or not such a model would give accurate predictions of sea-level change for sites close to the glaciers, the results of this initial analysis were compared with those obtained for a more detailed model of the glacier coverage. Very high

resolution digital models of the Alaskan and Spitsbergen's glacier fields were prepared and the results for these ice sheet models compared with those of the generalised models (see Figure 3 for Alaska's glaciers).

The global pattern does not change much when applying the digitised data set. But the comparison at geodetic sites suggests that the position of the glaciers has a very strong impact on the character of sea-level change and vertical deformation for sites close to the glaciers.

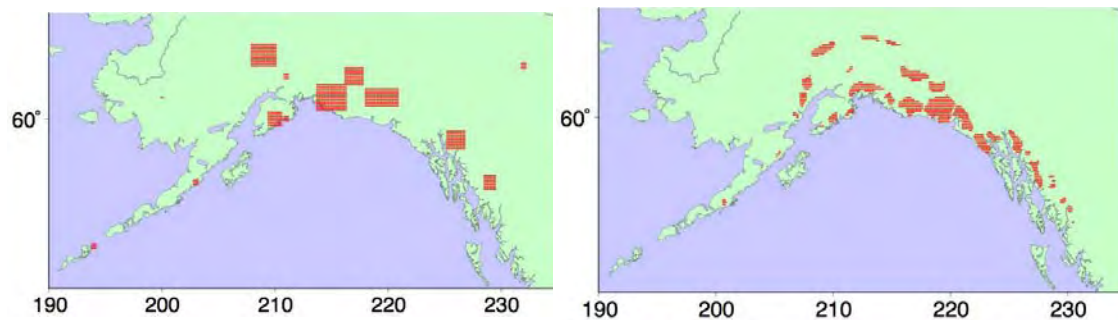


Figure 3: Comparison between locations and areas of glaciated regions in Alaska of generalised data set (left plot) and digitised data set (right plot).

However, the results of the current model do not closely reflect the amplitudes of observed relative sea-level changes at existing tide gauge stations or uplift rates at GPS stations. In the examples of Alaska and Spitsbergen the estimates at geodetic sites are much smaller than the observed values. Therefore comparisons to other studies for the Alaska and Spitsbergen regions and refinements of the global model have been undertaken.

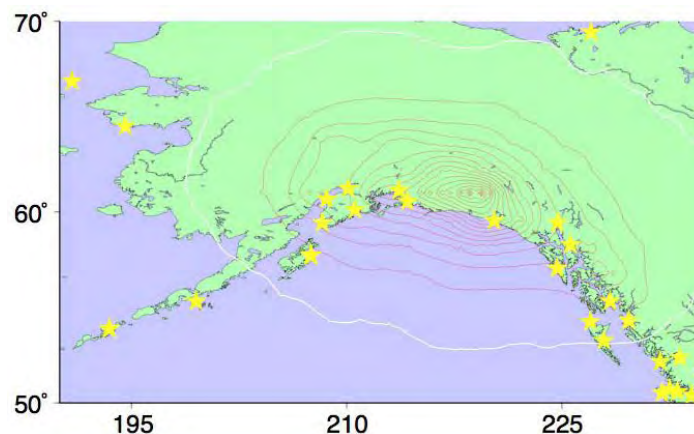


Figure 4: Spatial distribution of sea-level changes in Alaska and Canada applying the digitised areas. The contour interval is 0.1mm per year. Stars are indicating the location of PSMSL tide gauge sites.

References

Changes in sea level. In: Climate Change 2001: The Scientific Basis. Contribution of Working Group I to the Third Assessment Report of the Intergovernmental Panel on Climate Change Church, J. A., Gregory, J. M., Huybrechts, P., Kuhn, M., Lambeck, K., Nhuan, M. T., Qin, D., & Woodworth, P. L. edited by J. T. Houghton, Y. Ding, D. J. Griggs, M. Noguer, P. J. v. d. Linden, X. Dai, & C. A. Johnson, Cambridge University Press, Cambridge, United Kingdom and New York, NY, USA, 881pp.

Contribution of glacier melt to sea-level rise since ad 1865: A regionally differentiated calculation Zuo, Z. and Oerlemans, J. *Climate Dynamics*, **13**, 835-845

Laser Ablation U-Th dating of molluscan shells from Mediterranean interglacial deposits

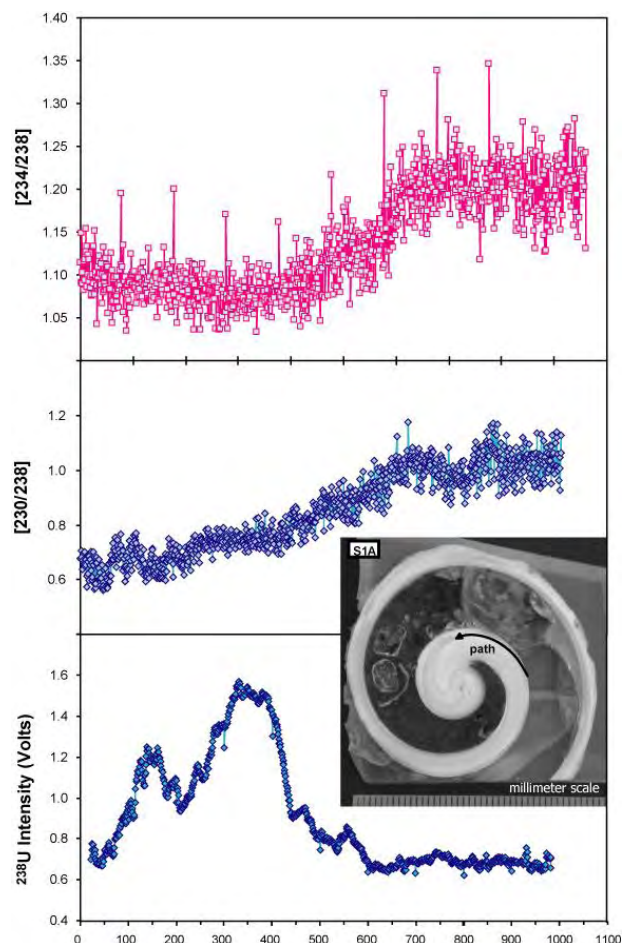
Andrea Dutton¹, Stephen Eggins¹, Fabrizio Antonioli², Kurt Lambeck¹

Research School of Earth Sciences, The Australian National University, Canberra, Australia

²ENEA, RAgency for New Technologies, Energy and Environment, 00166 Rome, Italy

We have examined a number of fossil gastropod shells belonging to the species *Strombus bubonius* with respect to their minor and trace element content, to determine the potential for precise and accurate U-series dating of these shells using a laser ablation system coupled to a MC-ICP-MS. These specimens were collected from Italy, Spain, and Tunisia and are associated with a fauna thought to represent the incursion of warm waters into the Mediterranean region during the last interglacial marine isotope substage 5e. Our objective was to explore the possibility of dating these shells using a U-Th laser ablation technique similar to that reported in Eggins et al. (2003) and Pike et al. (2005) and to test the hypothesis that these shells grew during the 5e substage of the last interglacial. Our findings were four-fold: 1) minor and trace element concentrations appear to contain fine-scale oscillations that may reflect the environmental influence of daily/tidal variability; 2) the uranium profiles along cross-sections do not display expected patterns of diffusive transport of uranium from the external environment into the shell as commonly observed in bone material (e.g., Pike et al. (2002)); 3) relative abundances of U and Th isotopes can change dramatically within a transect of the shell; 4) the concentration of U (and particularly Th) in these particular specimens is too low to provide ages with the precision necessary to rule out the possibility that these shells grew during the 5a and 5c highstands of the last interglacial.

Figure 1. Activity ratios are displayed in the upper two panels with relative concentration of uranium plotted in the lower panel. Data are plotted as consecutive data points, each spaced at ~166 μm in real distance across the shell. These parameters show high variability across the thickness of the shell and do not display expected diffusion profiles in uranium concentration. Inset shows location of laser path on shell.



Eggins, S., Grun, R., Pike, A. W. G., Shelley, M., Taylor, L. (2003) ^{238}U , ^{232}Th profiling and U-series isotope analysis of fossil teeth by laser ablation-ICPMS. *Quaternary Science Reviews*, **1** **22**, 1373-1382.

Pike, A. W. G., Eggins, S., Grun, R., Hedges, R. E. M., and Jacobi, R. M. (2005) U-series dating of the Late Pleistocene mammalian fauna from Wood Quarry (Steeley), Nottinghamshire, UK. *Journal of Quaternary Science* **20**, 59-65.

Pike, A. W. G., Hedges, R. E. M., and Van Calsteren, P. (2002) U-series dating of bone using the diffusion-adsorption model. *Geochimica et Cosmochimica Acta* **66**, 4273-4286.

Paired single-specimen analysis of foraminiferal stable isotope and element/Ca compositions: Exploring seasonal variability in the early Paleogene greenhouse climate

Andrea Dutton¹ and Stephen Eggins¹

¹ *Research School of Earth Sciences, The Australian National University, Canberra, Australia*

The objective of this investigation is to ascertain the seasonal variability in temperature and salinity of sea surface waters in the tropical Pacific during the late Paleocene and early Eocene by measuring the Mg/Ca and oxygen isotope composition of each individual foraminifera within a sample population. We paired these two analyses at the individual level by combining laser-ablation techniques to characterize the elemental composition with minimal damage to the specimen, followed by single-specimen stable isotope analysis using conventional gas source mass spectrometry techniques. This study represents the first example of directly pairing multiple paleoceanographic proxies on the same specimens which is an important advance as it presents the real possibility of extracting twice as much information from the same size sample.

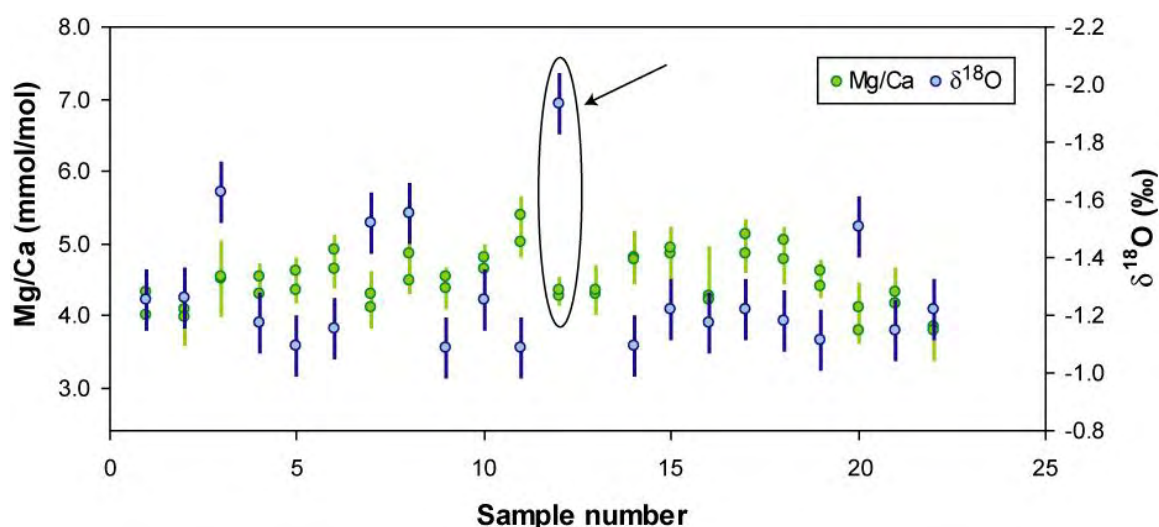


Figure 2. Mg/Ca values were measured using laser-ablation ICP-MS on two different chambers of each test. Oxygen isotope data represent whole-shell analyses that were conducted after laser ablation analysis. In general, the oxygen isotope data appear to track surface water temperatures, as represented by the Mg/Ca data, but in several instances departures from this relationship (e.g., see arrow) represent the influence of variable surface water salinity on the $\delta^{18}\text{O}$ signal.

Interlaboratory calibration of element/Ca ratio measurements using ICP-OES and ICP-MS

Andrea Dutton¹ and Stephen Eggins¹

¹ *Research School of Earth Sciences, The Australian National University, Canberra, Australia*

This international calibration effort grew out of discussions during a workshop on foraminiferal Mg/Ca that was held during the 8th International Conference on Paleoceanography, 2004. The first step in normalizing measurements between laboratories is to ascertain if there are analytical biases related to basic sample preparation, introduction into the instrument, and measurement on different types of instruments. To this end, we participated in an interlaboratory calibration study and prepared replicate dissolutions of three different powdered carbonate standards and analyzed the Mg/Ca and Sr/Ca compositions using a Varian Vista ICP-OES located in the Department of Earth and Marine Sciences, and also on the PQ2 ICP-MS housed in the Research School of Earth Sciences. Our results appear to agree well with published (accepted) values of minor element composition in these standards, although the internal precision on the ICP-OES appears to have deteriorated significantly over the past year resulting in accurate, yet less precise results than desired. This effect may be in some way related to the deterioration of the detection limits on this instrument and/or to the increase in drift observed during continuous instrument operation that has become characteristic within the past year. Nonetheless, the ICP-OES appears to have superior sensitivity and precision to the ICP-MS and remains our preferred method of analysis for applications to foraminiferal (and coralline) carbonate solution samples. Our participation of this study also serves to increase the international profile of The ANU in the field of marine science and paleoceanography and to establish the ANU as one of the leading facilities world-wide capable of producing reliable and accurate results in this subdiscipline.

Free Oscillations of the Earth after the Sumatra-Andaman earthquake

H. McQueen¹, S. Rosat², T. Sato², & K. Lambeck¹

¹ *Research School of Earth Sciences, The Australian National University, Canberra, Australia*

² *National Astronomical Observatory of Japan, Mizusawa*

The M_w 9.3 Sumatra-Andaman earthquake of 26 December 2003 triggered large amplitude Earth oscillations which were monitored on the superconducting gravimeter at the Mt Stromlo gravity station for over three months. A complex series of strong multimode vibrations continued for several weeks followed by a longer term signal of the more persistent modes of the whole Earth, dominated by the fundamental OS0 breathing mode, providing a constant reminder of the huge amount of energy released by the event. Signals generated by the December earthquake were still being recorded in March when a second major earthquake on a neighbouring plate boundary re-excited the vibrations.

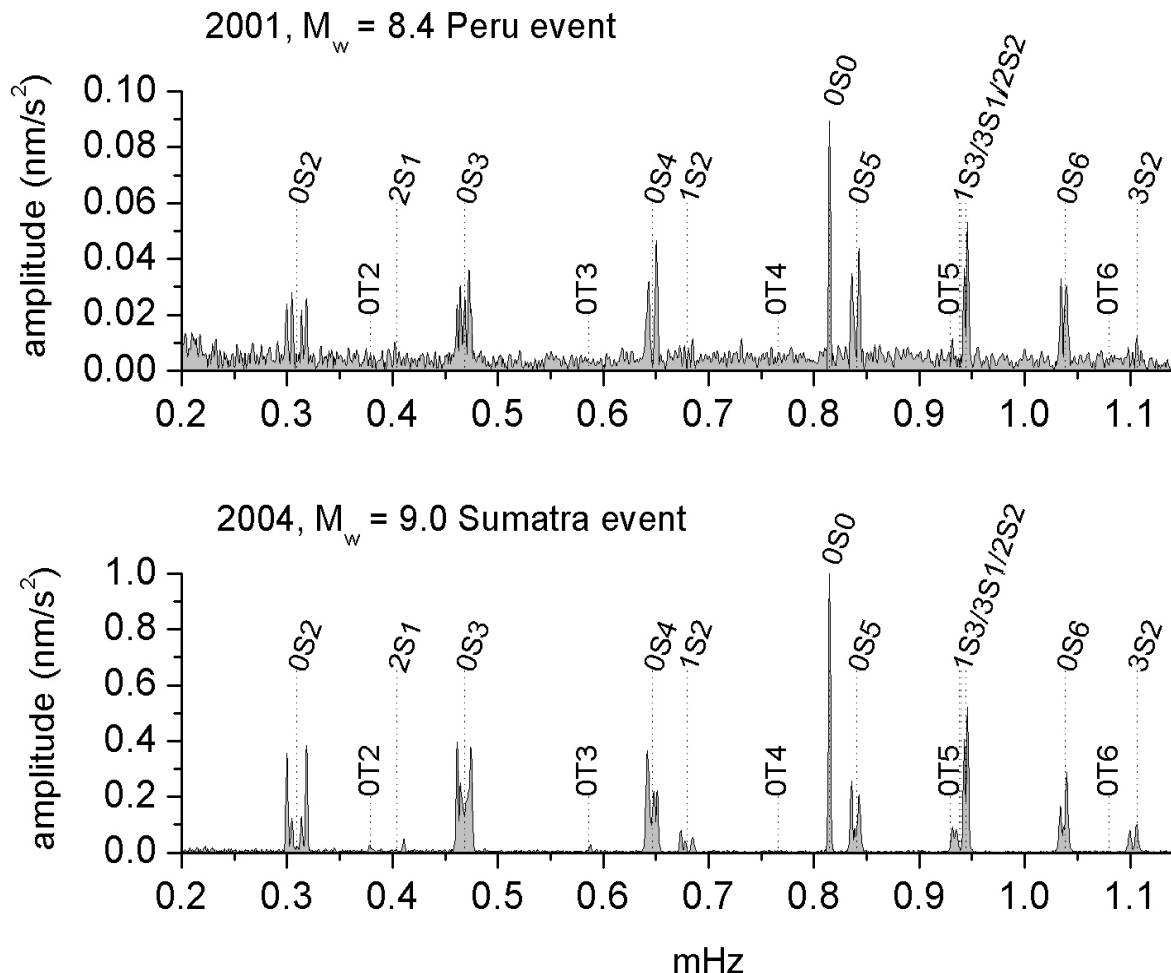


Figure 1. A comparison of the amplitude spectra of SG data at Canberra (240 h) after the 2001 M_w 8.4 Peru event with the 2004 M_w 9.03 Sumatra-Andaman earthquake showing the greatly improved spectral resolution from the 2003 event (from Rosat et al 2005).

The large amplitude and long duration of the vibrations provided a higher resolution spectrum of Earth's free vibrations than any event since the installation of the SG at the site and provided unprecedented detail in the splitting of fundamental modes due to rotation and inhomogeneity inside the Earth. The excitation of various modes of vibration by an earthquake depends on both its magnitude and mechanism and different earthquakes distribute their energy differently. The Sumatran earthquake was a relatively shallow event on a low angle fault and while it generated some very large low order modes it did not excite the elusive Slichter mode of oscillation in the Earth's core to a detectable level in the SG spectra.

The Superconducting Gravimeter at Mt Stromlo is the most sensitive instrument for monitoring gravity fluctuations and is one of four operating in the southern hemisphere. It is operated by RSES in collaboration with the Japanese National Astronomical Observatory, Mizusawa, as part of the Global Geodynamics Project, an international network of gravimeters attempting to detect motions in the earth's deep interior, infer details of its internal structure, and provide information on a range of problems in global geodynamics. Data from the site is regularly archived at the GGP data centre (<http://ggp.gfz-potsdam.de>)

References

Rosat, S., Sato, T., Imanishi, Y., Hinderer, J., Tamura, Y., McQueen, H., Ohashi, M. 2005 High-resolution analysis of the gravest seismic normal modes after the 2004 Mw = 9 Sumatra earthquake using superconducting gravimeter data *Geophys. Res. Lett.*, **32**, 3, L13304 10.1029/2005GL023128

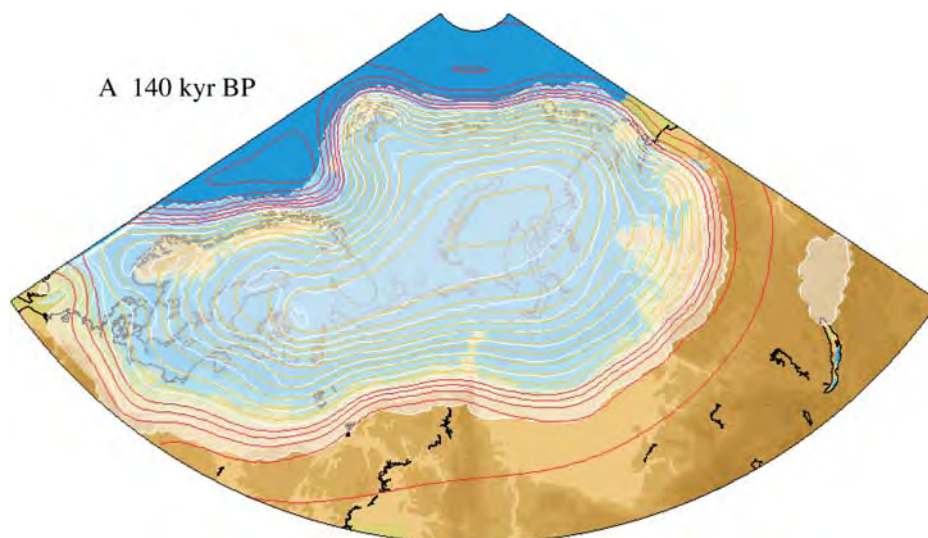
Glacial rebound and sea-level change: solutions for ocean-volume fluctuations, ice sheets and mantle rheology

Kurt Lambeck, Tony Purcell, Jason Zhao, Andrea Dutton

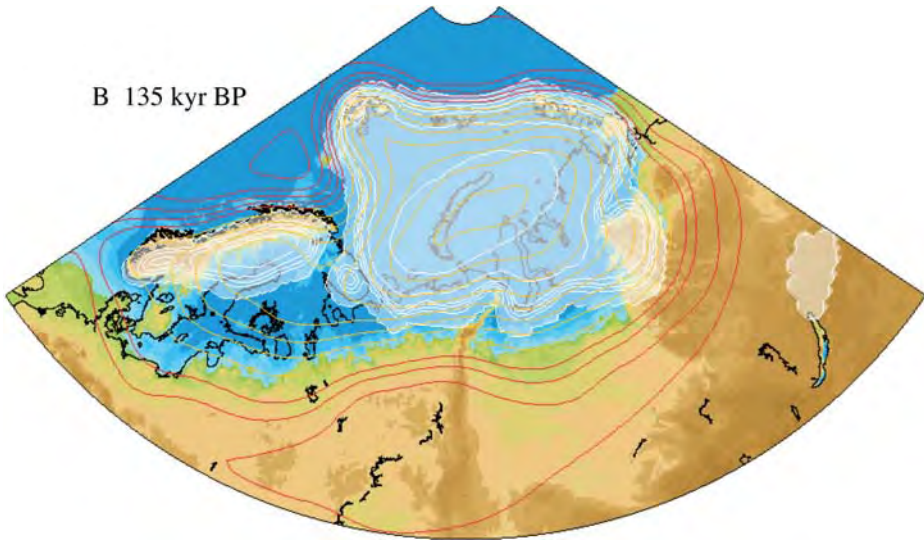
Research School of Earth Sciences, The Australian National University, Canberra, Australia

As ice sheets melt or grow, the load on the earth's surface changes and the planet's shape and gravity field is modified. This is seen in a range of geological, geophysical and geodetic observations. An important geological observation is the height and elevation of former shorelines above or below present sea level. Geodetic observations include the radial displacement of the crust or the acceleration of satellites as the gravity field changes. Inversion of such observations provides information on the Earth's rheology and on the history of the ice sheets. The rheological results are robust and the main emphasis of current work is on improving models of the ice sheets. This is achieved through a combination of field, laboratory, and numerical modelling.

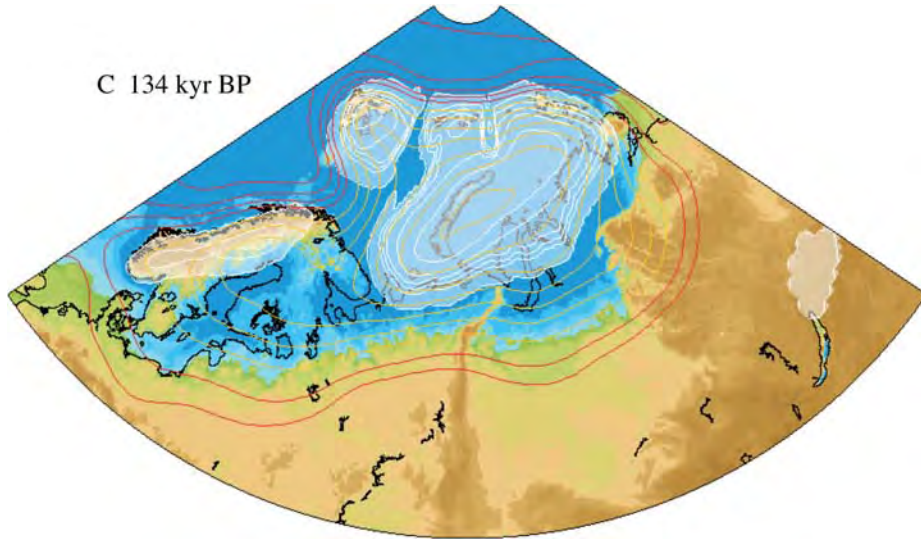
Study areas included in 2005 projects include Scandinavia and Arctic Russia (see below), The Baltic Sea (through a joint project with Shiyong Yu and Bjoern Berglund of Lund University, Sweden), Greenland (through a joint project with Charlotte Sparrenbom of Lund University, Sweden), the Gulf of Mexico (through a joint project with Alex Simms of Rice University, USA), the Mediterranean (through joint projects with Marco Anzidei of INGV, Rome, and Fabrizio Antonioli of ENEA, Rome), and Singapore (through a joint project with Michael Bird, now at St Andrews, Scotland).



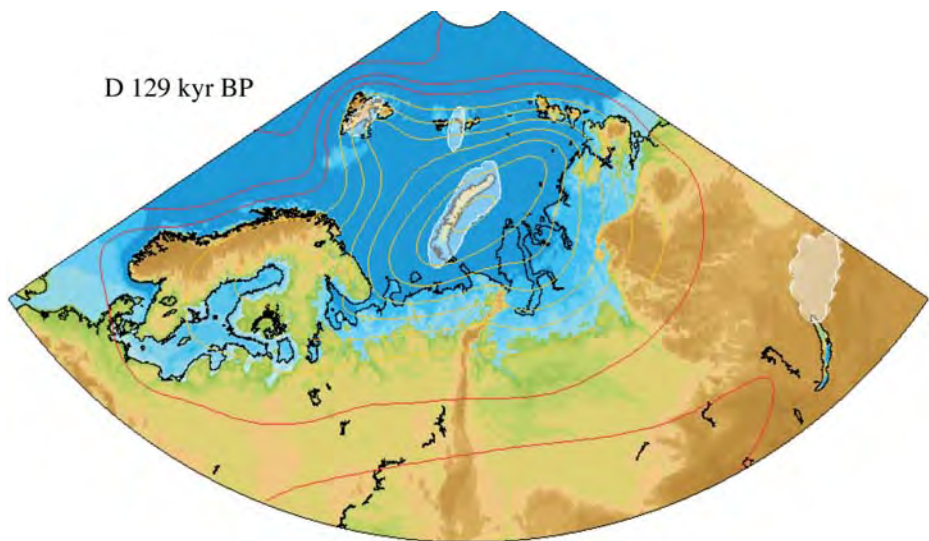
B 135 kyr BP



C 134 kyr BP



D 129 kyr BP



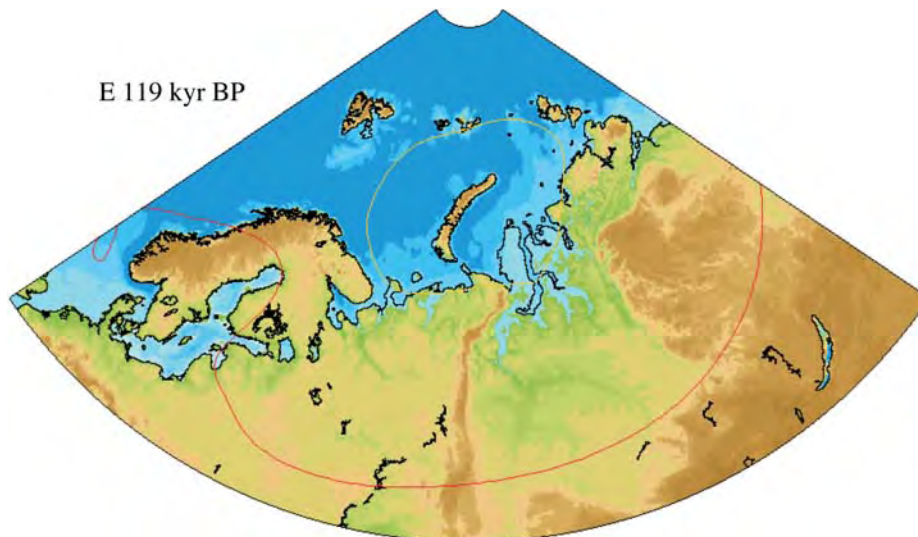


Figure 1 (A-E). Palaeogeographical reconstruction for selected epochs for Eurasia from the time of the penultimate glacial maximum to the stadial corresponding to MIS 4. The areas covered by grounded ice are shown by the white translucent areas with ice thickness contours (white lines) at 250 m intervals from 0 to 1000 m and at 500 m interval thereafter. The contours of negative and zero sea level change are in red and positive values in yellow (e.g. the 200 m contour represents palaeoshorelines that are now 200 m above sea level). For (A) to (C) the negative contours are at 50 m intervals and the positive contours are at 100 m interval. For (D) and (E) the negative contours are at 25 m intervals and the positive contours are at 50 m intervals. The palaeo-shoreline locations are defined by the green-blue boundary and palaeo-topography above coeval sea level is indicated by the green and brown colour gradations at 25, 50, 100, 200 m and higher elevations. Palaeo-water depths are defined by the blue colour gradations at -25, -50, -100, -200 m and deeper depths. The ocean depths and land elevations are with respect to sea level for the specified epoch. Water depths of enclosed bodies are with respect to the sill elevation that defines the enclosed basin.

The focus of the glacial rebound work in 2005 has been on Arctic Eurasia from the time of the penultimate glacial maximum (MIS 6 or the Late Saalian at ~145,000 years ago) up to the present. The aim of this work is to establish constraints on the ice thickness and ice margins for some of the major phases of the last glacial cycle that are independent of glaciological or climate assumptions. The penultimate glacial maximum was one of the largest ice sheets over northern Europe and the Russian arctic, extending from the British Isles to the Taymyr Peninsula. This was followed by the Eemian Interglacial and by a series of alternating stadials and interstadials over Russia and Scandinavia culminating in the last glacial maximum at ~ 20,000 years ago, at the end of which the next cycle of glaciation started.

The principal outcomes are: the completion of compilations of field evidence for the ice margin locations and shoreline elevations and sea levels across the region; the inversion of this data for ice thickness during the principal glaciations corresponding to the marine isotope stages 6, 5d, 5c and 4; and the palaeo-geographic reconstructions for these periods.

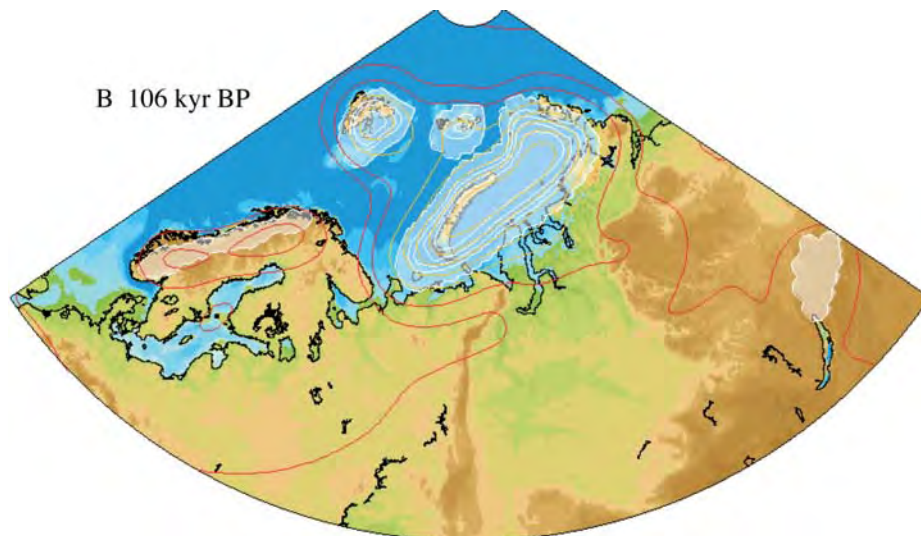
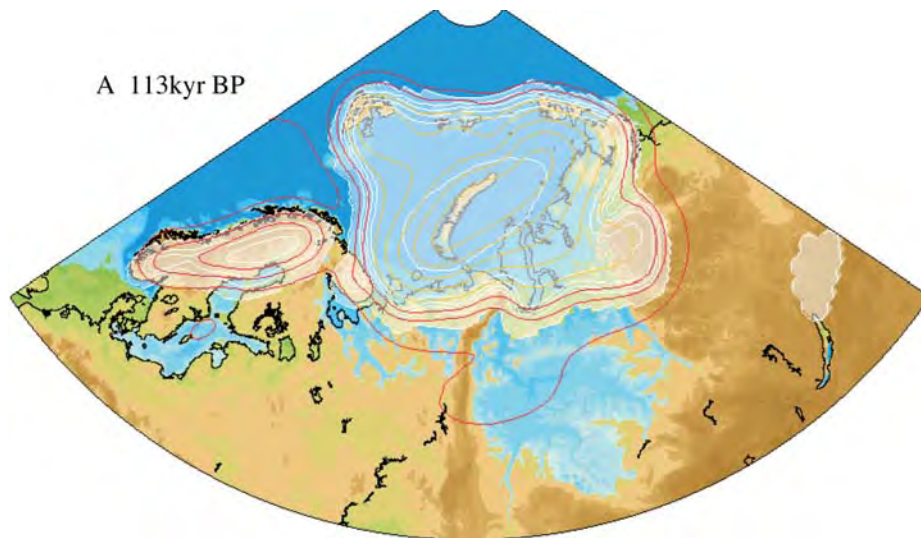
During the Late Saalian the ice extended across northern Europe and Russia with a broad dome centred from the Kara Sea to Karelia that reached a maximum thickness of *c.* 4500 m and ice surface elevation of *c.* 3500 m above sea level. A secondary dome occurred over Finland with ice thickness and surface elevation of 4000 m and 3000 m respectively (Figure 1). When ice retreat commenced, and before the onset of the warm phase of the Early Eemian, extensive marine flooding occurred from the Atlantic to the Urals and, once the ice retreated from the Urals, to the Taymyr Peninsula. The Baltic – White Sea connection is predicted to have closed at about 129 kyr BP although large areas of arctic Russia remained submerged until the end of the Eemian (Figure 1).

During the stadials (MIS-5d, 5b, 4) the maximum ice was centred over the Kara-Barents Seas with a thickness not exceeding *c.* 1200 m. Ice dammed lakes and the elevations of sills are predicted for the major glacial phases and used to test the ice models (Figure 1). For example, large lakes are predicted for west Siberia at the end of the Saalian and during MIS-5d, 5b and 4, with the lake levels, margin locations and outlets depending *inter alia* on ice thickness and isostatic adjustment. Comparison with the field evidence then permits further inferences about the ice margins and ice thickness. The results are to appear in *Boreas*. Subsequently the investigation has been continued from MIS-4 to MIS-2 to include the period of rapid changes in ice cover over Scandinavia and to provide constraints on the European and Russian ice sheets for the complete interval from MIS 6 to the present.

Related to this investigation is the study of sea-level fluctuations in the Mediterranean during the last interglacial (MIS 5e). The Mediterranean lies on the forebulge of the Late Saalian ice sheets and the present elevations of 5e shorelines are *inter alia* a function of the Stage 6 and subsequent ice sheets. The predicted Eemian sea-level signal for these locations is distinctly different from that at sites further from the former ice sheets and the differences are determined by the ice and earth model parameters. The amplitudes of the signals at both sites are determined by these parameters and by the ice volumes during the interglacial. The comparison of the data from the Mediterranean with far-field evidence from Western Australia indicates that land-based ice volumes during the middle and later parts of the Eemian were less than during the present interglacial by as much as 5 m sea-level equivalent (Figure 2). Related work in the Mediterranean includes the study of speleothems from submerged caves and dating of molluscan shells to refine the sea level curve for the past and earlier cycles and further work on the use of Roman-era fish tanks as sea-level indicators (see Anzidei et al., 2005).

A second focus has been on the stress evolution in the crust during a glacial cycle to answer specific questions about the stability of the crust during and after major glaciations. What is the evolution of the state of stress in the crust during a glacial cycle and how does the crust respond to the superpositioning of these stresses on long-term background stress fields? If

these questions can be resolved it becomes possible to estimate the likelihood of fault reactivation during future glacial cycles in areas that may otherwise be appropriate for the long-term storage of nuclear waste. These questions have been investigated for waste repository sites in Sweden, using the past glacial cycle as representative of future cycles and it has been possible to show that fault stability enhancement or reduction is strongly dependent on location relative to the ice sheets and that the glacial-load stress is a factor to be considered in any final decisions on repository site locations.



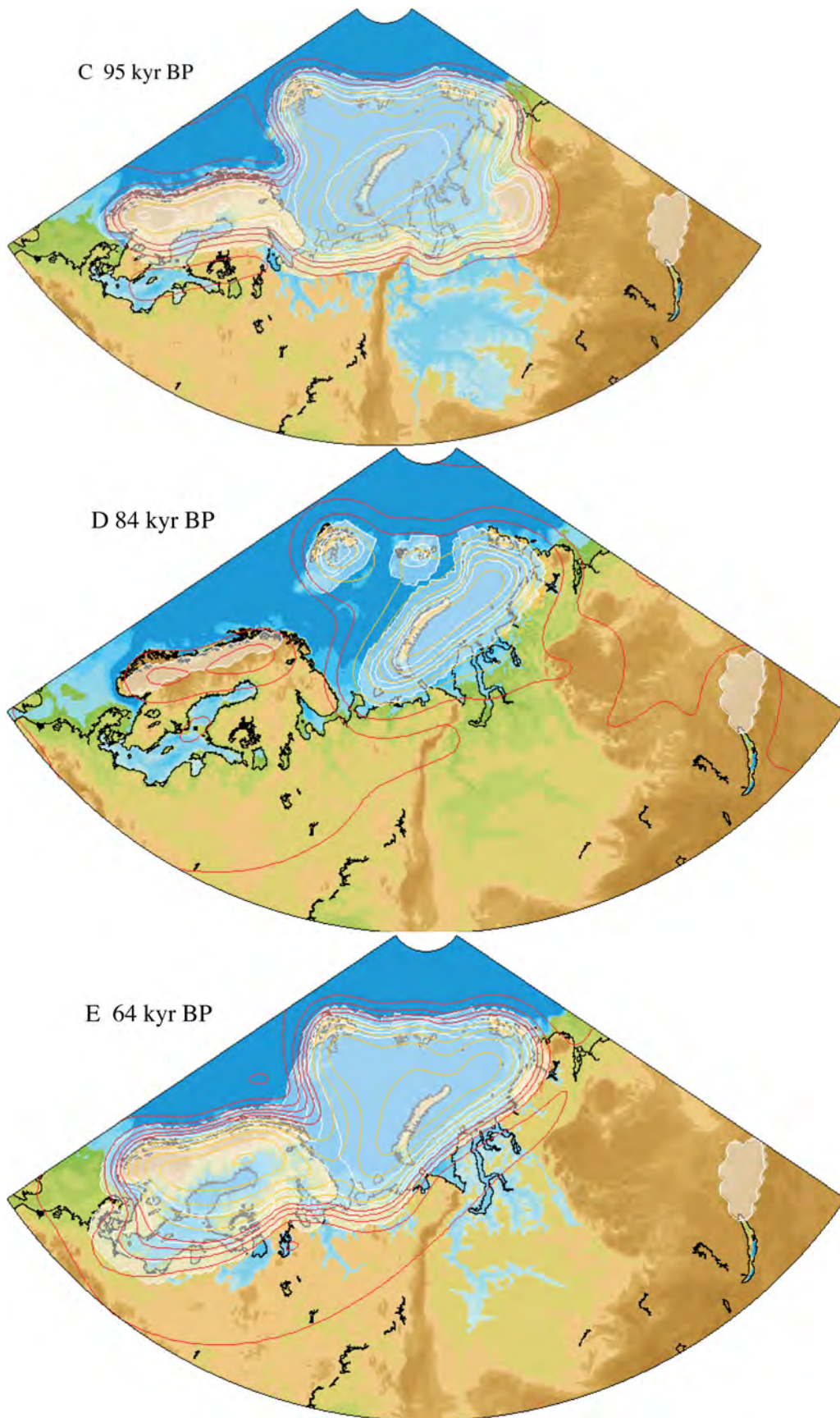


Figure 2: Same as Figure 1 but for the post Eemian period. The rebound contours are the same as in Figure 1 (D).

References:

- Lambeck, K., Purcell, A. 2005; Sea-level change in the Mediterranean Sea since the LGM: model predictions for tectonically stable areas. *Quaternary Science Reviews*, **24**, 1969-1988.
- Anzidei, M., Benini, A., Lambeck, K., Antonioli, F., Esposito, A., Surce, L. 2005. Siti archeologici costieri di età romano come indicatori della variazioni del livello del mare: un'applicazione al mare Tirreno (Italia centrale). In *Evolución Palaeoambiental de Los Puertos y Fondaderos Antiguos en el Mediterráneo Occidental*. L. de Maria and R. Turchetti, Eds, Rubbetino, Rome, pp115-126.
- Lambeck, K. 2005. Glacial load stresses: Can existing faults or other zones of crustal weakness be reactivated during glacial cycles? In *Expert Panel Elicitation of Seismicity Following Glaciation in Sweden* (Eds S. Hora and M. Jensen). Statens strålskyddinstitut rapport 2005:20 pp 85-106. Stockholm, Sweden.
- Sparrenbom, C.J. Bennike, O., Bjorck, S., Lambeck, K., 2006. Relative sea-level changes since 15000 cal. Yr BP in the Nanortalik area, southern Greenland. *J. Quaternary Science*, **21**, 29-48.
- Sparrenbom, C.J. Bennike, O., Bjorck, S., Lambeck, K., 2006. Holocene relative sea-level changes in the Qaqortoq area, southern Greenland. *Boreas* 35(2) (in press)
- Lambeck, K., Purcell, A., Funder, S., Kjær, K., Larsen, E., Möller, P., 2006. Constraints on the Late Saalian to early Middle Weichsellian ice sheet of Eurasia from field data and rebound modeling. *Boreas* (in press).

SEISMOLOGY 2005

Work in Seismology covers a variety of studies using wave propagation processes to study the nature of the Earth. The many strands of the research combine field observations, computer modelling and inversion and extensive data analysis to exploit the favourable location of Australia for seismic studies.

Professor Brian Kennett was awarded the Jaeger Medal for Australian Earth Sciences from the Australian Academy of Sciences in May 2005 and later in the same month was elected as a Fellow of the Royal Society of London, with a citation that included work on the structure beneath the Australian Region.

The main focus of research in Seismology is the investigation of the three-dimensional structure of the Earth using probing via seismic waves generated by earthquakes or man-made sources. This work builds on the extensive efforts of deployments of portable instruments across Australia and in East Antarctica, with developments in interpretation, seismic tomography and theoretical and computational work on seismic wave propagation.

Four portable stations are still in place in the Australian Antarctic Territory with stations deep into the interior, data retrieval and some station recovery was planned by Dr Reading for this 2004-2005 summer season, but has been hampered by logistic considerations

The long running Tasman Line experiment was completed this year and all 20 stations have been recovered. The data has made significant contributions to the resolution of structure in the neighbourhood of the transition from Precambrian to Phanerozoic Australia, both from surface wave tomography and in the mapping of crustal structure using receiver functions. In particular the nature of the transition in lithospheric structure at depth is quite complex and there are suggestions of a three distinct steps in lithospheric thickness. Efforts are being made to exploit gradient information from the 3-D shear wavespeed models to pin down the nature of the transitions.

The long-term data from the Tasman Line experiment has also been used to examine the use of waveform correlation methods to recover the impulse response between a pair of stations. It has proved possible to get satisfactory results for station separations up to 2000 km, with the fundamental mode Rayleigh wave the most prominent feature on the recovered records. The preliminary analysis shows clear lateral variations in Rayleigh wave group velocity across the area covered by the stations, indicating horizontal variations in crustal structure.

A major deployment of short-period recorders has been made in Eastern Victoria; when completed this survey will tie in with the earlier MALT surveys undertaken by Monash and Flinders Universities to provide high density coverage across almost all of Victoria. A much smaller deployment

commenced in South Australia in December in the neighbourhood of Mt. Gambier with the aim of determining whether there are any residual velocity anomalies associated with this area of relatively recent volcanism (6000 B.P.).

As part of an ARC funded Linkage Project with Dr M. Keep from the University of Western Australia and Dr P. Cummins from Geoscience Australia, a combined group has deployed eight broadband instruments across northwestern Western Australia to provide a network for improved location of smaller seismic events and structural studies. It is hoped that this will help to delineate the neo-tectonic trends both on-shore and off-shore.

Jingming Duan and Scott Savage have kept the Warramunga seismic and infrasound arrays running at a high performance level during the year. Tony Percival has provided valuable relief support at the WRA array again this year in addition to his regular work on the support and enhancement of the solid-state instruments for short-period recording. He has been able to dramatically increase the memory capacity using new generation flash-cards. Forty of the upgraded instruments are in use in the current EVA experiment.

A successful ARC LIEF application this year, in association with the University of Adelaide and Macquarie University, will provide support for 15 new recorders with combined seismic and electromagnetic recording capabilities. We hope that this will lead to synergies between the different methods of Earth sounding.

AUSTRALIAN STUDIES

B.L.N. Kennett, A. Reading, N. Rawlinson, M. Heintz, S. Fishwick, K. Procko, E. Saygin, A. Abdulah

The configuration of earthquake belts around Australia provides a wealth of events at suitable distances to be used as probes into the seismic structure of the upper mantle. The few permanent seismic stations have been supplemented with extensive deployments of portable broadband stations for periods of a few months at each site. The broad band records have been used in a variety of studies of 3-D structure.

Surface wave tomography is based on matching seismic waveforms on individual paths and then mapping the path-specific constraints on shear structure into a 3-D model. Higher frequency body wave arrivals are refracted back from the variations in structure in the mantle and are particularly sensitive to discontinuities in structure. Observations out to 3000 km provide coverage of the structures down through the transition zone. For northern Australia, the combination of short-period and broadband observations provides detailed information on both P and S wavespeeds and attenuation structure.

There is a complex pattern of 3-D structure beneath the Australian region. The cratonic region in the centre and west is underlain by a thick mantle lithosphere extending to around 200 km depth with fast wavespeeds (especially for S waves). However, the mobile belt in Central Australia has comparatively low wavespeeds to at least 75 km depth with fast lithospheric material beneath. In the asthenosphere the S wavespeeds diminish and there is significant attenuation. Beneath the eastern zone of Phanerozoic outcrop the lithosphere is generally thinner (less than 140 km) and the asthenosphere beneath has a pronounced low velocity zone for S again with high attenuation.

Surface wave tomography

S. Fishwick, B.L.N. Kennett and A.M. Reading

The extraction of information on 3-D shear wavespeed structure from surface waves proceeds in two main steps. Firstly a path specific model is found by matching the characteristics of segments of the observed seismograms with theoretical results. Both the fundamental and higher mode Rayleigh waves on the vertical component are exploited in the frequency band from 0.007 to 0.02 Hz. The seismogram matching requires a good knowledge of the event location and the source mechanism, and is most effective for events with magnitude greater than 5.4 for which reliable centroid moment tensor solutions are available.

The second stage of the surface wave tomography is to use the assembly of path constraints to build a 3-D model. The present images of the shear wavespeed have been obtained by using a B-spline representation of the velocity variation at each depth. The inversion proceeds with an initial pass to retrieve large scale structure with an 8 degree knot spacing, and then the knot spacing is refined to allow the introduction of smaller scale structure.

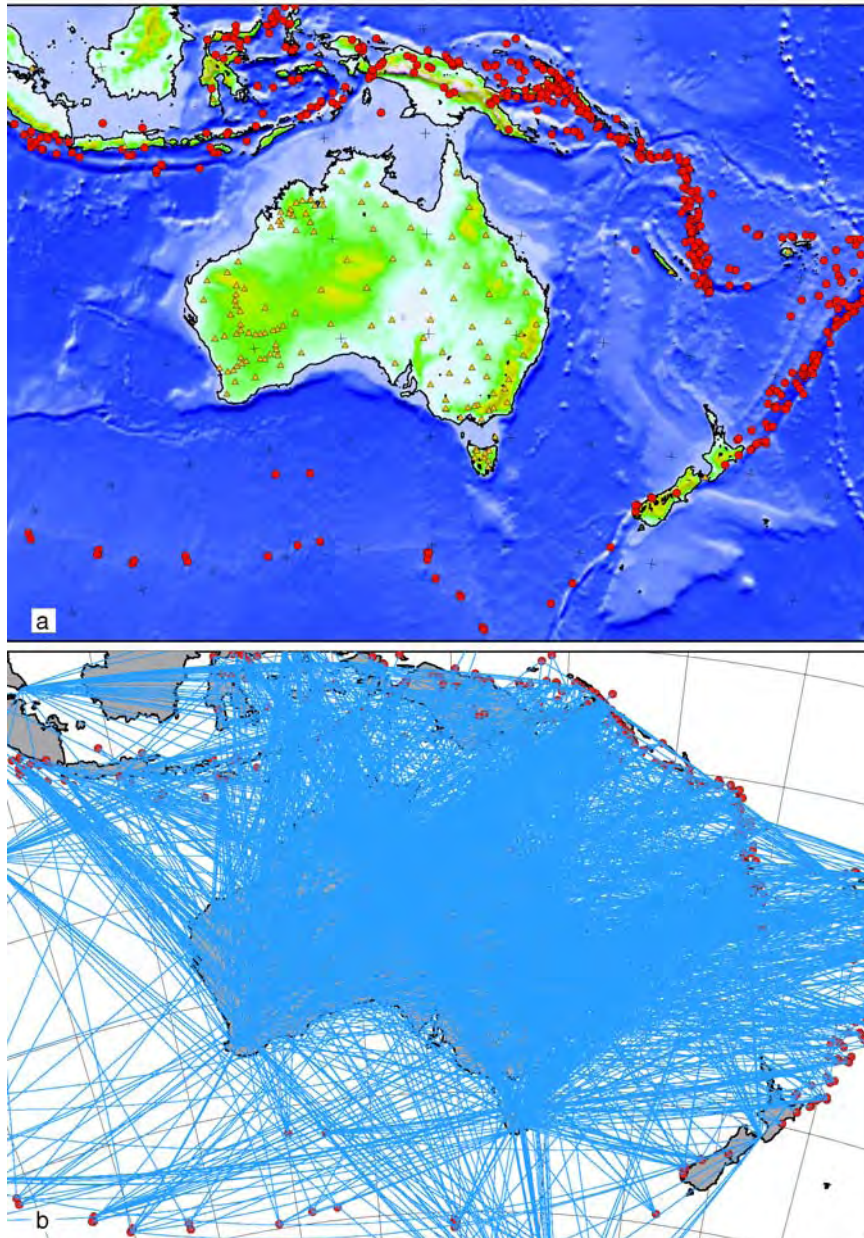


Figure 1: Configurations of earthquakes, stations and paths used in the surface wave tomography.

Nearly 2000 paths have been used in the current model, with as many as possible taken from the portable stations to achieve as comprehensive a distribution of crossing paths as possible and thereby obtain good resolution of structure. The distribution of sources and recorders is shown in Figure 1(a), and the path density for the tomographic inversion is displayed in Figure 1(b). The distribution of earthquake sources and available data mean that some regions are more densely sampled, but across the continent we have good coverage and crossing paths as is needed for reliable tomographic results. In the earlier stages of the surface wave studies the 3-D models changed markedly as new data was added since there was a major effect on path constraints. Now, however, the current results are robust over the continent. Nevertheless sampling in the oceanic regions to the south is still somewhat

limited and further refinement can be expected in this area once new events are captured.

Figure 2 shows the distribution of shear wavespeed as a function of depth at 50 km intervals, displayed as deviations from the continental reference model ak135 (Kennett et al, 1995). The S wavespeed in the mantle for model ak135 increases slowly with depth from 4.49 km/s at 75 km depth to 4.55 km/s at 225 km and there is no zone of lowered seismic wavespeeds. Shear wavespeeds lower than the ak135 values can readily be produced by the influence of increased temperature, but very fast wavespeeds associated with the cratonic elements are likely to require some chemical or textural component. The advantage of ak135 is that it provides a common reference for both surface wave and body wave studies.

The inversion for the image of shear wavespeed structure has been carried out in a way that emphasises contrasts in velocity structure and so reveals structural trends, but probably over-estimates the range in seismic wavespeeds. We have employed a 2 degree knot spacing in the B-spline representation and have restricted attention to the frequency range 0.007-0.02 Hz in the analysis of the surface wave portion of the seismograms to minimise influences of coupling between higher modes; as a result the potential resolution of structure in the images of shear wavespeed is at a horizontal scale of approximately 200 km and a vertical scale of about 30 km. Strong localised wavespeed variations should be detected, but cannot be reliably imaged.

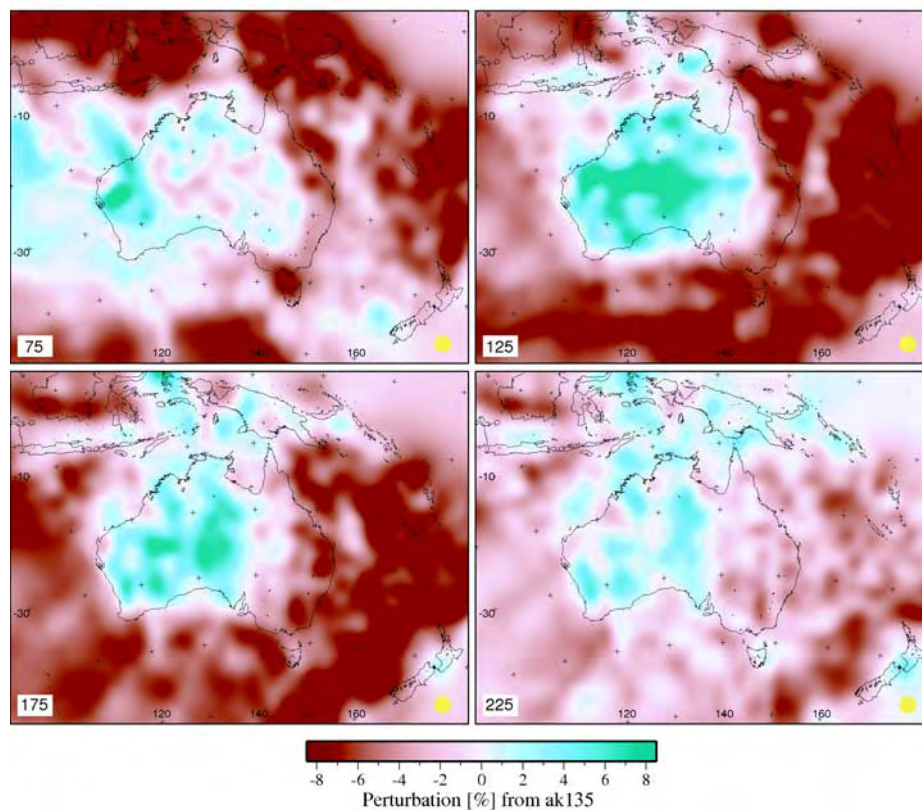


Figure 2: Shear wavespeed anomalies relative to the ak135 model.

The images of mantle shear wavespeed structure start at 75 km depth (Figure 2a) to minimise any influence from crustal structure, particularly from the zones of rather thick crust in the North Australian Craton and in southeast Australia. The maximum sensitivity of the Rayleigh waves at 50 s period (0.02 Hz) is located below the crust at 75 km depth, so that the surface-wave portion of the seismograms provides a dataset primarily sensitive to upper mantle structure. The deviations of shear wavespeed from the reference model are substantial, with higher wavespeeds generally in central and west Australia compared to the eastern margin of the continent.

At 75 km depth the pattern of seismic velocities is quite complex. There are zones of slower wavespeed in central Australia in the regions affected by the Alice Springs orogeny (~300 Ma) surrounded by faster S velocities. Most of western Australia has fast shear wavespeeds with the fastest velocities reached beneath the Capricorn orogen separating the Pilbara and Yilgarn cratons. The slower wavespeeds in the southwest of Australia at 75 km depth appear to correlate with the presence of a distinct gneissic terrain within the Yilgarn craton, also seen in receiver function studies (see 2003 Annual Report).

On the eastern margin of the continent, the shear wavespeeds are much lower than in central Australia and there is a fairly close correspondence with the regions with recent volcanism in the Newer Volcanics Province of Victoria and South Australia, extending into Bass Strait, and in the Atherton region of northern Queensland. The presence of the Lord Howe Rise is indicated by shear wavespeeds somewhat faster than its surroundings.

The pattern of wavespeeds in the mantle changes sharply by 125 km depth, and now the centre and west of the Australian continent are uniformly fast. The transition in central Australia, with depth, from modestly slow to fast wavespeeds is comparable to the available vertical resolution, and suggests a very rapid transition in material properties, rather than a change in thermal regime. At this depth the transition from elevated to lowered wavespeeds relative to the ak135 reference model extends to the east of the outcrop of Precambrian rocks, and so differs from most recent versions of the "Tasman Line". The Phanerozoic belt in eastern Australia has a thin zone of high wavespeeds in the lithosphere extending to about 100 km and beneath this there is a zone of lowered wavespeed which extends along most of the east coast of Australia, as seen in Figure 2(b),(c). The low seismic wavespeeds extend to the east beneath the Tasman Sea, where sea floor spreading ceases.

By 175 km depth (Figure 2c) the region of faster shear wavespeeds is concentrated to the west of 140° E. Within this zone there are clear indications of substructure in the sub-cratonic lithosphere; as, for example, the two distinct patches of fast wavespeed beneath the Yilgarn Craton. In the east, the zone of strongly lowered seismic velocities beneath the eastern margin of Australia and the Tasman Sea continues and is most likely associated with increased temperatures.

The general level of wavespeed contrast is significantly reduced at 225 km depth, Figure 2(d), for both fast and slow velocities. Nevertheless, there is still a distinct contrast in seismic wavespeeds across the continent, with a sharp gradient in seismic wavespeeds close to 140 E. There is only a small displacement from the corresponding transition at 175 km depth, so that the edge of the fast wavespeeds must have a relatively steep dip. High wavespeeds persist to at least 225 km over much of the cratonic region, notably beneath the Proterozoic North Australian Craton and in the Archaean Yilgarn. However, at greater depth new trends in faster wavespeed structure appear, e.g., a roughly east-west feature along the southern coast of Australia is present below 250 km. It is therefore difficult to define a clear base to the cratonic lithosphere from these surface wave results.

Regions such as the Kimberley Block in northwestern Australia appear to maintain a distinct character compared with their surroundings to significant depth. This suggests that the lithosphere is able to retain its character over very long periods of time and that there is the potential for using the nature of the seismic images to gain insight into the way the lithosphere might have been assembled.

As is apparent from Figure 2, the major change in mantle structure below 150 km depth occurs on an approximately north-south trend close to 140 E. To the west of this line the higher velocities extend coherently to 200 km or below, whilst to the east the area of elevated wavespeed hardly extends below 150 km, with a further step to thinner lithosphere along the eastern margin. It is possible that this set of transitions reflects the accretion of a continental block to the original core of Australia before the prominent Palaeozoic subduction events in the Lachlan Fold belt. There is no simple relation between the structures in the mantle and the conventional Tasman line that represents the eastern limit of surface exposure of Precambrian material.

Figure 2 shows the variation in seismic wavespeeds with no allowance for possible anisotropy and thus directional dependence of the speed of propagation of the Rayleigh surface waves. If sufficient crossing paths pass through a specific patch, we can use the variations in wavespeed as a function of direction of travel to extract estimates of the azimuthal anisotropy in shear wavespeed using an approximation based on near horizontal propagation of shear energy that is well satisfied by the fundamental mode contribution. To secure adequate data sampling we employ a 4 degree knot spacing in the inversion for azimuthal anisotropy and thereby confine attention to the longer spatial wavelengths in the seismic structure.

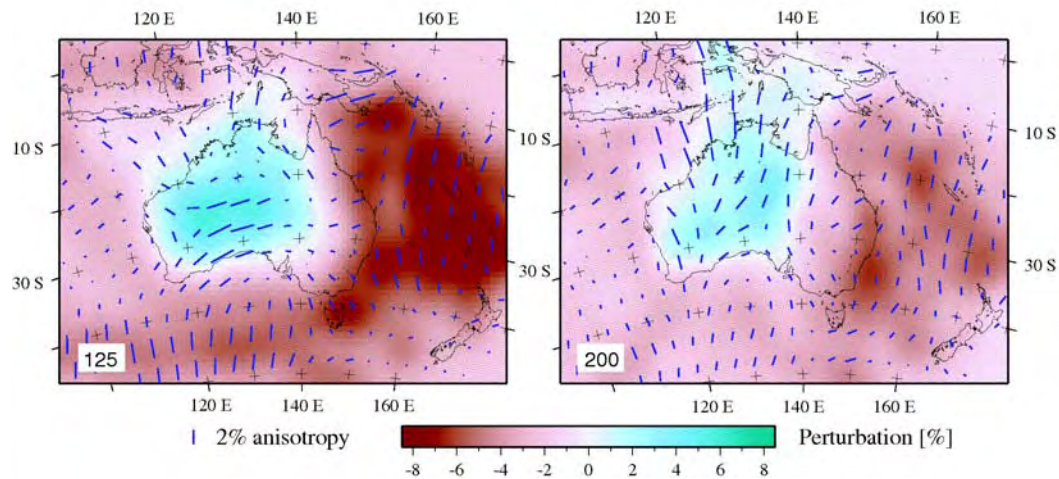


Figure 3: Inversion for azimuthal anisotropy for the rayleigh wavetrains, indicating a clear change in pattern in depth, with deeper directions more closely aligned to absolute plate motion.

The results of our inversion displayed in Figure 3 confirm the earlier studies of Debayle and Kennett (2000, 2003) that had more restricted path coverage. The pattern of azimuthal anisotropy across the continent shows a distinct change from a strong east-west component at around 100 km depth, likely to be due to "frozen" stress patterns, to a near north-south orientation at 200 km (close to the absolute plate motion). This change in the direction of the fast axis of the azimuthal anisotropy with depth, within the zone of faster wavespeeds, appears to be confined to the Australian continent. The change may well be a consequence of Australia's rapid motion northwards (approximately 7 cm/yr) imposing strains on the base of the lithosphere that induce orientation of mineral assemblages.

Body wave Anisotropy

M. Heintz

The structure of the upper mantle beneath the Australian continent is investigated using teleseismic shear-wave splitting to extract seismic anisotropy. Measurements have been performed on data recorded at 190 sites with portable broadband seismic recorders, covering almost the entire surface of the continent since 1992. The average time span of the various deployments, primarily designed for surface wave tomography, is six months, which is rather limited for shear wave splitting analysis. However, the data set does provide a full continental scale survey using the reasonably favourable distribution of seismicity from Australia. Seismic anisotropy has the potential to provide insights into the lithospheric structure and the possible mechanical coupling between the crust and the upper mantle, but prior results for Australia have indicated relatively small levels of splitting and a complex pattern of anisotropy from shear wave splitting. These results are confirmed with our new and far more extensive measurements across the whole continent.

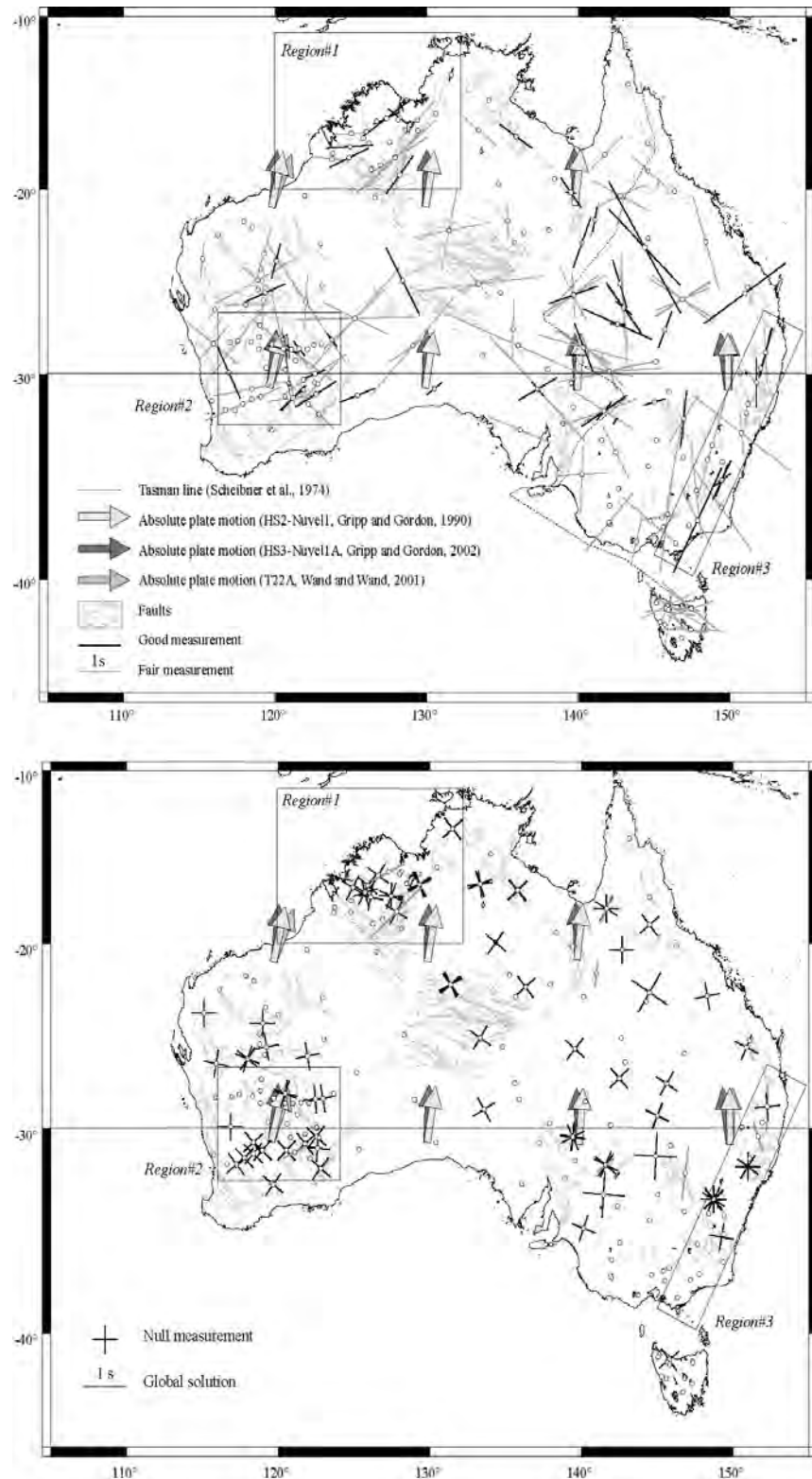
The observations of shear wave splitting of body wave phases (SK(K)S and PK(K)S) show little consistency at or between stations and is not correlated with the almost north-south absolute plate motion (APM) from recent models. Results from shear wave splitting analysis performed using the method of [1], together with the global solutions computed for a few stations using a set of events to solve for the splitting parameters [2], are shown below. The present study extends the preliminary results of [3] to a much larger number of stations spanning the whole continent.

Despite the good potential coverage of backazimuth with respect to the useful distance range (i.e. between 85 and 150°), the short time span of recording at most of the portable stations does not allow the recording of many events with large magnitude (>5.5) and good signal-to-noise ratio. The new Tasman Line project with a duration of 2 years may however allow the recording of more numerous suitable events.

At the continental scale, the pattern of anisotropy from shear wave splitting is rather complex, and we do not highlight any simple relation between the anisotropy and absolute plate motion (APM). If mantle flow is envisioned as the main source of anisotropy as suggested by the results obtained from surface waves [4],[5, 6] (at least below 150 km depth), we might consider rather complex deviations of the mantle flow around the numerous cratonic blocks building the continent to accommodate the nearly north-south APM of the Australasian plate with the scattered directions of anisotropy measured at the surface. Surface wave tomographic results suggest that the base of the lithosphere may well have a rather complex form. Mantle flow-related anisotropy can therefore not be completely ruled out.

Despite the limited geological outcrop, especially in Phanerozoic eastern Australia, that is almost entirely covered by sedimentary basins, and to the limited amount of reliable measurements, no direct correlation is seen between the measured orientation of the fast polarisation planes of shear waves relative to North and the known superficial structures. Having a closer look at the data, some correlations between the splitting parameters and the structural trends along, for instance, the Halls Creek orogen bordering the eastern edge of the Kimberley basin or along the New England and Lachlan fold belts in the southeastern part of the continent, may however be highlighted.

Figure 1: Directions of fast shear wavespeed.



In the Kimberley block (region #1, fig.1), the directions of anisotropy measured within the framework of the portable experiments (1997-1998) show various orientations. In the eastern part, the directions are oriented 50-60°, sub-parallel to the structural trend of the Halls creek orogen, whereas in the western part, the directions are close to 90° and are not obviously related to the structural trend of the King Leopold orogen. However, only one measurement per station has been considered as reliable along the King Leopold orogen, and splitting parameters can only be correctly interpreted in the context of a large number of measurements covering a range of backazimuths.

In the southern part of the Yilgarn cratonic block, two main directions of anisotropy are observed on both sides of 30°S latitude (region#2). The N40/50°W directions of anisotropy observed north of this line are parallel to some regional faults. South of 30°S latitude, a set of 10 stations recorded the same event (day 00341, latitude 39.57°, longitude 54.80°, depth 30 km, magnitude 7.5) and the coherence between the individual results per station is particularly striking because extending over 600km, whereas the pattern of anisotropy from shear wave splitting is usually expected to vary in continental areas that experienced long and complex history such as Precambrian platforms: all stations indeed exhibit a null result which corresponds either to an absence of anisotropy beneath the stations or to the polarization plane of the fast S-wave oriented N45/50°E or N40/45°W (fig.6c). A N40/45°W orientation of the polarisation plane of the fast S-wave would match pretty well to the global NW-SE trend of the faults in the southwestern part of the Yilgarn craton; however, despite the good consistency of the results at the deployment scale, no firm interpretation can be envisaged on the basis of a single measurement per station.

The results from permanent stations, with a long span of recording, are essentially null (see [7-10]). The pattern of azimuthal anisotropy derived from surface waves is, on the other hand, striking. It is possible that the changes in azimuthal anisotropic properties revealed by the surface waves lead to very little net splitting for a wave travelling nearly vertically. Due to the different wavelengths of both types of waves, they are not sensitive to the same structures, and the superficial structures of the continent vary at such a short scale that it is not possible to compare both sets of results. The two sets of observations may either emphasize different phenomena, or indicate a much more complex form of anisotropy.

REFERENCES

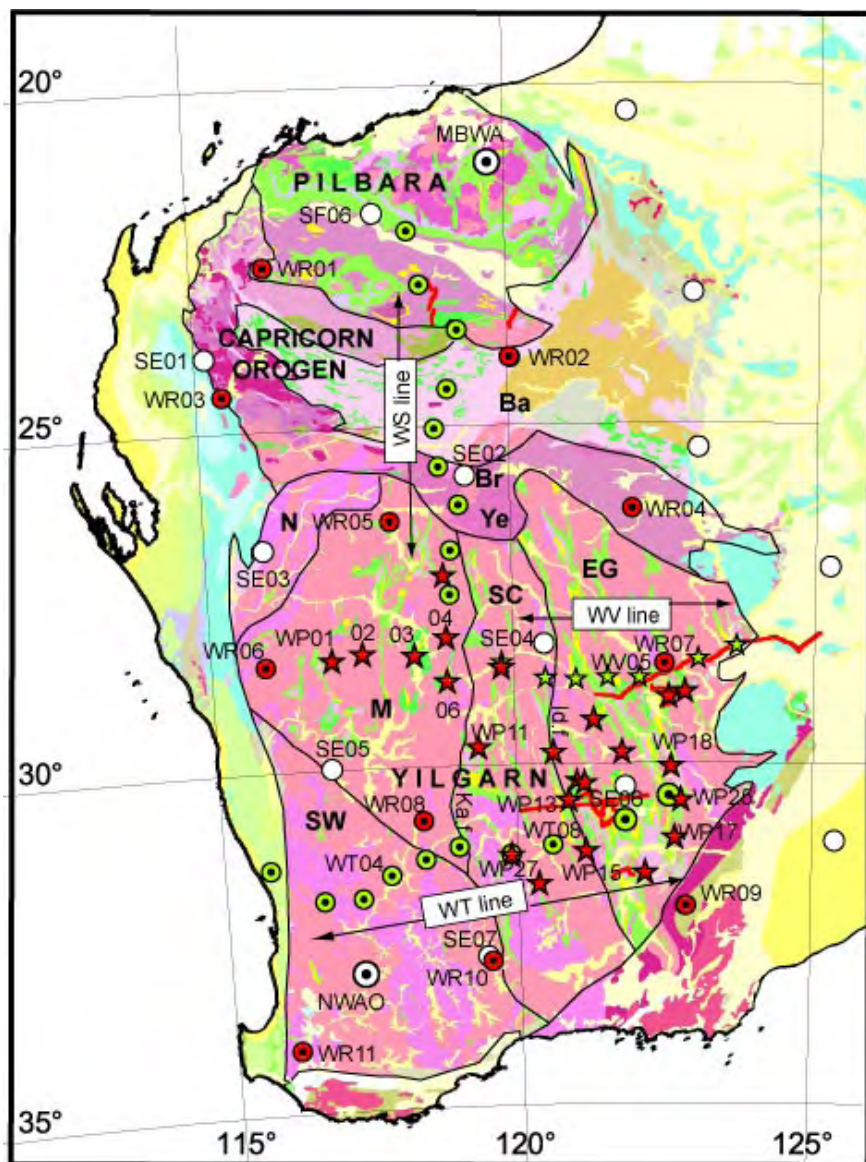
- [1] P.G. Silver and W.W. Chan, Shear wave splitting and subcontinental mantle deformation, *Journal of Geophysical Research* 96(B10), 16429-16454, 1991.
- [2] C.J. Wolfe and P.G. Silver, Seismic anisotropy of oceanic upper mantle : shear wave splitting methodologies and observations, *Journal of Geophysical Research* 103(1), 749-771, 1998.
- [3] G. Clitheroe and R.D. Van der Hilst, Complex anisotropy in the Australian lithosphere from shear-wave splitting in broad-band SKS records, *AGU Monograph Series*, 1997.

- [4] E. Debayle and B.L.N. Kennett, The Australian continental upper mantle : structure and deformation inferred from surface waves, *Journal of Geophysical Research* 105(11), 25423-25450, 2000.
- [5] F.J. Simons, A. Zielhuis and R.D. Van Der Hilst, The deep structure of the Australian continent from surface wave tomography, *Lithos* 48, 17-43, 1999.
- [6] E. Debayle and B.L.N. Kennett, Anisotropy in the Australian upper mantle from waveform inversion, *Annales Geophysicae* 16, 37, 1998.
- [7] L.P. Vinnik, L.I. Makeyeva, A. Milev and A.Y. Usenko, Global patterns of azimuthal anisotropy and deformations in the continental mantle, *Geophysical Journal International* 111(3), 433-447, 1992.
- [8] N. Girardin and V. Farra, Azimuthal anisotropy in the upper mantle from observations of P-to-S converted phases; application to Southeast Australia, *Geophysical Journal International* 133(3), 615-629, 1998.
- [9] G. Barruol and R. Hoffmann, Upper mantle anisotropy beneath Geoscope stations, *Journal of Geophysical Research* 104, 10757-10773, 1999.
- [10] S. Ozalaybey and W.P. Chen, Frequency-dependent analysis of SKS/ SKKS waveforms observed in Australia; evidence for null birefringence, *Physics of the Earth and Planetary Interiors* 114(3-4), 197-210, 1999.

RECEIVER FUNCTION STUDIES

A.M. Reading, E.Saygin, B.L.N. Kennett, M. Heintz

The deep crustal structure across the West Australian Craton has been determined using receiver function analysis of broadband records from temporary seismic stations. These stations were deployed in a series of experiments using both widely-spaced station configurations and denser coverage in the form of lines/groups of stations. Data from the permanent stations, MBWA and NWAO, were also included. The improved coverage obtained from the combined deployments allows investigation of seismic structure over the whole craton at a resolution greater than the scale of the main terrane groups. We are thus able to investigate the variations in crustal structure across the West Australian Craton in terms of craton assembly and crustal evolution.



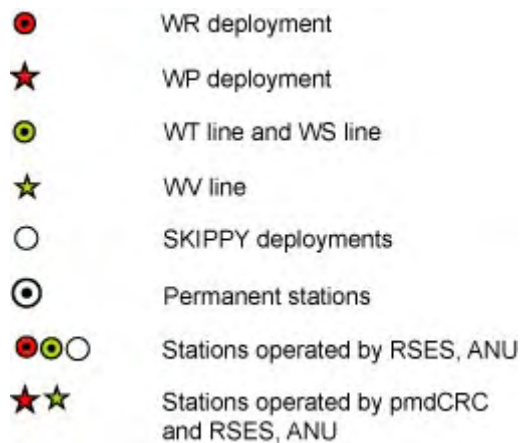
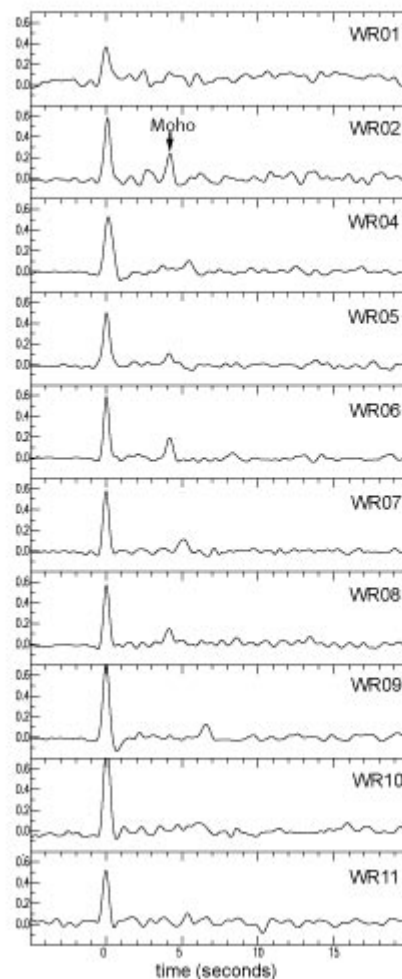


Figure 1: Receiver functions studies in western Australia

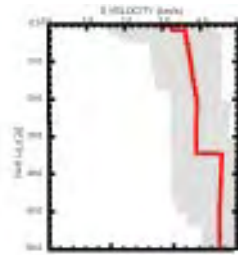
We find remarkable consistency of structure within several of the individual Precambrian terranes, most notably the Pilbara, Murchison and Southern Cross. Some systematic variability in seismic structure exists across more extensive terranes, notably towards the edge of the craton. The structure beneath orogenic belts is more variable and shows a less pronounced seismic Moho.

Figure 2: Variation of receiver functions for WR stations

We confirm that receiver function methods can be used to delineate the extent of Precambrian terranes in regions where geological exposure of the surface is limited and provide an effective alternative to active source seismic techniques for deep crustal targets

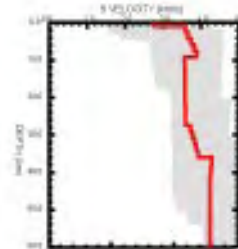


Murchison



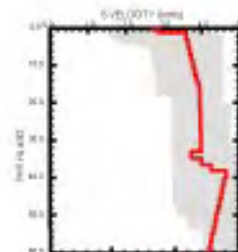
Moho depth 34 km (e.g. WR06)
Very sharp
Simple upper crust
Low velocity in lower crust
Structure very consistent across terrane

Southwest



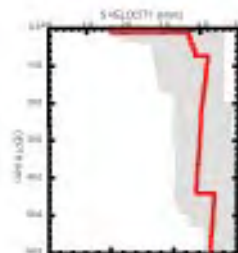
Moho depth 36 km (e.g. WT04)
Sharp away from terrane edges
Discontinuity in upper crust
High velocity gradient zone above Moho
HVGZ thickens towards the west

Southern Cross



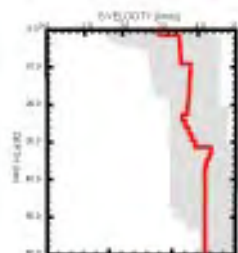
Moho depth 38 km (e.g. WT08)
Very sharp
Simple upper crust
Constant velocity lower crust
Structure consistent across terrane

Eastern Goldfields



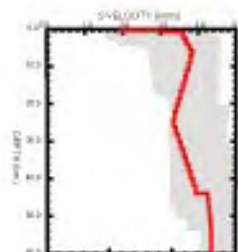
Moho depth 42 km (e.g. WW05)
Moderately sharp
Discontinuity in upper crust
Lower crust velocity gradients variable
Structure generally very variable
Moho much shallower towards the south

Pilbara



Moho depth 32 km (e.g. MBWA)
Very sharp
Discontinuity in upper crust
Low velocity in lower crust
Moho deeper in the south of the craton

Capricorn Orogen



Moho depth 44km (e.g. WR04)
Broad
Discontinuity in upper crust
Velocity gradient throughout lower crust
Structure variable
Moho sometimes hard to define

Figure 3: Summary of variation in crustal character across Western Australia terranes.

LITHOSPHERIC STRUCTURE OF TASMANIA FROM TELESEISMIC TOMOGRAPHY

N. Rawlinson, A.M. Reading and B.L.N. Kennett

The tectonic evolution of Tasmania (SE Australia) in the early to mid Palaeozoic and its relationship with the Phanerozoic terranes of eastern mainland Australia is not well understood, due in part to a lack of information on the deep structure and composition of its lithosphere. In 2001 and 2002, an array of 72 short period and broadband seismic recorders with a nominal spacing of 15 km was deployed across northern Tasmania (Figure 1), with the aim of imaging the underlying crust and upper mantle using 3-D teleseismic travelt ime tomography.

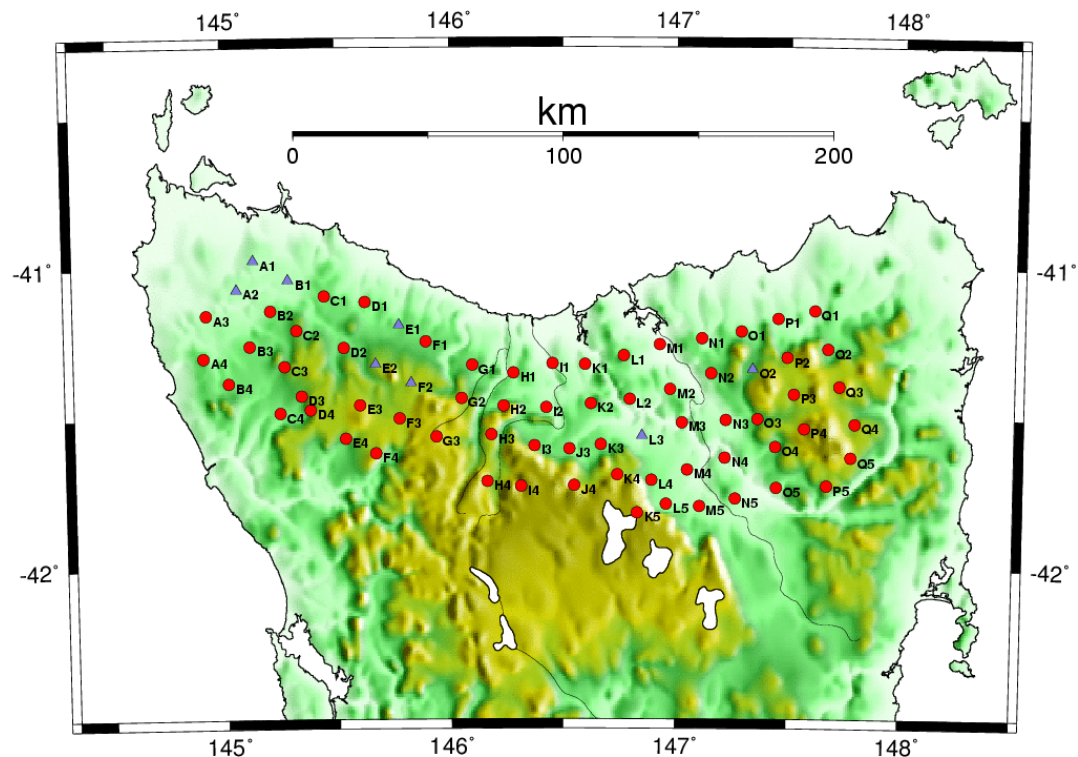


Figure 1: Locations of the 64 short period (red dots) and eight broadband (purple triangles) stations that comprise the TIGGER seismic array in northern Tasmania.

Using a recently developed and robust adaptive stacking technique, a total of 6520 (see Figure 2) relative P-wave arrival times have been picked from 101 distant earthquake records spanning a four month period. A new iterative non-linear tomographic procedure based on a subspace inversion scheme and the fast marching method (FMM), a grid based eikonal solver, is used to map residual patterns as P-wave velocity anomalies. The resultant images show significant lateral perturbations in P-wave velocity structure (up to 10%) from a modified ak135 reference model (Figure 3).

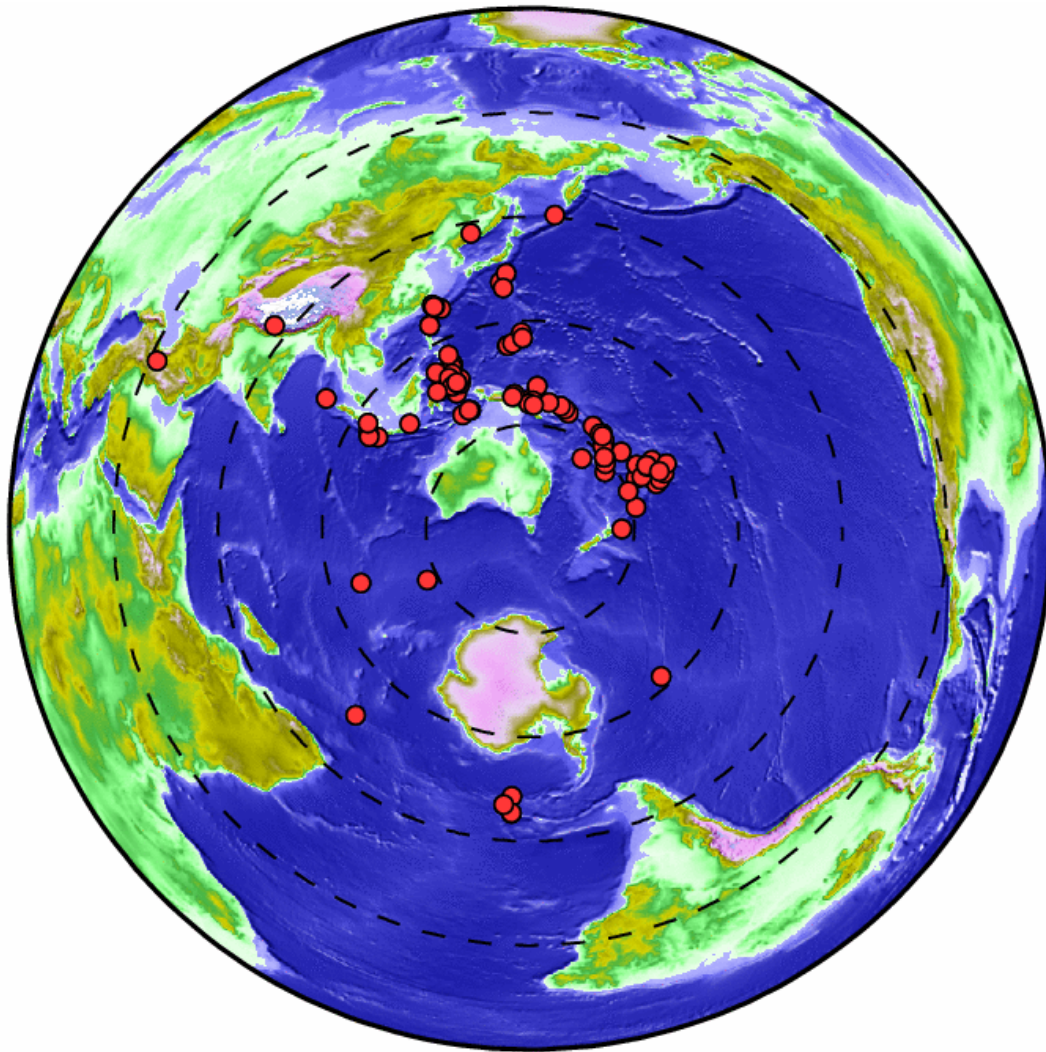


Figure 2: Distribution of the 101 teleseismic events (red dots) used in the tomographic inversion for the 3-D seismic structure beneath northern Tasmania. Dashed circles represent equidistant curves from the centre of the TIGGER array contoured at 30 degree intervals.

Geological inferences made from the TIGGER results include: (1) Within the crust, the first-order E-W velocity variations strongly support the idea that eastern Tasmania is underlain by dense rocks with an oceanic crustal affinity, contrasting with the continentally derived siliciclastic lower crustal rocks of western Tasmania; (2) there is no evidence to support the presence of a crustal scale suture zone (the "Tamar Fracture System") in the vicinity of the Tamar river; (3) an easterly dipping zone of high velocity material beneath the Rocky Cape Group and Arthur Lineament may be related to remnant subduction of oceanic lithosphere associated with the mid-Cambrian Delamerian Orogeny, which played a major role in the Phanerozoic subduction-accretion assemblage of eastern Australia.

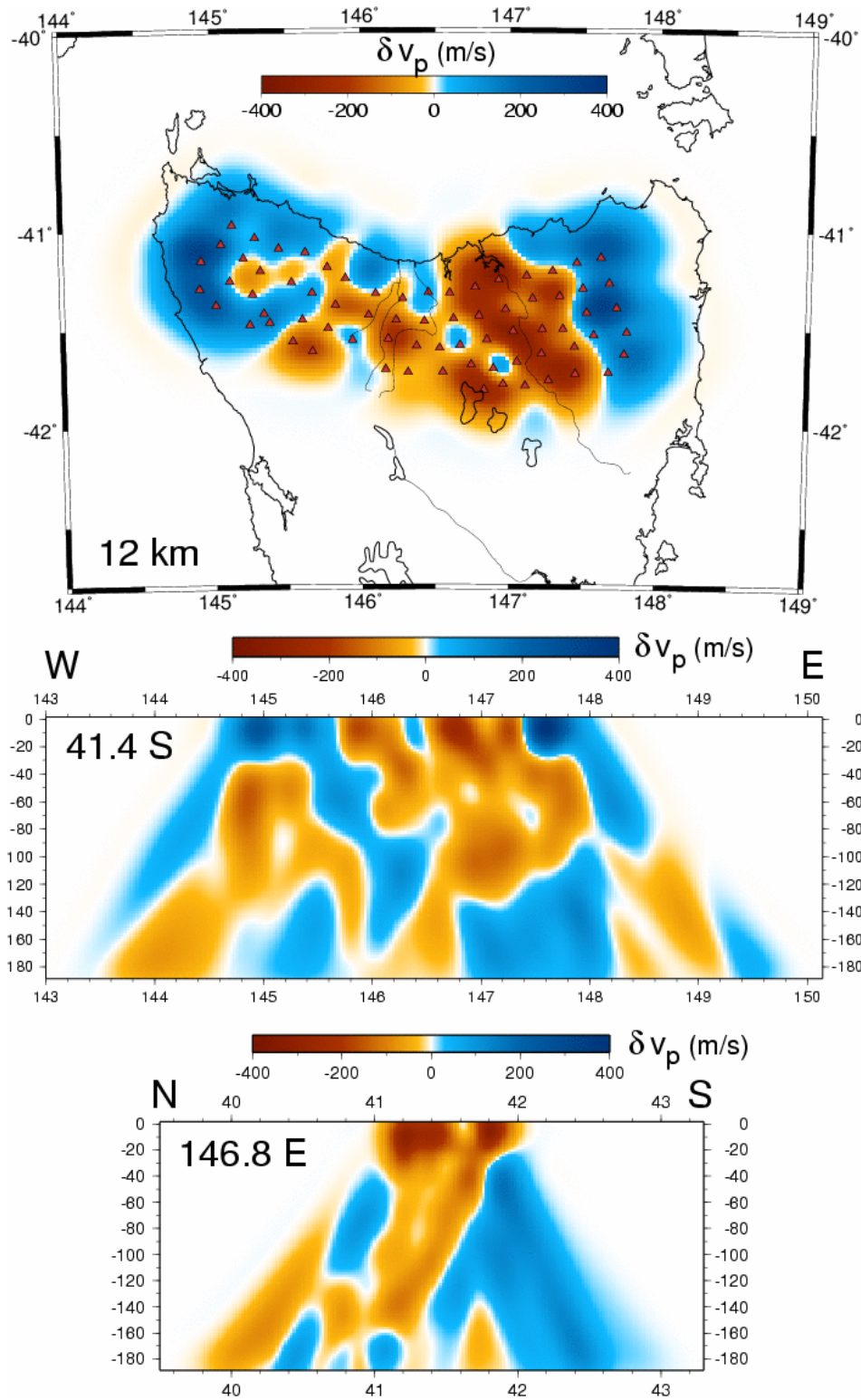


Figure 3: Slices through the 3-D teleseismic tomography model of northern Tasmania. P-wave velocity perturbations are shown relative to a modified form (adjusted using crustal velocities from a refraction survey) of the ak135 global reference model. Note the E-W trend of fast-slow-fast velocities in the crust, and the easterly dipping "slab" of elevated velocity in the lithospheric mantle between 145 and 146.5 E.

THE SEAL EXPERIMENT

N. Rawlinson, B.L.N. Kennett and M. Heintz

The SEAL (South East Australia Linkage) experiment began in November 2004 with the deployment of 20 vertical component short period seismometers in southern New South Wales and northern Victoria (see Figure 1) for a period of approximately five months. The main purpose of SEAL is to link together past and future high density passive seismic arrays to provide continuous coverage of teleseismic data across a large region of south east Australia. As shown in Figure 2, SEAL spans the MALT (1998-2000), QUOLL (1999) and EVA (scheduled for 2005) arrays, and covers an important region of the continent which includes the transition from the Delamerian Orogen to the Lachlan Orogen, and parts of the Stawell, Bendigo, Melbourne and Tabberabbera Zones.

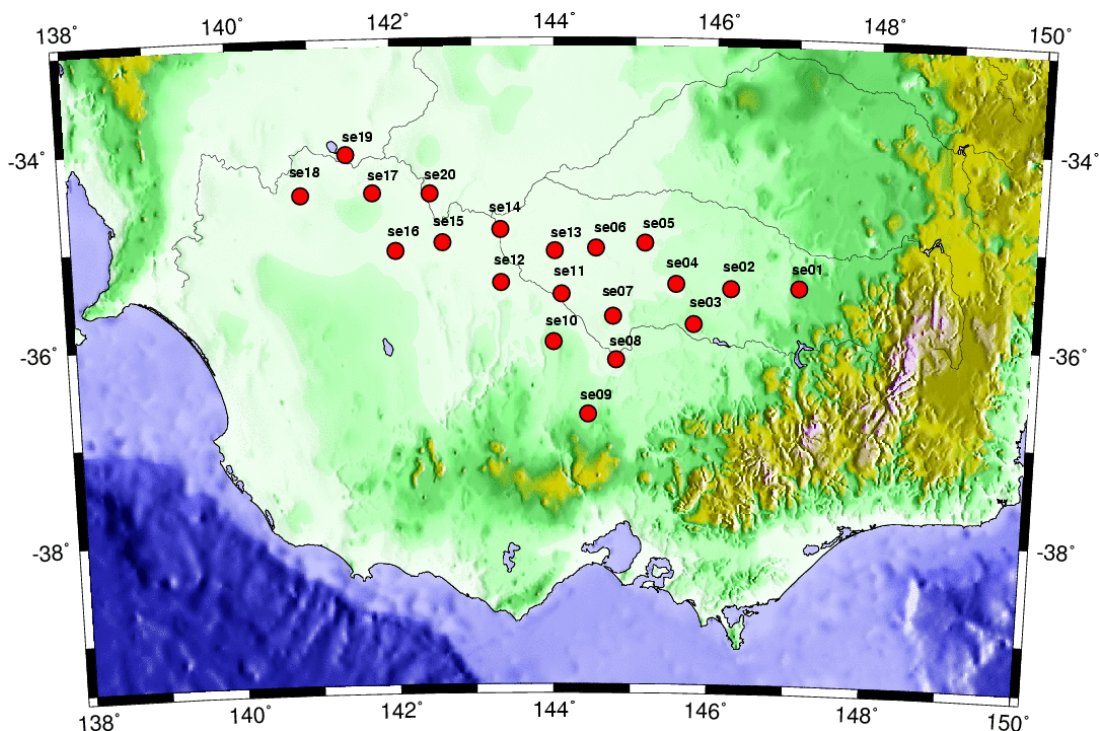


Figure 1: Locations of the 20 short period stations that make up the SEAL experiment.

Although SEAL will be used to independently assess the structure of the upper mantle using 3-D teleseismic tomography, the ultimate goal is to combine teleseismic data from all stations shown in Figure 2 in a joint inversion for the high resolution structure of the lithosphere beneath south east Australia. This will help us to answer fundamental geological questions about the Phanerozoic evolution of eastern Australia

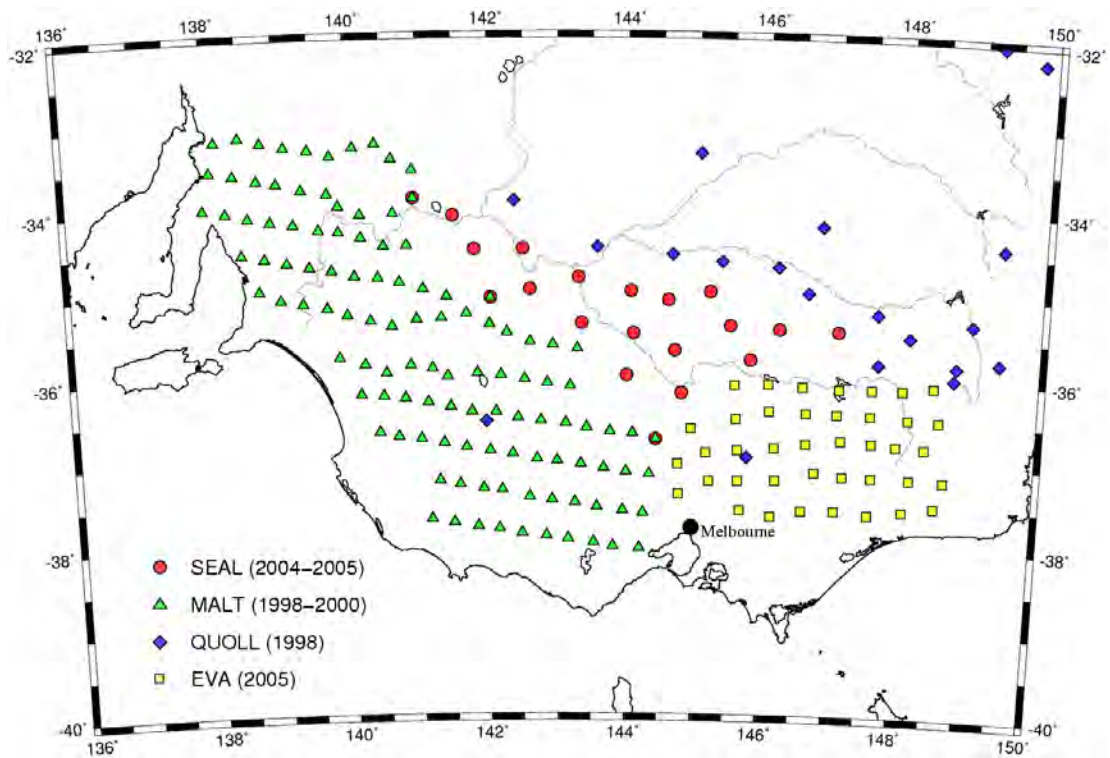


Figure 2: SEAL links together past and future teleseismic array experiments. Combining teleseismic data from all four arrays will allow tomographic images of unprecedented detail to be constructed.

ANTARCTIC STUDIES

A. Reading

During the Antarctic summer of 2004/05, most of the SSCUA broadband stations installed in East Antarctica (2002/03/04) were retrieved. Data from the majority of stations are excellent, although aircraft problems prevented any access to the two most southerly sites. The aims of the SSCUA deployment, to find out more about 1) The tectonic structure and history and 2) the neotectonics and mantle dynamics of East Antarctica, may now be addressed through the processing and interpretation of this unique dataset.

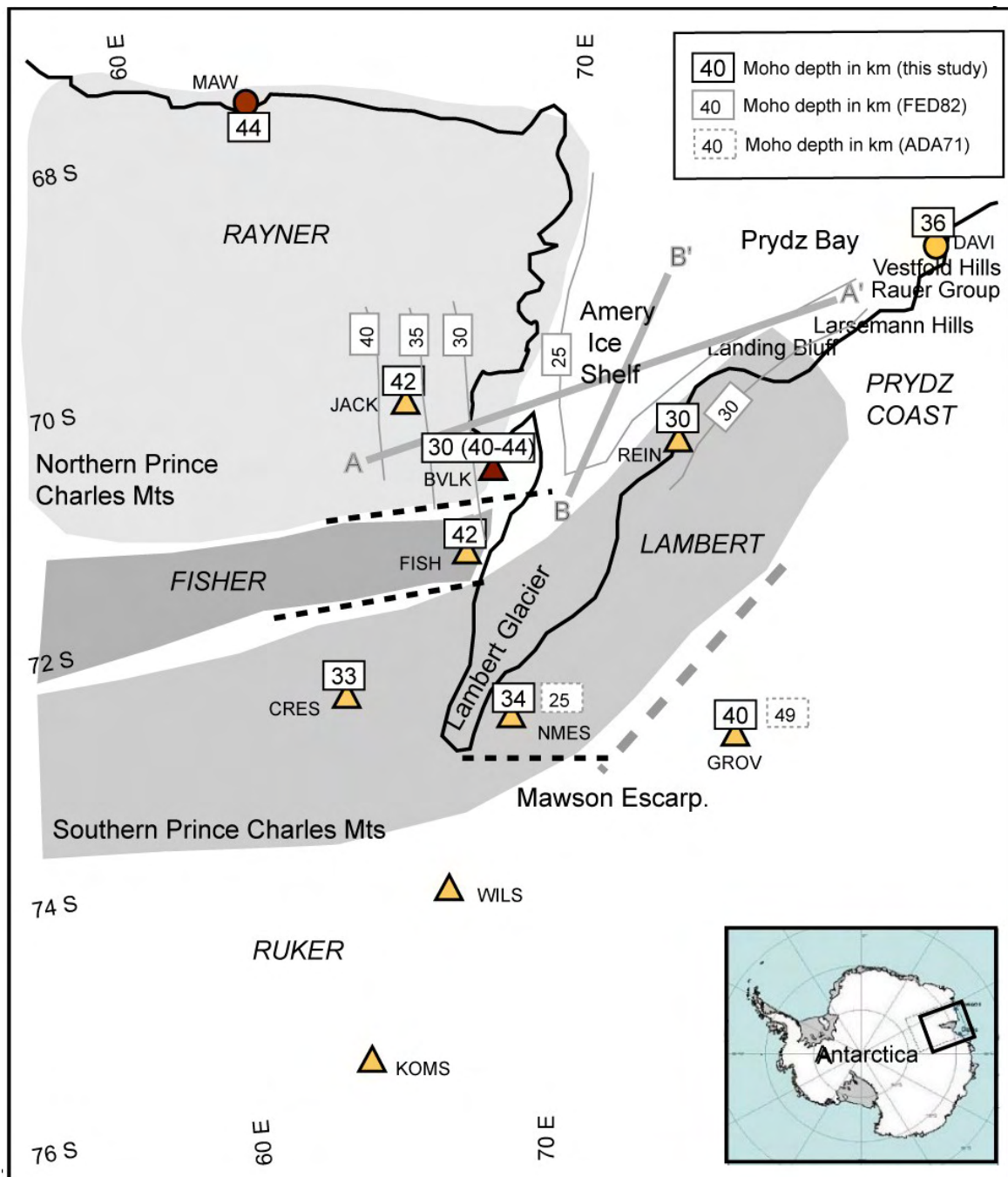


Figure 1: Moho Depth derived from receiver function modelling

Figure 1 shows the results of receiver function modelling for Moho depth across the region of the deployment. A major tectonic province boundary was found between stations FISH and CRES and may mark the southern extent of the pre-Gondwanan continent of greater India. The Moho beneath GROV, in the Grove Mountains, shows a very different structure from NMES, in the Northern Mawson Escarpment. Other data analysis, e.g. modelling surface waves to deduce the structure in the upper mantle, is in progress.

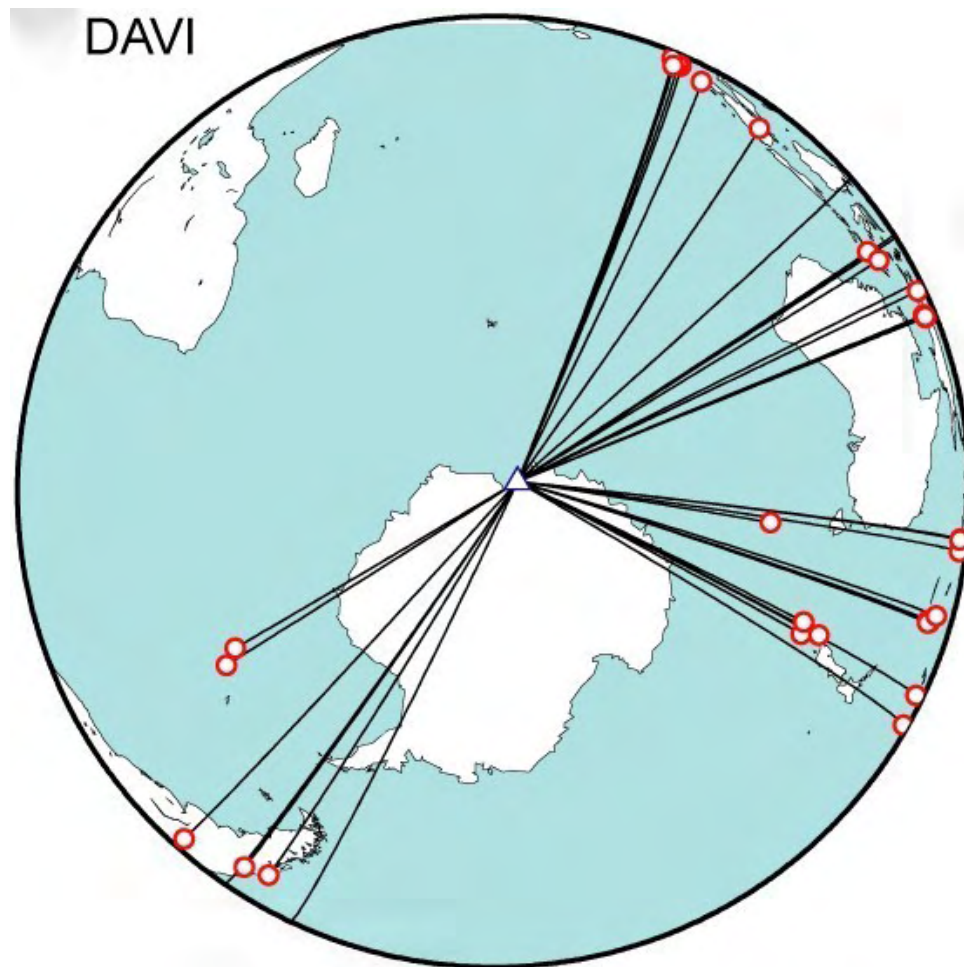


Figure 2: Events recorded at Davis station

Recording continues at the mains-powered station DAVI, at Davis, the Australian Antarctic Division year-round base. Figure 2 shows well-recorded source-receiver paths to date.

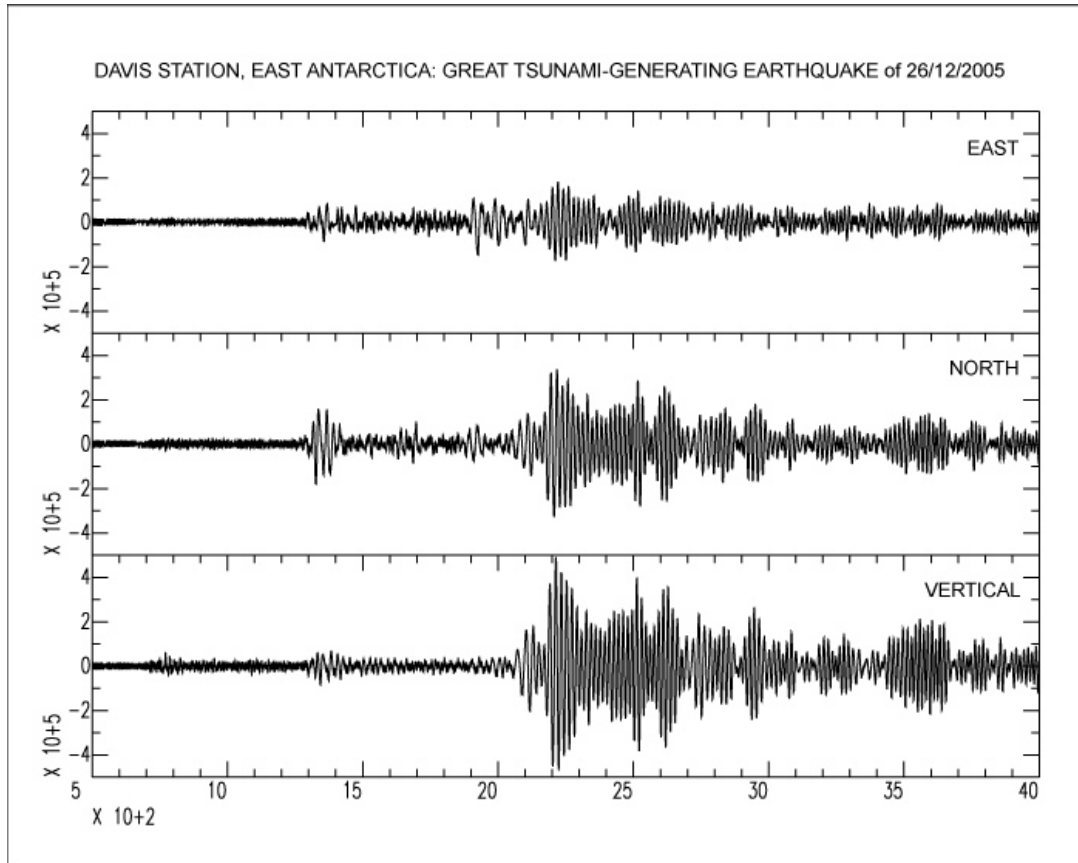


Figure 3: The great Sumatara-Andaman earthquake of 2004 December 26 as recorded at Davis station

Figure 3 shows a three-component record of the great earthquake of 26/12/2005, which generated a devastating Tsunami, recorded at DAVI. Wild-life is present at all but the most remote sites in Antarctica. Figure 4 shows an Adelie penguin 'inspecting' a broadband station equipment set after retrieval.



Figure 4: Inquisitive penguin

Multiple phases in 3-d with the fast marching method

M. de Kool, N. Rawlinson, M. Sambridge

A new scheme based on the Fast Marching Method (FMM) in spherical coordinates has been developed to track phases comprising any number of reflection and transmission branches in 3D layered media. A multi-stage approach which treats each layer that the wavefront enters as a separate computational domain is used. At each interface, FMM is reinitialized to track the impinging wavefront as either a reflection back into the incident layer or a transmission through to the adjacent layer. Notably, the method does not require an irregular mesh to be constructed in order to connect interface nodes to neighbouring velocity nodes which lie on a regular grid. To improve accuracy, local grid refinement is used in the neighbourhood of a source point where wavefront curvature is high.

In addition to computing simple refracted waves, reflected waves and more complex multiples, reflections which are not the first to arrive (e.g. the global PP phase) can also be tracked. The new scheme also allows various global phases from distant events to be computed through a spherically symmetric earth model to the boundary of a local 3-D model, after which FMM is used. This feature is useful for teleseismic tomography. Finally, conversions between P and S phases at interfaces can also be tracked.

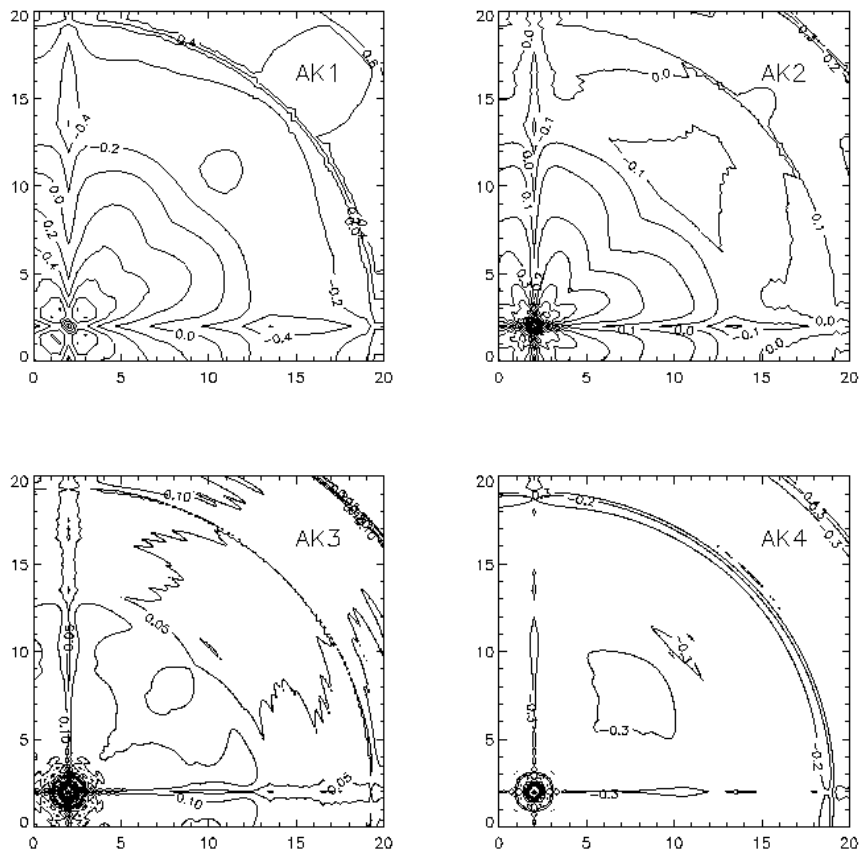


Figure 1: Summary of P-wave arrival time errors in the ak135 reference model using the new scheme. All four cases model a region extending 20 degrees in latitude and longitude and 1000 km in depth. The source is located at 100 km below the surface. AK1 - 21x41x41 nodes; AK2 - 41x81x81 nodes; AK3 - 81x161x161 nodes; AK4 - 81x161x161 nodes. Models AK1-AK3 explicitly include interfaces, while AK4 does not. Contour labels are in seconds.

A series of systematic tests have been carried out with the new method in order to verify its accuracy, efficiency and robustness. In particular, it has been shown that various global phases can be computed to an acceptable accuracy through the ak135 reference model (see Figure 1). The scheme can also be used to track complex crustal phases that may be encountered in coincident reflection, wide-angle reflection/refraction or local earthquake surveys. Figure 2 shows a variety of phases that have been tracked in the presence of a realistic subduction zone, which includes several layer pinch-outs and a subducting slab. Our numerical tests show that the new scheme is a practical and robust alternative to conventional ray tracing for computing a range of phases in layered media at a variety of scales.

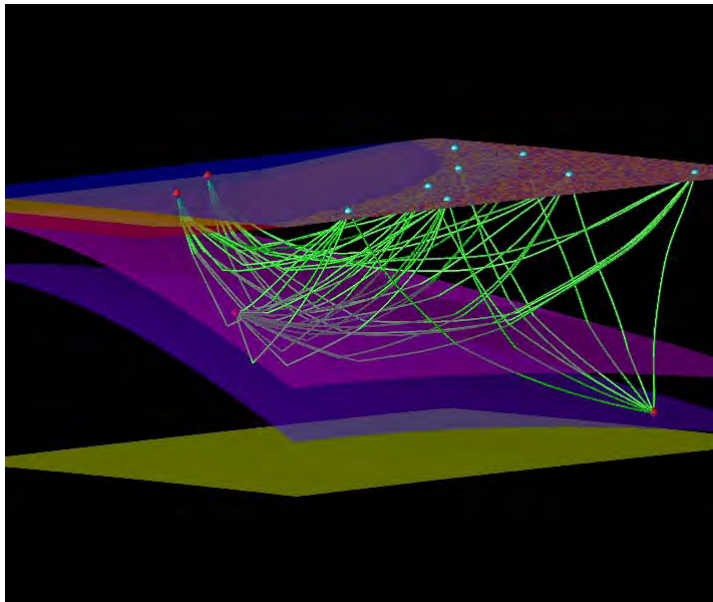


Figure 2: Ray paths in a complex layered geometry. The model consists of a coast line, a sediment layer beneath the ocean, continental crust, oceanic crust subducting under the continent, and part of the upper mantle. Seismic sources are represented by red diamonds, receivers by blue spheres. Two of the sources are on the ocean surface, another two are located in the subducting slab. An array of eight receivers is distributed over the land area. Velocity is laterally inhomogeneous in the continental crust. A selection of ray paths representing direct arrivals and reflections from the top and the bottom of the subducting slab is shown.

The complete software package is freely available on the Internet at: <http://rses.anu.edu.au/seismology/fmmcode/>

The relationship of the seismic source and subduction zone structure for the 2004 December 26 Sumatra-Andaman Earthquake

B.L.N. Kennett, P.R. Cummins [*Geoscience Australia*]

Studies of the 2004 December 26 Sumatra-Andaman earthquake indicate that the rupture and subsequent down-dip slip of the Mw 9.3 event propagated with variable speed as it progressed northwards.

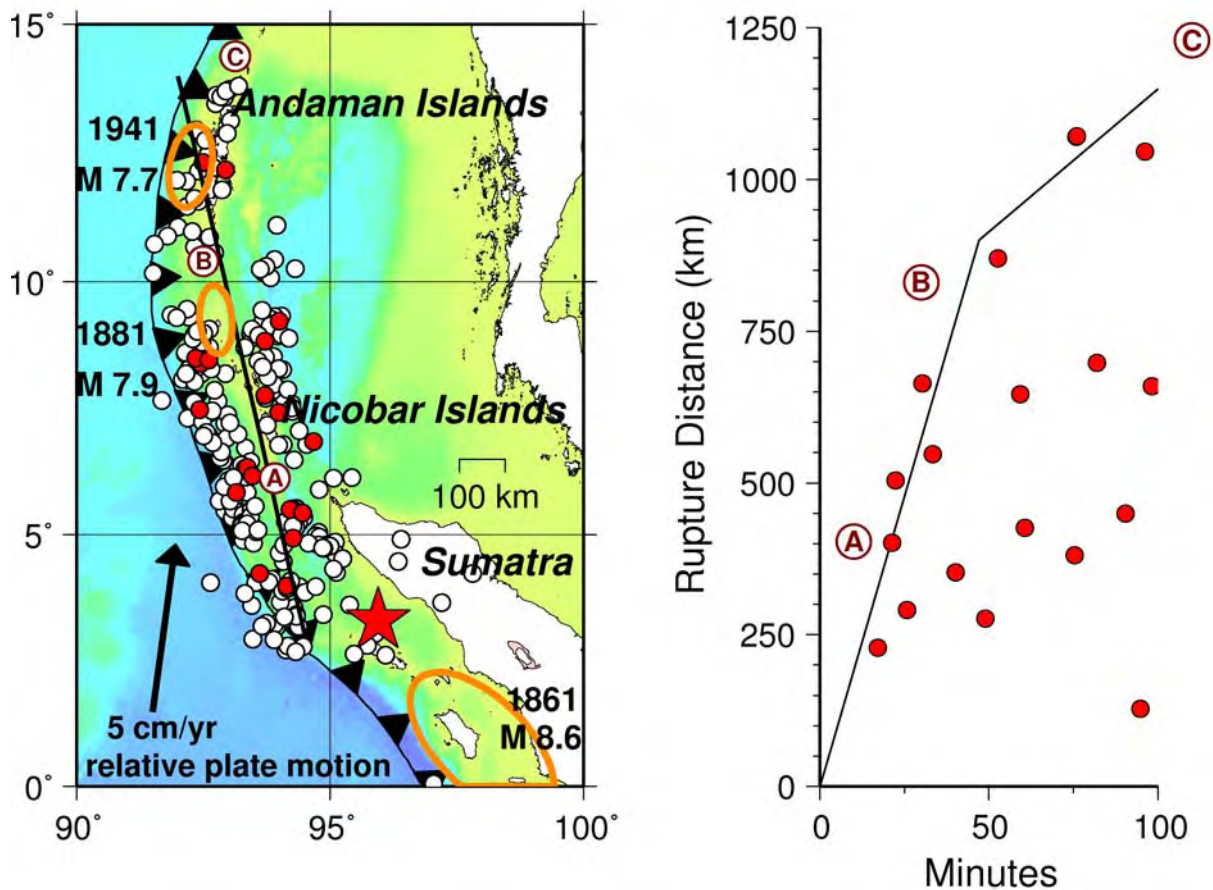


Figure 1: The aftershocks of the 2004 December 26 event, in the 60 days after the earthquake, superimposed on a topographic map of the Sumatran-Nicobar-Andaman arc. The deep basin behind the arc has been produced by back-arc spreading in the Andaman sea. The shallower water to the west marks the northern extremity of the 90E ridge. The approximate rupture areas of major historical earthquakes are outlined (after Bilham). The Great Sumatran Earthquake of 2005 March 28 (Mw 8.7) initiated at the northern end of the 1861 rupture area. **A** corresponds to the area originally suggested as the northern limit of rupture from body-wave inversions, but which now appears to be a temporary reduction in slip, **B** to the end of the main tsunamigenic segment and the likely terminal point for the highest frequency radiation, and **C** indicates the northern extension required to match geodetic and low frequency normal-mode observations. The aftershocks occurring within the first 100 minutes following the earthquake are plotted in red and the others in yellow. The rate at which the occurrence of aftershocks spread out along the

strike of the rupture area (as indicated by the heavy black line on the map) is shown in the righthand panel, where it can be seen that a change in the onset of aftershock occurrence occurs close to point **B**.

The transitions between different behaviour for the source correspond to changes in the physical properties of the subducted slab along the Sumatra-Andaman arc revealed by multi-wavespeed seismic tomography. For the Sumatra to Andaman arc segment the presence of sources within the slab provide useful constraints on the structure and careful resolution tests (as in [19]) indicate that resolution of the order of 1 degree or better can be achieved along most of the arc, between 50 and 200 km depth. The low level of shallow seismicity means that there is little capacity to image above 50 km.

The tomographic images reveal both changes in the shape of the subducted slab progressing from Sumatra to the Andaman Islands, and variations in the physical properties of the slab material.

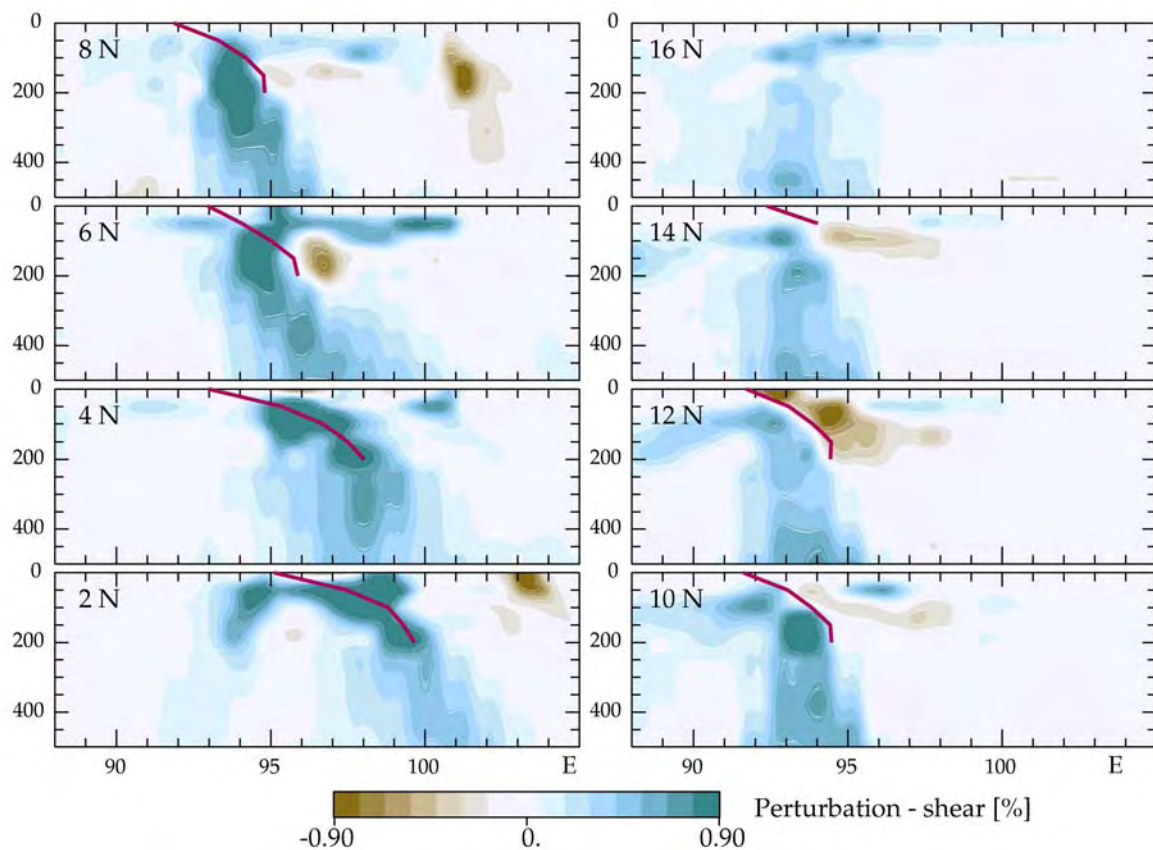


Figure 2: East-west cross-sections through the S wavespeed model displayed as deviations from the ak135 reference model. The subducted slab shows up through faster shear wavespeeds. Note the intrusion of a shallow low velocity zone at 12N linking across to beneath the back-arc spreading centre at 95E.

The superimposed dark red line in each section is taken from the representations of the upper surface of the subduction zone derived from seismicity patterns by Gudmundsson and Sambridge. The two independent estimates of the shape of the subduction zone agree very well.

The transition from rapid slip to dominantly slower slip near 6.5N and the end of the main zone of tsunamigenic source at 10N lie in each case just to the south of localised features where changes in the physical properties of the slab are indicated from the ratio of shear wavespeed to bulk sound speed, these features are associated mainly with bulk-modulus variations. The changing morphology of the subduction zone is associated with changes in physical properties, that are manifest in the tomographic images and have modified the character of the slip along the 1500 km long arc segment that ruptured during this great earthquake.

The cross-sections at 2N and 4N are somewhat oblique to the trend of the subduction zone, but still illustrate clearly the presence of a shallowly dipping segment down to around 150 km with steeper dip at greater depth. From 6N northwards the line of section is close to orthogonal to the subduction zone and so the apparent dip is more representative of the actual situation. Between 6N and 8N we see a distinct steepening of the dip of the deeper part of the slab.

In the section from the Nicobar to the Andaman Islands from 10N the slab becomes nearly vertical at intermediate depth. This geometry for the subducted slab is presumably a result of slab roll-back associated with the formation of the Andaman back-arc basin and spreading centre.

The changes in the morphology of the slab are accompanied by changes in the physical properties of the slab material as can be through the ratio of shear wavespeed and bulk-sound speed.

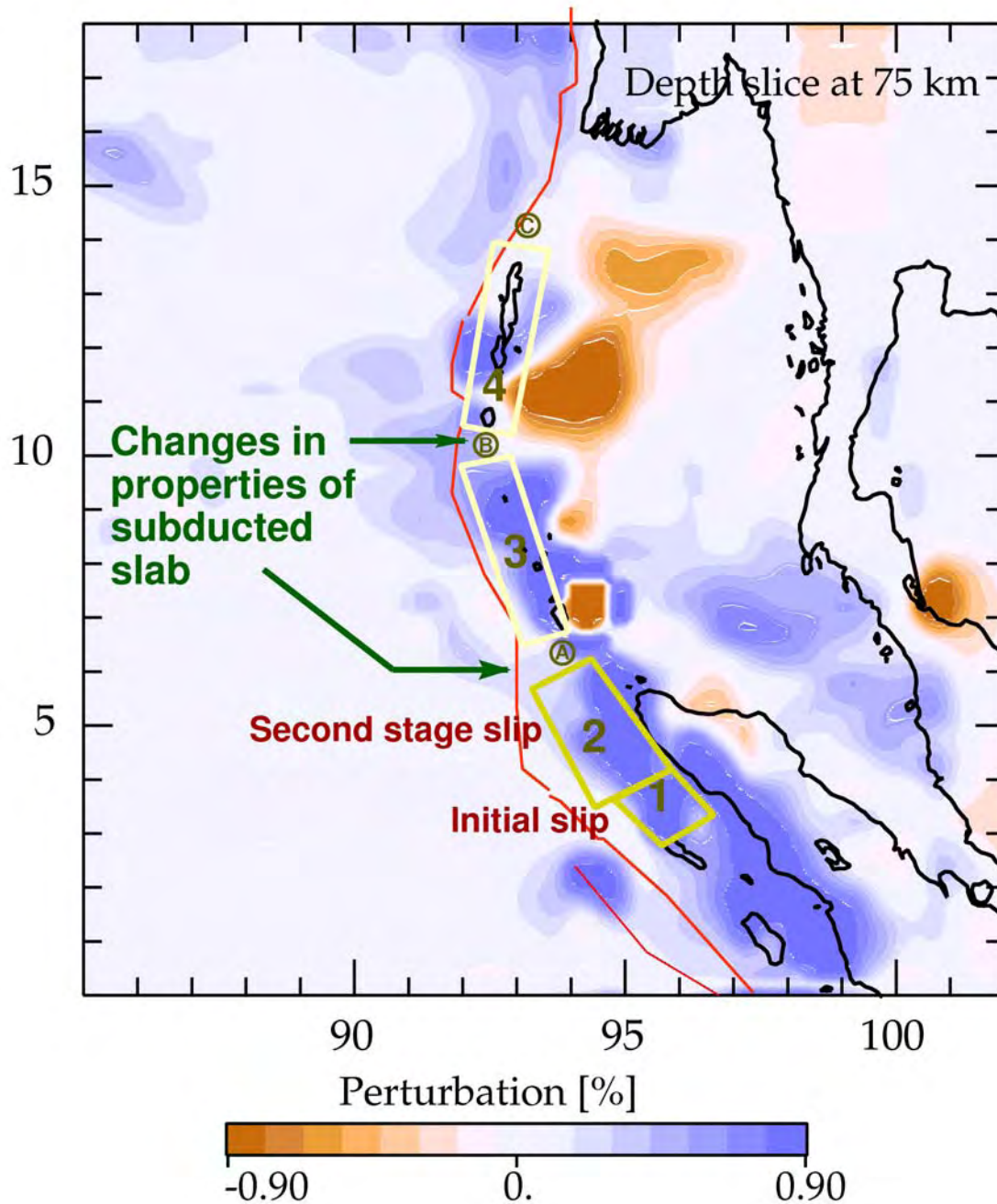


Figure 3: Contrasts in the ratio of shear wavespeed and bulk-sound speed at 75 km derived from joint tomography and their correspondence with changes in the character of the earthquake source.

We can summarise the source character for the 2004 December 26 event through a sequence of four source segments as in Figure 3. Rupture along the entire zone from 1 to 4 is indicated from the distribution of aftershocks. A common feature of the different representations of the rupture process for the 2004 December 26 event is a division into segments with a change of strike and rupture properties near points A and B in figure \ref{fse06} [12,13]. We envisage the faulting as occurring at the upper surface of the

subducting plate and differences in coupling with the overlying plate should play a major role in determining slip rate.

Nevertheless we find a strong correlation with the features of the tomographic images of subduction zone structure in the upper part of the steeper segment of the slab, particularly when we allow for the oblique convergence along the arc (Figure 3). There are clear modifications in the physical properties at the top of the subducting plate near point **A** (at 7N) and point **B** (at 10N). The northern feature **B** seems to link to the spreading system in the back arc basin, but feature **A** is distinct and separated.

The zones of modified physical properties revealed by the multi-wavespeed seismic tomography, may well correspond to accommodation zones to slab deformation in roll-back or to incipient tears imposed by the geometry of the subduction. It is likely that the differences in physical properties that we have been able to image below 50 km, thanks to the presence of intermediate depth earthquakes, extend back into the shallower portions of the slab, which we are not able to image (because there were few shallow events in the last 30 years).

The 1500 km long rupture zone crosses three distinct slab regimes and these contribute to the detailed behaviour of this great earthquake. The propagation of the rupture front for the thrust component along the interface between the slab and the overlying plate is affected by the physical properties and geometrical configuration of the slab, leading to barriers that have to be overcome before the next segment comes into action. These barriers are dictated by the nature of the subducted slab itself, and we can see their influence where the slab signature at greater depth is modified.

A typical horizontal length scale for a distinct segment of a subduction zone is around 500 km, and changes in the physical properties of the slab are likely to modify, or stop, rupture even in a mega-thrust event. This will give events of magnitude up to about Mw 8.8 for a 500 km long rupture. Only for a truly great earthquake such as the 2004 Aceh-Andaman event is there sufficient energy in rupture to overcome multiple physical barriers within the slab.

ANSIR

Director: B.L.N. Kennett

The contract with the Commonwealth of Australia for the Australian National Seismic Imaging Resource Major National Research Facility (ANSIR) came to an end in June 2005. The owners ANU and Geoscience Australia have agreed to continue for a further two years retaining the ANSIR label but the new designation **National Research Facility in Earth Sounding**. Applications for equipment access may now be made at any time.

2005 has proved to be a busy year with a wide range of activities. The broadband equipment continued to be heavily used. Short-period stations were used in the SEAL experiment and the new EVA experiment in Southern Victoria.

Reflection work in 2005 has seen over 700 km of reflection profile collected in the Tanami desert (NT,WA) including some work at mine scale. This was closely followed by work in NSW on the transition between the Thomson and Lachlan orogens that was slightly curtailed by rain. The minivibrator has received more use than of late.

The continuing demand for equipment led to a collaborative bid by ANU, Adelaide, Macquarie to the ARC LIEF program to supplement the available ANSIR equipment which was successful. Fifteen sets of recorders equipped with both seismic and electromagnetic sensors will be purchased in 2006.

The full range of experiments carried out in 2005 is shown in the table below.

2005 ANSIR Timetable

<i>Proponent</i>	<i>Institution</i>	<i>Location</i>	<i>Jan</i>	<i>Feb</i>	<i>Mar</i>	<i>Apr</i>	<i>May</i>	<i>Jun</i>	<i>Jul</i>	<i>Aug</i>	<i>Sep</i>	<i>Oct</i>	<i>Nov</i>	<i>Dec</i>
Reading, Kennett	ANU, RSES	Antarctica	A7	A7	A7	A7	A4							
Kennett	ANU, RSES	Tasman Line NSW,NT,QLD,SA,VIC	B24											
Cummins	GA, PIRSA	Flinders Ranges, SA	B8	B8	B8	B8	B8	B8						
Roach	U Tasmania	Macquarie Island	S6	S6	S6	S6								
Rawlinson	ANU	SE Australia	S20	S20	S20	S20	S20							
Rawlinson	ANU	E. Victoria							S20	S20	S20	S40	S40	S40
Kennett.Heintz	ANU	Mt Gambier											B8	B8
Huston	GA, NTGS, GSWA	Tanami, NT-WA					VR	VR	VR					
Goleby	GA	Tanami, NT-WA						S25	S25					

Robson	GSNSW	Broken Hill									VR				
Robson	GSNSW	Thomson-Lachlan									VR	VR			
Collins	GA	Echuca					mv								
Chaudury	Sydney Gas	Sydney basin									mv				
Poole	BHP Coal	Appin												mv	
Sherlock	CO2CRC	Otway basin										mv			
Benshemesh	Monash Univ	Marsupial Moles, NT	G32												

Equipment Key

S - Short period instruments (+number)
B - Broad band instruments (+number)
A - Broad band instruments in Antarctica (+number)
R - Reflection recording system
V - Vibrators
mv - Minivibrator
G - Geophone strings

Further details of the National Research Facility and its activities can be found at the [ANSIR](#) website.

CENTRE FOR ADVANCED DATA INFERENCE 2005

CADI activities

The Centre's operations are based on collaborative projects with other groups/centres in the Earth Sciences which are supported through partial funding of doctoral and post-doctoral fellowships, and an a visitor program. The Centre also provides access to parallel processing on a large cluster of performance PC's (called TerraWulf) funded by an Australian Research Council LIEF grant.

The main body of the report provides a survey of some of the strands of work in CADI during 2005. This year projects have been conducted in geomorphology, probability theory, statistical inference techniques, structural seismology, airborne geophysics, earthquake seismology, computational mineral physics and geodesy. This year saw continued development of the CADI inversion toolkit whereby CADI visitors and project participants have a simple interface to both software and hardware facilities.

CADI also had several visitors during the year, who used the facilities and interacted with staff and students. The main visitors were from Geoscience Australia, Leeds University, Univ. of Aarhus, Imperial College, London, and Univ. of Victoria, Wellington.

Tracking Multiple Arrivals in Phase Space

J. Hauser, M. Sambridge, and N. Rawlinson

Multipathing is the result of continuous and/or discontinuous variations in seismic wave speed causing a wave to travel to a receiver by more than one path. This means that at a given receiver multiple arrivals from the same source are observed. First arrival ray paths tend to avoid slow regions of a velocity model. Later arrivals do not avoid slow regions and hence contain additional information about the velocity field. However, current state of the art algorithms for the calculation of travel times only provide first arrivals.

A three dimensional phase space can be created from two dimensional normal space by simply using the local normal direction to the wavefront as the third coordinate. This phase space representation of a wavefront is known as the bicharacteristic strip (see Figure 1). A seismic wavefront in normal space can develop sharp corners and become self intersecting. In a Lagrangian wavefront tracking approach a given density of points on the wavefront has to be maintained in order to describe the wavefront adequately. However adding points to a self intersecting wavefront with sharp corners in normal space is difficult.

The bicharacteristic strip is not self-intersecting because the two intersecting segments of a wavefront have different local normal directions and a sharp corner of the wavefront in two dimensional normal space becomes a smooth line in three dimensional phase space (Figure 1). Points can thus be added to the bicharacteristic strip, and hence to the wavefront, using a simple linear interpolation or a weighted average.

Our implementation of a Lagrangian wavefront tracking algorithm differs from previous algorithms in the refinement of the wavefront which is performed in phase space. Wavefront tracking in phase space has not been extensively investigated in seismology, particularly in applications outside of the exploration field. Figure 2 illustrates how including later arrivals can increase the ray path coverage for a velocity structure with a strong low velocity anomaly. Including observed later arrivals routinely in the inversion for the velocity structure therefore has the potential to improve existing tomographic models.

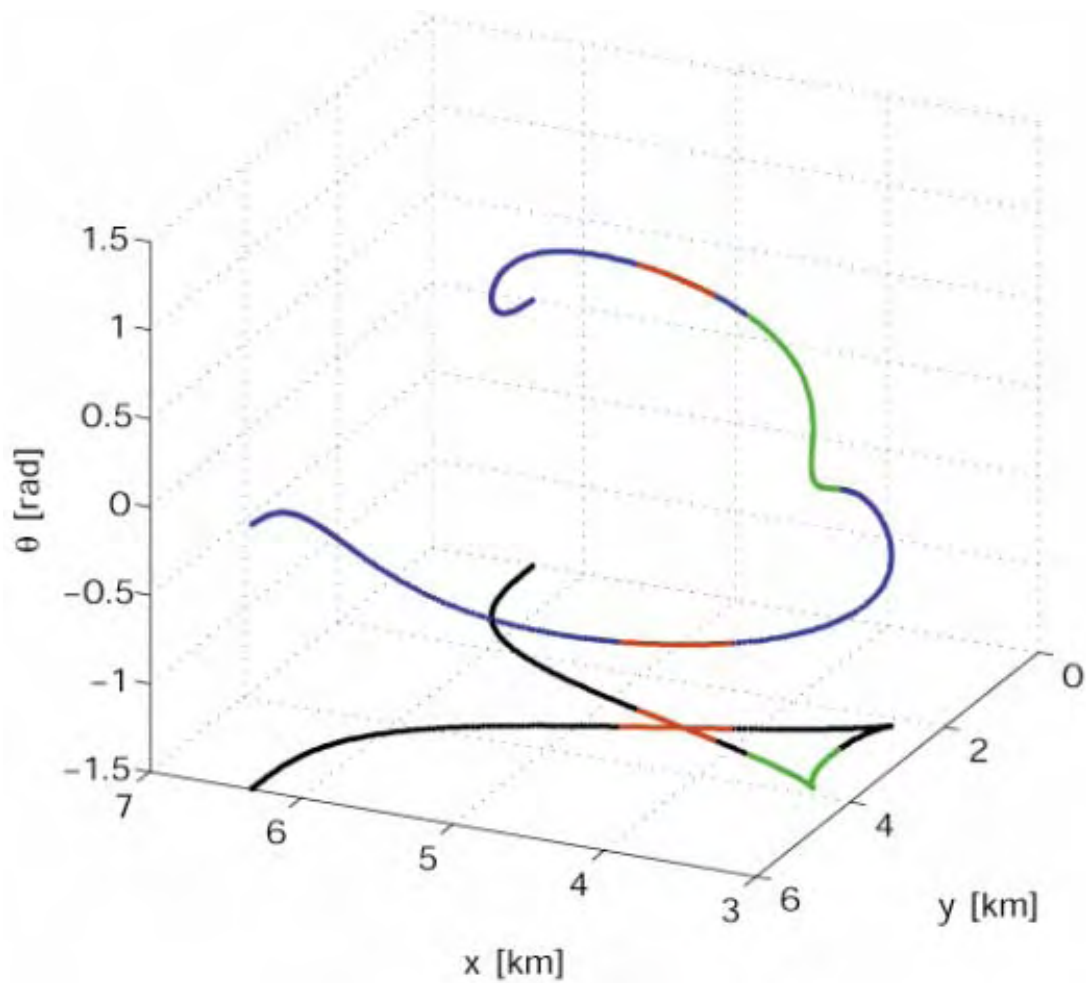


Figure 1: Swallow tail pattern of a wavefront. The sharp corners in normal space (green segments) are given by a smooth representation in phase space. The intersecting segments in normal space (red lines) are not intersecting each other in phase space.

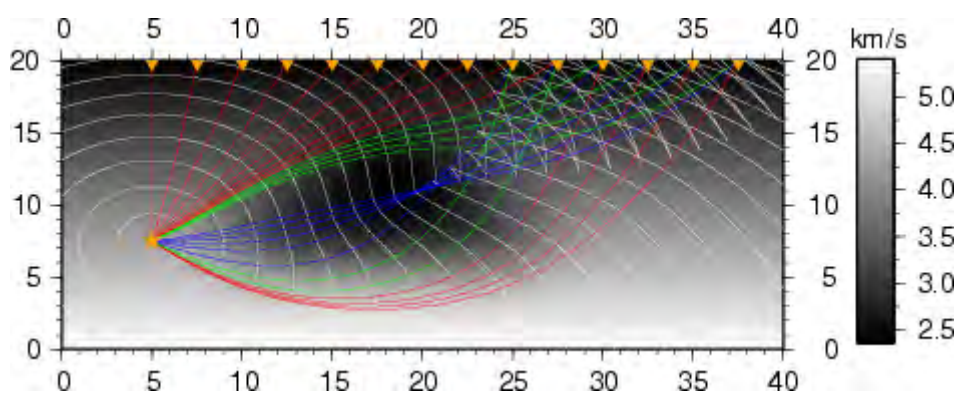
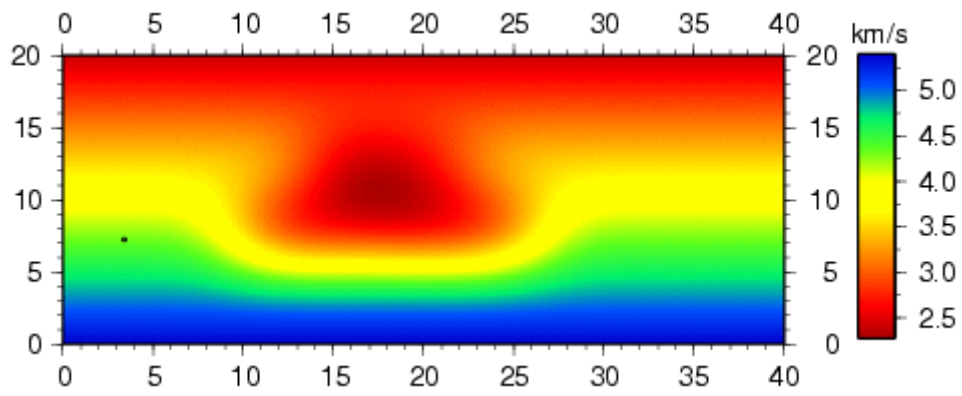


Figure 2: Wavefronts and corresponding raypaths for first (red), second (green) and third (blue) arrivals for a velocity structure with a strong low velocity anomaly.



Animation 1: Wavefront developing a swallow tail pattern as it travels through a low velocity region.

Multiple Seismic Phases in 3-D with the Fast Marching Method

M. de Kool, N. Rawlinson, & M. Sambridge

A new scheme based on the Fast Marching Method (FMM) in spherical coordinates has been developed to track phases comprising any number of reflection and transmission branches in 3D layered media. A multi-stage approach which treats each layer that the wavefront enters as a separate computational domain is used. At each interface, FMM is reinitialized to track the impinging wavefront as either a reflection back into the incident layer or a transmission through to the adjacent layer. Notably, the method does not require an irregular mesh to be constructed in order to connect interface nodes to neighbouring velocity nodes which lie on a regular grid. To improve accuracy, local grid refinement is used in the neighbourhood of a source point where wavefront curvature is high.

In addition to computing simple refracted waves, reflected waves and more complex multiples, reflections which are not the first to arrive (e.g. the global PP phase) can also be tracked. The new scheme also allows various global phases from distant events to be computed through a spherically symmetric earth model to the boundary of a local 3-D model, after which FMM is used. This feature is useful for teleseismic tomography. Finally, conversions between P and S phases at interfaces can also be tracked.

A series of systematic tests have been carried out with the new method in order to verify its accuracy, efficiency and robustness. In particular, it has been shown that various global phases can be computed to an acceptable accuracy through the ak135 reference model (see Figure 1). The scheme can also be used to track complex crustal phases that may be encountered in coincident reflection, wide-angle reflection/refraction or local earthquake surveys. Figure 2 shows a variety of phases that have been tracked in the presence of a realistic subduction zone, which includes several layer pinch-outs and a subducting slab. Our numerical tests show that the new scheme is a practical and robust alternative to conventional ray tracing for computing a range of phases in layered media at a variety of scales.

The complete software package is freely available on the Internet at: <http://rses.anu.edu.au/seismology/fmmcode>

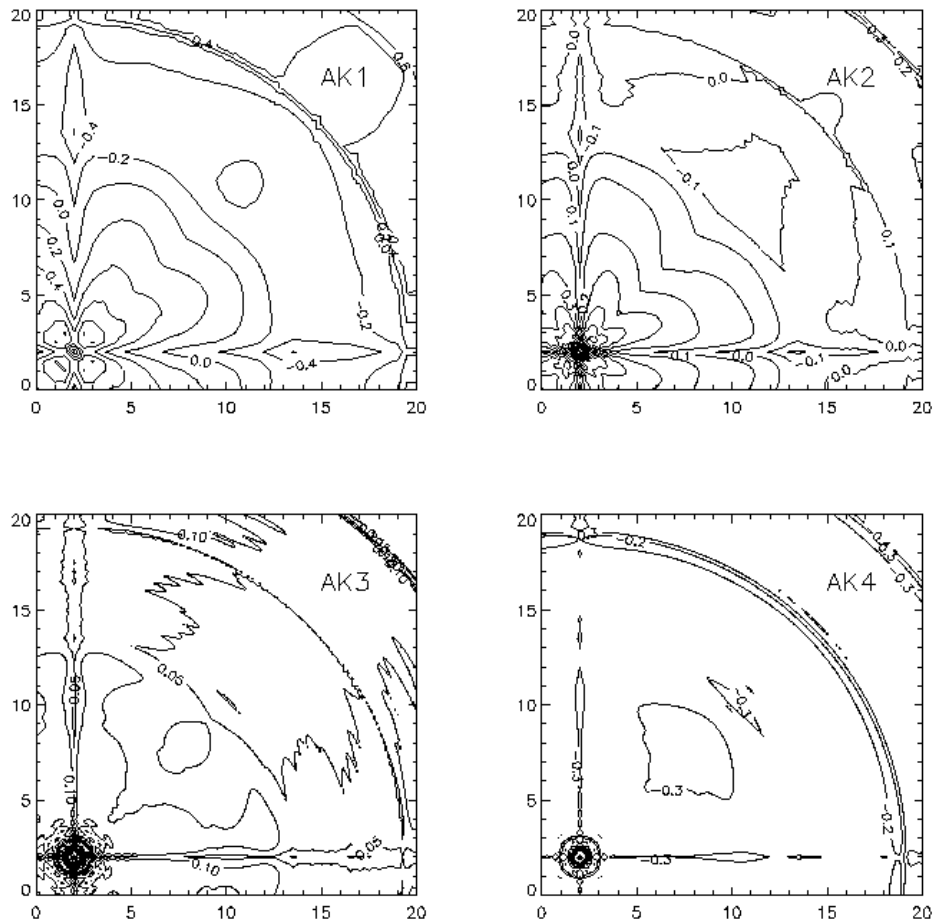
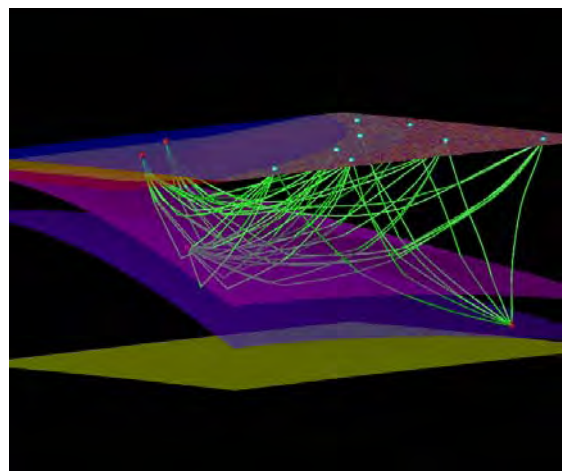


Figure 1: Summary of P-wave arrival time errors in the ak135 reference model using the new scheme. All four cases model a region extending 20 degrees in latitude and longitude and 1000 km in depth. The source is located at 100 km below the surface. AK1 - 21x41x41 nodes; AK2 - 41x81x81 nodes; AK3 - 81x161x161 nodes; AK4 - 81x161x161 nodes. Models AK1-AK3 explicitly include interfaces, while AK4 does not. Contour labels are in seconds.

Figure 2: Ray paths in a complex layered geometry. The model consists of a coast line, a sediment layer beneath the ocean, continental crust, oceanic crust subducting under the continent, and part of the upper mantle. Seismic sources are represented by red diamonds, receivers by blue spheres. Two of the sources are on the ocean surface, another two are located in the subducting slab. An array of eight receivers is distributed over the land area. Velocity is laterally inhomogeneous in the continental crust. A selection of ray paths representing direct arrivals and reflections from the top and the bottom of the subducting slab is shown.



Markov chain Monte Carlo extensions to the CADI toolkit

P. Rickwood, M.Sambridge

Standard Markov chain Monte Carlo

Markov chain Monte Carlo sampling is a method of sampling from a probability distribution by constructing a Markov chain that has the desired distribution as its stationary distribution. Surprisingly, this can be easy to do even in the usual case where the desired distribution is unknown.

An efficient parallel implementation of the Markov chain Monte Carlo algorithm has been included in the [CADI toolkit](#). This allows scientists wishing to use the algorithm on a cluster to do so with little effort. No parallel/MPI programming is required of the scientist, for example.

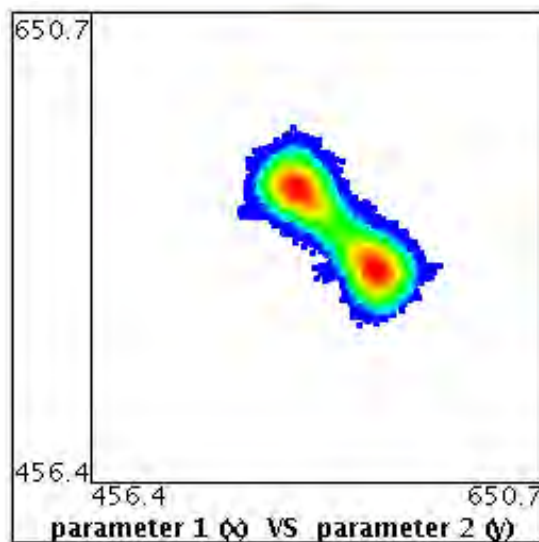


Figure 1: The image shows a simple 2 dimensional distribution that has been sampled by the Markov chain Monte Carlo technique. Red indicates regions of high probability. The Markov chain spends most of its time in regions of high probability: specifically, the amount of time spent in any particular region is proportional to the probability density of that region. We can see that the Markov chain has not been running long enough to visit areas with very low probability, and these areas show up as white.

The parallel Markov chain Monte Carlo sampling procedure implemented has been used in the completion of the [Sea-level modelling work](#). Future internal uses will include mixture modelling of thermochronology data.

Variable Dimension Markov chain Monte Carlo

In situations where a probability distribution of fixed dimension is being sampled, the Markov chain Monte Carlo technique has been in use for decades. More recently, however, the technique has been extended to cover cases where several probability distributions (possibly of different dimension) can be sampled at once. This is termed, somewhat obscurely, Reversible Jump Markov chain Monte Carlo (see ¹).

Having a Markov chain that can sample a variable dimension probability distribution is helpful in solving the *model comparison* problem. This problem occurs in situations where you have two (or more) theories/models, and wish to directly compare the two models, to see which one is better model for a

particular purpose. Simply choosing the model that best predicts/fits observed data is not the correct way of deciding which is the best model. This is especially the case where the models are differently parameterized (i.e. they have differing numbers of parameters). Reversible Jump Markov chain Monte Carlo allows direct comparison of differently parameterized models. Specifically, it calculates a probability distribution over all models, so that one may say how probable a particular model is compared to another model. Figure 2 shows a specific example.

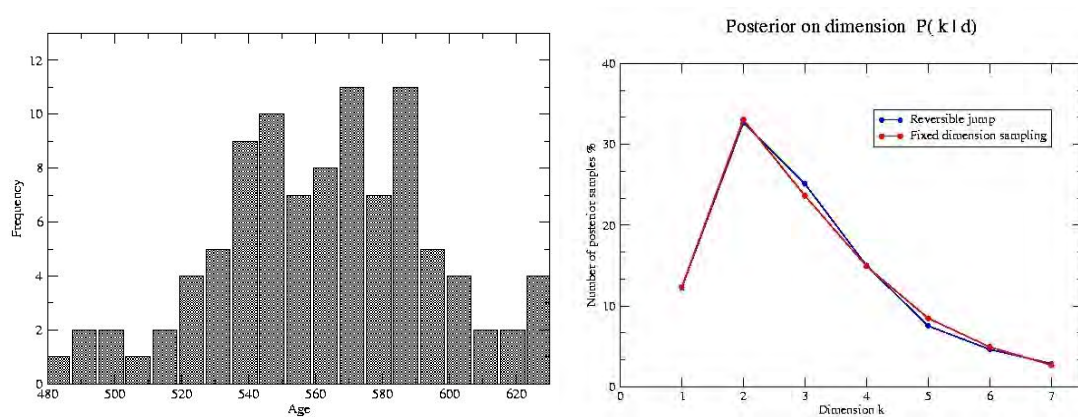


Figure 2: The left picture shows synthetic data generated from 2 normal distributions with means/stddevs of 540/30 and 570/30. The right figure shows that, after considering different numbers of normal distributions, variable dimension Markov chain Monte Carlo sampling has decided that a mixture of two normal distributions best explains the observed data. The result obtained using David Green's AutoMix Reversible Jump Markov chain Monte Carlo software is shown (in blue) alongside our implementations results (in red) to illustrate the equivalence of the techniques.

A parallel version of a variable dimensional Markov chain Monte Carlo sampler has been implemented and included in the CADI toolkit. While the implemented algorithm is not exactly the same as Greens Reversible Jump MCMC, it performs essentially the same computation. How efficient and stable the technique is compared to other trans-dimensional samplers is an open question, and comparisons with other variable dimension samplers are planned in future.

¹Green, P.J., 1995. Reversible jump Markov chain Monte Carlo computation and Bayesian model determination, *Biometrika*, **82**, 711-32.

Evaluation of Automatic Differentiation Tools

M.Sambridge, P.Rickwood

Computer programs can be viewed as black-boxes that, given some inputs \mathbf{x} compute outputs \mathbf{y} . So in mathematical terms, we can view a computer program as a vector valued function with \mathbf{x} in the domain and \mathbf{y} in the range. Viewing computer programs in this way has prompted people to consider the task of finding the derivatives of programs. In other words, if a computer program can be regarded as some mathematical function f , then does it have a derivative, and, if so, can we compute it?

Programs as functions

It turns out that almost all computer programs can be viewed as mathematical functions and, moreover, are almost always piece-wise differentiable. This can initially be difficult to accept, since we think of computer programs as containing many elements that we think of as non-differentiable, such as if statements and loops, but the easiest way to persuade oneself that this is the case is to consider that, for a program that does [halt](#) for every input, every execution of that computer program can be represented by a sequence of simple instructions. Consider, for example, the following program:

```
x = INPUT
y = 1.0
if (x <= 1.0) then
  return y
else
  while (y <= 10.0) then
    y = y*x

    x = x+0.5
  end while
  return y
end if
```

Depending on the input variable \mathbf{x} , this program can be represented by any of the following sequences of instructions.

1. $y = 1.0$; return y
2. $y = 1.0$; $y = y*x$; $x = x+0.5$; return y
3. $y = 1.0$; $y = y*x$; $x = x+0.5$; $y = y*x$; $x = x+0.5$; return y
4. $y = 1.0$; $y = y*x$; $x = x+0.5$; $y = y*x$; $x = x+0.5$; $y = y*x$; $x = x+0.5$; return y
5. and so on....

Each of these sequences can be viewed as a function of \mathbf{x} , and the derivative of the output \mathbf{y} w.r.t \mathbf{x} is well defined. *Automatic Differentiation* is a field of study with the aim of producing tools that, given a computer program \mathbf{p} , will generate another computer program \mathbf{p}' that computes the derivative of \mathbf{p} . In the simple example just presented, is easy for us to just write down this "derivative program":

```
x = INPUT
y = 1.0
dy = 0.0
dx = 1.0
if (x <= 1.0) then
  return dy
else
  while (y <= 10.0) then

    y = y*x

    dy = dy*x + y*dx

    x = x+0.5
  end while
  return dy
end if
```

In general however, this is not a trivial task, and a human attempting to do it will make mistakes. Automatic Differentiation tools aim to automate the creation of this "derivative program".

Reverse (adjoint) and Forward modes

There are two different methods of calculating the derivative of a computer program. They are the 'forward' method and the 'reverse' method. Without going into the details, for a function \mathbf{f} defined by program \mathbf{p} with \mathbf{n}_i inputs and \mathbf{n}_o outputs, the forward mode calculates the derivative \mathbf{f}' in $\mathbf{O}(\mathbf{n}_i)$ time, while the reverse method calculates the derivative in $\mathbf{O}(\mathbf{n}_o)$ time¹. In other words, in forward mode, the computational cost of calculating the derivative is dependent on the dimension of the domain of \mathbf{f} , while in reverse mode it is dependent on the dimension of the range of \mathbf{f} . In most computational problems, \mathbf{n}_i is less than \mathbf{n}_o , so it is the reverse mode that is more useful, but it is also more difficult to implement, as the control flow of the program must be reversed.

Current tools and how they perform

We investigated two different Automatic differentiation tools on four different problems, and tried to get each to produce a derivative program in both forward and reverse mode. We checked the results using finite difference.

The tools were:

1. TAF: Regarded as the leader in the field by most, we obtained an evaluation licence from the [commerical vendor](#) for the purposes of this study.
2. Tapenade: Developed in France at [INRIA](#). Free to use. Not as full-featured as TAF, and the differentiation programs produced are not as efficient as the ones produced by TAF. Nice graphical user interface, as well as command line.

The programs we differentiated were:

Gibbs free energy	A program that solves the Gibbs free energy differential equation.
Receiver function	Seismic receiver function calculation
Ray tracing in 2D medium	A program that calculated the travetimes of rays originating at a point-source and travelling through a 2D heterogeneous medium. See figure 1.
Fast Marching wave-front tracking	fast marching method program tracks the first-arrival wavefront from a seismic source through a heterogenous velocity medium.

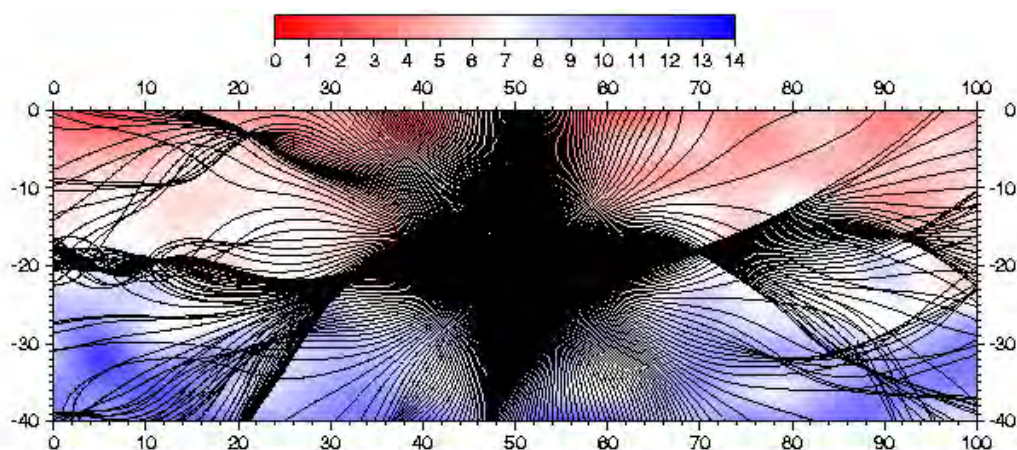


Figure 1: An example of the ray paths calculated by the ray-tracing program. The program calculates the travetime of a large number of rays originating at some source and travelling through a heterogeneous velocity medium.

Results

The most illuminating result was TAF's result for reverse mode on the Gibbs free energy problem, where we were able to vary the number of input parameters and hence show clearly the independence of the reverse mode on the number of input parameters.

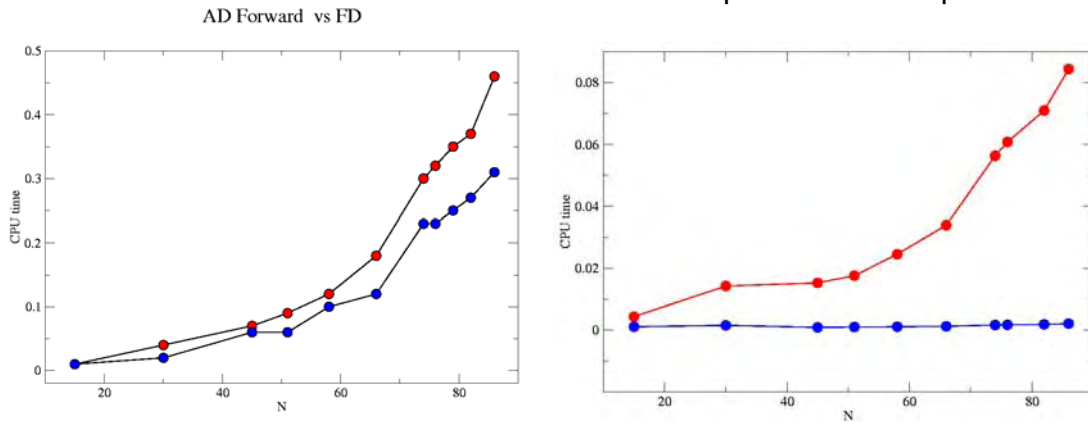


Figure 2: Shows the computational cost of forward and reverse mode for varying numbers of input parameters in the Gibbs free energy program. The left figure shows the cost of forward mode (blue) compared to finite difference (red) for increasing numbers of input parameters. The right figure shows the same for reverse mode. The computational cost in reverse mode is clearly independent of the number of input parameters.

The results were mixed. For the simpler programs (Gibbs free energy and receiver function) both tools produced correct derivatives (verified by finite difference), but for the more complicated ones, TAF failed in reverse mode on both and in forward mode on the fast marching program.

Because tafenade only understands a subset of valid fortran 90, it was only able to differentiate the gibbs free energy program, and in this case it was significantly slower than TAF in reverse mode. Results for TAF were better, but still not ideal.

	Gibbs	Receiver	Ray-trace	Fast marching
TAF (fwd mode)	Correct	Correct	Correct	Didn't work
TAF (rev mode)	Correct	TAF program returned incorrect derivative	TAF program did not return (after 24 hours)	Didn't work

In future work, we plan to further investigate TAF. In particular, TAF contains a facility for giving 'hints' to allow for more efficient differentiation in reverse mode, and we plan to use these hints to see what programs TAF can differentiate. Codes of several hundred thousand lines have been differentiated successfully, so large geo-physical codes may be within reach of the tool. This is ongoing work.

1. See [here](#) for an explanation of computational complexity.

Calibration and Inversion of Airborne Geophysical Data

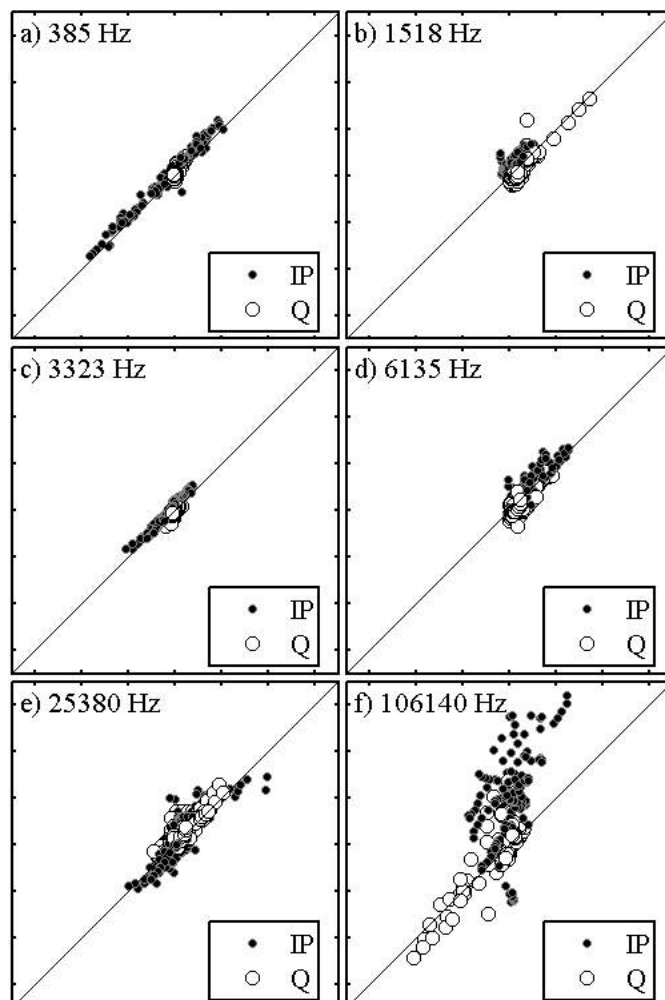
R. Brodie and M. Sambridge

During 2005 we have further developed and refined the [holistic approach](#) (Brodie and Sambridge, 2004) for calibration, processing and inversion of airborne frequency-domain electromagnetic data. The holistic approach is a method for simultaneously calibrating, processing and inverting frequency-domain airborne electromagnetic data. A spline-based 3-D layered conductivity model covering the complete survey area is recovered through inversion of the entire raw airborne dataset and available independent conductivity and interface-depth data. To account for systematic calibration errors, such as incorrect gain factors and zero-level drift, the holistic inversion formulation includes a mathematical model of the such errors. By taking account of these elements in the inversion, the need to pre-process the airborne data prior to inversion is eliminated.

Over the past year further development work has shown that a more accurate recovery of temporal system bias can be achieved through a more suitable parameterisation which allows us to take advantage of its smoothly varying character. Figure 1 shows that estimates of bias from the holistic inversion calibration model and high altitude zero-level observations compare well. As a result, we have concluded that the improved method may lead to data acquisition cost savings by elimination of the high altitude zero-level observations that are conventionally required for estimating bias (Brodie and Sambridge, 2005).

Figure 1: Observed high altitude zero-levels (horizontal axis) versus those predicted from the holistic calibration model (vertical axis).

An improved formulation of the regularisation terms in the inversion now allows expression of reference model and roughness constraints directly in terms of the more accessible and intuitive real physical quantities, instead of abstract basis function coefficients, has been implemented. Further refinements to the coding has allowed inversion of a larger portion of a dataset,



which has improved the overall stability of the inversion. Application of the method to raw survey data has shown that inversion models obtained from the holistic inversion are superior to those from conventional sample-by-sample 1-D inversion of fully processed data. Figure 2a shows that the layer two thickness estimates from a conventional inversion are negatively impacted by elongate artefacts in the north-south flight line orientation which are caused by residual systematic calibration error in the data. Furthermore, Figure 2b shows how the error-normalised data misfits are large and systematically related to individual survey flights or lines. In contrast, Figure 3a and b show that the holistic inversion of raw survey data has accounted for systematic calibration error since they are largely free of artefacts and the data-misfits are much smaller.

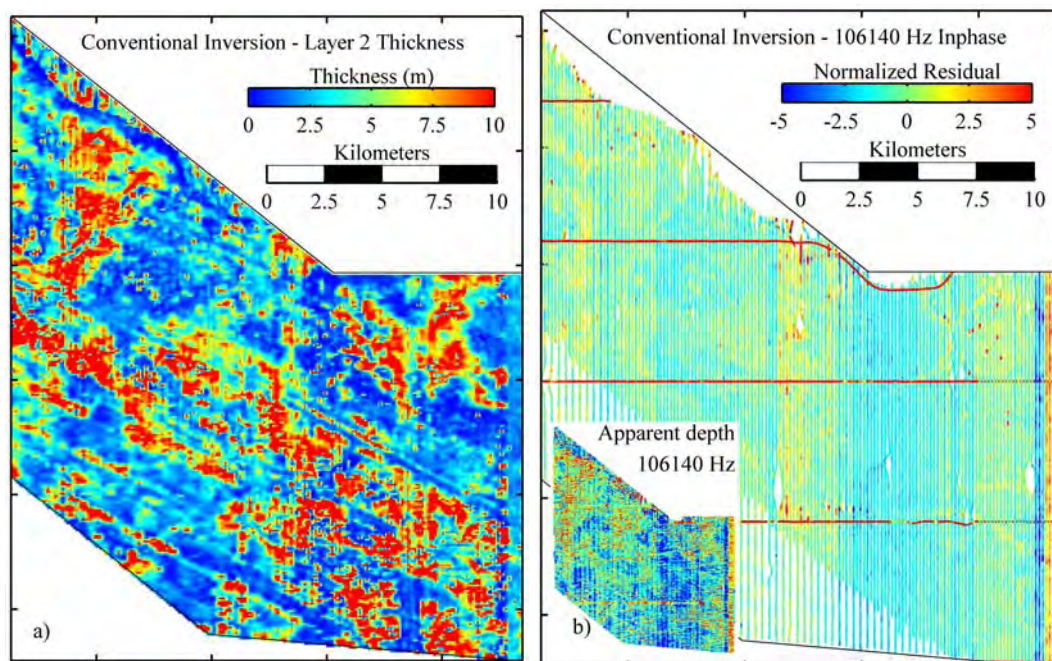


Figure 2: Results from the conventional sample-by-sample inversion; a) layer two thickness, and b) error normalized 106140 Hz inphase residuals.

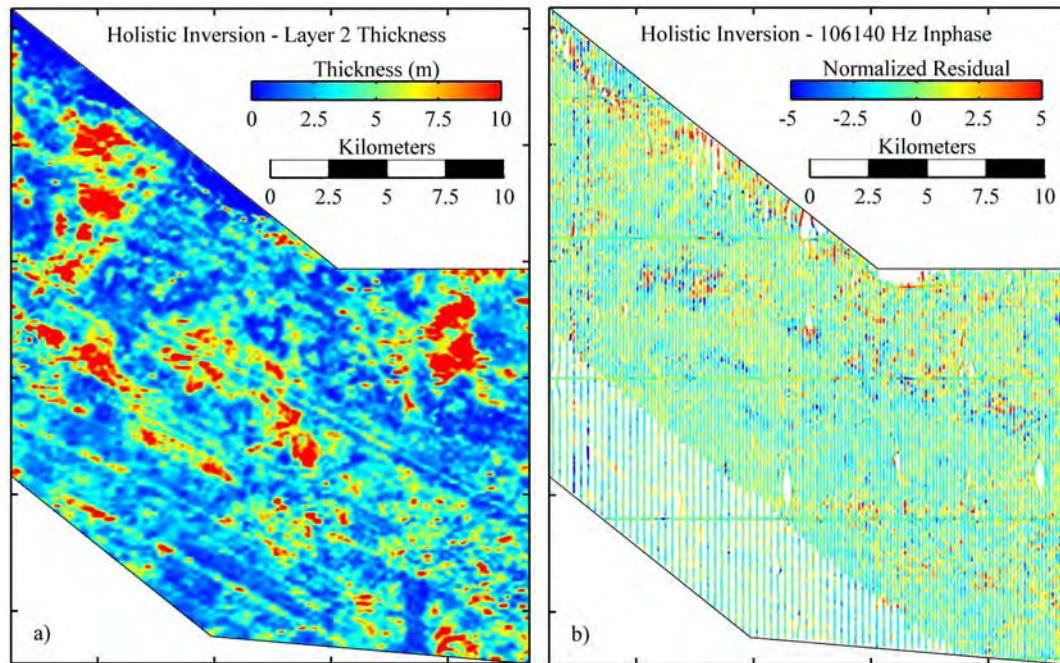


Figure 3: Results from the holistic inversion; a) layer two thickness, and b) error normalized 106140 Hz inphase residuals.

Further work has commenced on the feasibility of applying the holistic approach in survey areas where little prior information, such as sophisticated conceptual models, downhole conductivity or interface depth data are available. This work aims to allow/encourage wider adoption of the method (e.g. by airborne survey contractors) as a routine processing tool for complete datasets. More generic vertically smooth models, requiring many more layers and hence parameters will thus be required. Progress to date has been on implementing the vertical roughness constraints and parallelisation of the code to allow it to be run on a distributed architecture computer so that the larger inversion is possible.

References:

Brodie, R. and Sambridge, M., 2004, Holistically calibrating, processing and inverting frequency-domain AEM surveys: 17th Geophysical Conference and Exhibition, ASEG, Extended Abstracts.

Brodie, R. and Sambridge, M., 2005, A holistic approach to inversion of frequency-domain airborne EM data: submitted to Geophysics.

Terrawulf cluster computer

Various

This year the Terrawulf computational Facility has been used for a range of new projects covering the fields of Seismic surface wave imaging, Probabilistic inverse Theory, Computational Earth Materials, Geodesy, Earthquake location, and Elastic wave propagation. Projects established in 2004 have continued in a number of areas, with most usage taken up by applications in Sea level inversion for Coral Reef age and heights, and inverse problems in geomorphology. These projects have involved staff across the School with three of the four areas, as well as collaborators nationally (e.g. Geoscience Australia) and overseas (e.g. Universities of Rennes and Grenoble in France) as well as Dalhousie University in Canada). Below are a selection of highlighted projects.

Airborne frequency domain inversion

R. Brodie

The Terrawulf facility has been employed for conventional sample-by-sample 1-D inversion of airborne frequency-domain electromagnetic data carried out as part of the [Calibration and Inversion of Airborne Geophysical Data project](#). It has also been utilised in testing the feasibility of parallel computation in the "[holistic inversion](#)" of airborne electromagnetic data to allow the inversions with a greater number of unknowns since the method is currently limited by memory as a standalone application. To date this work has shown that the forward modelling part of the holistic inversion scales almost linearly on the Terrawulf, while solving of the linear system scales at around 25% efficiency for up to the use of 16 processors.

Surface wave imaging

K. Visser and B. Kennett

In recent years much work has been done using fundamental surface waves to image the earth. The tomographic models resulting from fundamental mode surface waves, however, suffer from a limited depth resolution. Improving the depth resolution can be done using higher mode surface waves. However, they are very difficult to measure because they overlap in the time domain as well as in the frequency domain with the fundamental mode. Yoshizawa and Kennett developed a new technique for multimode dispersion measurements using a fully non-linear waveform inversion for path specific 1-D profiles. This method is in principle able to measure both the fundamental as well as the higher modes with even coverage. It further provides much needed uncertainties from the measurements. We adapted the

method of Yoshizawa and Kennett to be able to run it automatically on all available seismograms in international databases (Oxford, IRIS). The process needs ten minutes per seismogram, which made it interesting to work with the terrawulf cluster. We use the terrawulf cluster to run the process on, up to 107, seismograms simultaneously. This significantly improves the calculation time needed for the millions of seismograms available.

Earthquake relocations in the Tonga-Kermadec

T. Nicholson, M. Savage, M. Sambridge

We are relocating all the earthquakes in the global EHB catalogue within the Tonga/Kermadec region using the Empirical Travel Time (ETT) approach of Nicholson et al. (2004), for estimating 3-D travel times. This is pilot project for a much larger study to relocate all the events in the EHB catalogue. The intention is to produce a high quality global data set for seismic tomography and other uses.

Coda wave interferometry

D. Robinson and M. Sambridge

Coda wave interferometry (CWI) is a new technique that can be used to constrain the distance between nearby events from comparisons of the coda waves they generate. The limitations of CWI are not yet fully understood. In this project the Terrawulf was used to perform numerical experiments for understanding the limitations of CWI. Experiments made use of a recently developed 3D elastic wave propagation code which exploited the parallel computing capability of the Terrawulf.

Geodetic Analyses

P. Tregoning

In 2005, the Terrawulf facility was used for the first time for the analysis of Global Positioning System (GPS) data. Using the GAMIT software and the full suite of nodes, it was possible to process 5 years of global data (up to 150 sites per day) in around 40 hours. The same analysis on conventional desktop systems would have taken several months to complete. This enormous increase in processing speed made it possible to conduct tests of many new models within the overall GPS analysis, tests that were simply unfeasible otherwise. Comparisons were made of four different mapping functions for modelling the propagation delay of the transmitted signals by the troposphere (Boehm et al, 2005a, 2005b), the effect on GPS analysis of implementing a more accurate model for the deformation caused by the solid Earth tide

(Watson et al., 2006) as well as extensive testing of models for the periodic and non-periodic elastic deformation of the Earth caused by atmospheric pressure loading (Tregoning and van Dam, 2005).

Computational Mineral Physics

A. Walker

Access to large scale computational facilities is an essential prerequisite for any project involving computational mineral physics. The terrawulf was therefore an important resource for this years foray into ab initio modelling at RSES. One major result of the calculations was the elucidation of a novel model of water weakening of olivine, as reported elsewhere in this volume

A second example of the type of calculation enabled by the terrawulf cluster was a combinatorial study of the interaction of hydrogen with trivalent impurity ions such as iron and aluminium in forsterite. For each element there are hundreds of possible configurations with hydrogen bonded to oxygen close to a the impurity ion and, for each impurity, the energy of the defect must be evaluated. Furthermore, accurate methods using density functional theory and requiring days of CPU time per configuration are required to extract meaningful results. As the terrawulf's communications backbone is not optimised for rapid inter-processor communication large numbers of calculations were performed in parallel, rather than performing each individual calculation in parallel. Initial analysis of the results suggests that the each ion type has a strong preference for one or the other octahedera site in olivine and that a hydroxyl group occupies an adjacent vacant octahedera.

References:

Boehm, J., A. Niell, P. Tregoning, H. Schuh, The GMF: A new empirical mapping function based on numerical weather model data, to be submitted to *Geophys. Res. Lett.*, Nov. 2005.

Boehm, J., P.J. Mendes Cerveira, H. Schuh, P. Tregoning, The impact of tropospheric mapping functions based on numerical weather models on the determination of geodetic parameters, *IAG Proceedings, Cairns, Aug. 2005, in press, Sept. 2005.*

Tregoning, P. and T. van Dam, Atmospheric pressure loading corrections applied to GPS data at the observation level, *Geophys. Res. Lett.*, 32, L22310, doi:10.1029/2005GL024104, 2005.

C. Watson, P. Tregoning, R. Coleman, The impact of solid Earth tide models on GPS time series analysis, to be submitted to *J. Geodesy*, Nov. 2005.

Coda wave interferometry and constraints on relative earthquake locations

D. Robinson, M. Sambridge and R. Snieder

Traditional earthquake location techniques involve triangulation of an earthquake hypocenter using the arrival time of the first arrival, or some other phase at 3 or more stations. It is well documented that single earthquake techniques are susceptible to errors in the velocity models (e.g. Lin and Shearer, 2005 and Lay and Wallace, 1995). Modern techniques such as the double difference method can be used to reduce the error from inaccurate velocity models by using pairs of earthquakes to reduce the dependence of the location algorithm on travel path. For example, Waldhauser and Ellsworth (2000) demonstrate how use of their double difference earthquake location algorithm leads to improvements in relative location between events by an order of magnitude. At the heart of the double difference algorithm is a measure of the time lag between direct arrivals, or known phases using a cross correlation. That is; the double difference algorithm does not use the entire waveform. A technique that uses the entire seismic waveform will use more information and therefore has the potential to improve earthquake locations further.

Snieder and Vrijlandt (2005) demonstrated how coda wave interferometry (CWI) can be used to directly estimate source separation between two earthquakes with identical source properties using the cross correlation of seismic waveforms measured at the same station. These estimates do not require detailed knowledge of the velocity model and are hence not susceptible to velocity errors. Moreover, the CWI utilises the coda, a component of the waveform that is not traditionally exploited.

This project aims to link CWI with travel time inversion of the body waves to provide new constraints on relative earthquake location. Numerical experiments are currently being conducted to explore the the limitations of CWI. For example, Figure 1 demonstrates results for two synthetically generated waveforms in a 3D Gaussian random field. The waveforms were generated using the software pmcl3d which was kindly supplied by Kim Olsen (*pers. comm.*, 2005). Currently a small bias is observed in the CWI estimates, the source of which is not yet understood.

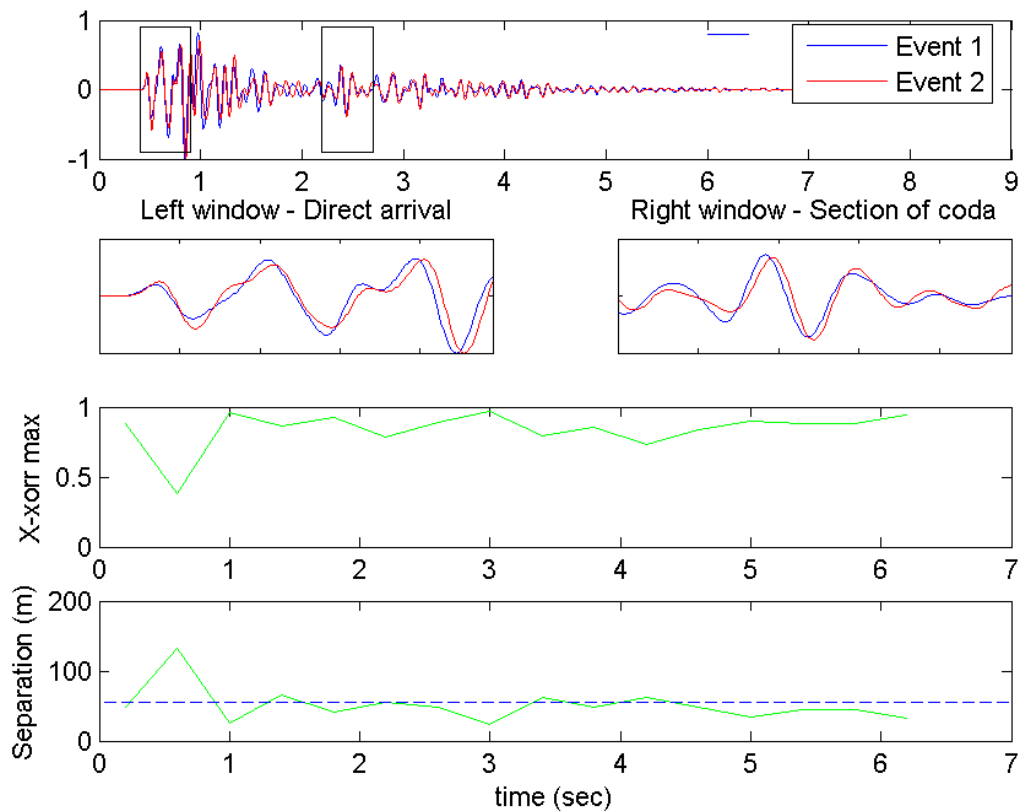


Figure 1: Results of the synthetic tests. The uppermost plot illustrates the synthetic waveforms recorded at a pseudo receiver filtered between 1 and 3 Hz. Illustrations on the second row depict the similarity of the direct arrivals (left) and the differences between coda (right). The third row illustrates the maximum of the normalised cross-correlation as a function of window centroid for a sliding time window with length depicted by the blue bar in the top plot. The green line of the final plot represents the estimated separation as a function of sliding window centroids. The blue dashed line represents the known separation between the synthetic sources. The results indicate a small bias in the CWI estimate.

REFERENCES

Lay, T. and Wallace, T. C., 1995, *Modern Global Seismology*: Academic Press.

Lin, G. and Shearer, P., 2005, Tests of relative earthquake location techniques using synthetic data: *Journal of Geophysical Research* 110 (B04304), doi:10.1029/2004JB003380.

Snieder, R. and Vrijlandt, M., 2005, Constraining the source separation with coda wave interferometry - Theory and application to earthquake doublets in the Hayward Fault California: *Journal of Geophysical Research* 110 (B04301), doi:10.1029/2004JB003317.

Waldhauser, F. and Ellsworth, W.L., 2000, A double difference earthquake location algorithm - method and application to the northern Hayward Fault, California: *Bulletin of the Seismological Society of America* 90 (6), 1353-1368.

***PRISE* Introduction**

The ***PRISE*** Group operates as a unique entity within the Research School, with the principal charter to provide external access to the Research School's specialised equipment and expertise in the areas of geochronology, isotope geochemistry and major and trace element geochemistry. Members of the ***PRISE*** Group seek support from a wide range of external funding sources; projects undertaken range from collaborative research projects supported by research grants through to fully commercial projects. The level of expertise is internationally recognised with high acclaim.

Areas of current personal research activity undertaken by members of the ***PRISE*** Group include:

- The rock record from 2600 to 2000 million years ago preserves evidence for dramatically fluctuating greenhouse and icehouse climates at the same time as, and possibly caused by, change from an oxygen-deficient to an oxygen-rich atmosphere. Although the global changes are well-documented, correlation of their timing and duration between continents is poorly constrained. This project aims to redress that problem by producing a precise calibration of the global time scale for the oxidation of Earth's atmosphere between 2.6 and 2.0 billion years ago through the analysis of the rock records in Australia, Canada and South Africa. It will provide a much needed time framework within which long-term feedback between atmospheric composition and climate can be understood
- Geochemical studies of the early solar system are being conducted to investigate physical conditions leading to assembly of the terrestrial planets and the chronology of events that shaped the Earth and Moon. Primitive objects from the solar nebula and samples from the Earth, Moon, Mars, and differentiated asteroids are being analysed. This research aims to (1) understand the astrophysical environment of the inner solar system, (2) establish high-resolution absolute timescales for early geological events including planetary differentiation and impact histories, and (3) identify the characteristics and provenance of small bodies present during the early stages of planetary development.
- Recycling of oceanic lithosphere into the mantle at subduction zones is a fundamental part of the earth's plate tectonics. Isotopic characteristics of many lavas indicate that this recycled material is present in upper mantle melting zones. This suggests that these lavas derive from partial melting of complex, mixed sources composed of ancient recycled oceanic crust with low melting temperatures, and normal peridotite with much higher melting temperatures. There is little understanding of how such heterogeneous material melts and the sorts of liquids it produces. This project is using high-pressure-temperature experiments and major, minor and trace element analysis of experimental run products to investigate the melting behaviour of mixed mantle sources.

- The concept of a Snowball Earth has stimulated much discussion and ongoing research. A fundamental criterion is the absolute timing of the glaciogene events on a global scale. This project involves the study of stratigraphically well-constrained rocks in North America, Africa, Australia and South America with the principal aim being to place absolute age constraints on the glaciogene events and so enable one to draw comparisons and contrasts with other correlated horizons. Preliminary results from this and other studies show that some glaciogene events are globally coincident, whilst others are clearly outside the bounds of a single coeval, coincident Snowball Earth event.

Constraints on the Mesoarchaean crustal development of the central Kaapvaal Craton, South Africa

Richard A. Armstrong,¹ Cristiano Lana^{2*}, Wolf U. Reimold² and Roger L. Gibson²

¹ *Research School of Earth Sciences, The Australian National University, Canberra 0200, Australia*

² *Impact Cratering Research Group, School of Geosciences, University of the Witwatersrand, Private Bag 3, P.O. Wits 2050, South Africa*

**Present address: Impacts and Astromaterials Research Centre, Imperial College London, Royal School of Mines, South Kensington Campus, UK, SW7 2AZ*

The Kaapvaal Craton does not contain the oldest rocks on Earth, but it does contain one of the most comprehensive and continuous Archaean geological records from ~3.6 Ga onwards (Hunter 1974; De Wit *et al.* 1992; Poujol *et al.* 2003). It is thus an excellent laboratory for the development of geodynamic models of crustal and lithospheric growth.

de Wit *et al.* (1992) proposed a two-stage evolution for the craton, with the initial cratonic shield having grown through collisional tectonics and vertical magmatic accretion between 3600 and 3200 Ma, and subsequent lateral accretion along the margins of the Shield between 3200 and 3100 Ma. Field mapping, geochemical analysis, and U-Pb zircon and monazite dating have confirmed de Wit *et al.*'s (1992) model for the eastern parts of the craton (Armstrong *et al.*, 1990; Kamo and Davis 1994; De Ronde and De Wit 1994; Lowe 1994, 1999). Formation and accretion of the younger crustal fragments in the western and northern parts of the craton appears to have coincided broadly with partial melting of pre-existing >3200 Ma tonalite-trondhjemite-granodiorite (TTG) suites at mid- to lower-crustal levels and emplacement of 3200-3100 Ma high-level granite-granodiorite-monzogranite (GGM) batholiths throughout the already formed Kaapvaal Shield (Robb *et al.* 1991; De Wit *et al.* 1992; De Wit 1998; Moser *et al.* 2001; Poujol *et al.* 2003). The latter event has been interpreted by some workers as having been responsible for the establishment of a thick, stable lithospheric crust, which was capable of supporting the large late Neoproterozoic to Paleoproterozoic volcano-sedimentary basins (Robb *et al.* 1991; De Wit *et al.* 1992; Kamo and Davis 1994; De Wit 1998; Moser *et al.* 2001; Poujol *et al.* 2003).

In the central parts of the craton, we have concentrated our studies in the unique exposure within the 2-billion year impact site now preserved as the Vredefort Dome, integrating lithological and structural mapping, geochemistry and SHRIMP U-Pb dating to elucidate the tectonic history of the crystalline basement. Previous studies have suggested a link between an ~3.1 Ga high-grade metamorphic event recorded in mid-crustal rocks of the Vredefort dome and partial melting of the >3200 Ma tonalite-trondhjemite-granodiorite (TTG) suites in the Kaapvaal Shield (Hart *et al.* 1999; Moser *et al.* 2001; Flowers *et al.* 2003; Poujol *et al.* 2003). Moser *et al.* (2001) and Flowers *et al.* (2003) have suggested that this metamorphic event was followed by coupling

of the cratonic mantle and the Archaean protocontinental crust shortly before stabilization of the craton at *ca.* 3080 Ma. However, whilst evidence of partial melting of >3200 Ma TTG crust is observed elsewhere in the eastern and, to some extent, central parts of the craton, our new SHRIMP results indicate that emplacement of oldest sialic rocks (TTG suites) in the core of the dome occurred *after* the assembly of the Kaapvaal Shield at 3200 Ma.

Our results suggest a three-stage magmatic and tectonic evolution commencing with multiple intrusions of 3150-3107 Ma TTG rocks during the ductile deformation events D1 and D2. The chemical compositions of the TTG rocks, together with the geochronological data, suggest that they were probably derived from partial melting of hydrated oceanic crust in an island arc setting. The TTG and greenstone sequences were later partially melted and intruded by 3090-3080 Ma leucosomes and other granitoids during the upper amphibolite- to granulite-facies regional metamorphism and the development of a kilometer-scale, NW-trending, S3 high-strain zone. S3 and the high-grade metamorphic event are related here to tectonic collision of the Vredefort island arc terrane with the >3200 Ma Kaapvaal Shield to the east. The final Mesoarchaean structural event recorded in the core of the dome was associated with the collapse of the thickened crust along NE-trending, normal dip-slip, peak-to-retrograde, subhorizontal mylonitic shear zones (D4). The collapse was probably associated with, or was shortly followed by, the emplacement of 3060-3017 Ma aplite dykes. This extension may be linked to the rifting that accompanied the outpouring of the 3070 Ga Dominion Group volcanic sequence.

These new results from the crystalline basement rocks of the Vredefort Dome show that the tectonic history of this part of the craton is significantly different to other well-documented parts of the craton. The amalgamation of the craton as it is presently preserved probably occurred through lateral accretion of substantial blocks of crust at varying times, but it is clearly a complex process combining crustal blocks that potentially had very different tectonic histories.

Armstrong R.A., Compston W., Retief E.A., Williams L.S., and Welke H.J. (1991) Zircon ion microprobe studies bearing on the age and evolution of the Witwatersrand Basin. *Precambrian Research*, 53, 243-266

De Ronde C.E.J., De Wit M.J. (1994) Tectonic history of the Barberton greenstone belt, South Africa: 490 million years of Archaean crustal evolution. *Tectonics*, 13, 983-1005.

Flowers R.M., Moser D.E., Hart R.J. (2003) Evolution of the amphibolite-granulite facies transition exposed by the Vredefort impact structure, Kaapvaal Craton, South African Journal of *Geology*, 111, 455-470

de Wit M.J., Roering C., Hart R.J., Armstrong R.A., de Ronde C.E.J., Green R.W.E., Tredoux M., Pederdy E., Hart R.A. (1992) Formation of an Archaean continent. *Nature*, 367, 553-562.

- de Wit, M.. (1998) On Archaean granites, greenstones, cratons and tectonics: does the evidence demand a verdict? *Precambrian Research*, 91, 181-226.
- Hunter, D.R. (1974) Crustal development in the Kaapvaal Craton. The Archean. *Precambrian Research*, 1, 259-294.
- Moser, D.E., Flowers, R.M., Hart, R.J. (2001) Birth of the Kaapvaal Tectosphere 3.08 billion years ago. *Science*, 291, 465-468.
- Poujol M., Robb L., Anhaeusser C.R., Gericke B. (2003) Geochronological constraints on the evolution of the Kaapvaal craton, South Africa. *Precambrian Research*, 127, 181-213.
- Lowe, D.R. (1994) Accretionary history of the Archean Barberton Greenstone Belt (3.55-3.22 Ga), southern Africa. *Geology*, 22, 1099-1102
- Lowe D.R. (1999) Geological evolution of the Barberton greenstone belt and vicinity in Geologic evolution of the Barberton greenstone belt, South Africa (D.R. Lowe and G.R. Byerly, editors). *Geological Society of America Special Paper*, 329, 287-312
- Robb, L.J., Davis, D.W., Kamo, S.L. (1991) Chronological framework for the Witwatersrand Basin and environs: towards a time-constrained depositional model. *South African Journal of Geology*, 94, 86-95.

Constraining depositional ages for Neoproterozoic siliciclastic sequences through detrital zircon ages: a ca.770 Ma maximum age for the lower Uinta Mountain Group

C. Mark Fanning, Carol M. Dehler, Paul K. Link, Laura D. DeGrey,

Research School of Earth Sciences, Australian National University, Canberra ACT 0200

Department of Geology, Utah State University, Logan, UT 84322, U.S.A.

Department of Geosciences, Idaho State University, Pocatello, ID 83209 U.S.A.

It is difficult to obtain accurate and reliable time constraints on siliciclastic Neoproterozoic rocks where tuffaceous horizons are absent; the so-called "curse of the Neoproterozoic sandstones" (Link et al., 1993). Further, even where tuffaceous rocks are present they often contain recycled zircon and so there may not be a unique interpretation of a "magmatic" component that dates the sequence. One mechanism to place time constraints on such siliciclastic and volcanoclastic sequences is via the detrital zircons, specifically by examining the youngest coherent age grouping in the detrital age spectrum. Detrital zircon age data is principally used to determine the provenance of a sediment, and from that provenance, draw conclusions about possible correlations and sources. Many detrital zircon age spectra contain a few analyses that are close to or within uncertainty of the inferred depositional age of the sediment. In some cases, this young age population may be younger than an existing prejudiced interpreted time of deposition and so a coherent young age peak (ie 3 or more grains) will place constraints on the maximum age of deposition. The Uinta Mountain Group (UMG) of northeastern Utah is one such siliciclastic Neoproterozoic succession that has limited constraints on the time of deposition. From correlations based on fossil, C isotope and lithological evidence with the Chuar Group of the Grand Canyon region, the top of the western UMG (Red Pine Shale) is placed at ca.740 Ma (Dehler et al., 2001). Few if any age constraints are available for the eastern UMG, nor for the lower parts of the sequence. An initial 60-grain sampling of the formation of Outlaw Trail, ~ 1km from the base of the 4-7 km thick (UMG) in the Swallow Canyon quadrangle, eastern Uinta Mountains, found a single zircon with an age of ca.760 Ma. Other components of that detrital zircon spectrum include a significant Grenville age cluster, grains derived from 1.45 Ga A-type granites, Meso- to Paleoproterozoic grains and the usual smattering of Archaean grains. In order to obtain a credible maximum depositional age constraint, a population, rather than a single young grain, is necessary. From the analysis of 128 single zircon grains from two separate samplings of the same outcrop and 4 analytical sessions, there are 4 grains that are within analytical uncertainty and give a concordia age of ca.770 Ma. These four grains are igneous in origin as interpreted from CL images, but the grain morphologies show clear evidence for surface transport; ie they are not primary volcanic grains. This ca.770 Ma age group is the youngest coherent component within the 128 grain population and therefore constrains the maximum age on deposition near the base of the eastern UMG. These data show that detrital zircon age determinations can not

only be used for provenance information and but where a significant youngest component is determined, it constrains the maximum depositional age.

Link, P.K., Christie-Blick, N., Devlin, W.J., Elston, D.P., Horodyski, R.J., Levy, M., Miller, J.M.G., Pearson, R.C., Prave, A., Stewart, J.H., Winston, D., Wright, L.A., Wrucke, C.T. (1993) Middle and Late Proterozoic stratified rocks of the western Cordillera, Colorado Plateau, and Basin and Range province: in Reed, Jr., J.C., Bickford, M.E., Houston, R.S., Link, P.K., Rankin, D.W., Sims, P.K., Van Schmus, W.R. (Eds), *Precambrian: Conterminous U.S.* Geological Society of America, *The Geology of North America*, Vol. C-2, 463-596.

Dehler, C.M., Elrick, M., Karlstrom, K.E., Smith, G.A., Crossey, L.J., and Timmons, J.M., 2001, Neoproterozoic Chuar Group (ca. 800–742 Ma), Grand Canyon: A record of cyclic marine deposition during global cooling and supercontinent rifting. *Sedimentary Geology* **141–142**, 465–499

The oxidation state of Fe in mantle garnets: implications for diamond stability during metasomatic events.

Greg Yaxley¹, Andrew Berry^{1,2}, Hugh O'Neill¹ and Alan Woodland²

¹ Research School of Earth Sciences, The Australian National University, Canberra ACT 0200, Australia

² Institut für Kristallographie, Universität Frankfurt, Frankfurt/M, Germany

Determination of $\text{Fe}^{3+}/(\text{Fe}^{2+} + \text{Fe}^{3+})$ in garnet from kimberlite-bourne peridotite xenoliths is essential in calculating lithospheric mantle oxidation state (ie. oxygen fugacity; $f\text{O}_2$) in the garnet peridotite stability field. Knowledge of deep lithospheric $f\text{O}_2$ is important in estimating diamond stability and in elucidating metasomatic history.

X-ray Absorption Near Edge Structure (XANES) spectroscopy offers a rapid and precise synchrotron-based microbeam technique for determining transition metal oxidation states in a range of geological materials, including volcanic glasses (e.g. Berry *et al.* 2003; Berry and O'Neill 2004). The aim of our study is to calibrate the technique for application to determination of $\text{Fe}^{3+}/\Sigma\text{Fe}$ in natural mantle-derived garnets, frequently recovered from regolith and drilling during diamond exploration programs.

Using the Australian National Beamline Facility at the Photon Factory, Tsukuba, Japan, we acquired Fe K-edge XANES spectra from a series of synthetic, well-characterised garnets on the compositional joins andradite – skiaigite - almandine ($\text{Ca}_3\text{Fe}_2^{3+}\text{Si}_3\text{O}_{12}$ - $\text{Fe}_3^{2+}\text{Fe}_2^{3+}\text{Si}_3\text{O}_{12}$ - $\text{Fe}_3^{2+}\text{Al}_2\text{Si}_3\text{O}_{12}$), which have $\text{Fe}^{3+}/\Sigma\text{Fe}$ varying from 1 to 0 (Woodland and O'Neill 1993; Woodland and Ross, 1994). The powdered samples were mounted on plastic film allowing simultaneous acquisition of fluorescence, absorption and Fe-foil energy calibration spectra. This visit to the ANBF was funded by the Australian Synchrotron Research Program.

Pre-edge peaks were subjected to background subtraction and best fits were determined by fitting a number of Gaussian components. The peak centroids varied linearly with $\text{Fe}^{3+}/\Sigma\text{Fe}$, as shown in Figure 1.

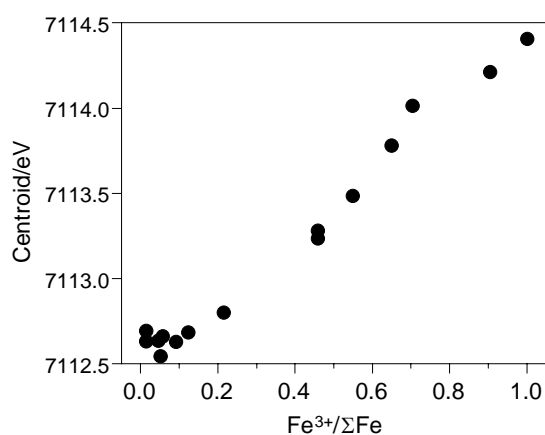


Figure 1. Plot of garnet $\text{Fe}^{3+}/\Sigma\text{Fe}$ against pre-edge peak centroid (eV) showing the linear correlation.

We have been granted further beamtime in 2006. During this visit, we will aim to investigate the nature of garnet compositional effects using an extended set of well-characterised synthetic and natural samples (e.g. Mössbauer spectroscopy).

In particular we will include Mg and Cr-bearing end-members. This should allow development of a full calibration applicable to natural mantle garnets.

Berry, A.J., O'Neill, H.S., Jayasuria, J.D., Campbell, D.J. and Foran, G.J., 2003. XANES calibration for the oxidation state of iron in a silicate glass. *American Mineralogist*, **88**, 967-977.

Berry, A.J. and O'Neill, H.S.C., 2004. A XANES determination of the oxidation state of chromium in silicate glasses. *American Mineralogist*, **89**, 790-798.

Woodland, A.B. and O'Neill, H.S., 1993. Synthesis and stability of $\text{Fe}_3^{2+}\text{Fe}_2^{3+}\text{Si}_3\text{O}_{12}$ garnet and phase relations with $\text{Fe}_3\text{Al}_2\text{Si}_3\text{O}_{12}$ - $\text{Fe}_3^{2+}\text{Fe}_2^{3+}\text{Si}_3\text{O}_{12}$ solutions. *American Mineralogist*, **78**, 1002-1015.

Woodland, A.B. and Ross, C.R., 1994. A crystallographic and Mössbauer spectroscopy study of $\text{Fe}_3\text{Al}_2\text{Si}_3\text{O}_{12}$ - $\text{Fe}_3^{2+}\text{Fe}_2^{3+}\text{Si}_3\text{O}_{12}$ (almandine-"skiagite") and $\text{Ca}_3\text{Fe}_2^{3+}\text{Si}_3\text{O}_{12}$ - $\text{Fe}_3^{2+}\text{Fe}_2^{3+}\text{Si}_3\text{O}_{12}$ (andradite-"skiagite") garnet solid solutions. *Physics and Chemistry of Minerals*, **21**, 117-132.

Detrital apatite geochemistry and its application in provenance studies

Andrew Morton^{1,2} and Greg Yaxley³

¹ *HM Research Associates Ltd., 100 Main Street, Woodhouse Eaves, Leics LE12 8RZ, UK*

² *Department of Geology and Petroleum Geology, University of Aberdeen, Aberdeen AB24 3UE, UK*

³ *Research School of Earth Sciences, The Australian National University, Canberra, ACT 0200, Australia*

Single-grain geochemical analysis by WDS electron-microprobe and LA-ICPMS of detrital apatites from Pliocene sandstones in the South Caspian Basin (Azerbaijan) and Devonian-Carboniferous sandstones from west of Shetland (UK) demonstrate that apatite geochemistry has significant potential in provenance analysis. Apatites in Pliocene sandstones deposited by the paleo-Kura river system, which drained the Lesser Caucasus region, were derived largely from mafic/intermediate and alkaline rocks. Apatite populations in Pliocene sediments transported by the paleo-Volga river system, which drained the Russian Platform, show greater compositional diversity, indicating supply from granitoids or other acidic rocks together with subordinate mafic/intermediate and alkaline rocks. Apatites in the Devonian-Carboniferous succession west of Britain were sourced predominantly by acidic rocks, either directly from Archaean gneisses or indirectly from metasedimentary rocks.

Since apatite is stable during burial in sedimentary basins, apatite geochemistry can be used to determine provenance of sandstones from the full range of diagenetic environments, although the instability of apatite during weathering means that the method will be difficult to apply to sandstones with prolonged weathering history. At present, identification of provenance using apatite geochemistry is limited by the lack of a comprehensive database on apatite compositions in some of the potential source rocks, particularly those of metamorphic origin. The role played by sediment recycling is another factor that requires consideration when reconstructing source areas on the basis of apatite compositions.